Title
Theory of the Ion-Channel Laser

Author
Whittum, D.H.

Publication Date
1990-09-01

Lawrence Berkeley Laboratory
UNIVERSITY OF CALIFORNIA

Accelerator & Fusion Research Division

Theory of the Ion-Channel Laser

D.H. Whittum
(Ph.D. Thesis)

September 1990

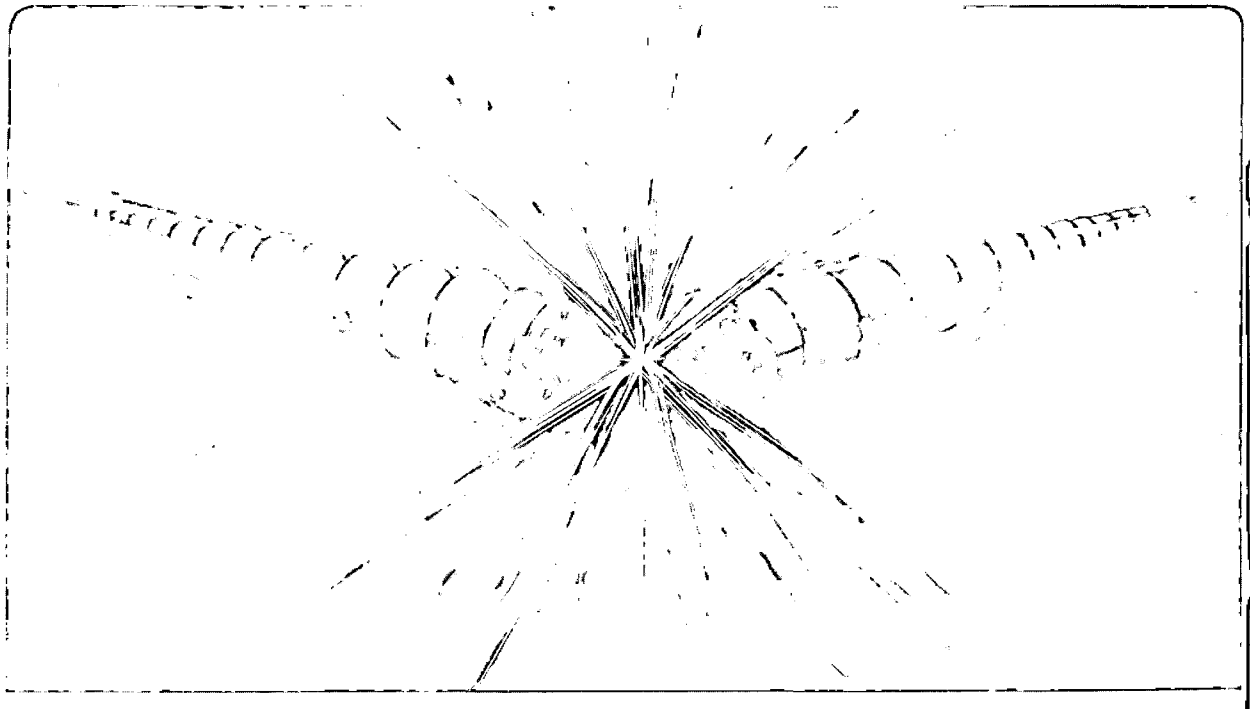

Prepared for the U.S. Department of Energy under Contract Number DE-AC03-76SF00098.

DISCLAIMER

LBL-29720

Theory of the Ion-Channel Laser

David H. Whittum
(Ph.D. Thesis)

September 1990

This work was supported by the Director, Office of Energy Research, Office of High Energy and Nuclear Physics, Division of High Energy Physics, of the US Department of Energy under contract DE-AC03-76SF00098.

Theory of the Ion-Channel Laser

David H. Whittum

Theory of the Ion-Channel Laser

by

David H. Whittum

Abstract

A relativistic electron beam propagating through a plasma in the ion-focussed regime exhibits an electromagnetic instability with peak growth rate near a resonant frequency $\omega \sim 2\gamma^2 \omega_\beta$, where γ is the Lorentz factor and ω_β is the betatron frequency. The physical basis for this instability is that an ensemble of relativistic simple harmonic oscillators, weakly driven by an electromagnetic wave, will lose energy to the wave through axial bunching. This "bunching" corresponds to the development of an rf component in the beam current, and a coherent centroid oscillation. The subject of this thesis is the theory of a laser capitalizing on this electromagnetic instability.

In Chapter 1 a historical perspective is offered. In Chapter 2, the basic features of relativistic electron beam propagation in the ion-focussed regime are reviewed.

In Chapter 3, the ion-channel laser (ICL) instability is explored theoretically through an eikonal formalism, analgous to the "KMR" formalism for the free-electron laser (FEL). The dispersion relation is derived,

and the dependence of growth rate on three key parameters (detuning δ, Pierce parameter ρ, and betatron parameter a_β) is explored. Finite temperature effects are assessed.

From this work it is found that the typical gain length for amplification is longer than the Rayleigh length and we go on to consider three mechanisms which will tend to guide the radiation. First, we consider the effect of the ion channel as a dielectric waveguide. We consider next the use of a conducting waveguide, appropriate for a microwave amplifier. Finally, we examine a form of "optical guiding" analgous to that found in the FEL.

In Chapter 4, the eikonal formalism is used to model numerically the instability through and beyond saturation. Results are compared with the numerical simulation of the full equations of motion, and with the analytic scalings. The analytical requirement on detuning spread is confirmed.

In Chapter 5 results are summarized and prospects for future work are considered.

Table of Contents

page

page

page

Figures

page

page

page

Tables

page

Acknowledgements

I thank Andrew M. Sessler, my research advisor, for training me to be a physicist. I am particularly indebted to him for teaching me how to give talks, when to make simple estimates, and how to write papers. Thanks to him, I think I have grasped the virtue of asking simple questions and making back-of-the envelope calculations. These skills I've found indispensable.

To John M. Dawson I owe my gratitude for taking seriously a speculative idea.

I owe my appreciation to Jonathan Arons, Joel Fajans and Edward Morse for taking the time to be on my committee, and to read this thesis.

I thank Donald B. Hopkins and Yehuda Goren for teaching me what I know about microwaves. I thank Jeffrey Tennyson for his cheerful willingness to talk about diverse issues (usually while jogging).

I am indebted to Simon S. Yu for accepting me as a student guest in the Beam Research Group at Lawrence Livermore National Laboratory, and for introducing me to many interesting problems of beam-plasma physics. His advice over the last four years and his many suggestions of new problems have been invaluable.

There are many others at LLNL who have helped to train me over the years, and I thank them for the numerous discussions, their helpful comments, and for occasionally taking me seriously. Among them are William A. Barletta, Yu-Jiuan Chen, George D. Craig, John F. Deford, William

M. Fawley, Tim L. Houck, V. Kelvin Neil, Thaddeus J. Orzechowski, Donald Prosnitz, Ernst T. Scharlemann, William M. Sharp, Henry D. Shay, John J. Stewart, and Glen A. Westenskow.

I wish to add my appreciation to Kuan-Ren Chen, Pisin Chen, Thomas Katsouleas, Warren Mori, Jaime R. Rosenzweig , and David U. L. Yu for many helpful discussions.

I wish to thank Shigenori Hiramatsu, Juni-ichi Kishiro, and Ken Takayama at the National Laboratory for High Energy Physics (KEK), for many discussions of their work and their experimental results, for their generous hospitiality, and especially for putting up with a graduate student theorist in their laboratory.

I wish to thank Hirobumi Saito for helpful comments and for very kindly showing me around the Institute of Space and Astronautical Science in Sagamihara-shi. I also wish to thank Makoto Shiho of the Japan Atomic Energy Research Insititute, Naka Fusion Research Establishment, for his hospitality, for his discussions of the LAX-1 project, and for the lengthy tour of his facility as well as JT-60.

I thank Glenn Joyce, Martin Lampe, Jarvis Leung, Gil A. Travish, and Jonathan S. Wurtele, for fruitful joint efforts. I also wish to thank Swapan Chattopadhyay and Kwan-Je Kim for their encouragement. I thank Ming Xie and Baruch Levush for helpful conversations.

I particularly wish to express my gratitude to William E. Drummond and M. Lee Sloan for introducing me to many problems of plasma physics and numerical simulation, at Austin Research Associates. I also wish to

thank George Bourianoff, Barry N. Moore, J. Robert Thompson, Karen Tweedy, John R. Uglum and Vernon Wong, for many delightful months of physics.

To Carol Adams, Darlene Moretti and Janet M. Wikkerwink I owe my thanks for their help and support.

To Mel Month, Marilyn Paul, and Susan Winchester, I owe my thanks for their hospitality, warmth and encouragement at the U. S. Particle Accelerator School.

To the soldiers of B Company, 2/159 Infantry (Mechanized) I owe my thanks for their encouragement. In particular, I wish to thank my platoon sergeant, SFC Ludwig, and my squad leaders, SGT Biscardi, CPL Cabanayan, CPL Sausedo, and CPL Garcia, for being *hoowha*. I also wish to thank my commander, CPT Sutherland, for giving me four weeks off to write this thesis.

The greatest debt I owe to Kinuko Sano for her encouragement and patience. *Arigato gozaimashita! Ikimasho!*

In relation to the specifics of this thesis, I am indebted to Jonathan S. Wurtele, and Ernst T. Scharlemann for vital discussions of detuning spread, and numerics. I thank Kuan-Ren Chen for pointing out the importance of the relativistic mass effect. I also appreciate helpful comments by Shigenori Hiramatsu and Ken Takayama concerning the ion-hose instability. I wish to thank Simon S. Yu, William M. Sharp, Martin Lampe and Glenn Joyce for vital discussions and joint efforts on the electron-hose instability. I am also indebted to John M. Dawson and Thomas Katsouleas for many essential conversations. Of course, it goes without saying that this work would never have gotten "off the ground" without the help of my research advisor, Andrew M. Sessler.

Dedication

This work is for Willie, as true a hound as ever roamed, mindful of his duties at home but mostly abroad, politely circumspect in regard to strangers, as befits a country dog, but ever my good friend. He will not be soon forgotten.

Chapter 1: Introduction

"All things hang like a drop of dew
Upon a blade of grass."
---W.B. Yeats

A relativistic electron beam propagating through a plasma in the ion-focussed regime exhibits an electromagnetic instability with peak growth rate near a resonant frequency $\omega \sim 2\gamma^2 \omega_\beta$, where γ is the Lorentz factor and ω_β is the betatron frequency.[1,2] The physical basis for this instability is that an ensemble of relativistic simple harmonic oscillators, weakly driven by an electromagnetic wave, will lose energy to the wave through axial bunching. This "bunching" corresponds to the development of an rf component in the beam current, and a coherent centroid oscillation. The subject of this thesis is the theory of a laser capitalizing on this electromagnetic instability.

In this introduction we review the historical background and motivation for the ion-channel laser, to include a brief history of beam-plasma physics and the subject of coherent radiation from intense relativistic electrons beams. In practice, these two fields overlap considerably, in that plasmas have been used to enhance efficiency in known radiation devices,[3,4,5]

and have been proposed to provide the coupling for novel radiation devices.[6,7] In the ion-channel laser (ICL), these two subjects are inseparable.

A. OVERVIEW OF BEAM-PLASMA PHYSICS

The essential features of beam propagation in an unmagnetized, preionized plasma may be described in terms of charge and current neutralization. A relativistic electron beam (REB) injected into a plasma *less dense* than the beam core ("underdense") expels plasma electrons from the beam volume, producing a non-neutral "ion-channel." The radial electric field due to the ions then focusses the beam ("ion-focussing regime" or IFR). A plasma *more dense* than the beam will neutralize the beam charge, so that the REB is focussed by its own magnetic field ("magnetic self-focussing"). A still denser plasma will partially neutralize the current, if the plasma skin depth is short compared to the beam radial size, and if the magnetic diffusion time is long compared to the beam length.

In the next chapter we will discuss these features in detail, specializing to the ion-focussed regime. First, however, we consider the historical context for the growing interest in the IFR.

1. Early work on beam-plasma physics

The earliest treatment of REB propagation in a plasma was given in 1934, by Bennett,[8] who considered the magnetically self-focussing regime.

This paper was followed in 1939 by work of Alfven,[9] who showed that, due to self-fields, an electron beam could not be propagated in *free space* at arbitrarily high current. The limiting current, or Alfven current, is $I_A=\gamma\beta_z I_0$, where I is the beam current, $I_0=mc^3/e\sim17$ kA, γ is the Lorentz factor for the beam and $\beta_z=v_z/c$, with v_z the velocity of the beam and c the speed of light. The electron mass is m and $-e$ is the electron charge. To exceed this limit some confining or focussing forces must be applied, and they may be either electric or magnetic, provided externally, or arising collectively from the addition of a plasma.

A second paper on self-focussing streams was published by Bennett in 1955.[10] In the same year, Budker published his work on propagation of partially charge-neutralized beams, motivated by the possiblity of accelerating lights ions.[11] Further work on ion-acceleration followed in 1957, by Veksler.[12,13] Eventually, interest in ion-acceleration led to the the Electron Ring Accelerator (ERA) concept.[14] From the ERA project, and related work on the "ASTRON" injector, we may trace the beginnings of work on induction linear accelerators for high current electron beams.

2. *Induction linear accelerators and beam-plasma physics*

At Lawrence Livermore National Laboratory (LLNL), this work began with the ASTRON I induction accelerator (1963), which was followed by the ASTRON II (1968). Under the SEESAW project funded by the Advanced Research Projects Agency (ARPA), the ASTRON was used to study REBpropagation in the atmosphere, for military applications.[15] After the

termination of the ASTRON program (1972), the ASTRON II was used as a tool for the study of beam-gas and beam-plasma interactions, and the Experimental Test Accelerator (ETA) was constructed on the old ASTRON II site (1977). ETA was sponsored by the Navy's Chair Heritage program, again to study propagation in the atmosphere.

Success with ETA lead to the construction of the Advanced Test Accelerator (ATA) at Site 300 (the high-explosives test site operated by LLNL near Tracy, California) in 1982. Most recently, a fifth induction linac, ETAII has been constructed (1987) on the site of the old ETA, which has been decommissioned.[16]

This is a rough outline of induction linac work at LLNL, just one lab among many. During the same period, induction linac work has been performed at the Atomic Weapons Research Establishment in England, Physics International, Ion Physics, Maxwell Laboratories, the Naval Research Laboratory, the Air Force Weapons Laboratory, the National Bureau of Standards, Sandia National Laboratories, and other labs. Induction linac work is also proceeding in Japan, notably at the National Laboratory for High-Energy Physics (KEK), the Institute for Laser Engineering at Osaka University, the Institute for Space and Astronautical Science, and the Naka Fusion Research Establishment of the Japan Atomic Energy Research Institute.

Space does not permit a thorough history or complete enumeration of induction linac work here, but this brief digression and the references will give some indication of the explosion of research during this period. Much of

this work was concerned directly or indirectly with beam-plasma interactions, and the proposals, papers and results which have accumulated could fill a small library.

3. Beam-plasma theory and experiment

Extensive treatments of the equilibria of a charge neutralized, and partially current neutralized, REB propagating in a plasma, were given in 1968 by Roberts and Bennett,[16] in 1970 by Bennett and Cox,[17] and Hammer and Rostoker,[18] and in 1971 by Lee and Sudan.[19] In 1976 a Fokker-Planck formulation of beam-plasma equilibria and an application of the *H*-theorem to this system were set down by E.P. Lee.[20] By the mid-1970's the beam-plasma community had grown quite large, and one finds review papers from around the world, for example R. Okamura, *et al.*,[21] and G. Wallis, *et al.*.[22] A more recent review of REB-plasma physics may be found in P. C. de Jagher, *et al.* [23]

An extensive literature exists on REB-plasma experiments. The first experimental work on magnetically self-focussing streams was published in 1966 by Graybill and Nablo.[24] The first observation of the acceleration of light ions was reported by Graybill and Uglum,[25] in 1970. A discussion of theory and results for REB propagation in connection with an REB-pumped N_2 laser is given by Yu V. Tkach, *et al.* [26] Some of the first results from experiments with REB heating of plasmas are discussed by MacArthur and Poukey, [27] and Prono, *et al.*[28] These papers are the first of scores of such papers published in

each area of application over the period 1960-1980, of which there are far too many to review in detail. Perhaps it is enough to note that over the last decade, ion-focussing has been successfully and routinely employed in the transport of high current beams for accelerator work and radiation research.[29,30,31,32] From this one might gather that the essential features of REB propagation are well in hand.

In fact, this is not quite true. At the Advanced Test Accelerator (ATA), at Lawrence Livermore National Laboratory (LLNL) extensive, experimental tests of beam propagation in the ion-focussed regime have been conducted over the last decade.[33] One particular application was to use the REB to drive an infrared FEL,[34] and this application provided a rigorous test of beam quality.[35] It was found that REB emittance degraded considerably in the ion-channel, much more than could be expected theoretically. As with the early experiments on fusion plasmas,[36] one might expect that some unknown, instability lurked in the data. In fact, the electromagnetic instability we will discuss in Chapter 3, coupled to ion-motion, may account for considerable emittance growth in a long pulse.

4. Novel beam-plasma concepts

We may summarize REB-plasma work during the period 1930-1980 as the study and application of the equilibria and instabilities of beams subject to various collective focussing forces. Most work involved long pulse lengths, in the range 10ns-1μs, for applications including light-ion acceleration,

plasma heating, microwave generation, gas-laser pumping and nuclear effects simulations. The applications are quite varied and this reflects the variety of regimes available in such a three-component plasma.[37]

More recently, interest has been growing in the regime of short pulse, low-emittance, high-current, high-energy beams, propagating through preionized, unmagnetized plasmas. Among the novel concepts proposed are the plasma lens,[38,39] the continuous plasma focus,[40,41] the plasma wakefield accelerator,[42,43,44] the beat wave accelerator,[45] a collective electron accelerator,[46] and the plasma emittance damper.[47,48]

Given the abundance of new ideas, it is helpful to remember that all have essentially one application: beam-handling. Typical beam-handling problems include transport, focussing, suppression of beam-breakup, and acceleration. For example, the foremost goal of accelerator physics today, is to design a high luminosity TeV-energy electron-positron collider of reasonable length.[49] To this end, plasmas have been proposed to accelerate beams to TeV energies in a few hundred meters, to focus the beams while overcoming theoretical limits[50] on conventional focussing and to neutralize self-fields at the interaction point,[51] thus overcoming certain limitations due to collective effects in beam-beam collisions.[52,53,54]

B. OVERVIEW OF FREE-ELECTRON RADIATION DEVICES

Coherent radiation from relativistic electron beams, usually in vacuum, also has been the subject of extensive work, in connection with the FEL,[55,56] the Cyclotron Auto-Resonant Maser (CARM),[57] and other FEL-like devices.[58,59,60,61] Applications for high power, coherent radiation may be found across the spectrum from the microwave to the X-Ray, from particle acceleration,[62,63] fusion,[64,65] communications and weapons,[66] to surface chemistry, medical and industrial applications.[67,68,69]

Probably the earliest work on the FEL is that of Motz,[70] and the "ubitron" work of Phillips[71] in the microwave regime, and Madey,[72] who proposed and demonstrated experimentally, that the FEL could be operated as an amplifier (and, subsequently, an oscillator) at visible wavelengths. The CARM concept grew naturally out of work on the gyrotron,[73] for which the CARM is the relativistic limit.

The CARM and the FEL are each fast-wave devices, in that the coupling of the beam to the fields occurs through a transverse electric field, with small electric field parallel to the beam velocity (corresponding to phase velocity of order *c*). This feature is shared with the ICL.

In general, fast-wave devices have a resonance relation of the form

$$\omega - k_z v_z = \omega_0, \tag{1.1}$$

near which maximum amplification of an input signal occurs. Here ω and k_z are the angular frequency and axial wavenumber of the signal field to be amplified. The beam propagates in the z-direction with velocity $v_z \sim c$. At the same time, external fields enforce a periodic transverse motion with angular frequency ω_0.

This resonance condition states that the Doppler shifted frequency of the signal field, should be close to the frequency of transverse oscillation of the electron. In this way the electron is resonantly driven and suffers a secular perturbation in its orbit. Viewed collectively, this secular drift produces a bunching of the beam. The system is unstable because the bunching of the beam causes the electrons to radiate more nearly in phase producing higher power, and thereby, more bunching.

For the CARM, $\omega_0 \sim eB_z/m\gamma c$, where B_z is the applied axial magnetic field. For the FEL $\omega_0 \sim k_w v_z$, where $k_w = 2\pi/\lambda_w$, with λ_w the spatial period ("wiggler" period) of the alternating dipole fields.

In fact, it is not hard to show, using the Maxwell-Vlasov equations, that for an ensemble of electrons subject to an arbitrary, periodic zeroth order orbit, such a resonant electromagnetic instability may ensue. This feature is exploited, for example, in the CARM, and in the quadrupole FEL (QFEL), proposed by Levush, *et al.*[74,75]. The QFEL makes use of a quadrupole focussing winding to capitalize on this instability and amplify microwaves. One shortcoming of the QFEL is that magnetic focussing channels tend to be weak

compared to FEL wigglers. Consequently, the frequency range, and gain are limited.

An analagous instability obtains for a REB propagating through an electrostatic focussing channel in the ion-focussing regme.[1,2] In this case the resonance relation of Eq. (1.1) applies, with $\omega_0=\omega_\beta$, where ω_β is just the betatron frequency of the ion-focussed beam,

$$\omega_\beta = \frac{\omega_p}{\sqrt{2\gamma}} . \tag{1.2}$$

The subject of this thesis is, roughly, to explain and expand on Eqs. (1.1) and (1.2), and to explore the consequences in detail.

Interestingly, experimental evidence has already been found, of coherent radiation from intense electron beams injected into overdense, unmagnetized plasmas.[76,77] Explanations offered for the high microwave power levels observed have included streaming instabilities, strong-turbulence, and virtual cathode oscillations. Kato *et al.*,[58] remark on the possibility of an FEL analogy based on jitter motion in "large-amplitude electrostatic waves generated by instability"; however, to date, no satisfactory theory has been set down to explain the measured power levels. We shall see that the ion-channel laser instability is likely an important contributing mechanism for the production of such radiation.

Now, unlike slow-wave devices, (the klystron or the magnetron,[78,79] for example) fast-wave devices require a cold beam, i.e., one with a small

spread in axial momenta, and small transverse temperature. This may be seen from the resonance relationship and the principle of Landau damping.[80] In general, one must require that the spread in detuning

$$\Delta\omega = \omega_0 + k_z v_z - \omega, \tag{1.3}$$

be small compared to the growth rate for the instability. Otherwise electrons slip out of phase with respect to the resonant particle (satisfying $\Delta\omega$=0) and, collectively, radiate less, so that gain is reduced. As in the FEL and CARM, detuning spread will turn out to be an important limitation on ICL performance.

C. SUMMARY

The diverse regimes of beam-plasma physics have been studied extensively over the last fifty years, and the list of novel applications grows wih each passing year. Free-electron radiation devices trace their origin to the burgeoning microwave work of the post-war era, and have flourished in the last decade, appearing in many varieties, with as many applications. Many features of each field will appear in our study of the ion-channel laser.

In the next chapter, we review the basic features of relativistic electron beam propagation in the ion-focussed regime. We go on to explore the ICL instability theoretically, in Chapter 3, and numerically, in Chapter 4. The

result of this work will be a theoretical formulation for the laser, including particle dynamics and radiation guiding, which will be summarized in terms of scaling laws encompassing laser performance and plasma constraints (ion-motion, etc.), with specific numerical examples for illustration. From this work, theory will be advanced to the state where practical experiments can be considered.

References

[1]D. H. Whittum, A. M. Sessler and J. M. Dawson, Phys. Rev. Lett. **64**, 2511 (1990).

[2]K. R. Chen, T. Katsouleas, and J. M. Dawson, "On the Amplification Mechanism of the Ion-Channel Laser", IEEE Trans. Plasma Sci. (accepted for publication).

[3]Addition of plasma to a backward-wave oscillator is discussed in Y. Carmel, *et al.*, Phys. Rev. Lett. **62**, 2389 (1989).

[4]Use of ion-focussing in the interaction region of a microwave FEL amplifier is proposed in K. Takayama and S. Hiramatsu, Phys. Rev. A **37**, 173 (1988). Experimental development of this concept is discussed in S. Hiramatsu, K. Ebihara, Y. Kimura, J. Kishiro, M. Kumada, H. Kurino, Y. Mizumachi, T. Ozaki and K. Takayama, Nucl. Instrum. Methods **A285**, 83 (1989).

[5]Use of ion-focussing in a short-wavelength FEL is proposed in W. A. Barletta and A. M. Sessler, *High Gain, High Power Free-Electron Laser: Physics and Application to TEV Particle Acceleration, Proceedings of the INFN International School on Electromagnetic Radiation and Particle Beams Acceleration*, edited by R. Bonifacio, L. De Salvo Souza, and C. Pellegrini (Elsevier Science Publishers B. V., Amsterdam, 1988) pp. 211-220.

[6]For a discussion of the transition free-electron laser, an FEL relying on periodic variations in plasma density to produce stimulated transition

radiation, see G. Bekefi, J. S. Wurtele, and I. H. Deutsch, Phys. Rev. A **34**, 1228 (1986).

[7]Use of a longitudinally varying ion density to make a "plasma laser" is proposed in A.T. Lin, P.K. Kaw and J.M. Dawson, Phys. Rev. A **8**, 2618 (1973).

[8] W. H. Bennett, "Magnetically Self-Focussing Streams," Phys. Rev. **45**, 890 (1934).

[9]H. Alfven, "On the Motion of Cosmic Rays in Interstellar Space," Phys. Rev. **55**, 425 (1935).

[10]W. H. Bennett, Phys. Rev. **98**, 1584 (1955).

[11]G. J. Budker, *Proceedings of the CERN Symposium on High Energy Accelerators and Pion Physics*, (CERN Service d'Information, Geneva, 1956), pp. 68-75.

[12]V. I. Veksler, At. Energ. (USSR) **2**, 247 (1957).

[13] Y. B. Fainberg, Sov. Phys.-Usp. **10**, 750 (1968).

[14]*Symposium on Electron Ring Accelerators*, University of California Radiation Laboratory Report No. 18103 (1968).

[15]D. Birx, "Induction Linear Accelerators", *Proceedings of the U. S. Particle Accelerator School*, edited by Melvin Month (AIP, 1989).

[16]T. G. Roberts and W.H. Bennett, Plasma Phys. **10**, 381 (1968).

[17]J. L. Cox, Jr., and W. H. Bennett, Phys. Fluids **13**, 182 (1970).

[18]D. A. Hammer and N. Rostoker, Phys. Fluids **13**, 1831 (1970).

[19]R. Lee. and R. N. Sudan, Phys. Fluids **14**, 1213 (1971).

[20]E. P. Lee, Phys. Fluids **19**, 60 (1976).

[21]R. Okamura, Y. Nakamura, and N. Kawashima, Plasma Phys. **19**, 997 (1977). This excellent review covers the basic features and applications of beam-plasma physics, together with a discussion of an experiment using short-pulse REBs (1 ns pulse, 500 keV energy, 2 kA current) for plasma heating.

[22]G. Wallis, K Sauer, D. Sunder, S. E. Rosinskii, A. A. Rukhadze and V. G. Rukhlin, Sov. Phys.-Usp. **17**, 492 (1975).

[23]P. C. de Jagher, et al. F. W. Sluijter, and H. J. Hopman, Physics Reports **167**, 177 (1988). This review omits a number of applications, however, it lists several interesting, old references on the use of the two-stream instability for pre-bunching in microwave devices driven by nonrelativistic beams.

[24]S. E. Graybill and S. V. Nablo, "Observations of Magnetically Self-focusing Electron Streams," Appl. Phys. Lett **8**, 18 (1966).

[25]S. E. Graybill and J. R. Uglum, J. Appl. Phys. **41**, 236 (1970).

[26]Yu. V. Tkach, Ya. B. Fainberg, I. I. Magda, G. V. Skachek, S. S. Pushkarev, and N. I. Gaponenko, Sov. J. Plasma Physics. **2**, 259 (1976).

[27]D. A. MacArthur and J. W. Poukey, Phys. Rev. Lett. **27**, 1765 (1971).

[28]D. Prono, B. Ecker, N. Bergstrom, and J. Benford, Phys. Rev. Lett. **35**, 438 (1975).

[29]W. E. Martin, G. J. Caporaso, W. M. Fawley, D. Prosnitz, and A. G. Cole, Phys. Rev. Lett. **54**, 685 (1985).

[30]G. J. Caporaso, F. Rainer, W. E. Martin, D. S. Prono, and A. G. Cole, Phys. Rev. Lett. **57**, 13 (1986).

[31]R. B. Miller, *Physics of Particle Accelerators*, edited by Melvin Month and Margaret Dienes, AIP Conf. Proc. **184**, Rita G. Lerner, series editor, (AIP, New York, 1989), Vol. 2, p. 1730.

[32]R. F Lucey, Jr., R. M. Gilgenbach, J. D. Miller, J. E. Tucker, and R. A. Bosch, Phys. Fluids B **1**, 430 (1989).

[33]"Electrostatic Channel Guiding: A Technological Breakthrough", *Energy and Technology Review* (March, 1985), (Lawrence Livermore National Laboratory, Livermore, 1985).

[34]T. W Meyer, R. L. Gullickson, B.J. Pierce, and D.R.Ponikvar, Nucl. Instrum. Methods **A285**, 369 (1989).

[35]The FEL interaction requires emittance less than a signal wavelength, $\varepsilon<\lambda$. C. Pellegrini, Nucl. Instrum. Methods **177**, 227 (1980).

[36]J. L. Bromberg, *Fusion*, (MIT, Cambridge, 1982).

[37]The large number of regimes may be seen from the existence of multiple time scales (beam current rise time, pulse length, electron plasma period, ion-plasma period, electron collision time), multiple length scales (beam radius, propagation length) and the dependence of the focussing on the beam energy, beam current, and the ratio of beam density to plasma density. (This assumes an unmagnetized, preionized, plasma, otherwise one should include the magnetic field and the ionization time scale.)

[38]P. Chen, Part. Acc. **20**, 171 (1987).

[39]J. J. Su, T. Katsouleas, J. M. Dawson, and R. Fedele, Phys. Rev. A **41**, 3321 (1990).

[40]P. Chen, K. Oide, A. M. Sessler, S. S. Yu, Phys. Rev. Lett. **64**, 1231 (1990).

[41]D. H. Whittum, *Proceedings of the Topical Conference on Research Trends in Nonlinear and Relativistic Effects in Plasmas*, (LaJolla Institute, 1990)

[42]P. Chen, J. M. Dawson, R. W. Huff, and T. Katsouleas, Phys. Rev. Lett. **54**, 693 (1985).

[43]J. B. Rosenzweig, D. B Cline, B. Cole, H. Figueroa, W. Gai, R. Konecny, J. Norem, P. Schoessow, and J. Simpson, Phys. Rev. Lett. **61**, 98 (1988)

[44]J. M Dawson, "Plasma Particle Accelerators," Sci. Am. **260**, 54 (1989).

[45]C. Joshi and T. Katsouleas, eds., *Laser Acceleration of Particles*, AIP Conf. Proc. No. **130** (AIP, New York, 1985).

[46]R. J. Briggs, Phys. Rev. Lett. **54**, 2588 (1985). This device falls into the category of wakefield accelerators.

[47]W. A. Barletta, in *Proceedings of the Workshop on New Developments in Particle Acceleration Techniques*, (CERN Service d'Information, Orsay, 1987), pp. 544-548.

[48]E. P. Lee, "Radiation Damping of Betatron Oscillations," Lawrence Livermore National Laboratory Report, UCID No. 19381, (unpublished, 1982)

[49]R. B. Palmer, *New Developments in Particle Acceleration Techniques*, edited by S. Turner, CERN Report No. 87-11, ECFA 87/110, Vol.1 (CERN, Geneva, 1987) pp. 80-120.

[50]K. Oide, Phys. Rev. Lett. **61**, 1713 (1988).

[51]D. H. Whittum, A. M. Sessler, S. S. Yu, and J. J. Stewart, Particle Accelerators **34**, 89 (1990).

[52]R. Hollebeek, Nucl. Instrum. Methods **184**, 333 (1981).

[53]P. Chen, *Physics of Particle Accelerators*, edited by Melvin Month and Margaret Dienes, AIP Conf. Proc. **184**, , Vol. 1, (AIP, New York, 1989) pp. 633-679.

[54]G. Bonvicini, E. Gero, R. Frey, W. Koska, C. Field, N. Phinney, A. Minten, Phys. Rev. Lett. **62**, 2381 (1989).

[55]Thomas C. Marshall, *Free-Electron Lasers*, (MacMillan, New York, 1985).

[56]C. W. Roberson and P. Sprangle, Phys. Fluids B **1**, 3, (1989).

[57]V. L. Bratman, G. G. Denisov, N. S. Ginzburg, and M. I. Petelin, IEEE J. Quantum Electron. **QE-19**, 282 (1983).

[58]A. Gover and P. Sprangle, IEEE J. Quantum Electron. **QE-17**, 1196 (1981).

[59]G. Bekefi and K. D. Jacobs, J. Appl. Phys. **53**, 4113 (1982).

[60]W. A. McMullin and G. Bekefi, Appl. Phys. Lett. **39**, 845 (1981).

[61]Y. Z. Yin and G. Bekefi, Phys. Fluids **28**, 1186 (1985).

[62]A. M. Sessler, "New Particle Acceleration Techniques", Phys. Today **41**, No. 1, 26 (January, 1988).

[63]A. M. Sessler, E. Sternbach, J. S. Wurtele, Nucl. Instrum. Methods **B40/41**, 1064 (1989).

[64]R. A. Jong and E. T. Scharlemann, *Proceedings of the Eighth International Free Electron Laser Conference*, edited by Kai Siegbahn and Erik Karlsson, Nucl. Instrum. Methods **A259**, 254 (1987).

[65]M. Shiho, *et al.*, "Recent results and future plans for the JFT-2M tokomak ECRH experiment", to be published in *Proceedings of the International Atomic Energy Association Technical Committee Meeting*, (Heifei, 1989).

[66]"Ground-Based Laser Defense Systems", *Energy and Technology Review* (September, 1989), Lawrence Livermore National Laboratory, (Livermore, CA).

[67]A. M. Sessler, "Prospects for the FEL", Lawrence Berkeley Laboratory Report No. 27034.

[68]Charles A. Brau, *Physics of Particle Accelerators*, edited by Melvin Month and Margaret Dienes, AIP Conf. Proc. **184**, Rita G. Lerner, series editor, (AIP, New York, 1989), Vol. 2, pp. 1615-1706. This excellent review article discusses both medical and industrial applications, to include molecular surgery, tumor vaporization, kidney-stone fragmentation, arterial welding, retina reattachment, cornea therapy, microfabrication of semi-conductor circuits and photoproduction of specialty chemicals and isotopes.

[69]*Free-Electron Lasers and Applications*, edited by Donald Prosnitz, SPIE (The International Society for Optical Engineering) Proc. No. **1227** (1990).

[70]H. Motz, J. Appl. Phys. **22**, 527 (1951).

[71]R. M. Phillips, IRE Trans. Elec. Dev. **7**, 231 (1960) and, by the same author, Nucl. Instrum. Methods **A272**, 1 (1988). "Ubitron" is an acronym for "undulating beam interaction."

[72]J. M. J. Madey, J. Appl. Phys. **42**, 1906 (1971).

[73]Also called the electron-cyclotron maser. R. Q. Twiss, Australian J. Phys. **11**, 564 (1958); J. Schneider, Phys. Rev. Lett. **2**, 504 (1959); A. V. Gaponov, Izv. Vyssh. Uchebn Zaved., Radiofizi. **2**, 450, 836 (1959).

[74]B. Levush, T. M. Antonsen, W. M. Manheimer, and P. Sprangle, Phys. Fluids **28**, 2273 (1985).

[75]T. P.Hughes and B. B. Godfrey Phys. Fluids **29**, 1698 (1986).

[76]K. G. Kato, G. Benford, D. Tzach, Phys. Rev. Lett. **50**, 1587 (1983).

[77]M. S. Di Capua, J. F. Camacho, E. S. Fulkerson, and D. Meeker, IEEE Trans. Plasma Sci. **16**, 217 (1988).

[78]R. E. Collin, *Foundations for Microwave Engineering*, (McGraw-Hill, New York, 1966).

[79]A. B. Bronwell and R. E. Beam, *Theory and Application of Microwaves* (McGraw-Hill, New York, 1947).

[80]L. D. Landau, J. Phys. USSR **10**, 25 (1946).

Chapter 2: Short Pulse Propagation

"One never ought to listen to the flowers. One should simply look at them and breathe their fragrance."
—Antoine de Saint Exupery

In this chapter, the basic features of REB propagation in the ion-focussed regime (IFR) are reviewed. In Sec. A, we discuss charge and current neutralization, and provide a working definition of the IFR. In Sec. B we consider in a more formal manner, equilibrium propagation in the IFR, and we apply our results to analyze the continuous plasma focus, recently proposed by Chen, *et al.*[1] In Sec. C we consider the dominant IFR instabilities: "ion-hose" and "electron-hose". In Sec. D, we enumerate certain important, but less dominant features, including scattering, beam-ionization, radiation and streaming instabilities.

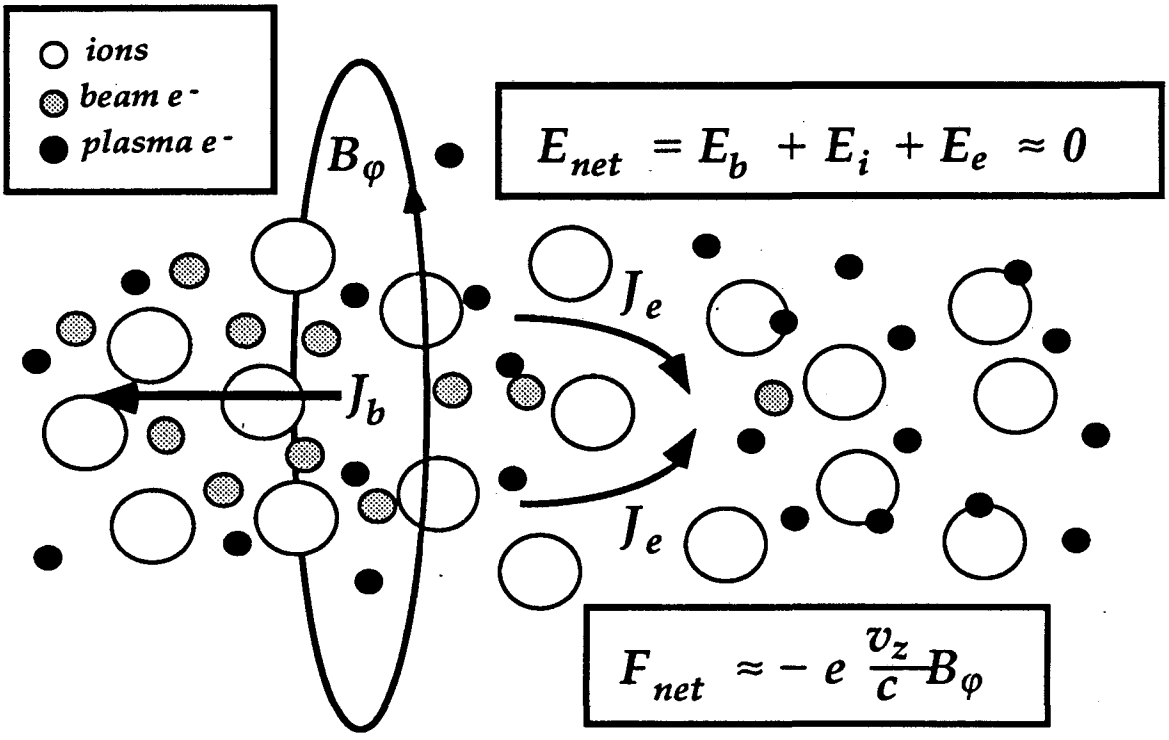

FIG. 2.1. A relativistic electron beam propagates through a preionized plasma, more dense than the beam core. A small fraction of plasma electrons are expelled (as indicated by the plasma electron current density J_e) to produce overall quasineutrality, so that the net electric field E_{net} (which is the sum of the fields due to the beam, ions, and plasma electrons, E_b, E_i, and E_e, respectively) vanishes. The net force on the beam, F_{net}, is then due to the beam magnetic field B_φ, i.e., the beam is magnetically self-pinched.

A. THE ION-FOCUSSED REGIME

Before embarking on detailed analytic work and to place this work in the appropriate context, it is helpful to review the simplest features of REB propagation: charge and current neutralization. In the course of this review, we will provide a working definition of the "IFR". We restrict ourselves

throughout to the case of a preionized, unmagnetized plasma, and neglect plasma electron collisions, recombination and attachment.

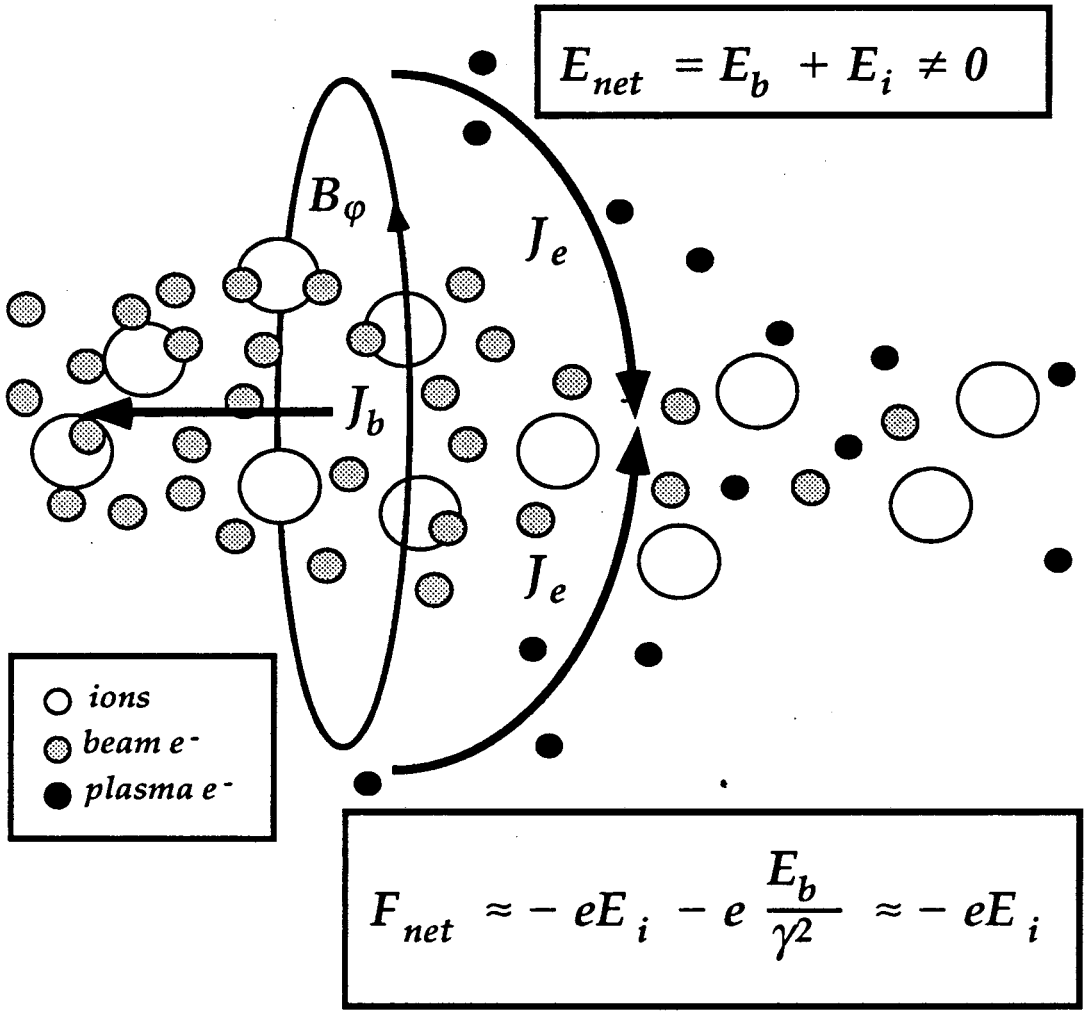

FIG. 2.2. A relativistic electron beam propagates through a preionized plasma, less dense than the beam core. All plasma electrons are expelled, producing a non-neutral column of ions, or "ion-channel." For a sufficiently dense plasma, such that $n_p >> n_b/\gamma^2$, the beam is then electrostatically focussed by the ion-charge. This is to be compared to Fig. 2.1.

Let us place ourselves at a fixed position in the plasma and watch the beam "arrive" (Fig. 2.1). We observe a rising current, a rising azimuthal magnetic field, a radial electric field and an induced axial electric field. The total electric field must, by Lenz's law drive a plasma current, J_e such as to oppose the rising beam current, as indicated in Fig. 2.1. Now, characteristically, plasma electrons will respond to imposed fields on the time scale of a plasma period, ω_p^{-1}, where $\omega_p^2=4\pi n_p e^2/m$, the electron charge is $-e$ and its mass is m. Thus if the current rises adiabatically on the ω_p^{-1} time scale, plasma electrons will flow out of the beam volume with only small radial plasma oscillations. The local plasma is then in a quasi steady-state. (We will take the ions to be fixed for the moment).

For early times, as the beam "head" is flowing past, there are many more plasma electrons than beam electrons, and the beam is charge neutralized and magnetically self-focussed, as indicated in Fig. 2.1. As the beam current continues to rise, the beam density on axis increases above the local ion charge density, and a channel is formed from which all plasma electrons have been quasi-statically evacuated.

Eventually, as the current rises still further, this "ion-channel" extends beyond the beam volume, as depicted in Fig. 2.2. In this limit, the transverse Lorentz force seen by a beam electron in the channel is

$$\vec{F}(r) = -e\left(\frac{1}{\gamma^2}+\beta_\perp^2\right)\vec{E}_b - e\,\vec{E}_i \,, \qquad (2.1)$$

where E_b is the radial electric field due to the beam and E_i is the field due to the ion charge, $E_i \sim 2\pi e n_p r$, with r the radial coordinate. The quantity $\beta_\perp = v_\perp/c$, with $v_\perp << c$ the transverse velocity. The speed of light is c and γ is the beam energy divided by the electron rest energy, mc^2.

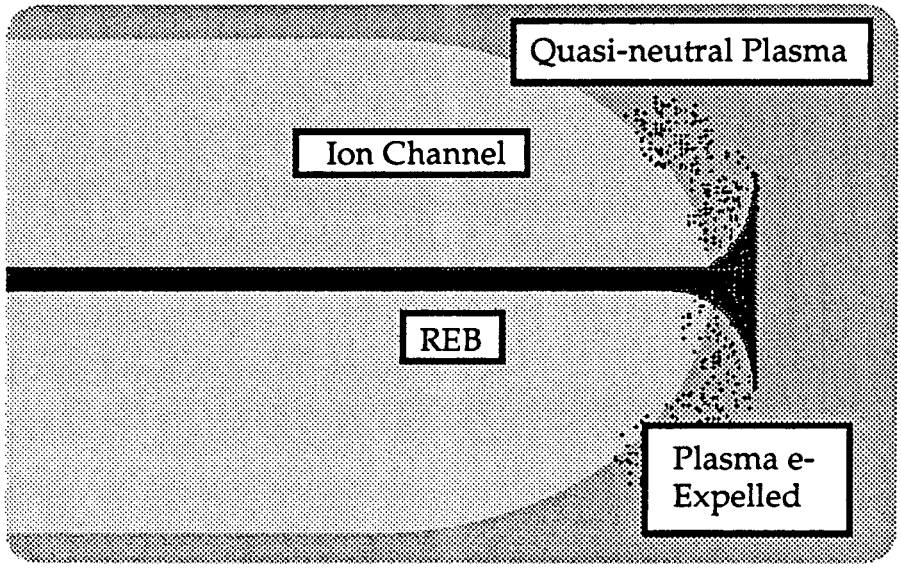

FIG. 2.3. The radial electric field of the beam expels plasma electrons from a large cylindrical volume, or "ion-channel". The beam head is weakly magnetically self-focussed, while the main-body of the beam is electrostatically focussed by the relatively immobile ions.

Now the primary motivation for sending a beam into a plasma is focussing and for focussing to be effective, the restoring force due to the ion charge should be much larger than the transverse Lorentz force on the beam due its self-fields. This imposes the Budker condition[2] on the plasma density,

$$n_b > n_p >> n_b \left(\frac{1}{\gamma^2} + \beta_\perp^2\right) \tag{2.2}$$

We shall refer to the regime constrained by these assumptions as the ion-focussed regime (IFR). In fact, as we have seen, no beam is ever entirely ion-focussed, since the beam head is always weakly magnetically self-focussed (Fig. 2.3).[3] For propagation over long distances, this distinction is important, since poor focussing at the beam head may result in significant "erosion". For the relatively short propagation lengths of interest here, this will turn out to be a minor effect, and we relegate further discussion of it to Sec. D.

With a definition of the "IFR" in hand, we proceed to a more quantitative treament of IFR equilibria.

B. EQUILIBRIUM PROPAGATION

In this section, we examine the features of equilibrium propagation in the IFR. In Sec. 1, we consider the steady-state plasma-electron flow subject to an adiabatically varying, specified beam current, using a cold-fluid model. In Sec. 2, we consider the ion-motion using a linearized cold-fluid model. In Sec. 3, we consider REB propagation through a background of rigid ions, subject to the fields determined in Secs. 1 and 2. We reserve to Sec. C discussion of dipole perturbations to the beam centroid.

1. Steady-state plasma electron flow

First, we consider the plasma flow subject to specified beam charge and current densities, with ions fixed. It will be convenient to change variables from z, t to z, s where $s=t-z/v_b$ is the displacement along the beam and varies from 0 at the beam head to τ (the pulse length) at the beam tail. The beam velocity is $v_b \sim c$. We will take the beam density to be specified in the form

$$\rho_{b0}(r,s) = -en_b(s)H(a-r), \tag{2.3}$$

where $-e$ is the electron charge, a is the beam radius, and H is the step function. The beam density on axis n_b varies with s, on the time-scale τ_r, the current rise time. As noted above, we assume throughout that current variation is adiabatic,

$$\boxed{\omega_p \tau_r >> 1}, \tag{2.4}$$

so that plasma oscillations are small in amplitude.

a. MHD Equations. With these assumptions, we calculate the equilibrium fields and plasma electron flow, using a cold fluid model.

Maxwell's equations in the Lorentz gauge are

$$\left\{\nabla_\perp^2 + \frac{\partial^2}{\partial z^2} - \frac{1}{c^2}\frac{\partial^2}{\partial t^2}\right\}\vec{A} = -\frac{4\pi}{c}\left(\vec{J}_b + \vec{J}_e\right) ,$$
$$\left\{\nabla_\perp^2 + \frac{\partial^2}{\partial z^2} - \frac{1}{c^2}\frac{\partial^2}{\partial t^2}\right\}\varphi = -4\pi\left(\rho_b + \rho_i + \rho_e\right) , \qquad (2.5)$$

where φ is the scalar potential and A is the vector potential. The transverse gradient is $\nabla_\perp$, and t is time. The beam, electron and ion charge densities are ρ_b, ρ_e, and ρ_i and the beam and plasma electron current densities are

$$\vec{J}_b \approx \rho_b c \beta_b \hat{z} ,$$
$$\vec{J}_e = \rho_e c \left(\beta_z \hat{z} + \beta_r \hat{r}\right) , \qquad (2.6)$$

where the plasma electron axial velocity is $v_z=\beta_z c$, and the radial velocity is $v_r=\beta_r c$.

In the adiabatic limit, we may simplify Eq. (2.5) with the "frozen-field" approximation, replacing the D'Alembertian operators with $\nabla_\perp^2$. This approximation neglects radiative effects and takes advantage of the slow variation of the beam fields in z, at fixed s. We will see that this amounts to the approximation $b/c\tau_r\gamma \ll 1$, which is typically well satisfied.

It is convenient to define dimensionless variables,

$$a_z = \frac{e A_z}{m c^2} ,$$
$$a_r = \frac{e A_r}{m c^2} ,$$
$$\phi = \frac{e\varphi}{m c^2} ,$$

$$\Delta = -\frac{\rho_e}{\rho_i},$$
$$\Sigma = -\frac{\rho_b}{\rho_i},$$

in terms of which Eq. (2.5) takes the form

$$\left(\frac{1}{r}\frac{\partial}{\partial r} r \frac{\partial}{\partial r}\right) a_z \approx k_p^2 (\Sigma \beta_b + \beta_z \Delta),$$
$$\left(\frac{1}{r}\frac{\partial}{\partial r} r \frac{\partial}{\partial r} - \frac{1}{r^2}\right) a_r \approx k_p^2 \beta_r \Delta,$$
$$\left(\frac{1}{r}\frac{\partial}{\partial r} r \frac{\partial}{\partial r}\right) \phi \approx k_p^2 (\Delta + \Sigma - 1). \tag{2.7}$$

Here, $k_p=\omega_p/c$. For reference, we note the expressions for the physical fields,

$$E_r \approx -\frac{mc^2}{e}\left(\frac{\partial \phi}{\partial r} + \frac{1}{c}\frac{\partial a_r}{\partial s}\right),$$
$$E_z \approx -\frac{mc}{e}\frac{\partial}{\partial s}\left(a_z - \frac{1}{\beta_b}\phi\right),$$
$$B_\theta \approx -\frac{mc^2}{e}\left(\frac{\partial a_z}{\partial r} + \frac{1}{c\beta_b}\frac{\partial a_r}{\partial s}\right), \tag{2.8}$$

where the azimuthal angle is θ, and $E_\theta=B_r=B_z=0$. The quantity $\beta_b=v_b/c$, where v_b is the beam axial velocity. We will take $\beta_b \sim 1$ below.

Next we set down the cold-fluid equations for the plasma electrons. In the beam frame, our system is translationally invariant, so derivatives in z at fixed s are zero. The continuity equation is

$$\frac{\partial}{\partial s}\left\{(1-\frac{\beta_z}{\beta_b})\,\Delta\right\}+c\,\frac{1}{r}\frac{\partial}{\partial r}r\{\beta_r\Delta\}\approx 0\,, \tag{2.9}$$

and this may also be rewritten

$$D\Delta+\Delta\left(\frac{\partial}{\partial s}\left\{(1-\frac{\beta_z}{\beta_b})\right\}+c\,\frac{1}{r}\frac{\partial}{\partial r}r\beta_r\right)\approx 0\,, \tag{2.10}$$

where D is the convective derivative along the flow,

$$D\approx(1-\beta_z)\frac{\partial}{\partial s}+\beta_r c\,\frac{\partial}{\partial r}\,. \tag{2.11}$$

The Lorentz force equation is

$$\begin{aligned} D(\gamma\beta_z) &\approx \frac{\partial}{\partial s}\left(a_z-\frac{1}{\beta_b}\phi\right)+\beta_r\left(c\,\frac{\partial a_z}{\partial r}+\frac{1}{\beta_b}\frac{\partial a_r}{\partial s}\right),\\ D(\gamma\beta_r) &\approx (1-\frac{\beta_z}{\beta_b})\frac{\partial a_r}{\partial s}+c\,\frac{\partial\phi}{\partial r}-c\beta_z\frac{\partial a_z}{\partial r}\,, \end{aligned} \tag{2.12}$$

where γ is now the Lorentz factor for the plasma electrons.

Now in principle, to describe the equilibrium, we may set $\beta_r=a_r=0$ and neglect all s-derivatives in Eqs. (2.7) and (2.12). In this case, the fluid equations, Eq. (2.12), reduce to a condition for radial force balance,

$$\boxed{\frac{\partial \phi}{\partial r} - \beta_z \frac{\partial a_z}{\partial r} \approx 0}, \tag{2.13}$$

valid where $\Delta \neq 0$. Equation (2.7) is unchanged except that we may set $a_r=0$.

Unfortunately, this steady-state approximation has left us with only three equations for the four unknowns ϕ, a_z, β_z, and Δ. In general, to close this system of equations, we must obtain an integral of the full s-dependent equations. Since these are non-linear partial differential equations, this would appear to be a formidable task. However, in the limit,

$$\beta_z >> \beta_r, \tag{2.14}$$

an integration is straightforward. We proceed to show that Eq. (2.14) is always valid for a sufficiently slowly rising current.

Now, from Lenz's law, we expect plasma electrons to stream backward in z, neutralizing the beam magnetic field at large radii, as is the case for overdense plasmas.[4] This implies that the electron density must vanish for $r<b$, for some channel radius b. Otherwise the electron density extends to $r=0$, where the net Lorentz force on a backward-drifting electron is outward, i.e., non-zero, contradicting Eq. (2.13). In this connection it is convenient to define a channel parameter,

$$\boxed{V = k_p b}, \tag{2.15}$$

which characterizes the magnetic shielding provided by the plasma drift in z. Small skin-depth corresponds to $V>>1$, and, as we shall see, a large axial drift, while large skin-depth corresponds to $V<<1$. [5]

Next, we estimate β_z. Qualitatively, we expect good magnetic shielding over a radial length c/ω_p, so long as the time for magnetic diffusion due to collisions is long compared to the electron beam pulse length. This magnetic diffusion time is of order $\tau_D \sim (k_p b)^2/\nu$, where ν is the plasma electron collision rate, and $k_p \sim \omega_p/c$. Consistent with our neglect of collisions we will assume $\tau << \tau_D$. In this case, the total plasma current contained within a skin-depth of the channel wall should be of order the total beam current. This gives $\beta_z \sim O(V^2)$, for $V<<1$, and $\beta_z \sim O(V)$ for $V \sim 1$.[6]

We may estimate β_r by assuming that any increase in beam charge must be balanced by plasma electron charge flowing outward through the channel wall. This gives

$$\beta_r \approx \frac{b}{c\tau_r} \approx \frac{V}{\omega_p \tau_r}.$$

Actually this is a bit of an overestimate of β_r, since charge may flow out axially.

With these estimates we have for $V<<1$

$$\frac{\beta_r}{\beta_z} \approx \frac{1}{\omega_p \tau_r} O\left(\frac{1}{V}\right), \tag{2.16}$$

We will assume that $\omega_p \tau_r >> 1/V$, so that $\beta_r << \beta_z$. The result $\beta_r << \beta_z$ for slowly rising current is not surprising, since in the limit of constant current, $\beta_r = 0$, while, on the other hand, β_z depends on the integral of E_z and is non-zero so long as the current is non-zero. (Indeed were β_z to vanish for non-zero current, the magnetic field would extend to large r, despite the presence of an intervening collisionless plasma, an unphysical result.)

Having established Eq. (2.14), we proceed to integrate the fluid equations by two methods. First, we will close this system of equations by iteration, in the limit $V << 1$. Next, we will obtain an integral of the motion (valid for arbitrary V) from the full s-dependent equations. This second method does not provide an explicit solution, but reduces the problem to one second-order, nonlinear, ordinary differential equation, which is easily solved numerically.

b. Large skin-depth limit (V<<1). Knowing that the electron density must vanish for $r<b$, we may solve Eq. (2.7) immediately for the potentials in that region. Suppressing the s-dependence, we have

$$\phi = \begin{cases} \frac{1}{4}\left(k_b^2 - k_p^2\right) r^2 + \phi(0) & ; r < a \\ -\frac{1}{4} k_p^2 r^2 + \frac{1}{4} k_b^2 a^2 \left(1 + 2\, ln(r/a)\right) + \phi(0) & ; a < r < b \end{cases}, \tag{2.17}$$

where $k_b^2=4\pi n_b e^2/m$. The vector potentials are

$$a_z=\begin{cases} \frac{1}{4}k_b^2 r^2 + a_z(0) & ; r < a \\ \frac{1}{4}k_b^2 a^2 (1 + 2\ ln(r/a)) + a_z(0) & ; a < r < b \end{cases}, \tag{2.18}$$

and

$$a_r(r) = a_r(b)\frac{r}{b}. \tag{2.19}$$

Boundary values at $r=b$ are,

$$\begin{aligned} &a_z(b) = a_z(0) + \frac{1}{4}U^2 (1 + 2\ ln(b/a)), \\ &\frac{\partial a_z}{\partial r}(b) = \frac{U^2}{2b}, \\ &\phi(b) = \phi(0) + \frac{1}{4}(U^2 - V^2) + \frac{1}{2}U^2\ ln(b/a), \\ &\frac{\partial \phi}{\partial r}(b) = \frac{1}{2b}(U^2 - V^2), \\ &\frac{\partial a_r}{\partial r}(b) = \frac{a_r(b)}{b}. \end{aligned} \tag{2.20}$$

and we have defined a current parameter

$$U = 2(I/I_0)^{1/2} \tag{2.21}$$

with $I_0=mc^3/e$~17 kA.

We proceed to linearize Eqs. (2.7) and (2.12), about the $V\rightarrow 0$ solution. In the $V\rightarrow 0$ limit, we know that $\beta_z \sim O(V^2)$. Inspection of the vacuum vector potential shows that $a_z \sim O(V^2)$ also. Equation (2.7) then implies $\phi \sim O(V^4)$ and can be neglected at lowest order. Equation (2.13) gives $V^2=U^2+O(U^4)$, or

$$b \approx a\left(\frac{n_b}{n_p}\right)^{1/2}\left(1+O\left(V^2\right)\right) \tag{2.22}$$

In this case, $\Delta \sim 1$ at lowest order. Inspection of Eq. (2.12) shows that β_r is of order $O(V^4)$. This gives $\beta_z \sim a_z$ through $O(V^2)$. From Eq. (2.7) it is then straightforward to solve for a_z. In addition, the continuity equation, Eq. (2.10) gives $\Delta_1=\beta_{z1}$. The $O(V^2)$ potentials and other quantities are then, for $r>b$,

$$\begin{aligned} a_{z1}(r) &= \Delta_1 = \beta_{z1} = -\frac{V}{2}\frac{K_0(k_p r)}{K_1(V)}, \\ \beta_{r1} &= \phi_1(r) = a_{r1}(r) = 0, \end{aligned} \tag{2.23}$$

and $\Delta_0=1$. Here K_0 and K_1 are the modified Bessel functions and the subscript n denotes a quantity of order $O(V^{2n})$. The constants in Eq. (14) are given by

$$\begin{aligned} a_{z1}(0) &= -\frac{1}{2}V^2\left\{\frac{K_0(V)}{V\,K_1(V)}+\ln(b/a)\right\}, \\ \phi_1(0) &= -\frac{1}{2}V^2\ln(b/a). \end{aligned} \tag{2.24}$$

We may check the $\beta_z<<1$ approximation, from Eq. (2.23), which gives,

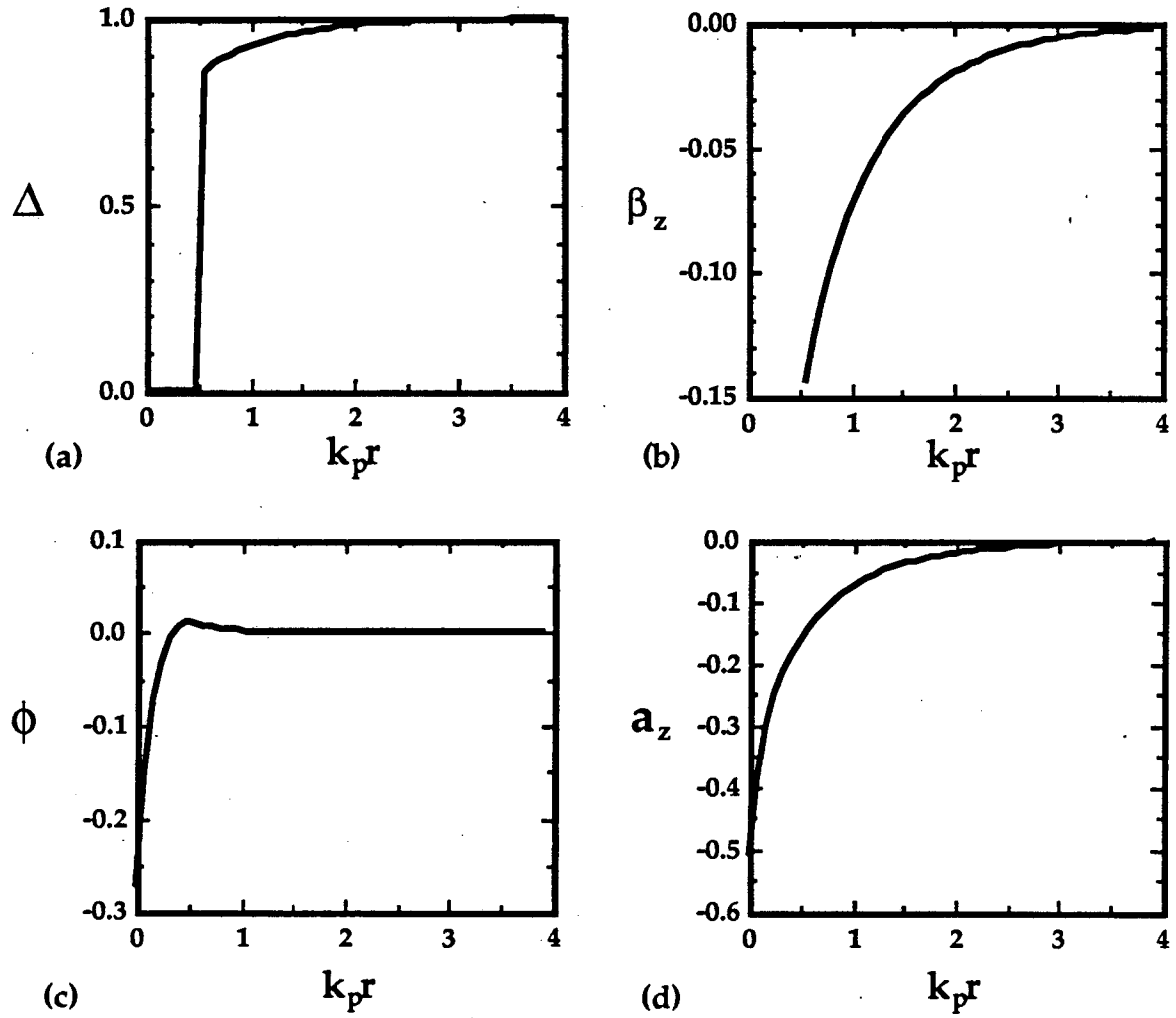

FIG. 2.4. The analytic solution in the large skin-depth approximation for U=0.5 (I~1 kA). (a)$\Delta=n_e/n_p$, the plasma electron density normalized to its initial value (b)$\beta_z=v_z/c$, the plasma electron axial drift velocity (c)the scalar potential and (d)the axial vector potential, normalized by e/mc^2. Due to the axial drift depicted in (b), electrons are "held off" the channel wall by the vxB force and this is reflected in the droop in the density in (a). This deficit of charge at the wall produces a small potential trough as depicted in (c), just adequate to balance the vxB force for the remaining electrons.

$$\beta_{z1}(b) \approx \frac{1}{2}V^2 \ln\left(\frac{V e^{\gamma_E}}{2}\right), \tag{2.25}$$

where we use the small argument expansions for the modified Bessel functions,[7]

$$K_0(z) \approx -\ln\left(\frac{z e^{\gamma_E}}{2}\right),$$
$$K_1(z) \approx \frac{1}{z},$$

and γ_E~0.5772 is Euler's constant. So, for example, β_{z1}~-10^{-2} for V~10^{-1}.

It remains to determine ϕ_2, the lowest order nonvanishing correction to ϕ. This is obtained from Eq. (2.13), radial force balance in equilibrium,

$$\phi_2(r) = \frac{1}{2}a_{z1}^2(r) = \frac{1}{8}\left(\frac{V}{K_1(V)}\right)^2 K_0(k_p r)^2$$

Note that the potential at r=0, is shifted slightly at $O(V^4)$, and is given by $\phi(0) \sim \phi_1(0)+\phi_2(b)$. The channel radius is then determined by the point where the radial Lorentz force vanishes,

$$V^2 \approx U^2 - \frac{1}{2}U^3\frac{K_0(U)}{K_1(U)} \approx U^2 - \frac{1}{2}U^4 \ln\left(\frac{U e^{\gamma_E}}{2}\right) + O(U^6) \tag{2.26}$$

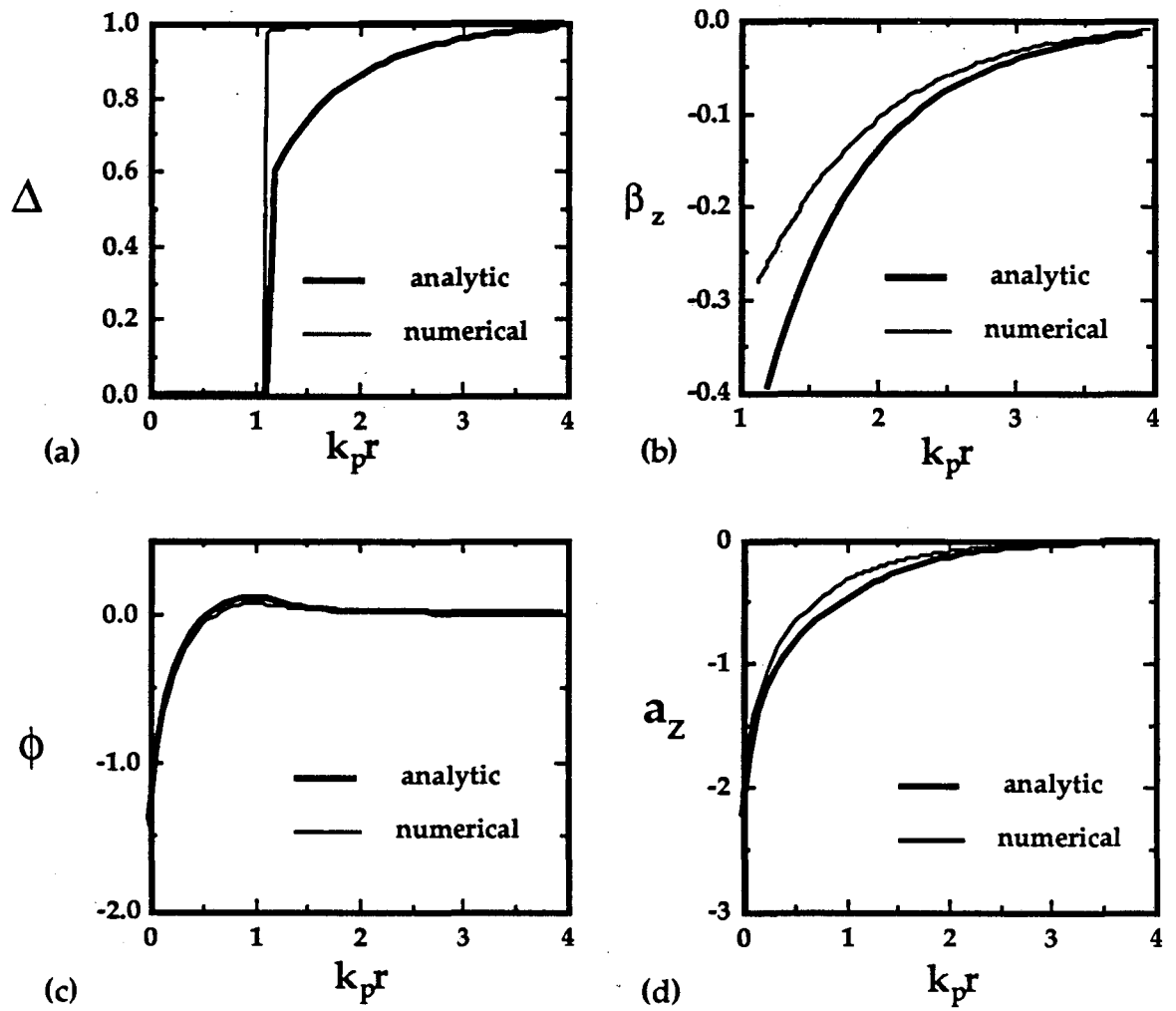

FIG. 2.5. Solution of Eq. (2.31) for ψ versus r, for U=1 (I~4 kA) compared to the analytic result of the V<<1 approximation.(a)$\Delta=n_e/n_p$, the plasma electron density normalized to its initial value (b)$\beta_z=v_z/c$, the plasma electron axial drift velocity (c)the scalar potential and (d)the axial vector potential, normalized by e/mc^2. Evidently at V~1, the small V approximation is fair for the potentials, while it errs noticeably for the plasma electron density .

More explicitly, in terms of the channel radius, this is

$$b \approx a\left(\frac{n_b}{n_p}\right)^{1/2}\left\{1 - \frac{1}{2}\left(\frac{I}{I_0}\right) ln\left(\frac{I}{I_0} e^{2\gamma_E}\right)\right\}.$$

So, for example, for I~1 kA, b is 5% larger than would be predicted by neglecting β_z.

Physically, Eqs. (2.25) and (2.26) show that the small axial drift (β_{z1}) of the plasma electrons results in a "vxB" force which tends to push electrons away from the channel wall. This results in an a depression in the plasma electron density (Δ_1) and an attractive electrostatic potential (ϕ_2). The associated radial electric field just balances the "vxB" force and maintains the equilibrium. For illustration, the analytic solutions for ϕ, a_z, β_z and Δ are depicted in Fig. 2.4 (a) for U=0.5 (I~1 kA).

c. General solution. In general, neglecting β_r reduces the Lorentz force law, Eq. (2.12) to the form

$$(1 - \beta_z)\frac{\partial}{\partial s}\gamma\beta_z = \frac{\partial}{\partial s}(a_z - \phi) \tag{2.27}$$

We integrate this from $s \rightarrow -\infty$, to obtain

$$\psi = a_z - \phi = 2\frac{tan(\zeta/2)}{1 + tan(\zeta/2)} \tag{2.28}$$

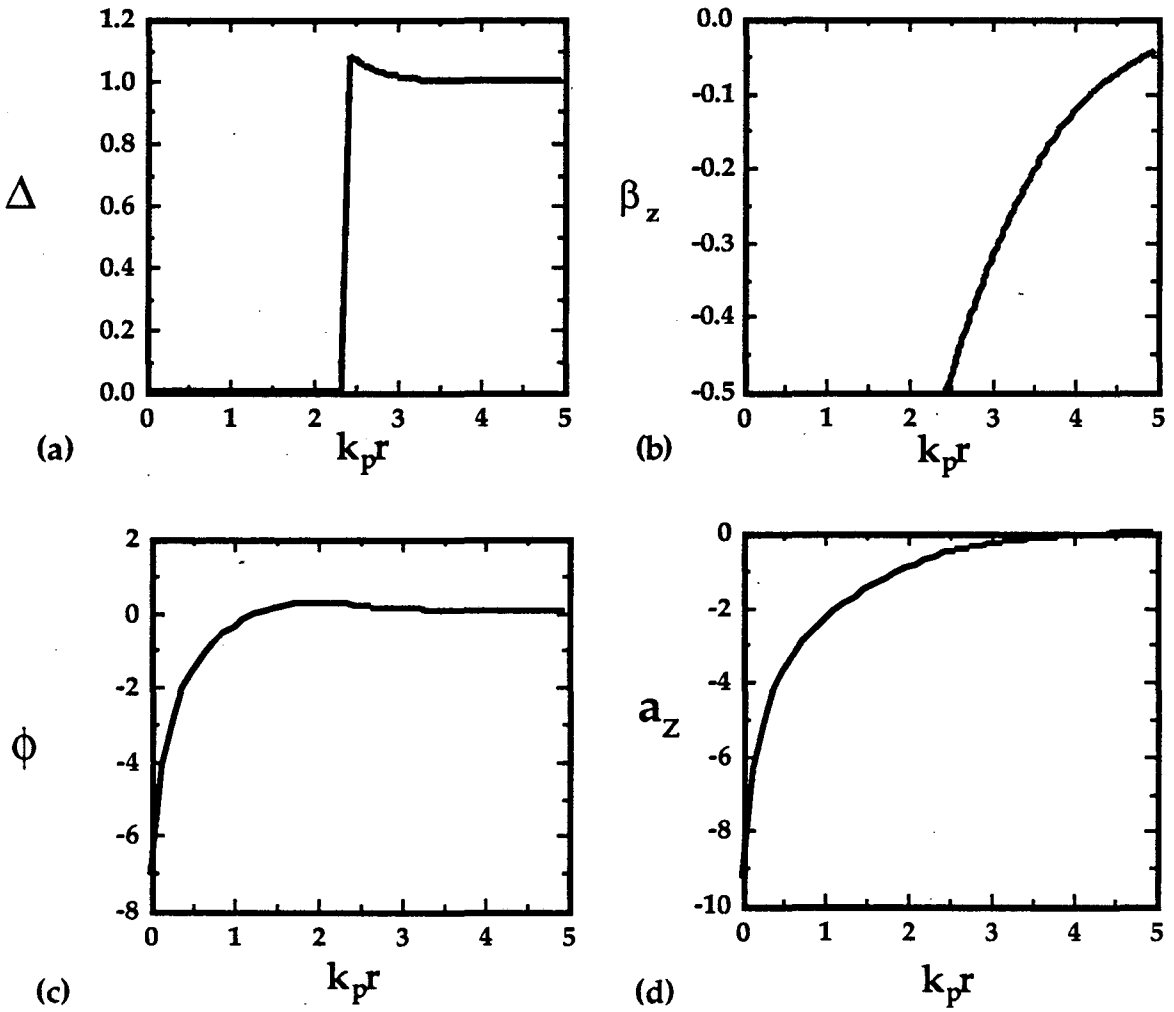

FIG. 2.6. Solution of Eq. (2.31) for ψ versus r, for U=2 (I~17 kA) compared to the analytic result of the $V<<1$ approximation.(a)$\Delta=n_e/n_p$, the plasma electron density normalized to its initial value (b)$\beta_z=v_z/c$, the plasma electron axial drift velocity (c)the scalar potential and (d)the axial vector potential, normalized by e/mc^2. Note that V~2.4 so that the channel radius $b\sim 1.2a(n_b/n_p)^{1/2}$ is 20% larger than would be given by charge neutrality at the wall. Thus (c) a large, attractive potential well forms corresponding to the deficit of charge in the annulus $2<k_p r<2.4$, as seen in (a). This sheath is mildly relativistic, as seen in (b), with energies of order 80 keV.

where $\beta_z=sin(\zeta)$, and we have taken a_z, ϕ and β_z to vanish at $s\rightarrow-\infty$. In terms of ψ,

$$\gamma = 1 + \frac{\psi^2}{2(1-\psi)},$$
$$\beta_z = \frac{\psi(2-\psi)}{2-2\psi+\psi^2}, \tag{2.29}$$

so that the flow is explicitly prescribed by the potentials. In this case, the equilibrium equations can be resolved into a single equation for ψ,

$$\frac{\partial^2\psi}{\partial\rho^2} = \left(\frac{1+\beta_z}{1-\beta_z}\right)^{1/2}\left(\frac{\partial\psi}{\partial\rho}\right)^2 + e^{2\rho}\frac{\beta_z}{1+\beta_z}, \tag{2.30}$$

where $\rho=ln(k_p r)$. All other quantities may be determined from ψ,

$$\frac{\partial a_z}{\partial\rho} = \frac{1}{1-\beta_z}\frac{\partial\psi}{\partial\rho},$$
$$\Delta = \frac{1}{1-\beta_z}\left\{1 - e^{-2\rho}\frac{\partial^2\psi}{\partial\rho^2}\right\},$$
$$\beta_z = \frac{\psi(2-\psi)}{2-2\psi+\psi^2}, \tag{2.31}$$

(This assumes that $\Sigma=0$ at and beyond the channel wall). Equation (2.30) is to be solved numerically on the interval $(\rho_0,+\infty)$, where $\rho_0=ln(V)$. The initial conditions are derived from Eq. (2.17),

$$\frac{\partial \psi}{\partial \rho}(\rho_0) = \frac{1}{2}U^2 ,$$

$$\psi(\rho_0) = 2\,\frac{1 - \sqrt{1 - \beta_z(\rho_0)^2}}{1 + \beta_z(\rho_0) - \sqrt{1 - \beta_z(\rho_0)^2}} ,$$

$$\beta_z(\rho_0) = 1 - \frac{V^2}{U^2} , \qquad (2.32)$$

and an iteration over V is required to obtain a finite solution at large ρ. Such a numerical iteration is straightforward, given the bounds, $U<V<2^{1/2}U$ (obtained from Eq. (2.32) using $-1<\beta_z(\rho_0)<1$).

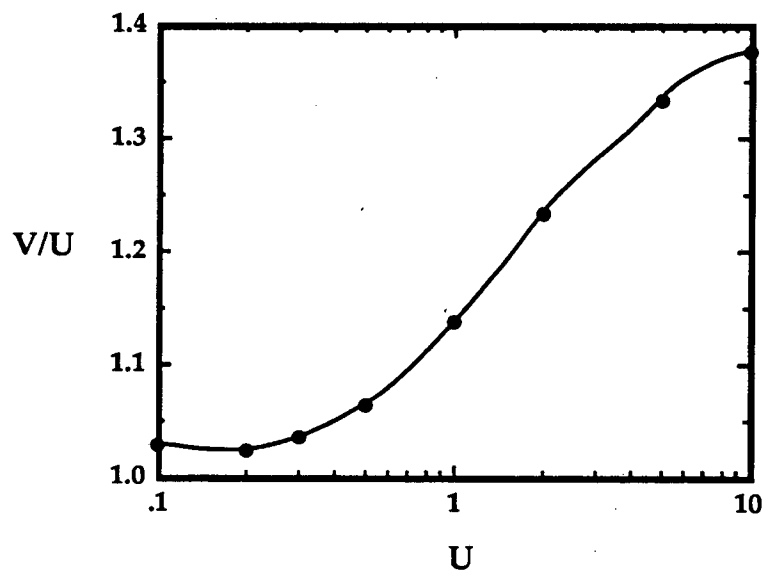

FIG. 2.7. The results of several numerical solutions of Eq. (2.30) have been collated to give V/U as a function of $U=2(I/I_0)^{1/2}$. This result is useful in that it gives the variation of channel radius with current as indicated in Eq. (2.33).

Regarding the character of the solution, we note that $\beta_z(\rho_0)<0$ implies $\psi(\rho_0)<0$. Physically, we expect β_z and therefore ψ to be monotone increasing to 0 at $\rho\to\infty$. On the other hand, from Eq. (2.32), we see that $\psi^{(1)}(\rho_0)>0$, and from Eq. (2.31) we see that $\psi^{(2)}(\rho_0)>0$. Since ψ must asymptote to 0 at $z\to\infty$, there will be an inflection point where $\psi^{(2)}(\rho_0)=0$. Thus we expect the solution to appear much as that of Eq. (2.23), rather similar to a modified Bessel function.

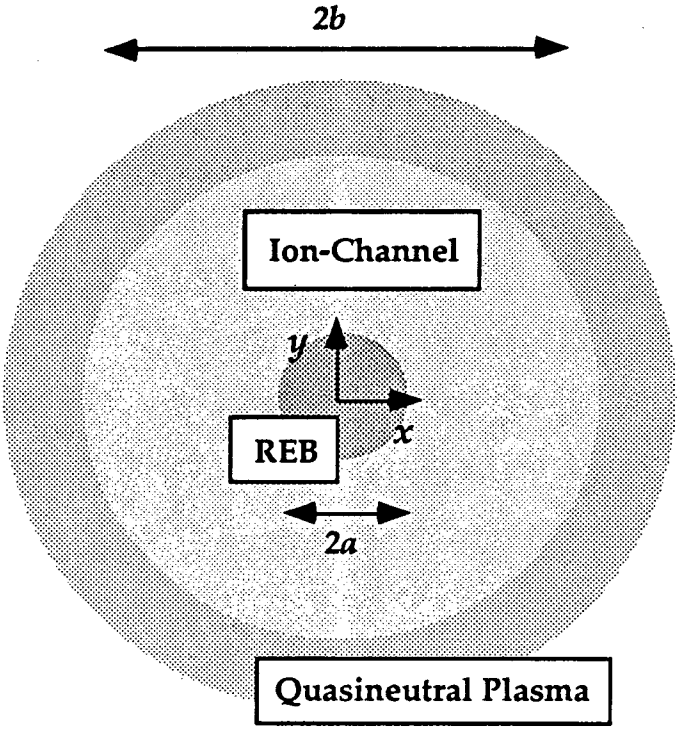

FIG. 2.8. An REB of radius a propagating through an underdense plasma, expels plasma electrons from the beam volume and beyond to produce an "ion-channel" of radius $b\sim a(n_b/n_p)^{1/2}$.

We have solved Eq. (2.31) numerically and results are displayed in Fig. 2.5 for U=1, with the results of the small-V approximation overlayed. In Fig. 2.6 results are displayed for for U=2. In Fig. 2.7, the results of several numerical solutions have been collated to give V/U as a function of U. We see that $V \sim U$ for U small, and $V \sim 2^{1/2}U$ for U large, as expected. This plot is instructive insofar as it provides the channel radius as a function of beam current, i.e.,

$$b = a\left(\frac{n_b}{n_p}\right)^{1/2}\left(\frac{V}{U}\right). \tag{2.33}$$

So, for example, for I~4 kA, U~1, and we see from Fig. 2.7 that V/U~1.15. Thus b is about 15% larger than predicted by the V<<1 result. For large currents we have

$$\lim_{I>>I_0} b = a\left(\frac{2\,n_b}{n_p}\right)^{1/2}.$$

From the work of this section, we have a simple picture of the plasma electron configuration in the IFR, in steady-state (Fig. 2.8). We know that for V<<1 (I<<4 kA) return current is fairly negligible, and the electrons reside at $r>b$, drifting very slowly backward in z. For V>1, return current effects become appreciable.

Before leaving this subject it is instructive to consider the single-particle plasma electron motion, as this yields some insight into the integral given by Eq. (2.28). The single-particle Hamiltonian is

$$H = \sqrt{m^2c^4 + (p_z + mca_z)^2c^2 + p_x^2c^2 + p_y^2c^2} - mc^2\phi ,$$

where the quantities p_x, p_y, and p_z are the canonical momenta in x, y, and z, respectively,

$$p_x = m\gamma v_x ,$$
$$p_y = m\gamma v_y ,$$
$$p_z = m\gamma v_z - mca_z ,$$
$$\gamma = \left\{1 - \frac{v_x^2 + v_y^2 + v_z^2}{c^2}\right\}^{-1/2} .$$

The particle velocity components are v_x, v_y, and v_z. Note that H may be written,

$$H = mc^2(\gamma - \phi) .$$

The variations in H and p_z are given by

$$\frac{dH}{dt} = (p_z + mca_z)\frac{c}{\gamma}\frac{\partial a_z}{\partial t} - mc^2\frac{\partial \phi}{\partial t} ,$$
$$\frac{dp_z}{dt} = -(p_z + mca_z)\frac{c}{\gamma}\frac{\partial a_z}{\partial z} + mc^2\frac{\partial \phi}{\partial z} .$$

On the other hand, we have already observed that the fields vary adiabatically as a function of $s=t-z/v_b$, so that

$$\frac{\partial}{\partial t} \approx - v_b \frac{\partial}{\partial z} ,$$

and $v_b \sim c$. In this case, we observe that

$$\frac{d}{dt}(H - p_z c) \approx 0 . \tag{2.34}$$

Equation (2.34) expresses momentum conservation in the translationally invariant beam-plasma system. For an initially cold plasma, we integrate this to obtain, $H-p_z c \sim mc^2$, so that

$$1 \approx \gamma(1 - \beta_z) + a_z - \phi .$$

It is not hard to show, for $\beta_r << \beta_z$, that this is just the integral of Eq. (2.28).

2. Ion collapse

Next, we consider the response of the ions to specified plasma electron and beam electron charge densities. We will work to linear order, using a cold fluid-model. Since ions drift very slowly the problem is essentially

electrostatic and can be described in terms of the scalar potential and ion-density, which we decompose as

$$\varphi = \varphi_0 + \varphi_1 ,$$
$$\rho_i = \rho_{i0} + \rho_{i1} .$$

Maxwell's equations reduce to the Poisson equation,

$$\nabla_\perp^2 \varphi_0 = -\, 4\pi(\rho_b + \rho_{i0}) ,$$
$$\nabla_\perp^2 \varphi_1 = -\, 4\pi\rho_{i1} ,$$

and the perturbed ion-density is governed by the cold fluid equations,

$$\frac{\partial \rho_{i1}}{\partial s} + \vec{\nabla} \bullet \left(\rho_{i0}\vec{v}_{i1}\right) \approx 0 \quad ,$$
$$\frac{\partial \vec{v}_{i1}}{\partial s} \approx -\frac{e}{m}\vec{\nabla}\varphi_1 \quad . \tag{2.35}$$

Combining Eqs. (2.35) and (2.34) then gives an equation for the perturbed ion density in terms of the beam density,

$$\left(\frac{\partial^2}{\partial s^2} + \omega_{io}^2\right)\rho_{i1} = -\,\omega_{io}^2(\rho_b + \rho_{i0}) , \tag{2.36}$$

where ω_{i0} is the ion-plasma frequency at zeroth order, $\omega_{i0}^2 = 4\pi n_{i0} e^2/m_i$, with m_i the ion-mass.[8] We may integrate Eq. (2.36) immediately to obtain,

$$\rho_{i1}(s) = -\omega_{io}\int_{-\infty}^{s} ds' \sin\{\omega_{io}(s-s')\}(\rho_b(s') + \rho_{i0}) \tag{2.37}$$

Not surprisingly, we see that ρ_b should vary rapidly on the ω_i time-scale to avoid collapse of the ion-channel and neutralization of the beam. Thus we expect $\omega_i\tau<<1$ will be required in order to self-consistently neglect ion-motion. To obtain a more quantitative estimate of the ion-density variation, we model the beam density with a square profile in s,

$$\rho_b(s) = -en_bH(a-r)H(s)H(\tau-s). \tag{2.38}$$

The integral of Eq. (2.37) then gives,

$$\rho_{i1}(s) = \{-en_{io} + en_bH(a-r)\}[1-\cos(\omega_{i0}s)]. \tag{2.39}$$

In terms of ion-density this is

$$\begin{aligned} n_i &\approx n_{io} + n_{i1} \\ &= n_{io}\cos(\omega_{i0}s) + n_bH(a-r)[1-\cos(\omega_{i0}s)]. \end{aligned} \tag{2.40}$$

(Note that this result is not valid in the limit $n_b\rightarrow 0$, since we have assumed an initially unneutralized ion-channel.) With this result we have an estimate for the variation in ion-density over the length of the beam,

$$\frac{n_{i1}(r,\tau)}{n_{io}} \approx \frac{1}{2}\left(\frac{n_b}{n_{io}}H(a-r)-1\right)(\omega_{i0}\tau)^2 , \tag{2.41}$$

and we assume $\omega_{i0}\tau<<1$ as noted above. Within the beam volume, this is

$$\frac{n_{i1}(a,\tau)}{n_{io}} \approx \frac{1}{2}\left(\frac{n_b - n_{io}}{n_{io}}\right)(\omega_{i0}\tau)^2 . \tag{2.42}$$

Thus for $n_b>>n_{i0}$, the time-scale for ion-motion within the beam volume is

$$\tau_{i1} \approx \sqrt{\frac{m_i}{m}}\,\omega_b^{-1} , \tag{2.43}$$

where $\omega_b^2=4\pi n_b e^2/m$. The condition for negligible ion-motion, $n_{i1}<<n_{i0}$ is then a constraint on the pulse length, $\tau<<\tau_{i1}$. Typically, we will consider the case where n_b is within a factor of a few of n_i, so that this costraint reduces simply to $\omega_i\tau<<1$.

There is in addition, a second ion time-scale, the time-scale for ion-neutralization of the beam. A simple estimate of the neutralization time may be made by following the motion of a single ion from initial position $r=b$, through to $r=0$ in specified beam and ion fields. This calculation provides a lower bound on the ion-neutralization time-scale,

$$\tau_{i2} \approx \frac{1}{4}\frac{b}{c}\left(\frac{m_i}{m}\right)^{1/2}\left(\frac{I_0}{I}\right)^{1/2} \approx \frac{1}{2\omega_i} . \tag{2.44}$$

From the work of this section, we see that to neglect ion-motion we must have a fairly short pulse (hence the title for this chapter). Putting this together with the adiabaticity assumption of the previous section, we see that our analysis applies to a particular range of pulse lengths,

$$\boxed{\omega_p^{-1} << \tau << \omega_i^{-1}} \tag{2.45}$$

In fact we shall find that quite a wide variety of beams fit this constraint.

3. REB Equilibrium

With a fair understanding of the ion and plasma electron motion, we now consider the beam equilibrium as it propagates through the channel. We will take the ion and plasma electron densities to be specified as obtained in the previous sections, and consider the motion of a single electron.

a. Single-particle Hamiltonian. From Eq. (2.14), we see that the motion of a beam electron is governed by the scalar and vector potentials

$$\begin{aligned} \phi &= \phi(0) + \frac{1}{4}\left(k_b^2 - k_p^2\right) r^2 , \\ a_z &= a_z(0) + \frac{1}{4} k_b^2 r^2 . \end{aligned} \tag{2.46}$$

and in general, we will consider an axially varying plasma density, $k_p=k_p(z)$. The single-particle Hamiltonian is

$$H = \sqrt{m^2c^4 + (p_z + mca_z)^2c^2 + p_x^2c^2 + p_y^2c^2} - mc^2\phi \,, \tag{2.47}$$

where the quantities p_x, p_y, and p_z are the canonical momenta in x, y, and z, respectively,

$$\begin{aligned} p_x &= m\gamma v_x \,, \\ p_y &= m\gamma v_y \,, \\ p_z &= m\gamma v_z - mca_z \,, \\ \gamma &= \left\{1 - \frac{v_x^2 + v_y^2 + v_z^2}{c^2}\right\}^{-1/2} . \end{aligned} \tag{2.48}$$

The particle velocity components are v_x, v_y, and v_z.

In the limit $p_z>>p_x,p_y$, and neglecting second order terms in a_z, Eq. (2.47) may be written

$$H \approx p_zc + \frac{m^2c^3}{2p_z} + \frac{p_x^2c}{2p_z} + \frac{p_y^2c}{2p_z} + mc^2(a_z - \phi) \,, \tag{2.49}$$

or

$$H \approx \underbrace{p_zc + \frac{m^2c^3}{2p_z}}_{H_{||}} + \underbrace{\frac{p_x^2c}{2p_z} + \frac{p_y^2c}{2p_z} + U}_{H_\perp} \,, \tag{2.50}$$

where, we identify the effective potential

$$\boxed{U = \frac{1}{4} m \omega_p^2 (x^2 + y^2) + mc^2 (a_z(0,s) - \phi(0,s))}, \tag{2.51}$$

and we restore the *s*-dependence of the constants of integration, for clarity. As indicated in Eq. (2.50), the energy is a sum of the energy of the axial motion ($H_{||}$), and the energy of the transverse motion ($H_{\perp}$).

b. Longitudinal wake in the IFR. Note that due to the s-dependence[9]

$$U(0,s) = mc^2\{a_{z1}(0,s) - \phi_1(0,s)\} \approx -\frac{1}{2} mc^2 V \frac{K_0(V)}{K_1(V)}, \tag{2.52}$$

H is not a constant of the motion, but varies according to,

$$\frac{dH}{dt} = \frac{\partial}{\partial s} U(0,s)$$
$$\approx -\frac{1}{2} mc^2 \frac{\partial}{\partial s}\left\{\frac{I}{I_0} ln\left(\frac{I}{I_0} e^{2\gamma_\varepsilon}\right)\right\}, \tag{2.53}$$

where we take the $V<<1$ limit. Equation (2.53) reflects the fact that electrons at the beam front must do work to induce a plasma return current. The plasma electrons deposit this energy in the beam tail.[10] In the terminology of accelerator physics,[11] Eq. (2.53), integrated over z, gives the "longitudinal

monopole wake potential" for IFR propagation.[12] The effect of this wake will be fairly negligible for our purposes, primarily because we will consider relatively short propagation lengths.[13]

c. Equations of motion. Next, we derive the equations of motion from the Hamiltonian of Eq. (2.50). In this connection, it is important to note, that by approximating the beam drift velocity by $v_z \sim c$, in evaluating the vector potential, the contribution to the Hamiltonian due to beam self-fields has been neglected,

$$U_b \approx \frac{1}{4} m c^2 k_b^2 r^2 \frac{1}{\gamma^2} .$$

This term is negligible in the limit $\gamma >> 1$, and typically has only a small effect on the particle motion. However, for a realistic beam profile (not a step profile), self-fields result in non-linear focussing and (as we shall see in Chapter 3) may produce damping of the ion-channel laser instability. We will neglect this effect for the remainder of this section.

From Eq. (2.50) the equations of motion are

$$\begin{aligned} \frac{dz}{dt} &= c - \frac{m^2 c^3}{2 p_z^2} - \frac{p_x^2 c}{2 p_z^2} - \frac{p_y^2 c}{2 p_z^2} \\ \frac{dp_z}{dt} &= - \frac{\partial U}{\partial z} . \end{aligned} \tag{2.54}$$

The equations for the transverse motion are,

$$\frac{d\vec{r}_\perp}{dt} = \frac{\vec{p}_\perp}{p_z} c$$
$$\frac{d\vec{p}_\perp}{dt} = -\frac{1}{2} m \omega_p^2 \vec{r} \ , \tag{2.55}$$

where we abbreviate

$$\vec{r} = (x, y) ,$$
$$\vec{p}_\perp = (p_x, p_y) .$$

Equation (2.55) may be rewritten as an equation for the transverse displacement alone,

$$\left(\frac{d^2}{dt^2} + \omega_\beta^2\right)\vec{r} = \vec{p}_\perp c \frac{d}{dt}\frac{1}{p_z}$$
$$= \frac{1}{4}\frac{\vec{p}_\perp}{p_z^2} m c^3 r^2 \frac{\partial}{\partial z} k_p^2 , \tag{2.56}$$

where ω_β is the "betatron frequency"[14] in the IFR,

$$\boxed{\omega_\beta = \omega_p \left(\frac{mc}{2\, p_z}\right)^{1/2}} \tag{2.57}$$

The main attraction of the IFR and the primary motivation for using a plasma in beam transport, is that ω_β, as given by Eq. (2.57), is much larger than that achievable with more conventional magnet focussing.

The transverse equation of motion simplifies when we take account of the fact that the axial momentum does not change appreciably. From Eq. (2.53),

$$\frac{\Delta p_z}{p_z} \approx -\frac{1}{4\gamma} a^2 \Delta k_p^2 . \tag{2.58}$$

Since, typically, $k_p a/\gamma^{1/2} << 1$, we have $\Delta p_z/p_z << 1$. In this case Eq. (2.56) is well-approximated by that of a 2-*D* simple harmonic oscillator,

$$\boxed{\left(\frac{d^2}{dt^2} + \omega_\beta^2\right)\vec{r} \approx 0} \tag{2.59}$$

The observation that a beam in the IFR may be considered as an ensemble of relativistic simple harmonic oscillators is the starting point, more or less for the analysis of the next chapter.

Since the the motion is Hamiltonian, the microscopic emittance is conserved, by Liouville's theorem. In addition, however, since focussing is linear, the rms normalized emittance

$$\varepsilon_n \approx \frac{1}{4}\gamma k_\beta a^2 , \tag{2.60}$$

is conserved (neglecting scattering, instabilities, etc.) for an adiabatic variation in k_β. This implies that an adiabatic increase in plasma density in z may be used to continuously focuss the beam to an ever-smaller spot size.

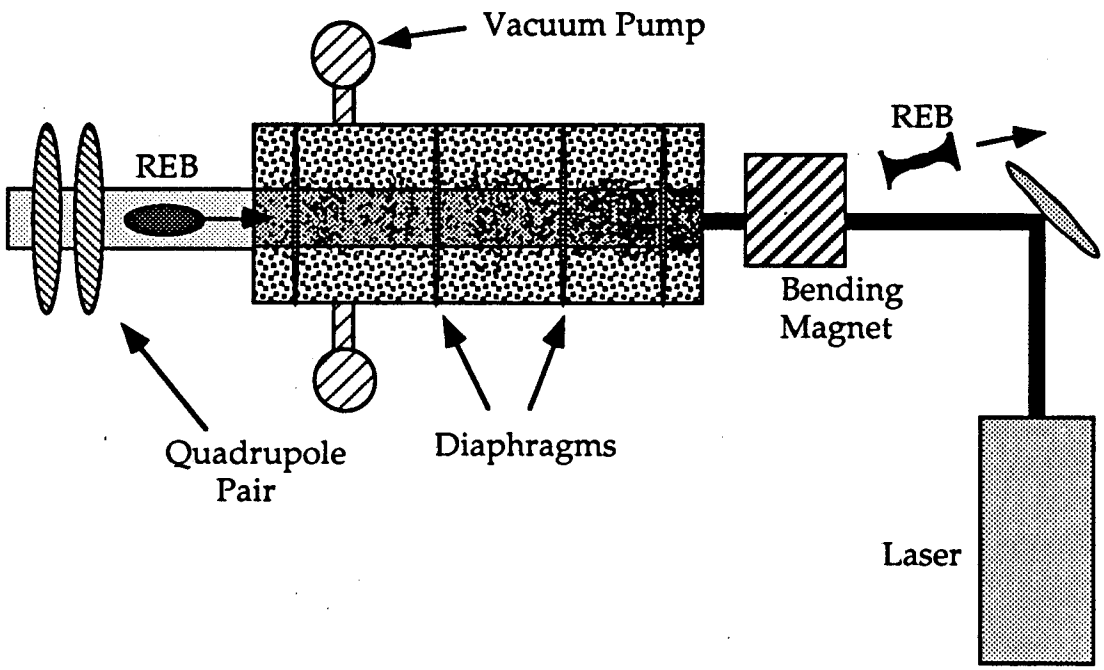

FIG. 2.9. Set-up for a "proof-of-principle" continuous plasma focus experiment, consisting of a pair of quadrupole magnets to control the initial beam spot size, a tank of gas with a density gradient maintained by differential pumping, and a laser used to form the plasma.

d. Continuous plasma focus. Chen, *et al.*[1] have proposed to take advantage of such continuous IFR focussing for application in a TeV linear electron-positron collider. In particular, they propose to focus the beam

continuously to a spot size smaller than can be achieved through conventional magnetic optics.[15] Such a focus also has application to the ion-channel laser, for, as we shall see in the next chapter, it is sometimes advantageous to focus the beam to a very small spot, not achievable with conventional magnetic optics. A schematic of a continuous plasma focus is depicted in Fig. 2.9.

Based on our work thus far, it is straightforward to derive some simple scalings for the continuous plasma focus. To transport the beam into the plasma without excessive emittance growth, k_β should vary adiabatically. This determines the initial plasma electron density, n_{pi}, in terms of the initial beam spot size, a_i,

$$n_{pi} \approx \frac{2\,\varepsilon_n}{\pi\,\gamma\,r_e\,a_i^4}, \tag{2.61}$$

where r_e is the classical electron radius.

As the beam is focussed to an ever smaller spot, the plasma density approaches the beam density and the character of the focussing changes. In the overdense regime, the ion space-charge is sufficient to neutralize the beam charge, so that the beam is focussed by its own magnetic field. This transition, from the underdense regime and ion space-charge focussing, to the overdense regime and beam self-pinching, occurs for a minimum beam radius, a_{min}, determined by setting $n_p=n_b$:

$$a_{min} \approx \varepsilon_n \left(\frac{2 I_0}{\gamma I}\right)^{1/2} \tag{2.62}$$

The density at this transition is

$$n_{pt} = \gamma \left(\frac{I}{I_0}\right)^2 \frac{1}{2 \pi r_e \varepsilon_n^2}, \tag{2.63}$$

and the betatron wavenumber at this density is

$$k_{\beta\, max} \approx \left(\frac{I}{I_0}\right) \frac{1}{\varepsilon_n}.$$

In the overdense regime, the effective betatron wavenumber provided by the beam magnetic field is

$$k_\beta \approx \left(\frac{I_{net}}{\gamma I_0}\right)^{1/2} \frac{1}{a},$$

where the net current, I_{net}, is the sum of the beam current and the plasma return current within the beam volume.[16] Since $I_{net} \leq I$, the maximum focussing strength is bounded: $k_\beta \leq k_{\beta max}$.

Therefore, once the beam spot size is focussed to a_{min}, the adiabatic focussing is complete. This establishes a limit on spot size in the continuous

plasma focus. However, for the low emittance, high energy beams of a TeV collider, this limit is far smaller than the beam spot size required. Therefore, the design final spot size, a_f, will usually be larger than the minimum possible spot size, a_{min}. In this case, the final density in the focussing section,

$$n_{pf} \approx \frac{2\,\varepsilon_n^2}{\pi\, r_e\, \gamma\, a_f^4},$$

will usually be much less than n_{pt}.

At the same time, a subject of ongoing interest, in TeV linear electron-positron collider design, is the reduction of coherent beam-beam effects: beamstrahlung and disruption.[17,18] One method which has been proposed is current neutralization in an overdense plasma at the interaction point (IP).[4] Beamstrahlung and disruption are suppressed due to plasma return currents which reduce the magnetic pinch forces seen by the two colliding beams.

Current neutralization requires a plasma skin depth short compared to the beam radial size, and a magnetic diffusion time long compared to the beam length. It is shown in Ref. 4 that the magnetic field reduction associated with an REB in a collisionless plasma scales as a function only of $k_p a$. Taking a reduction of 70% as a figure of merit, $k_p a_f \sim 2$ is required. To obtain partial current neutralization, without an increase in beam spot size, the adiabatic focussing cell should then be terminated within a distance $\lambda_{\beta f}$

of the IP with a nonadiabatic increase in plasma density to a value, n_{pc}, such that,

$$n_{pc} \approx \frac{1}{\pi r_e a_f^2}.$$

The length of this cell should be of order a few bunch lengths, and, to avoid defocussing due to plasma return currents, it should be less than the final betatron wavelength at the focusser exit. This implies, $c\tau < \lambda_{\beta f}$. If the adiabatic focusser is terminated with $n_{pf} < n_{pt}$, the beam may pinch as it enters the current neutralization cell. Pinching is negligible if the cell length is much less than $\lambda_{\beta min}$; this requires $c\tau < \lambda_{\beta min}$.

C. BEAM BREAK-UP IN THE IFR

Thus far we have considered only a cylindrically symmetric problem, where the beam centroid propagates down the center of the ion-channel. However, it is well-known in accelerator physics, that interaction with the guiding geometry can frequently result in instabilities coupled to the off-axis displacement of the beam centroid. In the IFR there are two such transverse "beam break-up" intstabilities: the "electron-hose" and "ion-hose" instabilities. In this section, we review the general features of beam break-up instabilities. We then go on to consider the particulars as they apply to the IFR.

1. The beam break-up equation

A relativistic electron beam injected off-axis into a beamline will have an electrostatic dipole moment. The axial current associated with this dipole moment will couple to the axial electric fields of the various structures along the beamline. The associated transverse Lorentz force will give a kick to beam slices to the rear, displacing them farther off-axis. In this way, an instability obtains.

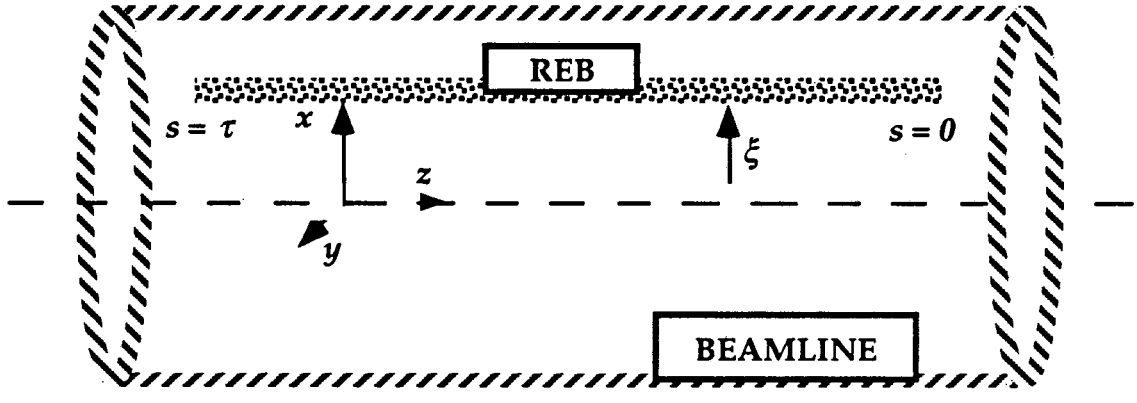

FIG. 2.10. A relativistic electron beam propagating in the z-direction (to the right), down the beamline. The beam head is at s=0, and the tail is at s=τ. The transverse beam break-up instabilities arise from an off axis perturbation ξ, which excites electromagnetic modes of the structures on the beamline. The Lorentz force associated with the mode fields then "kicks" follow-on beam slices, resulting in growth of the displacement ξ.

To make this quantitative, one considers the effect of a perturbation in the form of a small displacement, ξ, of the beam centroid, in the x direction

(Fig. 2.10). For definiteness we assume an unperturbed beam charge density of the form $\rho_{b0}=-en_bH(a-r)$, where H is the step function and r is the radial coordinate in the x-y plane. The perturbation to the beam charge density is then

$$\rho_{b1}(r,z,s) \approx -\, e n_b(s)\,\delta(a-r)\,\xi(z,s)\cos(\theta),$$

where θ is the azimuthal angle in the x-y plane. The variable $s=t-z/v_z$, indexes beam slices, $v_z\sim c$ is the axial beam velocity, and c is the speed of light. The beam extends from $s=0$ (the beam head) to $s=\tau$ (the beam tail). Beam electrons remain approximately at a fixed s, as they advance in z, down the beamline. The beam density $n_b(s)$ is proportional to the beam current is $I(s)$, which here will be assumed constant in s ("d.c. beam"). The perturbed current density is $J_{b1z}\sim\rho_{b1}c$.

With these perturbed charge and current sources, one solves Maxwell's equations for the perturbed scalar and vector potentials, for the beamline geometry of interest.[19] This procedure yields the fields as functionals of ξ. Writing out the Lorentz force equation, then gives a "beam break-up" equation for ξ, so called because of the deleterious effect the fields have on the beam. Generically, this equation takes the form[11]

$$\left(\frac{\partial}{\partial z}\gamma\frac{\partial}{\partial z}+\gamma k_\beta^2\right)\xi(z,s)=\int_0^s ds'\left(\frac{I(s')}{I_0}\right)W(s-s')\,\xi(z,s') \qquad (2.64)$$

$W(s-s')$, the wake potential,[20] is the Green's function which determines the Lorentz force on an electron at s, as it arrives at z, due to the fields generated by the beam segment at $s'<s$. In conventional accelerators, the focussing represented by the k_β term is provided by magnetic fields. In the IFR it is provided by the ion electrostatic field, as given by Eq. (2.57), with $k_\beta=\omega_\beta/c$.

We may solve Eq. (2.64) up to quadrature by Laplace transforming in s, solving the simple harmonic oscillator equation in z, and inverting the Laplace transform, to find

$$\xi(z,s)=\frac{1}{2\pi i}\int_{-i\infty}^{+i\infty}dp\,\frac{1}{p}exp(ps)\cos\left\{z\left[k_\beta^2-\left(\frac{I}{\gamma I_0}\right)w(p)\right]^{1/2}\right\}, \quad (2.65)$$

where $w(p)$ is the Laplace transform of the wake (the "impedance"[20]) and the initial condition $\xi(0,s)=H(s)$ is assumed. Given $w(p)$, it is usually straightforward to compute the asymptotic growth of the beam centroid oscillations, by applying the method of steepest descents to Eq. (2.65).[21]

In general, as discussed at length in Ref. 20, there are many wakes of different functional forms. For our purposes, one particular form is adequate for our discussion. This is the wake corresponding to a single undamped TM mode of a microwave cavity. Such a wake takes the form[22]

$$W(s)=W_0\sin(\omega_0 s), \quad (2.66)$$

where ω_0 is the resonant angular frequency of the mode, and the amplitude is given by

$$W_0 = r\omega_0^2 , \tag{2.67}$$

where r is the "shunt impedance per unit length"[23] for the mode. The solution of Eq. (2.65) for such a wake has been discussed extensively in the literature, and the distinction between the "weak" and "strong" focussing limits is worth noting.[24,25] Focussing is "weak" when $\lambda_\beta > L_g$, where L_g is the instability growth length, and $\lambda_\beta = 2\pi/k_\beta$ is the betatron period. In addition, one should distinguish between a pulse length which is short or long compared to the mode period. When the pulse length is short, the wake is approximately linear in s, giving rise to a "head-tail instability".[10] When the pulse length is longer the growth law is modified, and this is typically the case, for example, in induction linac work.[26]

We should add that we have actually written out a somewhat simplified form of the beam break-up equation. In general, k_β may vary in s, in z, and at fixed s, within a slice. This is an important feature in the strong-focussing regime, for it allows the accelerator physicist to attempt to damp what might otherwise be an incorrigible instability.

Such damping mechanisms require a spread or sweep in betatron wavenumber of order $\Delta k_\beta \sim 1/L_g$ This includes Landau damping due to a spread in energy within a beam slice,[23] "BNS damping" due to a sweep in energy from head to tail,[27] and "phase-mix damping" of BBU growth due to nonlinear focussing, arising from a radially non-uniform plasma.[28]

However, when focussing is weak, the condition $\Delta k_\beta \sim 1/L_g$ requires an impractically large spread ($\Delta k_\beta/k_\beta \sim 1/k_\beta L_g > 1$), and one must instead attempt to disrupt the resonances emodied in the impedance, $w(p)$, for example, by detuning successive cavities ("stagger tuning"), to produce phase-mixing in the driving term on the right side of Eq. (2.64).

We turn next to apply this formulation to the premier instabilities of the IFR, "electron-hose" and "ion-hose".

2. Electron-hose instability

Recently it has been shown[29] that IFR devices relying on an unneutralized ion-channel, surrounded by a quasineutral plasma, suffer from a hose instability, similar to the ion-hose instability,[30] and other varieties of two-species transverse coupling instability,[31] except that here the coupling is between the beam and the distant plasma electrons at the channel wall. In this section, we derive the growth length for this "electron-hose" instability.

The transverse wakefield corresponding to this "electron-hose" effect is calculated in the "frozen-field" approximation, for a low current, cylindrical beam. The asymptotic growth of beam centroid oscillations is computed and possible damping and saturation mechanisms are discussed.

As in previous sections, we assume an unperturbed beam charge density of the form $\rho_{b0}=-en_bH(a-r)$, where H is the step function, $-e$ is the electron charge, r is the radial coordinate in the x-y plane and a is the beam radius (Fig. 2.8). The beam density on axis is n_b and is a function of $s=t-z/c$, where t is time, z is axial displacement and c is the speed of light.

We will also assume that the collisionless plasma skin-depth, c/ω_p, is much larger than the channel radius. Thus $V=k_pb=2(I/I_0)^{1/2}<<1$, where $I_0=mc^3/e\sim17$ kA, and I is the beam current. We have seen that the axial plasma electron current, and drift velocity, are negligible in this limit. In this case, the equilibrium plasma electron charge density is $\rho_{e0}=-en_pH(r-b)$.

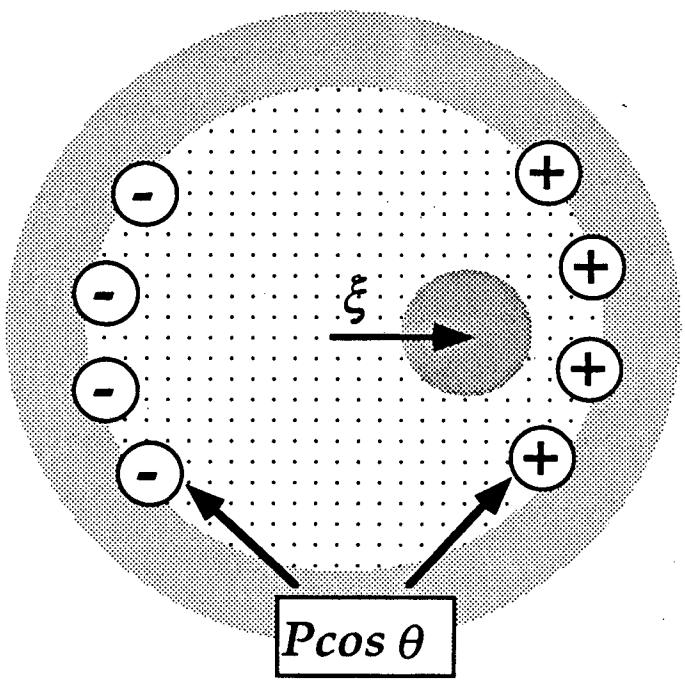

FIG. 2.11. A beam slice in the ion-channel is displaced by an amount ξ in the x-direction, inducing a polarization $P\cos\theta$ on the channel wall. The polarization responds to the beam dipole field as a simple harmonic oscillator with characteristic angular frequency ω_0. This image dipole then deflects follow-on portions of the beam. This is to be compared with the equilibrium depicted in Fig. 2.8.

We consider next the effect of a perturbation to the beam centroid (Fig. 2.11) in the form of a small displacement, ξ, of the beam centroid, in the x direction. The perturbation to the beam charge density is then $\rho_{b1}=-en_b\xi\delta(a-r)\cos\theta$, where θ is the azimuthal angle in the x-y plane. We proceed to compute the perturbed scalar and axial vector potentials, ϕ_1 and A_{z1}, and the perturbed plasma electron density ρ_{e1}, due to ξ.

Maxwell's equations in the Lorentz gauge are

$$\left\{\nabla_\perp^2+\frac{\partial^2}{\partial z^2}-\frac{1}{c^2}\frac{\partial^2}{\partial t^2}\right\}a_1=4\pi\rho_{e1}\ ,$$
$$\left\{\nabla_\perp^2+\frac{\partial^2}{\partial z^2}-\frac{1}{c^2}\frac{\partial^2}{\partial t^2}\right\}\phi_1=-4\pi(\rho_{b1}+\rho_{e1})\ . \tag{2.68}$$

where $a_1=A_{z1}-\phi_1$. The transverse gradient is $\nabla_\perp$. We will change variables from z, t to z, s and simplify Eq. (2.68) with the "frozen-field" approximation, in which the D'Alembertian operators are approximated by $\nabla_\perp^2$ and radiative effects are neglected. We shall find that this amounts to a neglect of $V/\gamma<<1$.

The perturbed plasma electron charge density is determined from the potentials through the electron cold-fluid equations,

$$\frac{\partial\rho_{e1}}{\partial s}+\vec{\nabla}\cdot(\rho_{e0}\vec{v}_{e1})\approx 0\ ,$$
$$\frac{\partial\vec{v}_{e1}}{\partial s}\approx\frac{e}{m}\vec{\nabla}\phi_1\ . \tag{2.69}$$

Inspection of Eq. (2.69) shows that ρ_{e1} consists entirely of a surface charge layer at $r=b$. Thus it is convenient to define,

$$P(z,s)\cos\theta = \int_{b^-}^{b^+} dr\ \rho_{e1}(r,\theta,z,s) \quad , \tag{2.70}$$

the dipole moment density induced on the channel wall by the beam charge.

In terms of ξ and P the potentials from Eq. (2.68) are

$$\phi_1 = 2\pi\cos(\theta)\begin{cases}(P - n_b e\xi)r & ;r < a\\ Pr - \dfrac{n_b e\xi a^2}{r} & ;a < r < b\\ (Pb^2 - n_b e\xi a^2)\dfrac{1}{r} & ;b < r\end{cases} \quad , \tag{2.71}$$

and

$$a_1 = -2\pi\cos(\theta)\begin{cases}Pr & ;r < b\\ \dfrac{Pb^2}{r} & ;b < r\end{cases} \quad . \tag{2.72}$$

The wall polarization is determined from ξ, through Eq. (2.69),

$$\left(\frac{\partial^2}{\partial s^2} + \omega_0^2\right)P(z,s) = \frac{a^2}{b^2}\omega_0^2 n_b e\xi(z,s) \quad , \tag{2.73}$$

where $\omega_0=\omega_p/2^{1/2}$. Thus P responds as a simple harmonic oscillator with characteristic angular frequency ω_0. This frequency differs from ω_p because the surface at $r=b$ is the boundary between a region of electron density n_p, and a region of zero density.

The Lorentz force law for the displacement of the beam centroid is

$$\left(\frac{\partial}{\partial z}\gamma\frac{\partial}{\partial z}+\gamma k_\beta^2\right)\xi=-\frac{e}{mc^2}\frac{\partial}{\partial x}a_1, \tag{2.74}$$

where $k_\beta\sim\omega_\beta/c$ is the betatron wavenumber. This describes the deflection of the beam by the image polarization on the ion-channel wall.

For an infinite beam and beamline, we may combine Eqs. (2.73) and (2.74), taking a perturbation varying as $\xi\propto exp(ikz-i\omega s)$, to obtain the dispersion relation,

$$\left(1-\frac{k^2}{k_\beta^2}\right)\left(1-\frac{\omega^2}{\omega_0^2}\right)=1 \tag{2.75}$$

Equation (2.75) predicts instability for real $\omega^2<\omega_0^2$ or real $k^2<k_\beta^2$ with growth rates diverging as $\omega^2\rightarrow\omega_0^2$, or $k^2\rightarrow k_\beta^2$ from below. As in the "rigid beam" model of the resistive-hose instability,[27] we expect these singularities to result in an instability which is absolute in both the beam and lab frames.

To obtain a more quantitative result, we solve the initial value problem for a semi-infinite beam and beamline. We invert Eq. (2.73) to obtain P, and using Eqs. (2.72) and (2.74), we obtain a beam break-up equation for ξ,

as in Eq. (2.65), where we identify the electron-hose "dipole wake potential" as $W(s)=W_0 sin(\omega_0 s)$, with

$$W_0 = 2\frac{\omega_0}{b^2}. \tag{2.76}$$

Comparing this result with Eq. (2.67) we see that this wake is formally identical to that of an undamped microwave cavity, with a shunt impedance per unit length of $2/\omega_0 b^2$, and a resonant frequency ω_0. Inspection of the beam break-up equation shows that with the scaling of z by $k\beta$, and s by ω_0, for γ, ω_0 independent of s and z, no free parameters remain. There is only one, universal solution for prescribed initial conditions.

We obtain this solution up to quadrature as in Eq. (2.68), and compute the asymptotic solution using the method of steepest descents to find

$$\xi(z,s) \approx \frac{2^{3/2}}{3^{5/4}\pi^{1/2}}\frac{A^{1/2}}{\omega_0 s}e^A \sin\left\{\omega_0 s - 3^{-1/2}A - \frac{\pi}{12}\right\}. \tag{2.77}$$

The term in the exponent is $A=(z/L_g)^{2/3}$, where the growth length is

$$L_g = \frac{2^3}{3^{9/4}}\left(\frac{\gamma I_0}{I}\right)^{1/2}\frac{1}{\sqrt{W_0 s}}, \tag{2.78}$$

or

$$L_g = \frac{2^2}{3^{9/4}\pi}\frac{\lambda_\beta}{\sqrt{\omega_0 s}}, \qquad (2.79)$$

and $\omega_0 s >> A >> 1$ is assumed. Thus when $\omega_0 \tau >> 1$ (adiabatic current rise) $L_g << \lambda_\beta$ and focussing is always weak with respect to electron-hose growth. This result is remarkable in that it predicts growth so rapid that ion-focussing should be considered ineffective, rendered so by the presence of free plasma electrons at the channel wall.

We turn next to consider mechanisms which will tend to reduce growth. We observe from the dispersion relation of Eq. (8), that there are in principle two methods of "curing" the electron-hose. We may diminish the resonance at $\omega^2 \rightarrow \omega_0^2$, or at $k^2 \rightarrow k_\beta^2$. On the other hand, since focussing is typically weak, damping mechanisms relying on a spread or sweep in betatron wavenumber, $\Delta k_\beta \sim 1/L_g$, are ineffective, as they require an impractically large spread, $\Delta k_\beta / k_\beta \sim 1/k_\beta L_g > 1$. This rules out Landau, BNS and phase-mix damping damping. (These conclusions contrast with those for resistive-hose growth,[32] where focussing is typically strong.)

Thus, to diminish electron-hose growth, we must look to the resonant coupling at $\omega^2 \rightarrow \omega_0^2$, and a number of mitigating factors suggest themselves. First, the electron-hose could be eliminated entirely by ionizing a channel of radius less than b. In this case, all plasma electrons are ejected to the beam-pipe wall, leaving no free plasma electrons at the channel edge. Alternatively, an axial variation in plasma density, as in the continuous plasma focus,[1] may

produce phase-mix damping. In this case, the plasma density should vary appreciably over a length $L_g<\lambda_\beta$.

Growth could also be reduced by varying the resonant frequency of plasma oscillations, through the external geometry. For example, if we add a conducting pipe of radius R to the problem, we find a resonant frequency $\omega_0' \sim \omega_0(1+b^2/2R^2)$, i.e., the image dipole, P oscillates at a slightly higher frequency, dependent on R. Thus a variation of the pipe radius on the scale of a growth length could in principle produce the effect of stagger tuning.

In addition, growth will be mitigated by the plasma return current, neglected in the approximation $V<<1$. In the low current limit we have considered, the electron-hose is formally analagous to the image-displacement effect in conventional accelerators.[33] Were a conducting boundary or a sufficiently dense plasma nearby, it would carry a dipole image current, and the combined Lorentz force on the beam due to the image fields would be a factor of $1/\gamma^2$ less than for the electric field term alone. On the other hand, to achieve even $V\sim 2$ requires $I\sim I_0$, a current larger than typically envisioned.

Ultimately, as a result of hosing, plasma electrons will be heated, and the instability will saturate. The simplest estimate would give saturation when $\xi\sim b$, corresponding to substantial growth in the beam emittance, and a significant electron temperature$\sim mc^2(I/I_0)$. In fact, this omits the subtler feature that, at lesser temperatures, the channel wall will take on the character of a Debye sheath, with a radial variation in the plasma frequency and a phase-mix reduction of the wake driving term. A simliar effect may

obtain due to beam "halo". In general, issues of saturation are best studied numerically, and such work is in progress.[34]

Finally, it is interesting to note that for an infinitely wide planar beam, the electron-hose dipole wake vanishes. This is because a one-dimensional dipole field vanishes outside the source. However, in this case one can show that there is a flute-like analog of the electron-hose, where ripples develop in the beam density and provide a coupling of the beam and the channel wall. Nevertheless, it may be possible that for ellipsoidal beams, electron-hose growth could be reduced with a sufficiently large aspect ratio.

For present purposes, we conclude from this work that for reliable propagation in the IFR, it is likely that a channel of radius less than b should be ionized to insure the absence of free plasma electrons at the wall. This is typically the case, for laser-ionized channels, for example.

3. Ion-hose instability

The ion-hose instability has been the subject of much work over the years, as it represents an important constraint on IFR propagation.[30] In this section, we derive the growth length for a short pulse ($\omega_i\tau<<1$).

We linearize the cold fluid equations, with an ion-density $\rho_i=\rho_{i0}+\rho_{i1}$, and consider a small dipole perturbation to the beam centroid as in the previous section. We find,

$$\left(\frac{\partial^2}{\partial s^2} + \omega_{io}^2\right)\rho_{i1} = -\omega_{io}^2\rho_{b1},$$

which is more or less Eq. (2.36), now for a different source term. (We neglect the monopole perturbation to the ion-charge density, which is small for short pulse lengths.) The solution may be written

$$\rho_{i1} = en_i\eta\,\delta(a - r)\cos(\theta),$$

where we may interpret η as the centroid of the ion-column or "hose"

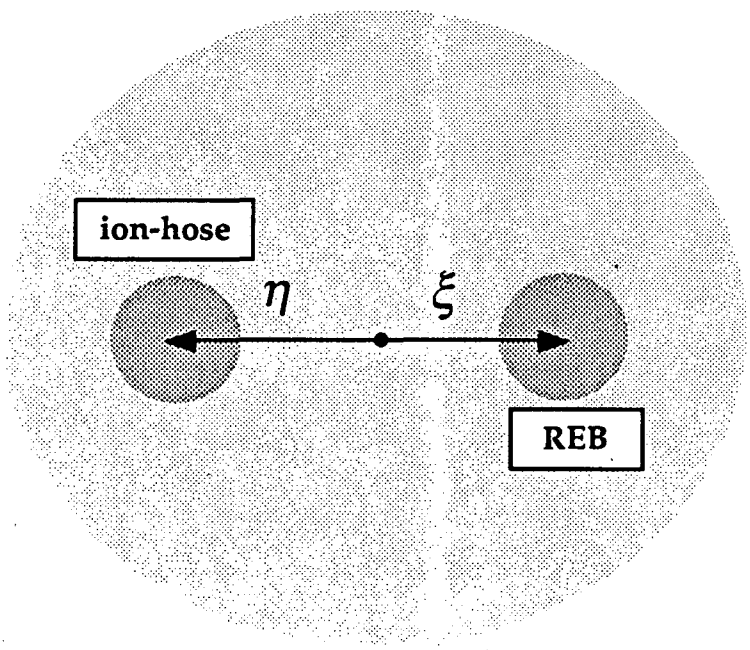

FIG. 2.12. A transverse displacement of beam centroid by an amount ξ, perturbs the ion-channel centroid (or "ion-hose"), here displaced by an amount η. The ion-hose then deflects follow on beam slices. Note that this figure is drawn to an exaggerated scale to illustrate the variables η and ξ. In fact, the beam and the hose are assumed to overlap very closely.

overlapping the beam. Following a procedure analagous to that for Eq. (2.72) and Eq. (2.74) we may then set down the coupled equations for the beam and hose centroids,

$$\left(\frac{\partial^2}{\partial s^2} + \omega_i^2\right)\eta = \omega_b^2\left(\frac{m}{m_i}\right)\xi ,$$
$$\left(\frac{\partial}{\partial z}\gamma\frac{\partial}{\partial z} + \gamma k_\beta^2\right)\xi = \gamma k_\beta^2\eta . \qquad (2.80)$$

Thus displacement of a beam slice off-axis produces a displacement of the ion-hose which then perturbs the motion of follow-on slices to the rear (see Fig. 2.12).

Solving for η up to a quadrature in ξ reduces Eq. (2.80) to the form of the beam break-up equation, Eq. (2.65), with

$$W_0 = 2\frac{\omega_i}{a^2} .$$

For ion-hose, however, unlike electron-hose, the pulse length is typically short compared to the time for ions to oscillate, as discussed in connection with Eq. (2.35). In this case, the sinusoidal wake is approximately linear,

$$W(s) \approx 2\frac{\omega_i^2}{a^2}s .$$

We take this into account in applying the method of steepest descents, and find that growth of the beam centroid oscillations varies as $exp(z/L_g)^{1/3}$, with growth length,

$$\boxed{L_g \approx \frac{2^6}{3^{9/2}}\left(\frac{I_0}{I}\right)\frac{\varepsilon_n}{(\omega_i \tau)^2}}, \qquad (2.81)$$

or, in practical units,

$$L_g \approx 0.32\ \lambda_\beta\ A\left(\frac{a}{1\,cm}\right)^2\left(\frac{1\,ns}{\tau}\right)^2\left(\frac{1\,kA}{I}\right).$$

We will typically accept this result as a constraint on pulse length, when we consider numerical examples for the ion-channel laser in the next chapter. However, typically $L_g > \lambda_\beta$, so that focussing is strong, and the instability is susceptible to BNS damping. In practice this may ameliorate growth considerably.

D. OTHER PLASMA EFFECTS

In this section, we enumerate and quantify certain fairly ubiquitous plasma effects which will tend to degrade beam quality in transit through the plasma. In general, these effects are much less severe than ion-hose and

electron-hose. However, they should be taken into account in any practical experiment.

1. Scattering

First, we consider emittance growth due to scattering. The total cross-section for small angle scattering is[35]

$$\sigma_s = \pi \left(\frac{2\ Zr_e}{\gamma}\right)^2 \frac{1}{\theta_{min}^2}. \tag{2.82}$$

For a fully ionized, quasineutral plasma, $\theta_{min} \sim \hbar/(\lambda_D mc\gamma)$, where λ_D is the Debye wavelength. However, for a partially ionized gas from which plasma electrons have been ejected, $\theta_{min} \sim \hbar/(bmc\gamma)$, for scattering from ions, and $\theta_{min} \sim \hbar/(amc\gamma)$ for scattering from neutral atoms. The atomic number is Z and $a \sim 1.4\ a_B\ Z^{-1/3}$, is the screening radius in the Thomas-Fermi model. The constant $\hbar = h/2\pi$, h is Planck's constant, and a_B is the Bohr radius, $a_B = \hbar^2/me^2$. It will be assumed that the ionization fraction, f, is sufficiently low that scattering with neutral atoms dominates.

The mean-square scattered angle per scattering event is

$$\langle \theta^2 \rangle = 2\,\theta_{min}^2\, ln\left(\frac{\theta_{max}}{\theta_{min}}\right). \tag{2.83}$$

The maximum scattering angle is $\theta_{max}=\hbar/(r_n mc\gamma)$ where $r_n \sim 0.5\ r_e A^{1/3}$ is the nuclear radius and A is the atomic weight. This gives,

$$\frac{\theta_{max}}{\theta_{min}} \approx 5.26 \times 10^4 (AZ)^{-1/3}$$

The rms scattering angle after traversing a length, z, of gas, $\Theta_{rms}(z)$, varies according to,

$$\frac{d}{dz}\Theta_{rms}^2 = n_0 \sigma_s \langle \theta^2 \rangle \approx 8\ \pi\ n_0 \frac{Z^2 r_e^2}{\gamma^2} ln\left(\frac{\theta_{max}}{\theta_{min}}\right), \tag{2.84}$$

where n_0 is the density of neutral atoms.[36] Emittance growth is then given by,[37]

$$\frac{d\varepsilon_n}{dz} = \frac{\gamma}{2\ k_\beta}\frac{d}{dz}\Theta_{rms}^2, \tag{2.85}$$

The change in normalized emittance in passing through the cell is then

$$\Delta\varepsilon_n = 2\ \frac{r_e Z^2}{f}\int_0^{L_p} dz\ k_\beta\ ln\left(\frac{\theta_{max}}{\theta_{min}}\right). \tag{2.86}$$

In the overdense regime, (e.g. at the beam head) envelope expansion is qualitatively different because the quasistatic beam equilibrium is maintained

by the beam magnetic field, rather than the (external) field of the ion charge (so that $k_\beta \propto 1/\varepsilon_n$ in Eq. [2.85]). As the beam expands, the focussing is reduced, with the result that the beam envelope exponentiates, on the scale of the Nordsieck length,[38]

$$L_N = \frac{1}{4\ \pi\ n_0\ r_e^2}\ \frac{\gamma I}{I_A}\ \frac{1}{Z^2\ ln\left(\frac{\theta_{max}}{\theta_{min}}\right)}, \tag{2.87}$$

where channel radiation has been neglected.

2. Radiation

Radiation in the ion-channel is of interest as a diagnostic, and of possible concern for its effect in producing energy spread on the beam. Two types of radiation are considered: bremstrahlung and synchrotron radiation due to the betatron motion.

Bremstrahlung may be characterized by the radiation length λ_R,[38]

$$\lambda_R^{-1} = \frac{16}{3}\alpha\ n_0\ r_e^2\ Z^2\ ln\left(\frac{233}{Z^{1/3}}\right), \tag{2.88}$$

where $\alpha = e^2/\hbar c$ is the fine structure constant. The fractional energy loss is then

$$\left(\frac{\Delta\gamma}{\gamma}\right)_B \approx \int_0^{L_p} \frac{dz}{\lambda_R} = \frac{16}{3}\alpha\ r_e^2\ Z^2\ ln\left(\frac{233}{Z^{1/3}}\right)\int_0^{L_p} n_0\ dz, \tag{2.89}$$

and this is typically very small.

Radiation due to the betatron motion takes on the character of wiggler radiation, for strong focussing ($\gamma\beta_\perp \geq 1$). The spectrum on axis is peaked at frequencies $\omega \sim 2\gamma^2 ck_\beta/(1+\gamma^2\beta_\perp^2)$. Integrated over all angles, the spectrum is characterized by the critical frequency, $\omega_c = 3\gamma^3 c/\rho$, where $\rho \sim 2^{1/2}/(k_\beta^2 a)$, is the effective bending radius. The angular distribution extends to angles of order $\beta_\perp$. Quantum effects are small provided $\Upsilon < 0.2$, where, $\Upsilon = \gamma^2 \lambda\!\!\!^{-}_c/\rho$, and $\lambda\!\!\!^{-}_c = \hbar/mc$ is the Compton wavelength.[39]

As in a damping ring, synchrotron radiation can decrease the normalized emittance of the beam.[40] However, this effect is typically small. Fractional energy loss is, for Υ small,

$$\left(\frac{\Delta\gamma}{\gamma}\right)_s = -\frac{2}{3}\frac{\alpha L_p}{\gamma \lambda\!\!\!^{-}_c}\Upsilon^2 , \tag{2.90}$$

where $\Delta\gamma$ is the change in γ and a constant λ_β is assumed.

3. Ionization

Ionization by the beam is of concern in determining the actual axial plasma density profile, and is of interest as a means of augmenting laser ionization at high plasma densities. Ionization is produced by the beam through electron impact, gas breakdown, and stripping of atoms and ions in the strong radial electric field at the beam "edge".

To accurately compute the net volume rate of ionization requires numerical solution of detailed rate equations, and modelling of the chemistry of the particular gas used. To estimate the effect of impact ionization, a phenomenological estimate must be made for the effective area into which secondary electrons are ejected.[41] Here we satisfy ourselves with a few simple estimates.

The time scale for ionization in the overdense regime via impact ionization of neutrals by beam electrons is $\tau_b \sim 1/(n_0 \sigma_{bi} c)$, where σ_{bi} is an effective ionization cross-section of order 10^{-18} cm^2.[42] For example, this ionization time is ~ 1 ps at a neutral density of $n_0 \sim 3 \times 10^{19}$ cm^{-3}.

The character of breakdown produced by long pulses is determined by the value of E/p, the ratio of radial electric field to pressure.[43] For very fine beams, E/p will be sufficiently large that secondary electrons are ejected far beyond the beam volume before they create additional ionization.

In addition, for short pulses, a key limitation is the formative time required for breakdown. This is roughly the time for one secondary electron accelerated in the beam field, to ionize one neutral, $\tau_e \sim 1/(n_0 \sigma_{ei} v_e)$, where σ_{ei} is the cross-section for ionization by secondaries and v_e is the secondary velocity. The quantity $\sigma_{ei} v_e$ peaks at secondary electron energies of order ~ 100 eV, with $\sigma_{e1} v_e \sim 10^{-7}$ - 10^{-8} cm^3/sec, depending on the gas.[44] For example, in N_2 this time scale is τ_e ~1 ps for $n_0 \sim 3 \times 10^{19}$ cm^{-3}.

The radial electric field at the beam edge will be adequate to strip an atomic electron with ionization potential, $\Delta\varepsilon$, for currents of order

$$I \approx \alpha^4 \frac{\sigma}{r_e}\left(\frac{\Delta\varepsilon}{e^2/a_B}\right) I_0 \qquad (2.91)$$

For very fine beams, this mechanism may fully ionize a channel larger than the beam, with some multiple ionization.

When field stripping may be neglected, plasma electrons are also lost through recombination on a time scale $\tau_{rc} \sim 1/(\alpha_r n_p)$, and through attachment on a time scale $\tau_a \sim 1/(\alpha_a n_0)$. Here, α_r and α_a are the recombination and attachment coefficients, respectively.[44] Taking recombination in N_2 as an example, $\alpha_r \sim 2\text{x}10^{-7}$ cm^3/sec, at electron energies ~ 1 eV.[45] At a density of $3\text{x}10^{19}$ cm^{-3}, $\tau_{rc} \sim$ 0.2 ps and this is quite short. However, α_r will be lower for more energetic electrons. In addition, despite recombination and attachment, the beam volume will become depleted of plasma electrons, provided the impact ionization time scale is short enough. This occurs because, as electrons go through successive ionizations and recombinations, they diffuse away from the beam center.

4. Streaming and other instabilities

A number of streaming instabilities arise in the IFR, and we note their growth rates here. Typically, they will have a negligible effect for parameters of interest in the ion-channel laser.

a.Buneman. We have taken plasma electrons to be collisionless. However, in the collisionless limit, instabilities may replace collisions in dissipating the energy of the secondaries.[46] In particular, the two-stream

(Buneman) instability will couple the electron motion to the ions on a time scale ν_{eiTS}^{-1}, where

$$\nu_{eiTS} = \frac{3^{1/2}}{2^{4/3}}\omega_p\left(\frac{m}{m_i}\right)^{1/3}, \tag{2.92}$$

This instability is mitigated by convection away from the beam, which continuously replaces the carriers of the return current with an unperturbed flow of plasma electrons.

b. Beam-plasma electron two-stream. In the magnetically self-focussed regime (at the beam head) beam electrons are subject to the longitudinal two-stream instability, due to the relative motion with respect to the plasma electron drift. The growth rate is

$$\nu_{beTS} = \frac{3^{1/2}}{2^{4/3}}\omega_p\left(\frac{n_b}{\gamma^3 n_p}\right)^{1/3}, \tag{2.93}$$

and this is typically small.

c. Beam-ion two-stream. In addition, the longitudinal two-stream instability will develop due to the relative motion of the beam over the ion background, on a time scale ν_{biTS}^{-1}, where

$$\nu_{biTS} = \frac{3^{1/2}}{2^{4/3}}\omega_i\left(\frac{\omega_b^2}{\gamma^3\ \omega_i^2}\right)^{1/3}, \tag{2.94}$$

where the limit $\omega_i^2 > \omega_b^2/\gamma^3$ is assumed. This time scale is long.

d. Weibel. In addition, in the overdense regime, when $k_p a$>O(1), (as for an eroded beam head) significant return currents flow within the beam volume and two adjacent plasma electron return current filaments attract. Filaments form and disrupt the intended current neutralization.[47] The growth rate for the Weibel or filamentation instability is

$$\nu_W = \omega_p \left(\frac{n_b}{\gamma\, n_p} \right)^{1/2} , \tag{2.95}$$

and this is typically small.

In addition to instabilities (a)-(d), there are resistive instabilities (resistive hose, sausage, hollowing, etc.).[28] We neglect these in the collisionless limit ($\nu\tau < 1$).

5. Channel formation and beam-head erosion

The analysis of the previous sections considered focussing of a long cigar shaped bunch, neglecting the details of channel evolution at the bunch head and tail (Fig. 2.3). We do not propose to treat this problem at length, merely to outline the issues involved.

In the discussion of Sec. A, we noted that the beam head always propagates in the weak magnetic-focussing regime. As a result, the beam head will expand due to emittance, self-fields, scattering, and decceleration due to

the induced axial electric field (longitudinal wake). In this way, the beam head gradually erodes.

These and other issues have been discussed in connection with erosion of long pulses injected into an unionized gas,[48] and for long pulses in a preionized plasma of radial extent comparable to the beam.[30] For this work, we will be interested in beams with relatively low emittance, and high energies (≥2 MeV), so that space charge effects are not dominant. Propagation lengths will be from centimeters to a few meters. In this limit, we will neglect erosion, since the plasma is preionized, the emittance is low, the energy is high, and the propagation length is short.

E. SUMMARY

In this chapter we have reviewed the basic features of REB propagation in unmagnetized, preformed plasma. We provided a working definition of the IFR, and delineated the features of the steady-state plasma electron flow, ion-collapse, and equilibrium beam propagation. We went on to consider the ion and electron hose instabilities and other deleterious plasma effects. The result of these considerations is a collection of practical constraints on IFR propagation.

We shall see in Chapters 3 and 4, that these constraints are important for a laser relying on IFR propagation. In practice, they force one to sacrifice pulse length for beam quality. Fortunately, as we shall see, efficiency and many other key figures of merit do not depend on pulse length.

There are a number of additional problems raised here that merit further work. Radiation from the plasma electrons during channel formation has not been addressed, and in light of Fig. 2.6(b), would be quite interesting. An analytical treatment of electron-hose in the limit of small skin depth ($V>>1$) remains to be performed. The utility of plasma heating via electron-hose in the IFR has not been assessed, but our simple estimate looks rather promising. In any case, it is evident from the work presented here that within the ion-focussed regime await many interesting and largely unaddressed problems for future work.

References

[1]Chen, K. Oide, A. M. Sessler and S. S. Yu, *Proceedings of the XIV International Conference on High Energy Accelerators*, Particle Accelerators, 31 (1990) pp. 7-19. See also Refs. 40 and 41 of Ch. 1.

[2] See Ref. 11, Ch. 1.

[3]In fact, if plasma electrons are not available to fill in the plasma after the beam has passed, then the tail is ion-focussed as well. This situation arises, for example, if, initally, insufficient plasma electron charge is created to balance the peak beam current. In this case, plasma electrons are expelled to the wall. Free plasma electrons are also destroyed if the pulse is sufficiently long for recombination or attachment. Indeed, this circumstance has been proposed by Briggs (Ref. 46, Ch. 1) as the basis for a novel wakefield accelerator.

[4]See Ref. 51, Ch.1.

[5]Not surprisingly, as we shall see in the next chapter, V serves to characterize the electromagnetic shielding or dielectric waveguide properties of the channel as well.

[6]This simple estimate, which assumes $n_e \sim n_p$, fails for $V>1$, implying the formation of a non-neutral, relativistic, plasma-electron sheath at high current, as we shall see below.

[7]I. S. Gradshteyn and I. M. Ryzhik, *Table of Integrals, Series, and Products*, translated by Alan Jeffrey, 4th ed., (Academic, New York, 1980), pp. 961.

[8]For singly-charged ions, $n_{i0}=n_p$, the initial plasma electron density. In general, $n_{i0}Z=n_p$, where Z is the average ion charge state.

[9]In Eq. (2.52), we have used the $V<<1$ result, in general one must use the solution of Eq. (2.30).

[10]Of course, when plasma electron collisions (or recombination or attachment) are added, the total beam energy is no longer conserved.

[11]K. L. F. Bane, *Physics of Particle Accelerators*, AIP Conf. Proc. **153**, edited by Melvin Month and Margaret Dienes (AIP, New York, 1987), pp. 972-1012.

[12]This is just the potential ψ, of the previous section, evaluated at $r=0$. The dependence on current is through the variable V. For simplicity we have considered the case $V\leq 1$, where this dependence is easily made explicit.. In general, it is straightforward to map ψ as a function of V, via numerical solution of Eq. (2.30) for a range of U.

We should also note, that, in general, there are additional terms varying on the ω_p^{-1} time-scale. These have been neglected in the limit $\omega_p\tau_r>>1$.

[13]In addition, the longitudinal wake produces a sweep in energy along the beam, but not a spread within a slice. Thus it will not result in damping of the fast-wave electromagnetic instabilities. However, in principle, it will tend to damp cumulative instabilities, in the "strong-focussing" regime, as discussed below, in Sec. C.

[14]This name arises from the original work on the "betatron". See, for example, Stanley Humphries, *Principles of Charged Particle Acceleration*, (John Wiley & Sons, New York, 1986).

[15]An additional advantage of continuous focussing for a TeV collider is the possibility of circumventing the "Oide limit" (Ref. 50, Ch. 1) on the spot size in a discrete focussing system.

[16]Note, however that focussing is non-linear and electrons at the beam edge see weaker focussing. Thus any estimate of k_β for a magnetically self-focussed beam is understood to be approximate.

[17]See Ref. 52, Ch.1, also G. Bonvicini, *et al.*, Phys. Rev. Lett. **62**, 2381 (1989).

[18]See Ref. 49, Ch.1.

[19]In general, this geometry may consist of dielectric, perfectly conducting, resistive, or free-space boundaries. In the most interesting cases, the problem of determining the electromagnetic modes is not analytically tractable and one resorts to numerical solution. See for example, J. DeFord, G. Craig, and R. McLeod, "The AMOS (Azimuthal Mode Simulation) Code, *Proceedings of the 1989 IEEE Particle Accelerator Conference*, edited by Floyd Bennett and Joyce Kopta, (IEEE, New York, 1989) pp. 1181-1183.

[20]Alexander W. Chao, *Physics of High Energy Particle Accelerators*, AIP Conf. Proc. **105**, edited by Melvin Month (AIP, New York, 1983), pp. 353-523.

[21]Typically these steepest descents calculations yield excellent agreement with the "exact" result computed numerically, even for only small growth. See for example, D. H. Whittum, A. M. Sessler and V. K. Neil, "Transverse resistive

resistive wall instability in the two-beam accelerator", Phys. Rev. A, (accepted for publication).

[22]W. K. H. Panofsky and M. Bander, Rev. Sci. Instrum. **39**, 206 (1968).

[23]V. K. Neil, L. S. Hall, and R. K. Cooper, Particle Accelerators **9**, 213 (1979).

[24]Y. Y. Lau, Phys. Rev. Lett. **63**, 1141 (1989).

[25]D. H. Whittum, G. A. Travish, A. M. Sessler, G. D. Craig, and J. F. DeFord, *Proceedings of the 1989 IEEE Particle Accelerator Conference*, edited by Floyd Bennett and Joyce Kopta, (IEEE, New York, 1989) pp. 1190-1192 .

[26]In addition, if the pulse length is long compared ot an rf period, then it may be short compared to a decay time for the mode (absolute instability), or long (convective instability). However, we have taken an infinite decay time in Eq. (2.66) and this distinction does not arise.

[27]V.E. Balakin, A.V. Novokhatsky, and V.P. Smirnov, *Proceedings of the 12th International Conference on High-Energy Accelerators*, edited by F.T Cole and R. Donaldson (Fermi National Accelerator Laboratory, Batavia, Illinois, 11-16 August 1984), pp. 119-120.

[28]E. P. Lee, Phys. Fluids **21**, 1327 (1978).

[29]D. H. Whittum, W. M. Sharp, S. S. Yu, M. Lampe, G. Joyce, "Electron-hose instability in the ion-focussed regime", (submitted to Phys. Rev. Lett.).

[30]H. L. Buchanan, Phys. Fluids, **30**, 221 (1987).

[31]L. J. Laslett, D. Mohl, and A. M. Sessler, *Proceedings of the Third All-Union National Conference on Particle Accelerators*, (Moscow, 1972).

[32]M. Lampe, W. Sharp, R. F. Hubbard, E. P. Lee, R. J. Briggs, Phys. Fluids **27**, 2921 (1984).

[33]R. J. Adler, B. B. Godfrey, M. M. Campbell, D. J. Sullivan, and T. C. Genoni, Particle Accelerators **13**, 25 (1983).

[34]Glenn Joyce and Martin Lampe (private communication).

[35]J. D. Jackson, *Classical Electrodynamics*, 2nd ed. (Wiley, New York, 1975).

[36]Evidently, scattering with neutral atoms dominates as long as $f < ln(a/r_n)/ln(b/r_n)$. This is typically the case for f ~10%, or less.

[37]B. W. Montague and W. Schnell, in *Laser Acceleration of Particles*, edited by Chan Joshi and Thomas Katsouleas, AIP Conf. Proc. **130**, (AIP, New York, 1985), p. 146.

[38]T. P. Hughes and B. B Godfrey, Phys. Fluids **27**, 1531 (1984).

[39]A. A. Sokolov and I. M. Ternov, *Radiation from Relativistic Electrons*, (AIP, New York, 1986).

[40]See Ref. 47, Ch.1.

[41]D.P. Murphy, M. Raleigh, R.E. Pechacek, and J. R. Grieg, Phys. Fluids **30**, 232 (1987).

[42]A. E. S. Green, Radiation Research **64**, 119 (1975); A. E. S. Green and T. Sawada, J. Atmos. Terr. Phys. **34**, 1719 (1972).

[43]P. Felsenthal, J. M. Proud, Phys. Rev. **139**, 1796 (1965).

[44]M. Mitchner and C. H. Kruger, Jr., *Partially Ionized Gases*, (Wiley, New York).

[45]F. J. Mehr and M. A. Biondi, Phys. Rev. **181**, 264 (1969).

[46]D. Prono, B. Ecker, N. Bergstrom, and J. Benford, Phys. Rev. Lett. **35**, 438 (1975); D. A. McArthur and J. W. Poukey, Phys. Rev. Lett. **27**, 1765 (1971).

[47]R. B. Miller, *Intense Charged Particle Beams*, (Plenum, New York, 1982).

[48]W. M. Sharp and M. Lampe, Phys. Fluids **23**, 2383 (1980).

Chapter 3:
Theory of the Ion-Channel Laser

". . . we are mere white horses of the sea . . ."
---Octavio Paz

"To disprove anything is very difficult,
but also to prove it."
---Hannes Alfven

In this chapter, we develop the theory of an ion channel "free-electron" laser amplifier (ICL),[1,2] consisting of a short pulse, low emittance REB copropagating in the IFR with an externally supplied electromagnetic wave. The ICL makes use of ion-focussing to transport the beam, and a resonance, akin to that of the planar wiggler FEL, to produce coherent radiation. Here, the wiggler is provided by the electrostatic field of the ion channel, analagous in some respects to the quadrupole FEL proposed by Levush, *et al.*[3,4,5]

In contrast to other proposed plasma-loaded rf devices,[6] no external magnets are used, and, in principle, no external structures (waveguides,

cavities) are required. However, in the microwave regime, the use of a waveguide can enhance the overlap of the beam and the rf signal, making the ICL comparable to the FEL as an rf power source.

In Sec. A, we briefly describe the concept, and the limitations of the theoretical model we will use. In Sec. B we develop an eikonal formalism rather simliar to that for the FEL. We derive the dispersion relation describing amplification in the initial exponential growth regime, and we assess the effect of spreads in axial momenta.

In Sec. C, we derive the dispersion relation by applying the method of characteristics to the Maxwell-Vlasov equations. We use this result as a check on the work of Sec. B and to assess the effect of detuning spread due to a realistic beam profile. From the work of Sec. B and C we will see that the Rayleigh length is typically rather short compared to the gain length, and so, in Sec. D, we go on to consider mechanisms which will guide the radiation.

In Sec. E, we summarize the scaling laws derived in Secs. B-D, and give some numerical examples. As a postscript, in Sec. F, we consider the modifications required to the theory of Sec. B, in the overdense regime. We also briefly discuss certain experimental evidence which shows some agreement with theory.

A. CONCEPT

The ICL consists of a tank of neutral gas, through which a plasma is produced, for example, by an ionizing laser pulse.[7] Within less than a recombination time, and with proper matching, as in a continuous plasma focus,[9] an REB is injected into the preformed plasma, propagating in the axial (+z) direction (Fig. 3.1). Co-propagating with the beam is an externally supplied electromagnetic wave.

We recall, from Chapter 2, that as the beam head propagates through the plasma, it expels plasma electrons from the beam volume, leaving fixed the relatively immobile ions to provide focussing for the remainder of the beam. For definiteness the beam density is assumed to be a step radial profile, with radius a. In this case, the unneutralized ions occupy a cylindrical volume of radius approximately $b \sim a(n_b/n_p)^{1/2}$ and this is the "ion channel", as depicted in Fig. 3.1(a).

As discussed in Ch. 2, it is assumed that the electrostatic pinch force due to this ion charge is much larger than the transverse force on the beam due to self-fields. This imposes the Budker condition[4] on the plasma density, $n_b > n_p > n_b/\gamma^2$, where n_b is beam density, n_p is the plasma density prior to channel formation, and γ is the beam Lorentz factor. As before, we assume adiabatic current rise ($\omega_p \tau_r >> 1$), and we neglect ion motion ($\omega_i \tau << 1$), where ω_p and ω_i are the electron and ion plasma frequencies.

In Ch. 2, Sec. B.3, we found that the zeroth order transverse motion of a beam electron is that of a relativistic, 2-D, simple harmonic oscillator subject to the potentials given by Eq. (2.46)

$$\phi = \phi(0) + \frac{1}{4}\left(k_b^2 - k_p^2\right)r^2 ,$$

$$a_z = a_z(0) + \frac{1}{4}k_b^2 r^2 .$$

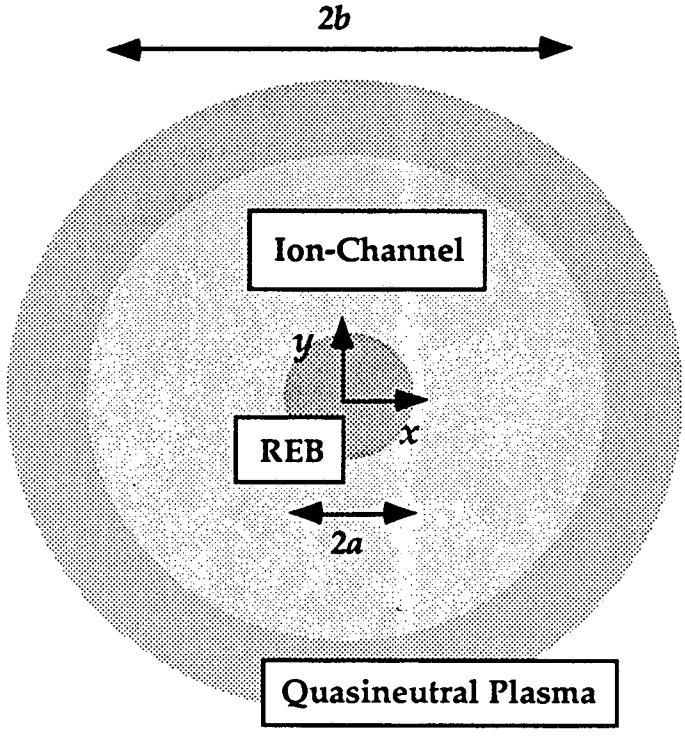

FIG. 3.1. (a)An REB, propagating through an underdense plasma, expels plasma electrons from the beam volume and beyond to produce an "ion-channel", which then focusses the beam, and causes it to radiate.

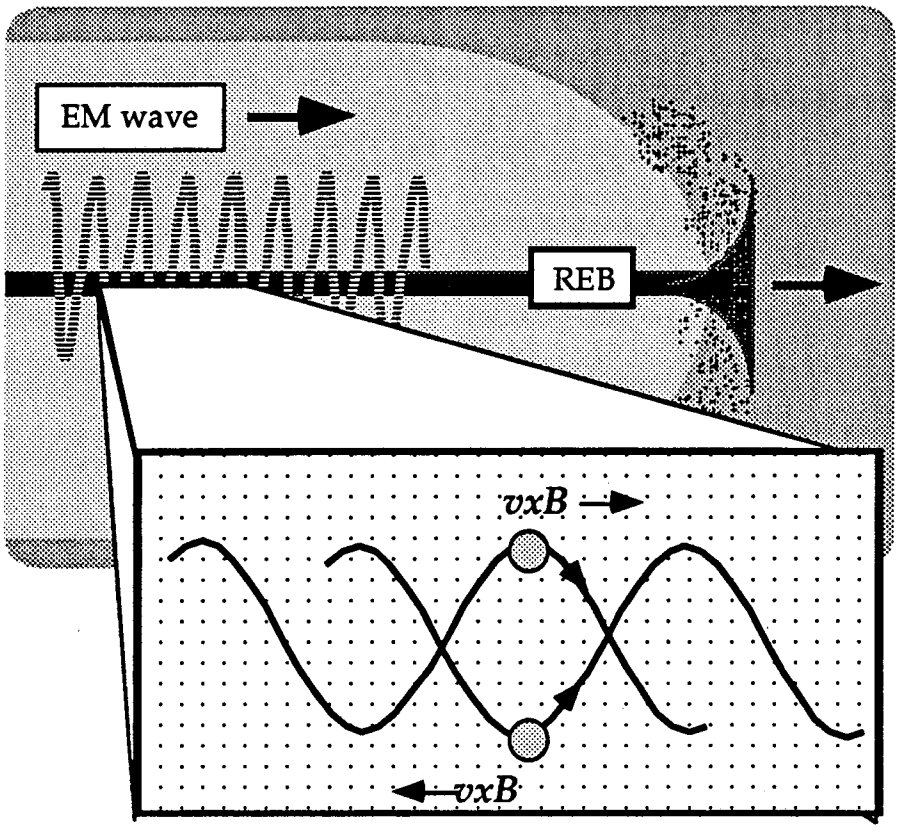

FIG. 3.1. (b)An electromagnetic wave copropagates with a relativistic electron beam in the ion-focussed regime. Beam electrons (indicated by circles in the inset) oscillate transversely (focussed by the ion electrostatic field), and are bunched axially by the ponderomotive force, much as in an FEL. This is essentially Fig. 2.3, with the addition of an electromagnetic wave.

The Hamiltonian was found to be (Eq. [2.50])

$$H \approx \underbrace{p_z c + \frac{m^2 c^3}{2 p_z}}_{H_{||}} + \underbrace{\frac{p_x^2 c}{2 p_z} + \frac{p_y^2 c}{2 p_z} + U}_{H_{\perp}}$$

where we identified the effective potential as (Eq. [2.51])

$$U = \frac{1}{4} m \omega_\beta^2 r^2 , \tag{3.1}$$

and we neglect small constants of integration. Inspection of the Lorentz force equation revealed that electrons undergo transverse oscillations at the "betatron frequency"[8] $\omega_\beta \sim \omega_p (mc/2p_z)^{1/2}$, where p_z is the axial momentum.

We turn now to consider the perturbation of the single particle motion by a linearly polarized electromagnetic wave.

B. EIKONAL FORMALISM

Now in the center of momentum frame, electrons are oscillating with upshifted frequency $\omega_1 \sim \gamma\omega_\beta$ and radiate incoherently. In the lab frame the frequency of radiation in the forward (+z) direction is $\omega \sim 2\gamma\omega_1 \sim 2\gamma^2\omega_\beta$.

In this section, we proceed to show that coherent radiation, near the frequency $\omega \sim 2\gamma^2\omega_\beta$, may be amplified. The essential feature of amplification is that an ensemble of relativistic simple harmonic oscillators, subject to a growing transverse electromagnetic wave, will give up energy to the field, through "axial bunching," if they are driven "weakly". Providing a definition of "weakly" and the sense in which it applies to a realistic beam is more or less the purpose of the detailed calculations which follow. "Axial bunching" refers to an induced correlation of longitudinal and betatron phase, which

corresponds to a coherent oscillation of the beam centroid. This will be described in some detail below.

1. Particle equations

To the equilibrium described in Sec. A, we introduce an electromagnetic wave linearly polarized in the y-direction, copropagating with the beam. We write the vector potential in terms of a dimensionless eikonal amplitude and phase, A and φ,

$$A_y = \frac{mc^2}{e} A \sin(\zeta) , \tag{3.2}$$

$$\zeta = k_z z - \omega t + \varphi . \tag{3.3}$$

The angular frequency is ω and the axial wavenumber is k_z. A and φ are assumed to vary slowly in time on the ω^{-1} scale, and in z on the k_z^{-1} scale.

The single-particle Hamiltonian is, in the limit $p_z >> p_x, p_y$, and neglecting second order terms in A,

$$H \approx \underbrace{p_z c + \frac{m^2 c^3}{2 p_z}}_{H_{||}} + \underbrace{\frac{p_x^2 c}{2 p_z} + \frac{p_y^2 c}{2 p_z} + U}_{H_\perp} + \underbrace{e \frac{p_y}{p_z} A_y}_{H_1} . \tag{3.4}$$

As indicated, the energy is a sum of the energy of the axial motion ($H_{||}$), the energy of the transverse motion ($H_\perp$) and a perturbation linear in the field

(H_1). The quantities p_x, p_y, and p_z are the canonical momenta in x, y, and z, respectively,

$$
\begin{aligned}
p_x &= m\gamma v_x \ , \\
p_y &= m\gamma v_y - \frac{e}{c}A_y \ , \\
p_z &= m\gamma v_z - \frac{e}{c}A_z \ , \\
\gamma &= \left\{1 - \frac{v_x^2 + v_y^2 + v_z^2}{c^2}\right\}^{-1/2} \ .
\end{aligned}
\tag{3.5}
$$

The particle velocity components are v_x, v_y, and v_z. Note that the correction to p_z due to A_z is typically small, $mca_z/p_z \sim v/\gamma$, where $v=I/I_0$ is Budker's parameter. We will neglect it in the following work, to take it up again in Sec. B.4 in the discussion of detuning spread.

The equations of motion derived from the Hamiltonian of Eq. (3.4) describe an electron drifting in z, subject to an axial "vxB" force as it oscillates in the potential well

$$
\begin{aligned}
\frac{dz}{dt} &= c - \frac{m^2 c^3}{2\,p_z^2} - \frac{p_x^2 c}{2\,p_z^2} - \frac{p_y^2 c}{2\,p_z^2} - mc^2 \frac{p_y}{p_z^2} A \sin(\zeta) \ , \\
\frac{dp_z}{dt} &= -k_z mc^2 \frac{p_y}{p_z} A \cos(\zeta) \ .
\end{aligned}
\tag{3.6}
$$

The y-motion consists of an oscillation in the ion channel potential, subject to the Lorentz force due to the signal field,

$$\frac{dy}{dt} = \frac{p_y}{p_z}c + \frac{mc^2}{p_z}A\sin(\zeta) ,$$
$$\frac{dp_y}{dt} = -\frac{1}{2}m\omega_p^2 y , \qquad (3.7)$$

and coupled to the z motion via p_z and A_y. The x-motion is a free oscillation in the potential well, which is however coupled to the axial motion via p_z (the relativistic mass effect),

$$\frac{dx}{dt} = \frac{p_x}{p_z}c ,$$
$$\frac{dp_x}{dt} = -\frac{1}{2}m\omega_p^2 x . \qquad (3.8)$$

In Eqs. (3.6)-(3.8), we have neglected derivatives of the slowly varying eikonal quantities, and their transverse gradients.

To make some progress in describing the particle motion, it is helpful to average over the rapid betatron motion. It is convenient to introduce dimensionless variables q_z, q_x, θ_x, q_y, and θ_y, such that

$$p_x = mcq_x \sin(\theta_x) ,$$
$$p_y = mcq_y \sin(\theta_y) ,$$
$$p_z = mcq_z . \qquad (3.9)$$

For A=0, q_x and q_y are constants and $d\theta_{x,y}/dt=\omega_\beta$. With averaging, Eq. (3.6) becomes

$$\frac{1}{c}\left\langle\frac{dz}{dt}\right\rangle = 1 - \frac{1}{2q_z^2} - \frac{q_x^2}{2q_z^2}\left\langle\sin^2(\theta_x)\right\rangle - \frac{q_y^2}{2q_z^2}\left\langle\sin^2(\theta_y)\right\rangle - \frac{q_y}{q_z^2}A\left\langle\sin(\zeta)\sin(\theta_y)\right\rangle,$$
$$\left\langle\frac{dq_z}{dt}\right\rangle = -k_z c\frac{q_y}{q_z}A\left\langle\cos(\zeta)\sin(\theta_y)\right\rangle, \tag{3.10}$$

where the angle brackets indicate the average over the betatron period. Noting the identities

$$\sin(\zeta)\sin(\theta_y) = \frac{1}{2}\left(\cos(\theta_y - \zeta) - \cos(\theta_y + \zeta)\right),$$
$$\cos(\zeta)\sin(\theta_y) = \frac{1}{2}\left(\sin(\theta_y + \zeta) + \sin(\theta_y - \zeta)\right), \tag{3.11}$$

we see that the averages will depend on the time variations of $\theta_y \pm \zeta$. In this connection we will neglect "jitter" in the axial motion, namely, that in the frame of reference co-moving with the beam (the "beam frame"), electrons execute a figure eight motion as they oscillate transversely, alternately slowing and speeding up with frequency $2\omega_\beta$, as they "climb" or "descend" the ion-channel potential. Specifically, the zeroth-order motion in z is

$$z = z_i + \bar{v}_z t + \frac{\xi_x}{k_z}\sin(2\theta_x) + \frac{\xi_y}{k_z}\sin(2\theta_y),$$
$$z_i = z_0 - \frac{\xi_x}{k_z}\sin(2\theta_{x0}) - \frac{\xi_y}{k_z}\sin(2\theta_{y0}). \tag{3.12}$$

where $z_0 = z(t=0)$, and the dimensionless quantities $\xi_{x,y}$ are given by

$$\xi_{x,y} = \frac{1}{8}\frac{k_z}{k_\beta}\frac{q_{x,y}^2}{q_z^2} \quad . \tag{3.13}$$

The quantity

$$\begin{aligned} \bar{v}_z &= c\left\{1 - \frac{2 + q_x^2 + q_y^2}{4 q_z^2}\right\} \\ &= c\left\{1 - \frac{1 + q_z h}{2 q_z^2}\right\} \end{aligned} \quad , \tag{3.14}$$

is the drift velocity in z, at zeroth order, averaged over the betatron period, and $h=H_\perp/mc^2$.

The effect of this jitter in z is to couple the beam to odd harmonics (angular frequencies ω' satisfying $\omega'-k_z v_z=(2n+1)\omega_\beta$, with n a non-zero integer). We will consider the limit $\xi_{x,y}<1$, and neglect these higher harmonics. From Eq. (3.13) we see that this is roughly the approximation that $q_x, q_y<1$, corresponding to a transverse motion which is nonrelativistic in the beam frame.

In addition we assume that the phase variable

$$\psi = \theta_y + \zeta \ , \tag{3.15}$$

is slowly varying on the time scale ω_β^{-1}, ie., the "detuning" parameter $\Delta\omega$,

$$\Delta\omega = k_z\bar{v}_z - \omega + \omega_\beta$$
$$= k_z c\left\{1 - \frac{1 + q_z h}{2q_z^2}\right\} - \omega + \frac{\omega_p}{\sqrt{2q_z}}, \qquad (3.16)$$

is small compared to ω_β. ψ represents the phase of the transverse motion measured with respect to the phase of the radiation field. For a fast wave, the condition, $\Delta\omega << \omega_\beta$ corresponds to an angular frequency $\omega \sim 2\gamma^2\omega_\beta$. Note that detuning depends only on q_z and h, not q_x or q_y individually. Thus the distribution in detuning may be determined in simple way from the Boltzmann distribution function for the beam. For the step radial profile, the distribution function is a delta function in h and q_z, and there is no spread in $\Delta\omega$.

The resonance condition $\omega \sim 2\gamma^2\omega_\beta$ states that the Doppler shifted frequency of the signal field, in the beam frame should be close to the frequency of transverse oscillation of the electrons in that frame. In this way the electron is resonantly driven and suffers a secular perturbation in its orbit ("bunching").

With these assumptions, Eq. (3.10) becomes

$$\frac{1}{c}\left\langle\frac{dz}{dt}\right\rangle = 1 - \frac{1}{2q_z^2} - \frac{q_x^2}{4q_z^2} - \frac{q_y^2}{4q_z^2} + \frac{1}{2}\frac{q_y}{q_z^2}A\cos(\psi);$$
$$\left\langle\frac{dq_z}{dt}\right\rangle = -\frac{1}{2}k_z c\frac{q_y}{q_z}A\sin(\psi), \qquad (3.17)$$

To average Eqs. (3.7) and (3.8) we differentiate, eliminating x and y,

$$\frac{d^2 p_x}{dt^2} + \frac{m\omega_p^2 c}{2 p_z} p_x = 0 \ ,$$
$$\frac{d^2 p_y}{dt^2} + \frac{m\omega_p^2 c}{2 p_z} p_y = -\frac{m^2 \omega_p^2 c^2}{2 p_z} A \sin(\zeta) \ . \tag{3.18}$$

Substituting the dimensionless eikonal variables of Eq. (3.18) then gives

$$\ddot{q}_y \sin(\theta_y) + 2\dot{q}_y\dot{\theta}_y \cos(\theta_y) + q_y\ddot{\theta}_y \cos(\theta_y) - q_y \sin(\theta_y)\dot{\theta}_y^2 + \omega_\beta^2 q_y \sin(\theta_y) = -\omega_\beta^2 A \sin(\zeta) \ , \tag{3.19}$$

and simlilarly for x. Here, the dot denotes the derivative with respect to t. Averaging these equations over the betatron period then gives,

$$\ddot{q}_x - q_x\dot{\theta}_x^2 + \omega_\beta^2 q_x = 0 \ ,$$
$$2\dot{q}_x\dot{\theta}_x + q_x\ddot{\theta}_x = 0 \ ,$$
$$\ddot{q}_y - q_y\dot{\theta}_y^2 + \omega_\beta^2 q_y = \omega_\beta^2 A \cos(\psi) \ ,$$
$$2\dot{q}_y\dot{\theta}_y + q_y\ddot{\theta}_y = -\omega_\beta^2 A \sin(\psi) \ . \tag{3.20}$$

At first order in A, these equations reduce to

$$\frac{d\theta_x}{dt} = \omega_\beta ,$$
$$\frac{dq_x}{dt} = -\frac{q_x}{2\omega_\beta}\frac{d\omega_\beta}{dt} ,$$
$$\frac{d\theta_y}{dt} = \omega_\beta\left(1 - \frac{A}{2q_y}\cos(\psi)\right) ,$$
$$\frac{dq_y}{dt} = -\frac{q_y}{2\omega_\beta}\frac{d\omega_\beta}{dt} - \frac{1}{2}\omega_\beta A \sin(\psi) , \qquad (3.21)$$

and we have formally neglected electrons with $q_y \sim O(A)$ or smaller. In Sec. 2.b. we will show that Eq. (3.21) is valid even in the limit $q_y \rightarrow 0$. Roughly, this is because all terms varying as $1/q_y$ are eventually multiplied by q_y, i.e., the complex eikonal variable $q_y exp(i\theta_y)$, is always well-defined, even if the phase is varying rapidly. The apparent divergence at $q_y \rightarrow 0$ simply shows that θ_y adjusts rapidly to a phase determined by the wave, independent of $\theta_y(0)$ and $q_y(0)$.

Combining these results and eliminating z in favor of ψ, the equations of motion take a form reminiscent of that found by Kroll *et al.*, for the FEL,[9]

$$\frac{d\psi}{dt} = k_z v_z - \omega + \frac{d\theta_y}{dt} + \frac{d\varphi}{dt} + \frac{1}{2}k_z c \frac{q_y}{q_z^2} A \cos(\psi), \tag{3.22}$$

$$\frac{d\theta_y}{dt} = \omega_\beta \left(1 - \frac{1}{2q_y} A \cos(\psi)\right), \tag{3.23}$$

$$\frac{dq_z}{dt} = -\frac{1}{2}k_z c \frac{q_y}{q_z} A \sin(\psi), \tag{3.24}$$

$$\frac{dq_y}{dt} = -\frac{1}{2}\left(\omega_\beta + \frac{1}{4}k_z c \frac{q_y^2}{q_z^2}\right) A \sin(\psi), \tag{3.25}$$

$$\frac{dq_x}{dt} = -\frac{1}{8}k_z c \frac{q_y q_x}{q_z^2} A \sin(\psi). \tag{3.26}$$

It is evident that ψ determines the sign and magnitude of all the perturbative effects of the field. In general, Eq. (3.22) shows that evolution of ψ is dominated by variation in v_z and θ_y, (since the first order term in Eq. (3.22) is small) which are themselves determined by variation in q_z, q_x and q_y. For a fast-wave ($\omega=ck_z$) Eq. (3.24) describes the slowing of particles with $\psi>0$ and the acceleration of particles with $\psi<0$, due to the z-component of the Lorentz force (the ponderomotive force). It is worth noting that, in general, dv_z/dt and dq_z/dt may have opposite signs depending on the wave phase velocity $\beta_\varphi=\omega/ck_z$. Differentiating Eq. (3.14), and using Eqs. (3.24) and (3.25), we find (neglecting $q_{x,y}<<1$)

$$\frac{1}{c}\frac{d\bar{v}_z}{dt} \approx -\frac{1}{2}k_z c \frac{q_y}{q_z^4}\left[1 - \frac{q_z^2}{2}\left(\beta_\varphi - \frac{v_z}{c}\right)\right] A \sin(\psi)$$

Thus for $\beta_\varphi > v_z/c + 2/q_z^2$, particles may be accelerated in z (due to a loss of transverse energy), while losing axial momentum. In fact, as we shall see below, $dH/dt = mc^2\beta_\varphi(dq_z/dt)$, so that in this case the total particle energy is decreasing as well.

The first term on the right in Eq. (3.25), as well as the first-order term in Eq. (3.23), are due to the y-component of the Lorentz force. These terms arise from the resonant perturbation of the transverse motion. In an FEL this effect is small; here, it will be non-negligible. The remaining terms in Eqs. (3.25) and (3.26) are due to the relativistic mass effect. The amplitude of the transverse motion drifts due to variation in ω_β, which varies with q_z.

2. Particle motion in a prescribed field

To gain some insight into these equations, we consider the motion of a test particle under the influence of a prescribed eikonal. We observe from Eqs. (3.22) and (3.23),

$$\frac{d\psi}{dt} = k_z\bar{v}_z - \omega + \omega_\beta + \frac{d\varphi}{dt} - \frac{\omega_\beta}{2q_y}A\cos(\psi) + \frac{1}{2}k_z c\frac{q_y}{q_z^2}A\cos(\psi)$$
$$\approx \frac{d\varphi}{dt} + \Delta\omega - \Pi A\cos(\psi) \quad , \quad (3.27)$$

where the parameter Π is given by

$$\Pi = \frac{\omega_\beta}{2 q_y} , \tag{3.28}$$

and arises from the θ_y variation of Eq. (3.23). This shows that particles with small q_y can be significantly "detuned" from resonance. This is because the phase of a driven harmonic oscillator varies rapidly when its initial amplitude is small.

Examining Eq. (3.27) it is tempting to think of $\Delta\omega>0$ as corresponding to a particle with energy "above resonance", as in an FEL. However, from Eq. (3.16) we see that $\Delta\omega$ depends on both v_z, (which increases with q_z) and ω_β, which decreases with q_z. Thus higher energy particles drift faster in z, but they oscillate more slowly. Depending on the wave phase velocity, more energetic particles may actually be below resonance, i.e., have $\Delta\omega<0$.

a. Bounce motion. To make this more precise, we differentiate Eq. (3.27) and subsititute from Eqs. (3.23)-(3.26), to obtain,

$$\frac{d^2\psi}{dt^2} \approx - \left\{ \Xi - \Pi \frac{d\psi}{dt} \right\} A \sin(\psi) - \Pi \frac{dA}{dt} \cos(\psi) , \tag{3.29}$$

where the "bunching" parameter Ξ is

$$\Xi = \frac{(k_z c)^2}{4 q_z^4} q_y \left\{ 2 + \frac{3}{4}(q_x^2 + q_y^2) - 2 \frac{\omega_\beta}{k_z c} q_z^2 \right\} ,$$

or

$$\Xi \approx \frac{(k_z c)^2}{2 q_z^4} q_y \left\{1 - \frac{\omega_\beta}{k_z c} q_z^2\right\} \tag{3.30}$$

This parameter describes the dependence of detuning on energy, including the relativistic mass effect, and the effect of the y-component of the Lorentz force, from Eq. (3.25). Evidently Σ depends sensitively on $k_z c$. For $\omega = k_z c$, $\Xi \sim \omega_\beta^2 q_y$, while $\Sigma = 0$ for $k_z c \sim \omega_\beta q_z^2$. In terms of the phase velocity the condition for $\Sigma = 0$ may be written

$$\beta_\varphi \approx \frac{\bar{v}_z}{c}\left(1 - \frac{1}{q_z^2}\right)^{-1}, \tag{3.31}$$

where we have set $\Delta\omega = 0$. Typically, such a phase velocity corresponds to a group velocity close to v_z. Thus Ξ varies from a value which (as it will turn out) is appreciable, to zero over a very small range of phase velocity $1 < \beta_\varphi < 1 + 1/2q_z^2$.

For A constant, Eq. (3.27) simplifies to

$$\frac{d^2\psi}{dt^2} = -\Sigma A \sin(\psi), \tag{3.32}$$

where $\Sigma=\Xi-\Pi\Delta\omega$. Thus ψ oscillates as in a nonlinear pendulum, a behavior reminiscent of the FEL or RF linac.[40] Equation (32) differs from the usual FEL result in an important way, however, in that Σ may in principle be negative. This feature is due to an extra degree of freedom, the y-motion, which is strongly coupled to the axial motion. (In the FEL the y-motion is prescribed to a good approximation.)

Inspecting Eq. (3.32) we note that the stable point for small oscillations is either $\psi=0$ or $\psi=\pi$ depending on whether $\Sigma>0$ or $\Sigma<0$. Considering first the fast-wave limit ($\omega\sim k_z c$), and using $\Xi\sim\omega_\beta^2 q_y$, we have

$$\Sigma \approx \omega_\beta^2 q_y \left\{1 - \frac{\delta}{2q_y^2}\right\}, \tag{3.33}$$

where we define the dimensionless detuning $\delta=\Delta\omega/\omega_\beta$. Thus, in general, the beam divides into two ensembles. Particles with $\delta>2q_y^2$ have stable point $\psi\sim\pi$, while those with $\delta<2q_y^2$ have stable point $\psi\sim0$. Furthermore, within each ensemble particles have an intrinsic spread in bounce frequency. This is quite different from the result for the FEL, where Ξ is replaced by a term proportional to the wiggler parameter, which is the same for all particles.

Note that for a beam with uniform $\delta<0$, *all* particles have stable point $\psi\sim0$. Conversely one may show that for a beam with uniform $\delta>0$, and for a wave with phase velocity larger than that given by Eq. (3.31), so that $\Xi<0$, *all* particles have stable point $\psi\sim\pi$.

From this discussion it is evident that, in general, the details of the bounce motion depends in detail on the wave phase velocity, through the bunching parameter. For example, in the slow-wave limit ($\omega >> k_z c$), Eq. (3.30) gives

$$\Xi \approx -\frac{1}{2}\omega_\beta k_z c \frac{q_y}{q_z^2} \quad , \tag{3.34}$$

so that

$$\Sigma \approx -\frac{1}{2}\omega_\beta k_z c \frac{q_y}{q_z^2}\left\{1 + \frac{\delta}{q_y^2}\frac{\omega_\beta q_z^2}{k_z c}\right\} . \tag{3.35}$$

Thus $\Sigma<0$, except for particles with $\delta<-q_y^2 k_z c/\omega_\beta q_z^2$. This result for Σ is lower than the fast-wave result by a factor of order $O(ck_z/2q_z^2\omega_\beta)$.

In general, the period of small oscillations ("bounce period") about $\psi \sim 0$ or π, is $2\pi/\Omega_0$ where, $\Omega_0^2 = |\Sigma| A$. For $\Sigma>0$, we may describe this motion with a bounce Hamiltonian

$$H_B = \frac{1}{2} p_\psi^2 + \Omega_0^2 (1 - \cos(\psi)) \quad , \tag{3.36}$$

where $p_\psi = d\psi/dt$ and at zeroth order $p_\psi \sim \Delta\omega$. (For $\Sigma<0$ the same description applies, with ψ interpreted as $\psi - \pi$). Unlike the case for the FEL, such a

Hamiltonian does not describe the motion of all particles, merely those with the prescribed values of δ and q_y.

Defining a dimensionless parameter $k^2=H_B/2\Omega_0^2$, we observe that the motion in ψ is bound for $k^2<1$, and unbound for $k^2>1$. For bound orbits the maximum excursion ψ_m is given by

$$cos(\psi_m) = 1 - \frac{H_B}{\Omega_0^2}, \tag{3.37}$$

or $sin(\psi_m/2)=k$. In either case, we may define the invariant action for the bounce motion,

$$J_B = \frac{1}{2\pi}\oint p_\psi d\psi, \tag{3.38}$$

where the integral is over a period of the motion. More explicitly, for bound orbits,

$$\begin{aligned} J_B &= \frac{2^{3/2}}{\pi}\Omega_0 \int_0^{\psi_m} d\psi \sqrt{cos(\psi) - cos(\psi_m)} \\ &= \frac{8}{\pi}\Omega_0 \int_0^{\pi/2} d\theta \frac{k^2 cos^2(\theta)}{\sqrt{1 - k^2 sin^2(\theta)}} \\ &= \frac{8}{\pi}\Omega_0 \{E(k^2) - (1 - k^2) K(k^2)\}, \end{aligned} \tag{3.39}$$

where $sin(\theta)=sin(\psi/2)/sin(\psi_m/2)$ and K and E are the complete elliptic integrals of the first and second kind.[10] For $\psi_m<<1$, $J_B \sim H_B/\Omega_0=0.5\Omega_0\psi_m^2$. For a slowly growing eikonal, Ω_0 increases, and the amplitude of small oscillations varies according to, $\psi_m \propto 1/\Omega_0^{1/2} \propto 1/A^{1/4}$. Thus particles are adiabatically bunched within the ponderomotive well (or "bucket") described by H_B. For larger amplitude oscillations, Eq. (3.39) must be inverted to obtain the variation in bounce amplitude ψ_m as a function of Ω_0.

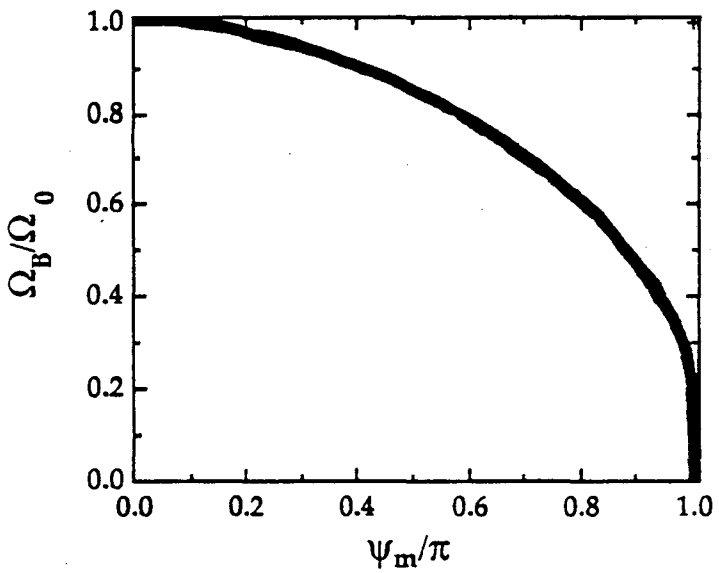

FIG. 3.2. Variation of bounce frequency with maximum excursion in ψ_m.

The angular frequency is

$$\Omega_B = \left\{ \frac{\partial J_B}{\partial H_B} \right\}^{-1} = \Omega_0 \frac{\pi}{2K(k^2)}, \tag{3.40}$$

and varies from Ω_0 for ψ_m small, to 0 for a particle with $\psi_m \sim \pi$, as depicted in Fig. 3.2. In the FEL, a similar bounce motion results in the amplification of frequencies in the range ω-Ω_0 to ω+Ω_0 ("sideband" instability). In the ICL, due to the intrinsic spread in Ω_0, one may expect a qualitatively different result for sideband growth.

Before leaving this section, we note, from Eq. (3.27), that in order for particles to bunch about $\psi \sim 0$ ($\Sigma > 0$), we must have $d\varphi/dt + \Delta\omega > 0$ on average. For stable point $\psi \sim \pi$ ($\Sigma < 0$), on the other hand we must have $d\varphi/dt + \Delta\omega < 0$ on average. This is because particles are being continually detuned from resonance by the transverse Lorentz force, with a sign depending on the wave phase velocity. Further insight into the importance of this detuning can be gained by examining the ponderomotive force in detail.

b. Ponderomotive force In the previous section we took the eikonal to be rigorously constant. Inspecting Eq. (3.29), however, we see that even a very small growth rate will alter the motion, in ψ, of particles with small q_y. This is because the phase of their transverse motion is determined for the most part by the wave, and not the initial values of q_y and θ_y. In this section, we examine such effects in detail. We take an exponentially growing eikonal since, as we shall find in the next section, the self-consistent solution of

Maxwell's equations is well-described by a sum of such terms, prior to saturation.

In principle, we can treat this problem most expeditiously through Eqs. (3.22)-(3.26). However, it is instructive and useful as a check of the eikonal equations, to solve the problem directly, using the full equations of motion.

We adopt a complex eikonal variable B given by

$$\begin{aligned} B &= A e^{i\varphi} \\ &= B_0 \exp(\Gamma t) , \end{aligned} \tag{3.41}$$

where $\Gamma=\Gamma_r+i\Gamma_i$ may be complex. In this case, $dA/dt=\Gamma_r A$, and $d\varphi/dt=\Gamma_i$. We assume that $|\Gamma|<<\omega_\beta$ so that growth is adiabatic on the betatron time-scale.

We proceed to solve for the particle motion directly from the Hamilonian of Eq. (3.8). The equations of motion are Eqs. (3.6) and (3.18):

$$\begin{aligned} \frac{dz}{dt} &= c - \frac{m^2 c^3}{2 p_z^2} - \frac{p_x^2 c}{2 p_z^2} - \frac{p_y^2 c}{2 p_z^2} - m c^2 \frac{p_y}{p_z^2} A \sin(\zeta) , \\ \frac{dp_z}{dt} &= - k_z m c^2 \frac{p_y}{p_z} A \cos(\zeta) . \\ \frac{d^2 p_x}{dt^2} &+ \omega_\beta^2 p_x = 0 , \\ \frac{d^2 p_y}{dt^2} &+ \omega_\beta^2 p_y = -mc\omega_\beta^2 A \sin(\zeta) . \end{aligned} \tag{3.42}$$

We adopt dimensionless complex variables, $p_j=mcIm(Q_j)$ for $j=x,y,z$. Since ω_β is slowly varying, the solution for the x-motion is just the WKB result,

$$Q_x = \left(\frac{\omega_{\beta 0}}{\omega_\beta}\right)^{1/2} q_{x0}\, exp\left(i\theta_{x0} + i\int_0^t dt'\omega_\beta(t')\right), \tag{3.43}$$

and we abbreviate $\theta_{x0}=\theta_x(0)$, $q_{x0}=q_x(0)$ and $\omega_{\beta 0}=\omega_\beta(0)$. To solve for the y-motion, we write decompose it into a sum of a free and a driven oscillation, $Q_y=Q_{yf}+Q_{yd}$, with Q_{yd} and dQ_{yd}/dt vanishing at t=0. These quantities obey,

$$\begin{aligned}
&\frac{d^2Q_{yf}}{dt^2} + \omega_\beta^2 Q_{yf} = 0\ , \\
&\frac{d^2Q_{yd}}{dt^2} + \omega_\beta^2 Q_{yd} = -\omega_\beta^2 A\, e^{i\zeta}\ .
\end{aligned} \tag{3.44}$$

The solution for the free-oscillation is just

$$Q_{yf} = \left(\frac{\omega_{\beta 0}}{\omega_\beta}\right)^{1/2} q_{y0}\, exp\left(i\theta_{y0} + i\int_0^t dt'\omega_\beta(t')\right), \tag{3.45}$$

where we abbreviate $\theta_{y0}=\theta_y(0)$, and $q_{y0}=q_y(0)$. Next we define $\Omega=\omega-k_z v_z+i\Gamma$, and rewrite the Q_{yd} equation as

$$\frac{d^2Q_{yd}}{dt^2} + \omega_\beta^2 Q_{yd} = -\omega_\beta^2 B_0\, exp(-i\Omega t + ik_z z_0 + i\zeta_1)\ . \tag{3.46}$$

The term $\zeta_1=k_z z_1$, where z_1 is the $O(A)$ drift in z. This may be neglected in Eq. (3.46) at first order in A. In addition, we neglect the variation in ω_β, at $O(A)$. Then we have

$$Q_{yd} \approx \frac{\omega_\beta^2}{\Omega^2 - \omega_\beta^2} B_0 \, exp(ik_z z_0) exp(-i\Omega t) \tag{3.47}$$

and we neglect terms which are small for times $t>1/\Gamma_r$. Using

$$\Omega^2 - \omega_\beta^2 \approx 2i\omega_\beta (i\Delta\omega + \Gamma) \tag{3.48}$$

Eq. (3.47) simplifies to

$$Q_{yd} \approx -i \frac{\omega_\beta}{2(i\Delta\omega + \Gamma)} B_0 \, exp(ik_z z_0 - i\Omega t) \tag{3.49}$$

Combining Eq. (3.45) and (3.49) we may write out explicitly the solution for the eikonal variables θ_y and q_y, defined in the previous section. We have

$$q_y(t) exp(i\theta_y(t)) = \left(\frac{\omega_{\beta 0}}{\omega_\beta}\right)^{1/2} q_{y0} exp\left(i\theta_{y0} + i\int_0^t dt' \omega_\beta(t')\right) + \rightarrow$$
$$- i \frac{\omega_\beta}{2(i\Delta\omega + \Gamma)} B_0 \, exp(ik_z z_0 - i\Omega t) \tag{3.50}$$

It is straightforward to show that this is the same solution one obtains using Eqs. (3.23) and (3.25). Thus, Eq. (3.50) confirms the eikonal equations for the y-motion, including the limit $q_y \to 0$.

The equation for Q_z is

$$\begin{aligned}\frac{dQ_z}{dt} &= -ik_z c\,\frac{p_y}{p_z} A e^{i\zeta} \\ &= \frac{-ik_z c}{q_z}\Im(Q_{yf} + Q_{yd})\, B_0\, exp(-i\Omega t + ik_z z_0 + i\zeta_1) \\ &= \frac{-ik_z c}{q_z}\left\{\Im(Q_{yf})(1 + i\zeta_1) + \Im(Q_{yd})\right\} B_0\, exp(-i\Omega t + ik_z z_0)\end{aligned}, \qquad (3.51)$$

and $q_z = Im(Q_z)$. We have neglected a q_{z1} term which is small in the limit $q_x, q_y << 1$. Neglecting jitter in z_1, we average this over a betatron period. It is useful to write Q_z as a sum of a first-order term and a second-order term, $Q_z = Q_{z1} + Q_{z2}$, where

$$\begin{aligned}\frac{dQ_{z1}}{dt} &= -\frac{k_z c}{2q_z} q_{y0}\left(\frac{\omega_{\beta 0}}{\omega_\beta}\right)^{1/2} B_0 e^{i\Psi_0}, \\ \frac{dQ_{z2}}{dt} &= -\frac{k_z c}{2q_z} q_{y0}\left(\frac{\omega_{\beta 0}}{\omega_\beta}\right)^{1/2} B_0 e^{i\Psi_0} i(\zeta_1 + \Psi_1) + i\frac{k_z c}{4q_z}\frac{\omega_\beta}{(-i\Delta\omega + \Gamma')}|B(t)|^2,\end{aligned} \qquad (3.52)$$

and we have defined phase variables

$$\Psi_0 = \theta_{y0} + i\,\omega_{\beta 0} t - i\Omega t + i k_z z_0 ,$$
$$\Psi_1 = \int_0^t dt' \left\{ \omega_\beta(t') - \omega_{\beta 0} \right\} . \tag{3.53}$$

Note that the phases Ψ_0 and Ψ_1 are slowly varying quantities, since $d\Psi_0/dt=\Delta\omega-i\Gamma$, and $d\Psi_1/dt=\omega_\beta-\omega_{\beta 0}$. Using Eq. (3.52) for Q_{z1} we can solve for Ψ_1 and ζ_1 (which replaces the variable z_1). For Ψ_1 we have, differentiating Eq. (3.53) twice,

$$\begin{aligned} \frac{d^2\Psi_1}{dt^2} &= \frac{d\,\omega_\beta}{dt} \\ &= -\frac{\omega_\beta}{2q_z}\frac{dq_z}{dt} \\ &= \frac{k_z c\,\omega_\beta}{4q_z^2} q_{y0}\,\Im\left(B_0 e^{i\Psi_0}\right) . \end{aligned} \tag{3.54}$$

The solution is

$$\Psi_1 \approx \frac{k_z c\,\omega_\beta}{4q_z^2} q_{y0}\,\Im\left(B_0 e^{i\Psi_0}\frac{1}{(i\Delta\omega+\Gamma)^2}\right), \tag{3.55}$$

neglecting small terms.

We obtain an equation for ζ_1 from Eq. (3.42), after differentiating once,

$$\frac{1}{k_z c}\frac{d^2\zeta_1}{dt^2} = \frac{d}{dt}\left(-\frac{1}{2q_z^2}\left\{1+\frac{\langle p_x^2+p_y^2\rangle}{m^2c^2}\right\}\right)$$
$$= \frac{1}{q_z^3}\frac{dq_z}{dt} - \frac{1}{2q_z^2}\frac{d}{dt}\frac{\langle p_x^2+p_y^2\rangle}{m^2c^2}, \tag{3.56}$$

where the brackets indicate an average over the betatron period and we neglect the small term proportional to $sin(\zeta)$ in Eq. (3.42). The averages are

$$\frac{\langle p_x^2\rangle}{m^2c^2} = \left[\frac{1}{2}\left(\frac{\omega_{\beta 0}}{\omega_\beta}\right)q_{x0}^2\right],$$
$$\frac{\langle p_y^2\rangle}{m^2c^2} = \left[\frac{1}{2}\left(\frac{\omega_{\beta 0}}{\omega_\beta}\right)q_{y0}^2\right] + \left(\frac{\omega_{\beta 0}}{\omega_\beta}\right)^{1/2} q_{y0}\,\Re\left\{\frac{i\omega_\beta}{2(i\Delta\omega+\Gamma)}B_0 e^{i\Psi_0}\right\}, \tag{3.57}$$

and we neglect second order terms. The terms in square brackets are small and will be neglected below. The derivatives are

$$\frac{d}{dt}\frac{\langle p_x^2\rangle}{m^2c^2} = \frac{1}{4}\frac{q_{x0}^2}{q_z}\frac{dq_z}{dt},$$
$$\frac{d}{dt}\frac{\langle p_y^2\rangle}{m^2c^2} = \frac{1}{4}\frac{q_{y0}^2}{q_z}\frac{dq_z}{dt} - \frac{1}{2}\omega_\beta q_{y0}\,\Im\left\{B_0 e^{i\Psi_0}\right\} \tag{3.58}$$

Substituting this in Eq. (3.56) gives

$$\frac{1}{k_z c}\frac{d^2\zeta_1}{dt^2} = \frac{1}{q_z^3}\left\{1-\frac{1}{8}(q_{x0}^2+q_{y0}^2)\right\}\frac{dq_z}{dt} + \omega_\beta\frac{q_{y0}}{4q_z^2}\Im\left(B_0 e^{i\Psi_0}\right). \tag{3.59}$$

From Eq. (3.52), using $q_z=Im(Q_z)$, we have at first order,

$$\frac{dq_z}{dt} = -\frac{k_z c}{2q_z} q_{y0}\,\Im\left(B_0 e^{i\Psi_0}\right)$$

Combining this result with Eq. (3.59) then gives,

$$\frac{d^2\zeta_1}{dt^2} = -\Xi'\Im\left(B_0 e^{i\Psi_0}\right), \tag{3.60}$$

where the parameter Ξ' is given by

$$\Xi' = \frac{(k_z c)^2}{2q_z^4} q_{y0}\left\{1 - \frac{\omega_\beta}{2k_z c} q_z^2\right\} \tag{3.61}$$

and we neglect $q_x, q_y << 1$. Ξ' differs from the bunching parameter Ξ of Eq. (3.30) because ψ includes θ_y in its definition, while ζ_1 does not (this is subsumed in Ψ_1). Integrating Eq. (3.59) we have

$$\zeta_1 = -\Xi'\Im\left(B_0 e^{i\Psi_0}\frac{1}{(i\Delta\omega + \Gamma)^2}\right). \tag{3.62}$$

Adding this result to that of Eq. (3.55) we have

$$\zeta_1 + \Psi_1 = -\Xi\,\Im\left(B_0 e^{i\Psi_0}\frac{1}{(i\Delta\omega + \Gamma)^2}\right), \tag{3.63}$$

where Ξ is the bunching parameter of Eq. (3.30).

Next, we substitute this result in Eq. (3.52), for Q_{z2}, to determine the axial ponderomotive force on a beam slice. We find

$$\left\langle \frac{dQ_{z2}}{dt} \right\rangle = \frac{k_z c}{4}\left\{ -\left\langle \frac{q_{y0}}{q_z} \frac{\Xi}{(-i\Delta\omega + \Gamma)^2} \right\rangle + \left\langle \frac{q_{y0}}{q_z} \frac{2i\Pi}{(-i\Delta\omega + \Gamma)} \right\rangle \right\} A(t)^2 , \tag{3.64}$$

where $\Pi=\omega_\beta/2q_y$, as defined in Eq. (3.28), and the brackets indicate an average over the beam slice. More explicitly, for the cold beam, we have

$$\frac{dp_z}{dt} = vmcA(t)^2 , \tag{3.65}$$

where

$$v = \frac{k_z c}{4}\left\{ -\left\langle \frac{q_{y0}}{q_z}\Xi \right\rangle \frac{2\Gamma_r(\Gamma_i + \Delta\omega)}{\left(\Gamma_r^2 + (\Gamma_i + \Delta\omega)^2\right)^2} + \left\langle \frac{q_{y0}}{q_z}\Pi \right\rangle \frac{2\Gamma_r}{\Gamma_r^2 + (\Gamma_i + \Delta\omega)^2} \right\} \tag{3.66}$$

or

$$v = \frac{k_z c}{4}\left\{ -\frac{(k_z c)^2}{2q_z^5} a_\beta^2 \left\{ 1 - \frac{\omega_\beta}{k_z c} q_z^2 \right\} \frac{2\Gamma_r(\Gamma_i + \Delta\omega)}{\left(\Gamma_r^2 + (\Gamma_i + \Delta\omega)^2\right)^2} + \rightarrow \right.$$
$$\left. + \frac{\omega_\beta}{q_z} \frac{\Gamma_r}{\Gamma_r^2 + (\Gamma_i + \Delta\omega)^2} \right\} . \tag{3.67}$$

Here we define a betatron parameter, a_β, analogous to the wiggler parameter in an FEL,

$$\boxed{a_\beta^2 = \langle q_y^2 \rangle = \langle q_z h \rangle} \tag{3.68}$$

For the round beam with step radial profile, as in Fig. 3.1(a),

$$a_\beta = 2^{-1/2} q_z k_\beta a \,, \tag{3.69}$$

and is initially the same for each particle. Considering the fast-wave limit, we have

$$\nu = \frac{\omega_\beta k_z c}{4 q_z} \left\{ - 2\,\omega_\beta a_\beta^2 \frac{\Gamma_r(\Gamma_i + \Delta\omega)}{\left(\Gamma_r^2 + (\Gamma_i + \Delta\omega)^2\right)^2} + \frac{\Gamma_r}{\Gamma_r^2 + (\Gamma_i + \Delta\omega)^2} \right\}. \tag{3.70}$$

This result is quite revealing. We note that for a beam with negligible transverse energy ($a_\beta^2 \to 0$), ν and Γ_r are of the same sign. Suppose that $\Gamma_r > 0$, corresponding to a growing eikonal. Then both the beam and the eikonal are gaining energy. Since energy is conserved, this is a contradiction. On the other hand, if $\nu < 0$ and $\Gamma_r < 0$ conservation of energy would also be violated. Thus in the limit $a_\beta^2 \to 0$, we must have $\Gamma_r \to 0$. This is just the well-known result that an ensemble of cold simple harmonic oscillators is stable against

electromagnetic perturbations. (Interestingly, this conclusion is reached without reference to the perturbed Maxwell's equations.)

Physically this is because the driven transverse velocity ($\propto \xi_{xd}$) in an eikonal of constant amplitude is ninety degrees out of phase with the electric field, as reflected in the factor of i multiplying Π in Eq. (3.64). Thus no net work is performed on the fields, on average. On the other hand, when the eikonal is growing, the driven motion absorbs energy from the wave, while the "free" oscillation does work on the fields, through axial (ζ_1) bunching. The relativistic mass effect tends to lessen the work done as reflected in the subtracted terms in Ξ' of Eq. (3.61). The relativistic mass effect in the phase of the transverse motion (Ψ_1) also reduces bunching by the same amount. We shall refer to the term Π generically as the "cold-beam dielectric term" or the "debunching" term.

From this we may understand the physical basis for the detuning, $d\psi/dt$, of Eq. (3.27). The quantity $d\varphi/dt+\Delta\omega$, which appears there is just $\Gamma_i+\Delta\omega$. From Eq. (3.70) we see that in the fast-wave limit, $d\varphi/dt+\Delta\omega>0$ is required to extract energy from the beam, while in the slow-wave limit $d\varphi/dt+\Delta\omega<0$ is required. On the other hand, in these limits particles tend to bunch about $\psi\sim 0$ or π, respectively, corresponding to a detuning $\Pi A\cos(\psi)$ (due to the resonant perturbation of the transverse motion) in Eq. (3.27) which approximaterly balances the detuning $d\varphi/dt+\Delta\omega$ (due to the resonant perturbation of the axial motion). More simply, the bunching wave velocity should always be less than the beam velocity. This has an analog in the FEL, where the instability is

stabilized for finite positive detuning.[11] As in the FEL, we shall find that even when $\Delta\omega$ is large and negative, $\Delta\omega+\Gamma_i$ is positive.

Inspecting the calculation of Eqs. (3.41)-(3.65) we see that amplification of the input signal is correlated with bunching in the variable $\zeta+\Psi$ (identified as ψ in the eikonal formulation) due to the axial component of the Lorentz force, much as in an FEL. We observe that this bunching is reduced due to the relativistic mass effect and due to the resonant damping of the transverse motion. Indeed, in the slow-wave limit ($k_z c<<\omega$), the relativistic mass effect and transverse damping dominate bunching, which occurs in the opposite sense as for axial bunching. A similar transition in bunching was examined by Chu and Hirshfield[12] for the cyclotron maser instability.

In summary, amplification will rely on the circumstance that a strongly driven harmonic oscillator *absorbs* energy in a growing wave, while a weakly driven harmonic oscillator, on the other hand, *loses* energy through axial bunching. Here the "strength" is just $(\Delta\omega+\Gamma_i)/\omega_\beta a_\beta^2$, and measures the size of the driven amplitude relative to the intial amplitude.

To make further progress in assessing the relative magnitudes of the debunching and bunching terms ($(\Delta\omega+\Gamma_i)/\omega_\beta a_\beta^2$), we will consult Maxwell's equations to determine the dependence of Γ_i on $\Delta\omega$ and the other parameters of the problem. We reserve this work for Sec. 3. We shall find that the cold beam dielectric has a significant effect on the conditions for amplification.

c. Invariants of the motion. Further insight into Eqs. (3.22)-(3.26) is gained by considering the constants of the perturbed motion. First, we note that energy varies according to

$$\frac{dH}{dt} = \frac{\partial H}{\partial t}$$
$$= -\omega mc^2 \frac{p_y}{p_z} A \cos(\zeta), \tag{3.71}$$

and with an average over the betatron period, this gives,

$$\frac{dH}{dt} \approx -\frac{1}{2}\omega mc^2 \frac{q_y}{q_z} A \sin(\psi). \tag{3.72}$$

Comparing this result with Eq. (3.24) shows that

$$\boxed{\Phi_z = H - \frac{\omega}{k_z} p_z} \tag{3.73}$$

is a constant of the perturbed motion. This also may be seen from translational invariance. Energy ΔH deposited in the fields, will correspond to a field momentum $\Delta p_z = (k_z/\omega)\Delta H$, and this axial impulse must be taken up by the particles, in the absence of external axial forces. This is quite different from the FEL, where the wiggler magnetic field can absorb axial momentum.

In addition, applying Eqs. (3.24) and (3.26) shows that the action of the x-motion

$$J_x = \frac{1}{2\pi}\oint p_x\,dx \approx \frac{m c^2}{2\omega_\beta}\frac{q_x^2}{q_z}, \tag{3.74}$$

is invariant under an adiabatic variation in ω_β, so that q_x^4/q_z is a constant. (Here, the integral is over one betatron period.)

A similar result obtains for the y-motion. Combining Eqs. (3.23) and (3.25) it is straightforward to show that

$$q_y\frac{dq_y}{dt} = \left\{\frac{\omega_\beta}{k_z c} + \frac{1}{4}\frac{q_y^2}{q_z^2}\right\} q_z\frac{dq_z}{dt}, \tag{3.75}$$

and this may be integrated to give

$$\frac{d}{dt}\left\{\frac{q_y^2}{\omega_\beta q_z} - 2\frac{q_z}{k_z c}\right\} = 0. \tag{3.76}$$

Combining this with Eq. (3.73) shows that

$$\boxed{\Phi_y = H - \omega J_y} \tag{3.77}$$

is a constant of the perturbed motion, where J_y is the action of the y-motion,

$$J_y = \frac{1}{2\pi}\oint p_y dy \approx \frac{mc^2}{2\omega_\beta}\frac{q_y^2}{q_z} \tag{3.78}$$

This result shows that a loss of particle energy ΔH, is accompanied by a decrease in the particle action by an amount $\Delta H/\omega$. In terms of quanta, we may say that the emission of a photon of energy $h\nu$ is accompanied by a loss of action by an amount h. This implies that amplification of the eikonal must be accompanied by a decrease in the area occupied by the beam in the y phase plane. In other words, if the phase of the transverse motion is such that the particle gives up energy to the field, then the transverse motion in y is coherently damped. It is important to point out however, that the motions in y and z are strongly coupled. Thus this result is consistent with Liouville's theorem, provided the area occupied in the z phase plane increases so as to keep the total phase-space volume constant. This result may also be adduced to explain the stability of the cold beam. If $J_y=0$ initially, then $\Delta J_y \geq 0$, since $J_y<0$ is unphysical. Therefore $\Delta H \geq 0$ and the electromagnetic field energy is non-increasing.

For a simple estimate of the y-emittance decrease we compute the variation in the rms normalized emittance in the y phase plane,

$$\varepsilon_{ny} = \sqrt{\langle y^2\rangle\langle p_y^2\rangle - \langle y\ p_y\rangle^2}\ , \tag{3.79}$$

where the brackets indicate an average over the betatron motion and a beam cross-section. This gives

$$\varepsilon_{ny}^2 = \frac{1}{4}\left\langle \frac{q_y^2}{q_z^2 k_\beta^2} \right\rangle \langle q_y^2 \rangle , \tag{3.80}$$

where the betatron wavenumber is $k_\beta \sim \omega_\beta / c$. The rms normalized emittance (in x or y) is initially

$$\varepsilon_n = \frac{1}{4} q_z k_\beta a^2 . \tag{3.81}$$

Noting that $\langle J_y \rangle = mc\varepsilon_{ny}$ and applying Eq. (3.77), it is straightforward to show that the change in rms emittance is

$$\frac{\Delta \varepsilon_{ny}}{\varepsilon_{ny}} \approx \frac{1}{a_\beta^2} \frac{\langle \Delta H \rangle}{H} , \tag{3.82}$$

where $\langle \Delta H \rangle$ is the average change in energy., and we have used $a_\beta = 2^{3/2}\varepsilon_n / a$. This provides a simple estimate of the y-emittance reduction in terms of the efficiency, $\langle \Delta H \rangle / H$. This also provides a useful upper bound to the efficiency, $\langle \Delta H \rangle / H < a_\beta^2$. (Obtained without reference to the perturbed Maxwell's equations).

Finally, we consider axial angular momentum,

$$L_z = xp_y - yp_x . \tag{3.83}$$

Applying Eqs. (3.7) and (3.8) we find that

$$\frac{dL_z}{dt} = \frac{1}{2}mc^2\frac{q_x}{q_z}A\cos(\psi + \theta_x - \theta_y) . \tag{3.84}$$

In this expression we may set θ_x-θ_y equal to its value at t=0. This shows that in general particles will feel a torque due to the perturbation. However, averaged over the ensemble, this torque is zero and no net spin is imparted to the beam, just as one would expect for interaction with a linearly polarized wave.

Table 3.1. Invariants of the single particle motion

Φ_x=-ωJ_x	*x-invariant (action)*
Φ_y=H-ωJ_y	*y-invariant (action, modified due to y-z coupling)*
Φ_z=H-(ω/ck_z)p_z	*z-invariant (conserved total axial momentum)*

These invariants have important implications for bunching. In particular, a loss of axial momentum is compensated in part (by an amount depending on the phase velocity ω/ck_z) by a loss of transverse energy (due to the relativistic mass effect and the resonant damping of the transverse motion). This explains the sensitivity of bunching to phase velocity. At the phase velocity given by Eq. (3.31), bunching is stationary with respect to

variations in axial momentum, brought about by interaction with the eikonal.

d. 1-Dimensional equations. With three integrals of the motion in hand, we may reduce the "KMR" equations for the ICL to just two equations, for q_z and ψ. The equations for ψ and q_z are

$$\begin{aligned}\frac{d\psi}{dt} &= k_z c\left[1 - \frac{2 + q_x^2 + q_y^2}{4q_z^2}\right] - \omega \rightarrow \\ &\rightarrow + \omega_\beta\left[1 - \frac{1}{2q_y} A\cos(\psi)\right] + \frac{1}{2}k_z c\,\frac{q_y}{q_z^2} A\cos(\psi)\,, \\ \frac{dq_z}{dt} &= -\frac{1}{2}k_z c\,\frac{q_y}{q_z} A\sin(\psi)\,.\end{aligned} \tag{3.85}$$

To eliminate q_x and q_y we first define two dimensionless integrals,

$$\begin{aligned}\phi_x &= \omega\frac{J_x}{mc^2}\,, \\ \phi_y &= k_z c\,\frac{J_y}{mc^2} - q_z\,,\end{aligned} \tag{3.86}$$

in terms of which,

$$\begin{aligned}q_x^2 &= 2\,\frac{\omega_\beta}{\omega} q_z \phi_x\,, \\ q_y^2 &= 2\,\frac{\omega_\beta}{k_z c} q_z(\phi_y + q_z)\,.\end{aligned} \tag{3.87}$$

The equations of motion then take a form involving only ψ, q_z and constants,

$$\frac{d\psi}{dt} = k_z c\left(1 - \frac{1}{2q_z^2}\right) - \omega + \frac{1}{2}\omega_\beta - \frac{\omega_\beta}{2q_z}\frac{k_z c}{\omega}(\phi_x + \phi_y) \rightarrow$$

$$+\left\{\frac{k_z c}{8q_z^3}\frac{\omega_\beta}{(\phi_y + q_z)}\right\}^{1/2} A\cos(\psi)\,, \tag{3.88}$$

$$\frac{dq_z}{dt} = -\left\{\frac{k_z c}{2q_z}(\phi_y + q_z)\right\}^{1/2} A\sin(\psi)\,. \tag{3.89}$$

It is tempting to try to formulate the problem in terms of a Hamiltonian parameterized by ϕ_x and ϕ_y. However, it is evident that ψ and q_z are not canonical variables.

To summarize this section, we observe from Eq. (3.89) that to simulate the fully 3-D problem including finite "temperature" effects, requires a distribution over four variables, corresponding to the intial values of ϕ_x, ϕ_y, q_z and ψ. Thus the problem has been reduced to a 1/2+3/2 D problem. However, the simplest model, corresponding to an intially cold beam (uniform in q_z, and $\phi_x+\phi_y$) requires a distribution over only two variables, the initial values of ψ and q_y. This is a 1/2+1/2 D, or in some sense, a 1-D problem.

3. Maxwell's equations

Having examined the single-particle motion, we consider next the feedback from the particles through the field equations. We will work in the Lorentz gauge and neglect the rf scalar potential. Maxwell's equations in terms of the vector potential A_y and the current density, J_y, are

$$\left\{\nabla_{\perp}^2 + \frac{\partial^2}{\partial z^2} - \frac{1}{c^2}\frac{\partial^2}{\partial t^2}\right\} A_y = -\frac{4\pi}{c} J_y \tag{3.90}$$

We take the radial mode to be specified, corresponding to a transverse wavenumber $k_\perp$, satisfying $k_\perp a << 1$ so that variation across the beam is negligible. We define the mode area, Σ

$$\Sigma^{-1} = \frac{|A_y(r=0)|^2}{\int dx dy\, |A_y|^2}, \tag{3.91}$$

(to be distinguished from the parameter employed in Eq. (3.32), passim) and the overlap integral $\eta = \pi a^2/\Sigma$. Without loss of generality, we take ω to satisfy the dispersion relation,

$$\omega^2 = c^2\left(k_z^2 + k_\perp^2\right) + \tilde{\omega}_{beff}^2, \tag{3.92}$$

where

$$\begin{aligned}\tilde{\omega}_{beff}^2 &= \frac{4\pi e^2}{\Sigma}\left(\frac{I}{I_o}\right)\left\langle\frac{1}{q_z}\right\rangle \\ &= \omega_{beff}^2\left\langle\frac{1}{q_z}\right\rangle,\end{aligned} \tag{3.93}$$

and the brackets indicate an average over the beam slice. We define $\omega_{beff} = \eta^{1/2}\omega_b$, with ω_b the beam-plasma frequency, $\omega_b^2 = 4\pi n_b e^2/m$.

a. Eikonal equations. Expressing A_y in terms of the eikonal quantities A and φ, from Eq. (3.2), and neglecting second derivatives, and products of derivatives, of A and φ, we obtain,

$$\left\{k_z\frac{\partial}{\partial z}+\frac{\omega}{c^2}\frac{\partial}{\partial t}\right\}(A\,e^{i\varphi})=i\,\frac{\omega_{beff}^2}{2c^2}\left\langle\frac{q_y}{q_z}exp(-i\chi)\right\rangle. \tag{3.94}$$

Here, we have introduced a new phase variable, $\chi=\psi-\varphi$. In this expression, an average has been performed over the period $2\pi/\omega$ and over all electrons at z,t, as indicated by the brackets. Making a change of coordinates from z,t to $s=t-z/v_z$ and t, gives

$$\underbrace{\left\{(1-\frac{c^2}{v_\varphi\bar{v}_z})\frac{\partial}{\partial s}+\frac{\partial}{\partial t}\right\}}_{slippage}(A\,e^{i\varphi})=i\,\frac{\omega_{beff}^2}{2\omega}\left\langle\frac{q_y}{q_z}exp(-i\chi)\right\rangle \tag{3.95}$$

where $v_\varphi=\omega/ck_z$. Following Bonifacio *et al.*,[13] we neglect the slippage term for $v_\varphi\sim v_z\sim c$ (fast-wave limit). This can also be written in terms of real variables as

$$\boxed{\begin{aligned}\frac{\partial A}{\partial t}&=\frac{\omega_{beff}^2}{2\omega}\left\langle\frac{q_y}{q_z}sin\ (\psi)\right\rangle,\\ A\frac{\partial\varphi}{\partial t}&=\frac{\omega_{beff}^2}{2\omega}\left\langle\frac{q_y}{q_z}cos\ (\psi)\right\rangle.\end{aligned}} \tag{3.96}$$

Combining Eq. (3.96) with Eqs. (3.22)-(3.26), we have the basic equations describing the ion-channel laser in the fast-wave limit.

Comparing Eq. (3.72) and (3.96) we see that the quantity

$$\boxed{E = \eta\omega_b^2\langle H\rangle + \frac{1}{2}\omega^2 A^2 mc^2}, \tag{3.97}$$

is a constant in t. This integral is proportional to the total energy of a beam slice and the comoving eikonal wave front.

b. Dispersion relaion To examine amplification, we adopt the complex eikonal $B=Ae^{i\varphi}$, in terms of which Eq. (3.96) is

$$\frac{\partial B}{\partial t} = i\,\frac{\omega_{beff}^2}{2\omega}\left\langle \frac{q_y}{q_z} exp(-i\chi)\right\rangle. \tag{3.98}$$

Expanding $\chi=\chi_0+\chi_1$ and $q_y=q_{y0}+q_{y1}$ in zeroth and first order terms, we have

$$\frac{\partial B}{\partial t} \approx \frac{\omega_{beff}^2}{2\omega}\left\langle exp(-i\chi_0)\left(\frac{q_{y0}}{q_z}\chi_1 + i\frac{q_{y1}}{q_z}\right)\right\rangle. \tag{3.99}$$

(In principle, there is also a perturbed q_z term, but it contributes at higher order in a_β^2.) The perturbed phase is determined from Eqs. (3.22)-(3.26), or equivalently, Eq. (3.29),

$$\frac{\partial^2 \chi_1}{\partial t^2} = -\left\{\Xi - \Pi\left(\frac{\partial \chi_0}{\partial t} + \frac{\partial \varphi}{\partial t}\right)\right\} A \sin(\chi_0 + \varphi) - \Pi \frac{\partial A}{\partial t} \cos(\chi_0 + \varphi) \tag{3.100}$$

Writing $\chi_1 = Im(\tilde{\chi}_1)$, we have

$$\frac{\partial^2 \tilde{\chi}_1}{\partial t^2} = -\Xi B e^{i\chi_0} - i\Pi \frac{\partial}{\partial t}\left(B e^{i\chi_0}\right)$$

(This result is roughly equivalent to the work of Eqs. (3.52), (3.54), and (3.61) combined.) We look for a solution $B(t) \propto exp(\Gamma t)$, and integrate Eq. (3.101) to obtain

$$\tilde{\chi}_1 \approx -\left\{\frac{\Xi}{(\Gamma + i\Delta\omega)^2} + \frac{i\Pi}{(\Gamma + i\Delta\omega)}\right\} B e^{i\chi_0} \tag{3.101}$$

neglecting small constants of integration. (Note that this derivation mirrors that given in Sec. 2b, except that here we used the eikonal equations (22)-(26), to arrive at the same result more quickly.)

The q_{y1} term is obtained by perturbing Eq. (3.25),

$$\frac{dq_{y1}}{dt} \approx -\frac{1}{2}\left\{\omega_\beta + \frac{1}{4} k_z c \frac{q_y^2}{q_z^2}\right\} A \sin(\chi_0 + \varphi)$$

which we integrate to find

$$q_{y1} \approx -\Im\left\{\frac{q_{y0}\Pi}{(\Gamma + i\Delta\omega)} B e^{ix_0}\right\}, \tag{3.102}$$

neglecting corrections of order a_β^2, and small constants of integraton.

Combining Eqs. (3.99), (3.101) and (3.102) gives the dispersion relation for the growth rate

$$\boxed{\Gamma = \frac{\omega_{beff}^2}{4\omega}\left\langle \frac{q_y}{q_z}\left\{\frac{i\Xi}{(\Gamma + i\Delta\omega)^2} - \frac{2\Pi}{(\Gamma + i\Delta\omega)}\right\}\right\rangle} \tag{3.103}$$

This result is fairly general and can be used to assess finite temperature effects, due to spreads in $\Delta\omega$, arising from spreads in v_z or ω_β, themselves due to spreads in transverse energy (h) or axial momentum (q_z). Before considering detuning spread, however, we analyze the case of a cold beam, corresponding to a step radial profile. In this case, the detuning $\Delta\omega$ is the same for each particle, and the resonant denominators may be removed from the average. The dispersion relation then takes the form

$$\boxed{\Gamma(\Gamma + i\Delta\omega)^2 + \mu^2(\Gamma + i\Delta\omega)\omega_\beta^2 = i(2\rho\omega_\beta)^3}, \tag{3.104}$$

where the "Pierce parameter",[14] ρ is given by

$$\rho^3 = \frac{\omega_{beff}^2}{32\,\omega\omega_\beta^3}\left\langle \frac{q_y}{q_z}\Xi \right\rangle$$
$$= \frac{\omega_{beff}^2}{32\,\omega\omega_\beta^3}\frac{(k_z c)^2}{2\,q_z^5}a_\beta^2\left\{1 - \frac{\omega_\beta}{k_z c}q_z^2\right\} \qquad (3.105)$$

For a fast-wave, this

$$\boxed{\rho = \left(\frac{I}{32\,q_z I_0}\right)^{1/3}} \qquad (3.106)$$

The constant μ is given by

$$\mu^2 = \frac{\omega_{beff}^2}{2\,\omega\omega_\beta^2}\left\langle \Pi\frac{q_y}{q_z}\right\rangle$$
$$\approx \frac{\omega_{beff}^2}{4\,\omega\omega_\beta q_z} \qquad (3.107)$$

and in the fast-wave limit, it is

$$\boxed{\mu^2 = 8\,\frac{\rho^3}{a_\beta^2}} \qquad (3.108)$$

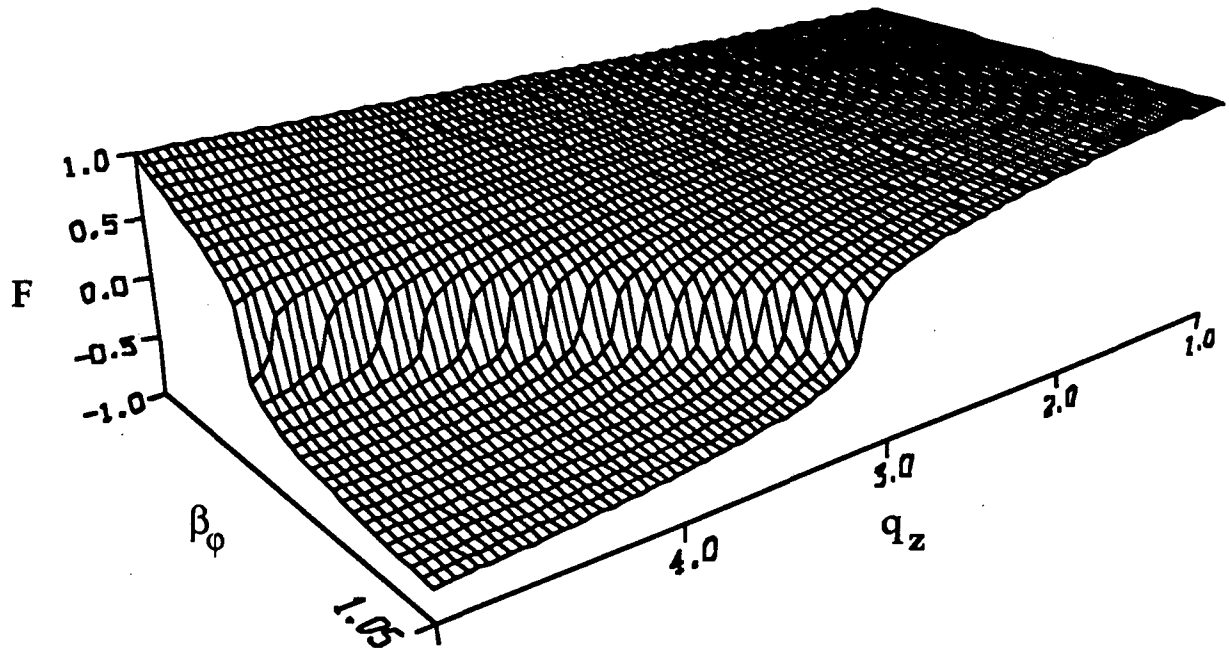

Fig. 3.3 (a)Variation of ICL Pierce parameter with wave phase velocity and momentum ($q_z=p_z/mc$), on resonance, as given by Eq. (3.110), for $1<\beta_\varphi<1.05$ and $1<q_z<5$.

As for the FEL,[15] the solution for the eikonal is then given by a superposition of three terms

$$A e^{i\varphi} = A_0 e^{i\varphi_0} \sum_{j=-1}^{+1} \alpha_j \, exp(\Gamma_j t) \tag{3.109}$$

where the Γ_j (j=-1,0,+1) are the three roots of the cubic gain equation. Taking $Ae^{i\varphi}=A_0e^{i\varphi_0}$ at t=0, with vanishing first and second derivatives, the constants α_j are determined from the roots according to

$$\alpha_j = \frac{\Gamma_k \Gamma_l}{\Gamma_j^2 - \Gamma_j \Gamma_l - \Gamma_j \Gamma_k + \Gamma_l \Gamma_k},$$

with j,l,k any permutation of -1,0,+1.

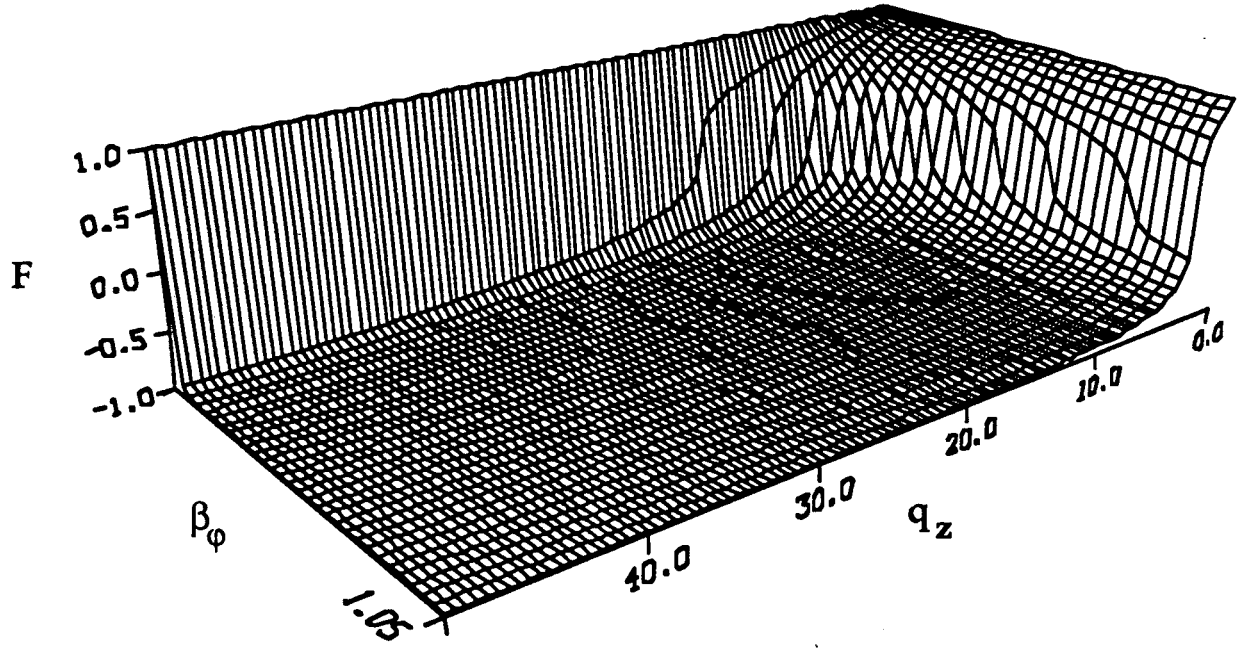

Fig. 3.3 (b)Variation of ICL Pierce parameter with wave phase velocity and momentum ($q_z=p_z/mc$), on resonance, as given by Eq. (3.110), for $1<\beta_\varphi<1.05$ and $1<q_z<50$.

Before analyzing the dispersion relation, it is important to note that ρ as given by Eq. (3.105) varies significantly with wave phase velocity. This is not surprising given the discussion of Eq. (3.30). To make this more explicit, we define a function $F(\beta_\varphi,q_z)$ such that

$$\rho = \left(\frac{I}{32 q_z I_0}\right)^{1/3} F(\beta_\varphi, q_z)$$

Making the approximation $\beta_z \sim 1 - 1/2q_z^2$, and using the resonance relation, $\omega(1 - \beta_z/\beta_\varphi) = \omega_\beta$, we find, from Eq. (3.105)

$$F(\beta_\varphi, q_z) = \left\{\frac{1 - 2q_z^2(\beta_\varphi - 1)}{1 + 2q_z^2(\beta_\varphi - 1)}\frac{1}{\beta_\varphi}\right\}^{1/3}, \tag{3.110}$$

where the real root is understood. This result is depicted in Fig. 3.3(a) and on a larger scale, in Fig. 3.3(b) We note that for $\beta_\varphi = 1$, $F = 1$, while for $(\beta_\varphi - 1)2q_z^2 >> 1$, $F \sim -1/\beta_\varphi < 0$ and increases slowly to zero, with increasing β_φ. Note that this is precisely the limit in which the relativistic upshift is negligible, i.e., $\omega_0 \sim \omega_\beta$.

c. Small μ, δ limit ("cubic gain regime"). In general the roots are rather different from those for the FEL, due to the μ term. Nevertheless, before plunging into a detailed analysis of the cubic, it is instructive to consider the limit of negligible μ (corresponding to $a_\beta^2 \sim \rho$ or larger) for the purpose of making simple estimates and comparisons with the $\delta, \mu \neq 0$ results. In this case the dispersion relation is

$$\Gamma^3 \approx i(2\rho\omega_\beta)^3 \tag{3.111}$$

i.e.

$$\Gamma_0 = 2\,\rho\omega_\beta\, exp(-i\pi/2)\,,$$
$$\Gamma_{\pm 1} = \pm\, 2\,\rho\omega_\beta\, exp(\pm\, i\pi/6)\,, \qquad (3.112)$$

and the constants α_j=1/3. (We will assume ρ>0, since the details for ρ<0 can be straightforwardly worked out, with the replacement $\Gamma_j^*=-\Gamma_{-j}$.)

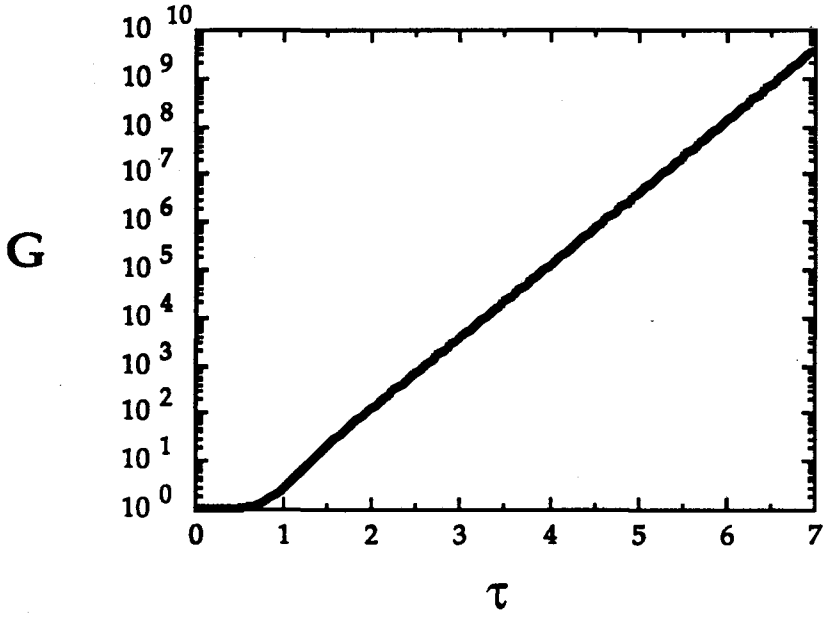

FIG. 3.4 (a)Gain, from Eq. (3.114), versus the normalized time coordinate $\tau=\rho\omega_\beta t$, for zero detuning.

The solution is

$$A\,e^{i\varphi} = \frac{1}{3}\left\{e^{-2i\tau} + 2\,e^{i\tau}\,cosh(\sqrt{3}\,\tau)\right\} A_0\,e^{i\varphi_0}\,, \qquad (3.113)$$

where $\tau=\rho\omega_\beta t$. Gain is given by

$$G(t) = \frac{A^2}{A_0^2}$$
$$= \frac{1}{9}\{3 + 2\cosh(2\sqrt{3}\tau) + 4\cos(3\tau)\cosh(\sqrt{3}\tau)\}, \quad (3.114)$$

and is plotted in Fig. 3.4(a).The phase advance varies according to

$$\tan(\varphi - \varphi_0) = \frac{\sin(\tau)2\cosh(\sqrt{3}\tau) - \sin(2\tau)}{\cos(\tau)2\cosh(\sqrt{3}\tau) + \cos(2\tau)}, \quad (3.115)$$

and is plotted in Fig. 3.4(b).

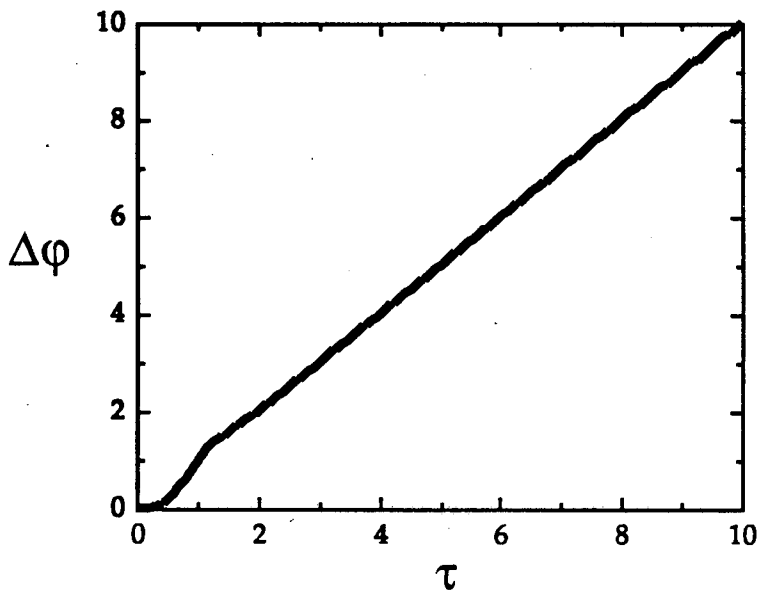

FIG. 3.4 (b)Phase advance, $\Delta\varphi=\varphi-\varphi_0$, from Eq. (3.115), versus the normalized time coordinate $\tau=\rho\omega_\beta t$, for zero detuning.

Growth is cubic for short times,

$$A e^{i\varphi} \approx \left\{ 1 + \frac{4}{3} i\tau^3 \right\} A_0 e^{i\varphi_0} , \tag{3.116}$$

and for longer times is exponential

$$A e^{i\varphi} \approx \frac{1}{3} exp(\sqrt{3}\,\tau + i\tau)\, A_0 e^{i\varphi_0} . \tag{3.117}$$

As a figure of merit we note the exponential gain length $L_g = c/Re(\Gamma_+)$, or

$$L_g = \frac{\lambda_\beta}{2\pi 3^{1/2}\rho} = \frac{2^{2/3}}{\pi 3^{1/2}} \left(\frac{\gamma I_0}{\eta I} \right)^{1/3} \lambda_\beta . \tag{3.118}$$

This is typically a few to one hundred betatron wavelengths, depending on η, I and γ.

With the solution for A in hand it is instructive to substitute this into Eq. (3.102) and solve for χ_1. In the limit $\tau > 1$, this gives

$$\chi_1 \approx \frac{1}{4} \frac{q_y}{\rho^2} A \sin(\varphi + \chi_0 + \frac{2\pi}{3}) .$$

Note that particles with small q_y are perturbed little. Maximum power is achieved near the onset of non-linearity and particle trapping, where the rms χ_1 is of order unity. At saturation we then find,

$$A^2 \approx 32 \frac{\rho^4}{a_\beta^2} . \tag{3.119}$$

Making use of Eq. (3.97), this gives an estimate for the efficiency $\varepsilon \sim \rho$, and the final output power $P_{out} \sim \varepsilon P_{beam}$, where $P_{beam} \sim mc^2(\gamma-1)I$ is the initial beam power.

We observe that the average energy lost by the beam is second order in A. Indeed, writing out Eq. (3.72) explicitly gives

$$\begin{aligned}
\left\langle \frac{dH}{dt} \right\rangle &\approx -\frac{1}{2}\omega mc^2 A \left\langle \frac{q_y}{q_z} \sin(\psi) \right\rangle \\
&\approx -\frac{1}{2}\omega mc^2 A \left\langle \frac{q_y}{q_z} \sin(\varphi + \chi_0) + \frac{q_y}{q_z} \cos(\varphi + \chi_0)\chi_1 \right\rangle \\
&\approx -\frac{1}{2}\omega mc^2 A \left\langle \frac{q_y}{q_z} \cos(\varphi_0 + \chi_0 + \tau)\chi_1 \right\rangle \\
&\approx -\frac{3^{1/2}}{2^4}\omega mc^2 \frac{a_\beta^2}{q_z \rho^2} A^2 .
\end{aligned} \tag{3.120a}$$

This energy loss from $v_y E_y$ work done by the particles is seen to arise from coherent oscillations in χ, at angular frequency $\rho\omega_\beta$ which are synchronous with those in the eikonal. In configuration space, this amounts to a slow drift in betatron phase, and axial position, which results in coherent beam centroid oscillations of ever growing amplitude.

More quantitatively, calculating the average y-momentum in a beam slice we find

$$\langle p_y \rangle \approx - mc \frac{1}{2^4} \frac{a_\beta^2}{\rho^2} A \sin(k_z z - \omega t + \varphi + \frac{2\pi}{3}) \quad (3.120b)$$

This result makes use of $\theta_{y1} \sim -0.5\chi_1$, which follows from differentiation of Eqs. (3.22) and (3.23). Equation (3.120) shows that a coherent oscillation of the beam centroid develops, and, near saturation, $\langle p_y \rangle \sim mca_\beta/2^{3/2}$. On the other hand, particles bunch in ψ as A grows. Thus an rf component develops in the beam current, at the same time that the beam centroid oscillations grow in amplitude. As we have seen, the result is coherent radiation.

d. Growth for finite μ,δ ("quadratic gain regime"). We shall find that the results of the last section are typically useful for simple estimates of the laser performance. However, they represent the optimal performance possible. In fact, the approximation $\mu=0$ omits some important features. In particular, a beam with a smooth distribution in transverse energy (i.e., a typical beam) will have a detuning spread of order $\omega_\beta a_\beta^2$. If μ is small, this detuning spread is large, and gain will be reduced. This circumstance motivates the more detailed study of the roots which we now undertake.

We proceed to solve Eq. (3.122). We define a dimensionless gain parameter ζ, and detuning δ,

$$\zeta = (i\Gamma - \Delta\omega) / \omega_\beta \ ,$$
$$\delta = \Delta\omega / \omega_\beta \ , \quad (3.121)$$

in terms of which the dispersion relation takes the form

$$\boxed{\zeta^3 + \delta\zeta^2 - \mu^2\zeta - 8\,\rho^3 = 0} \tag{3.122}$$

Note that since $Re(\Gamma)=\omega_\beta Im(\zeta)$, growing roots correspond to $Im(\zeta)>0$. In particular, for amplification ζ must be complex. In terms of dimensionless parameters

$$\begin{aligned} Q &= -\frac{1}{3}\mu^2 - \frac{1}{9}\delta^2 , \\ R &= -\frac{1}{6}\mu^2\delta + 4\,\rho^3 - \frac{1}{27}\delta^3 , \end{aligned} \tag{3.123}$$

and a discriminant,

$$\begin{aligned} D^2 &= Q^3 + R^2 \\ &= \left[4\,\rho^3 - \frac{1}{6}\delta\left(\mu^2 + \frac{2}{9}\delta^2\right)\right]^2 - \frac{1}{27}\left[\mu^2 + \frac{1}{3}\delta^2\right]^3 , \end{aligned} \tag{3.124}$$

the condition for the existence of complex roots, and amplification, is $D^2>0$.[16] Specifically, for $D^2>0$ there is one real root and one conjugate pair of complex roots. For $D^2=0$ all roots are real and at least two are equal. For $D^2<0$ all roots are real.

Definining two additional constants

$$S_{\pm} = (R \pm D)^{1/3}, \tag{125}$$

the roots of the dispersion relation are given by

$$\zeta_0 = S_+ + S_- - \frac{\delta}{3},$$
$$\zeta_{\pm} = -\frac{1}{2}(S_+ + S_-) - \frac{\delta}{3} \pm i\frac{\sqrt{3}}{2}(S_+ - S_-) \tag{3.126}$$

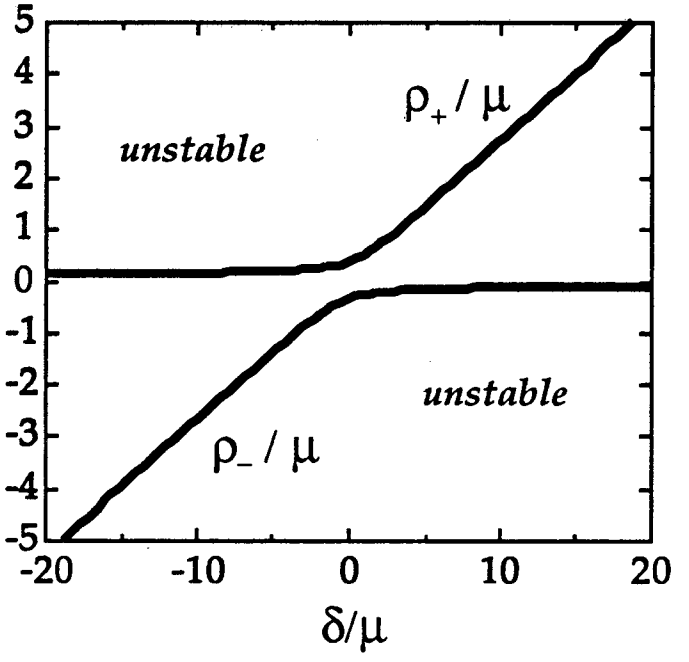

FIG. 3.5. The $\rho_{\pm}$ of Eq. 3.(130) are depicted as a function of detuning, δ. For gain, ρ must satisfy $\rho<\rho_-$ or $\rho>\rho_+$, i.e., the region of stability lies between the two curves shown.

For $D^2>0$, we have one growing root (ζ_+) one decaying root (ζ_-) and one purely real root (ζ_-). Inspecting Eq. (3.122) we observe that the dispersion relation is unchanged under the transformation $\zeta\rightarrow-\zeta$, $\delta\rightarrow-\delta$ and $\rho\rightarrow-\rho$. This simplifies

our analysis somewhat, in that we need consider only the case $\rho>0$. Conclusions reached there may be extended to the $\rho<0$ case by changing the appropriate signs and noting that when $D^2>0$, $\zeta_+=\zeta_-^*$.

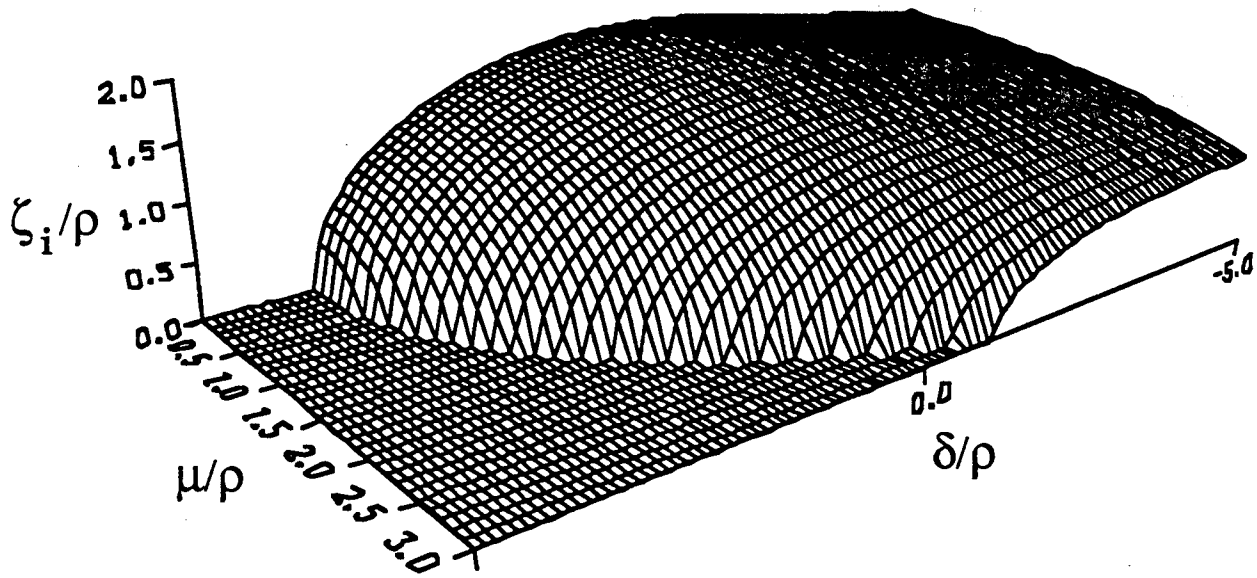

FIG. 3.6. (a)The normalized growth rate $\zeta_i=Im(\zeta_+)=Re(\Gamma)/\omega_B$ is plotted versus detuning, δ and the cold beam dielectric parameter μ. Note that the peak value $\zeta_i=3^{1/2}$ occurs at $\delta=\mu=0$.

It is also helpful, in analyzing the roots to note the standard relations between the roots of a cubic, which in this case are

$$\zeta_+ + \zeta_0 + \zeta_- = -\delta \ ,$$
$$\zeta_+\zeta_0 + \zeta_-\zeta_+ + \zeta_-\zeta_0 = -\mu^2 \ ,$$
$$\zeta_+\zeta_0\zeta_- = 8\rho^3 \ .$$

We may check Eq. (3.126) against the $\mu=\delta=0$ result, by taking the limit $\mu,\delta<<\rho$. We find,

$$\zeta_0 = 2\,\rho\left(1+\frac{1}{2^{5/3}3}\frac{\delta^2}{\rho^2}\right)-\frac{\delta}{3},$$
$$\zeta_\pm = -\,\rho\left(1+\frac{1}{2^{5/3}3}\frac{\delta^2}{\rho^2}\right)-\frac{\delta}{3}\pm i3^{1/2}\rho\left(1-\frac{1}{2^{5/3}3}\frac{\delta^2}{\rho^2}\right). \qquad (3.127)$$

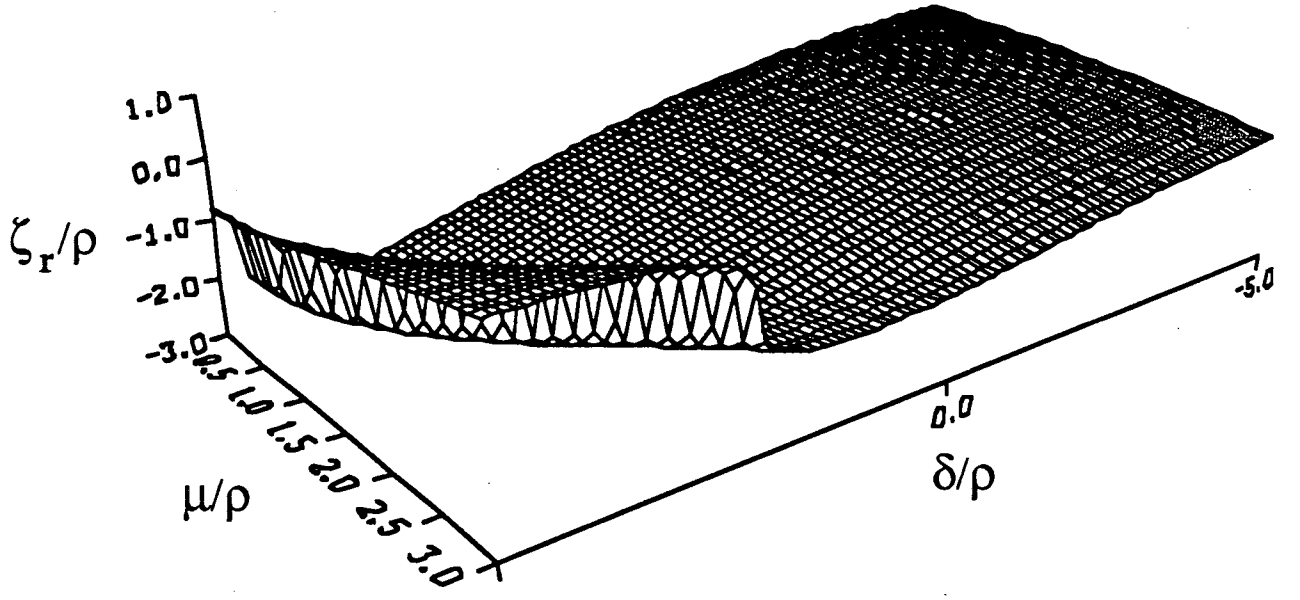

FIG. 3.6. (b) The real part of the root $\zeta_r=Re(\zeta_+)$ is plotted versus detuning, δ and the cold beam dielectric parameter μ, as in Fig. 3.6(a). Note that $Re(\zeta)=-(\Gamma_i+\Delta\omega)/\omega_\beta<0$ in regions where $Im(\zeta)\propto Re(\Gamma)>0$ (i.e., in regions where amplification occurs) as would be expected from the discussion of the ponderomotive force of Eq. (3.70).

The exponential growth length is $L_g\sim 1/k_\beta Im(\zeta_+)$, or

$$L_g \approx \frac{\lambda_\beta}{2\pi 3^{1/2}\rho}\left(1+\frac{1}{2^{5/3}3}\frac{\delta^2}{\rho^2}\right), \tag{3.128}$$

in agreement with the previous result.

In general, however, for μ or δ comparable to ρ, the condition $D^2>0$ yields a constraint on ρ, $\rho<\rho_-$ or $\rho>\rho_+$, where

$$4\rho_\pm^3 = \frac{1}{6}\delta\mu^2 + \frac{1}{27}\delta^3 \pm \frac{1}{3^{3/2}}\left\{\mu^2+\frac{1}{3}\delta^2\right\}^{3/2}. \tag{3.129}$$

This constraint did not appear in the previous treatment because we neglected detuning, and the cold beam dielectric effect represented by μ (i.e., we neglected particles with $q_y<A$). The $\rho_\pm$ are plotted versus δ in Fig. 3.5. We observe that on resonance ($\delta=0$) $|\rho|>\mu/2^{2/3}3^{1/2}$ is required for gain. For a fast-wave, this condition is $a_\beta^2>(2^{5/3}/3)\rho\sim\rho$. On the other hand, inspection of Eq. (3.130) reveals that for large negative detuning this constraint is reduced and gain is possible with $a_\beta^2<O(\rho)$, i.e., $\mu/\rho>2.8$.

To gain more insight into the condition for gain, we plot the growth rate, $Im(\zeta_+)$ given by Eq. (3.126), versus δ and μ in Fig. 3.6(a) and, on a larger scale, in Fig. 3.7. Immediately we observe that gain is not an even function of detuning. In fact, the instability is stabilized for a finite positive detuning, which for $\mu=0$ is $\delta/\rho\sim3.8$. As μ/ρ increases to $\mu/\rho\sim2.8$, this upper bound on δ decreases to 0. On the other hand, for any finite negative detuning, there is some range of μ which yields growth. Conversely, for any μ, there is some

negative detuning which yields growth. Interestingly, the growth rate is appreciable even for δ/ρ~-50. It should be added, however that the cubic is strictly valid only for δ<<1 and this constrains the maximum possible δ. (Thus for δ/ρ~-50 to make sense we must have ρ<1%).

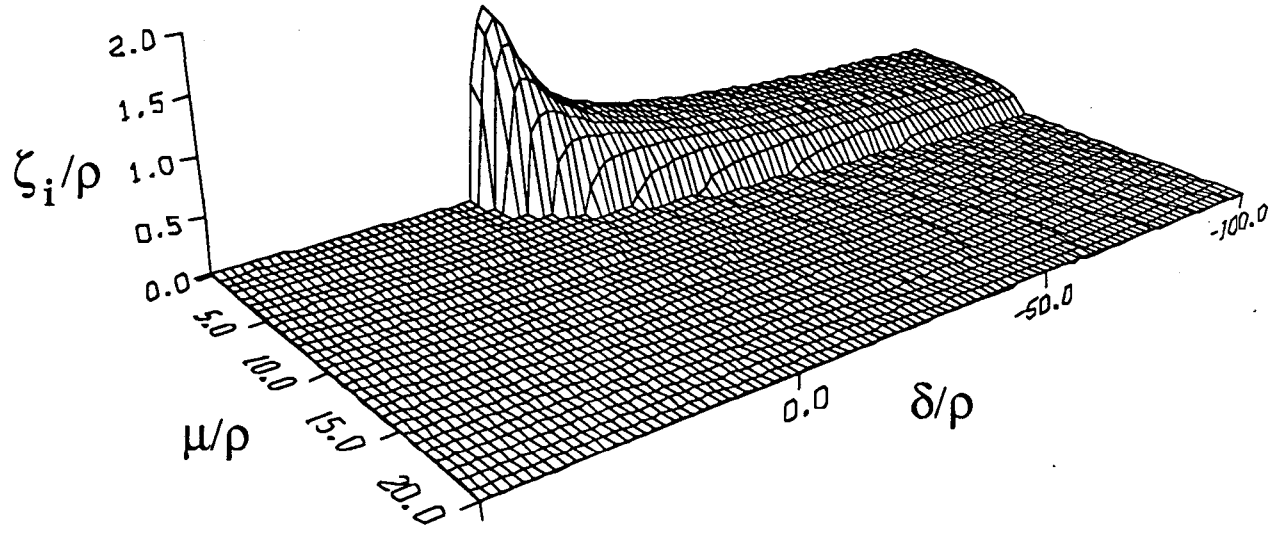

Fig. 3.7. Growth rate as in Fig. 3.6(a), for -100<δ/ρ<50 and 0<μ/ρ<20.

We may check this large δ behavior by solving Eq. (3.122) explicitly, in the limit $|\delta| >> \mu,\rho$. In this limit, we find

$$\zeta_0 \approx -\delta - \frac{\mu^2}{\delta},$$
$$\zeta_\pm \approx \frac{-\mu^2 \pm i\sqrt{32\,\rho^3|\delta| - \mu^4}}{2|\delta|}, \qquad (3.130)$$

and the threshold for gain in this limit is $\delta<-\mu^4/32\rho^3$. Far above threshold, $Im(\zeta_+)$ decreases slowly, as $1/|\delta|^{1/2}$, as seen in Figs. 3.6-3.8. More quantitatively, we may compute the maximum growth rate directly from Eq. (3.130). We find

$$\max_{\delta} \Im(\zeta_+) = 8\frac{\rho^3}{\mu^2} \approx a_\beta^2, \tag{3.131}$$

occuring at

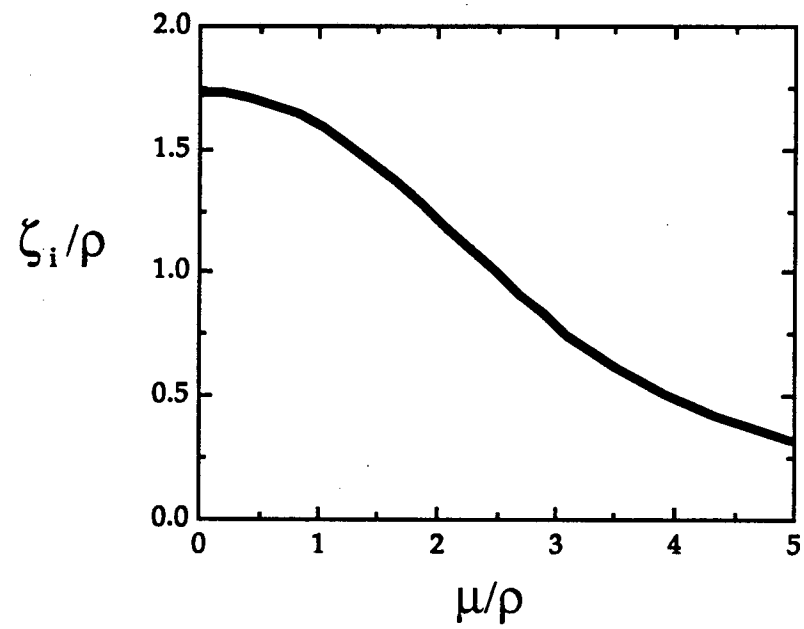

FIG. 3.8. The maximum growth rate $Im(\zeta_+)/\rho$ is plotted versus the cold beam dielectric parameter. The corresponding detuning is plotted in Fig. 3.9.

$$\delta \approx -\frac{1}{16}\frac{\mu^4}{\rho^3} \approx -4\frac{\rho^3}{a_\beta^4}, \tag{3.132}$$

and corresponding to

$$\zeta \approx \frac{8\rho^3}{\mu^2}(-1+i).$$

We observe that at this detuning, $Re(\zeta_+)=-\mu^2/2\,|\,\delta\,|=-8\rho^3/\mu^2\sim-2a_\beta^2$, corresponding to $\Gamma_i=-\Delta\omega+2a_\beta^2\omega_\beta$.

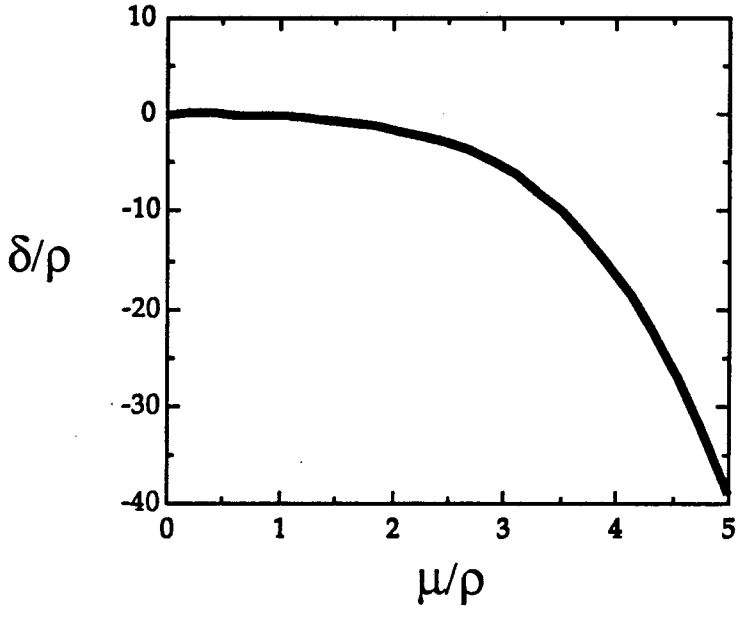

FIG. 3.9. The detuning corresponding to the growth rate depicted in Fig. 3.8, plotted versus the cold beam dielectric parameter.

The "exact" result computed numerically from Eq. (3.128) is depicted in Fig. 3.8, with the corresponding detuning in Fig. 3.9, giving good agreement. Practically, it is useful to have an estimate of the reduction in the peak growth rate due to the μ term. This is given numerically in Fig. 3.8. Analytically, in the limit $a_\beta^2 << \rho$, this is

$$\vartheta = \frac{\max_{\mu \neq 0} \Im(\zeta_+)}{\max_{\mu=0} \Im(\zeta_+)} = \frac{8}{3^{1/2}} \left(\frac{\rho}{\mu}\right)^2 \approx \frac{1}{3^{1/2}} \frac{a_\beta^2}{\rho} , \tag{3.133}$$

where we have used the fact that the maximum growth rate for $\mu=0$ is $Im(\zeta_+)=3^{1/2}\rho$, *and* $a_\beta^2/\rho \sim 8(\rho/\mu)^2$.

From the analysis of this section we have learned that the cold beam dielectric effect represented by the μ term in Eq. (3.122) tends to reduce growth, even eliminating growth for some range of δ and ρ. This was anticipated in the discussion of the ponderomotive force of Sec. 2.b. We have seen that the competition between the bunching (Ξ) and debunching (Π) terms depends on the ratio ρ/a_β^2. It also depends on detuning, since the pondermotive force may be varied by tuning the beam off-resonance.

To make this more explicit, and to check the calculation of the ponderomotive force of Eq. (3.70), we repeat the calculation of Eq. (3.120), in the case where the Π (or μ^2) term is not negligible. We have

$$\left\langle \frac{dH}{dt} \right\rangle \approx -\frac{1}{2}\omega mc^2 A \left\langle \frac{q_y}{q_z} \sin(\psi) \right\rangle$$
$$\approx -\frac{1}{2}\omega mc^2 A \left\langle \frac{q_{y1}}{q_z} \sin(\varphi + \chi_0) + \frac{q_y}{q_z} \cos(\varphi + \chi_0)\, \chi_1 \right\rangle$$
$$\approx -\frac{1}{2}\omega mc^2 A \Re \left\langle exp(-i\varphi - i\chi_0) \left[i\frac{q_{y1}}{q_z} + \frac{q_y}{q_z}\chi_1 \right] \right\rangle$$

We substitute from Eq. (3.101) for χ_1, and (102) for q_{y1} to obtain

$$\left\langle \frac{dH}{dt} \right\rangle \approx \frac{1}{4}\omega mc^2 A^2 \left\{ \left\langle \frac{q_y}{q_z} \Xi \right\rangle \Im \frac{1}{(\Gamma + i\Delta\omega)^2} + 2 \left\langle \frac{q_y}{q_z} \Pi \right\rangle \Re \frac{1}{(\Gamma + i\Delta\omega)} \right\}.$$

Taking the fast wave limit and writing this in terms of $\zeta_r = Re(\zeta_+)$ and $\zeta_i = Im(\zeta_+)$ we have

$$\left\langle \frac{dH}{dt} \right\rangle \approx \frac{1}{4 q_z}\omega mc^2 A^2 \left\{ 2 a_\beta^2 \frac{\zeta_r \zeta_i}{(\zeta_r^2 + \zeta_i^2)^2} + \frac{\zeta_i}{(\zeta_r^2 + \zeta_i^2)} \right\}.$$

This is just the result one obtains from Eq. (3.70), using $dH/dt = (\omega/ck_z)dq_z/dt$. By inspection we see that $\zeta_r < 0$ is required for gain. Since $\zeta_r = -(\Gamma_i + \Delta\omega)/\omega_\beta$, this just says that $\Gamma_i + \Delta\omega = d\varphi/t + \Delta\omega$ must be positive for gain. In this way the phase shift in the transverse motion due to the driving force is partially cancelled and particles may remain nearly stationary in ψ, resulting in a secular loss of energy. Said differently, detuning has increased the axial bunching with respect to the debunching effect represented by the "Π" terms of Eq. (3.29). (The same discussion applies to the slow-wave case, with the signs reversed)

4. Finite temperature effects.

Thus far we have considered a cold beam, for which all particles had identical detuning, $\Delta\omega$. In this approximation, all particles were resonant with the wave. Returning to the dispersion relation of Eq. (3.103), we see that a spread in detuning will alter the dispersion relation, and likely reduce growth. In this section, we quantify the effect of a detuning spread arising from a spread in axial momentum, q_z. We reserve for the next section a rigorous calculation of the effect of spread in transverse energy, h.

We define $\delta_0=<\Delta\omega>/\omega_\beta$ to be the dimensionless average detuning, and introduce a new particle variable $\delta_1=(\Delta\omega-<\Delta\omega>)/\omega_\beta$. Taking ζ to be defined as in Eq. (3.121) with "δ" replaced by δ_0, we rewrite Eq. (3.103) in the form

$$\zeta + \delta_0 = \mu^2 \left\langle \frac{1}{(\zeta + \delta_1)} \right\rangle + 8\,\rho^3 \left\langle \frac{1}{(\zeta + \delta_1)^2} \right\rangle .$$

We model the effect of momentum spread by taking particles to be uniformly distributed in the range $-\delta_s<\delta_1<\delta_s$. In this case the integrals are straightforward and we obtain the modified dispersion relation, (to be compared with Eq. (3.122)),

$$\boxed{\zeta + \delta_0 = \frac{\mu^2}{2\,\delta_s} ln\left(\frac{\zeta + \delta_s}{\zeta - \delta_s}\right) + \frac{8\,\rho^3}{\zeta^2 - \delta_s^2}} \qquad (3.134)$$

a. Cubic gain regime. First, we consider the limit of negligible μ. The dispersion relations is then cubic,

$$\zeta^3 + \delta_0\zeta^2 - \delta_s^2\zeta = 8\rho^3 + \delta_s^2\delta_0 \approx 8\rho^3 ,$$

and is identical to Eq. (3.122), provided we make the replacement $\mu^2 \rightarrow \delta_s^2$. Thus we may carry over all the conclusions from our analysis of finite μ effects. When $\delta_s < \rho$, the effect of the spread is small. When $\delta_s > \rho$ the coherent oscillations in χ_1, which in Eq. (3.120) contributed to the ponderomotive force are washed out, unless δ_0 is below the threshold detuning given by Eq. (3.131)

$$\delta_0 < -\frac{1}{32}\frac{\delta_s^4}{\rho^3} .$$

From Eq. (3.132), peak growth occurs for

$$\delta_0 = -\frac{1}{16}\frac{\delta_s^4}{\rho^3} ,$$

and the growth rate is reduced below the $\delta_0=\delta_s=0$ value by the factor from Eq. (3.133),

$$\vartheta = \frac{8}{3^{1/2}}\frac{\rho^2}{\delta_s^2} . \qquad (3.135)$$

Thus for $\delta_s \sim 3\rho$, the growth rate is reduced by a factor of two.

We may relate these constraints on δ_s to practical constraints on the beam through the dependence of detuning on q_z and h as given by Eq. (3.16). In the fast-wave limit this gives $\delta_s \sim 1.5 q_s/q_z$ for a momentum spread of $\pm q_s$. Equation (136) then requires $q_s/q_z \sim O(\rho)$ or less. For example, for $q_s/q_z \sim 2\rho$, the growth rate is reduced by a factor of two. For low ρ, as in the FEL, this imposes a stringent requirement on beam quality.

For a spread in transverse energy $\pm h_s$, $\delta_s \sim q_z h_s$. On the other hand, for typical beam profiles, $h_s \sim \sigma_h a_\beta^2/q_z$, where σ_h is a factor of order unity which depends on the beam profile. In this case $\delta_s \sim \sigma_h a_\beta^2$. Peak growth then occurs for a detuning

$$\frac{\delta_0}{\rho} = -\frac{\sigma_h^4}{16}\left(\frac{a_\beta^2}{\rho}\right)^4,$$

with a reduction in the growth rate from the $\delta_1=\delta_0=\mu=0$ result of

$$\vartheta = \frac{8}{3^{1/2}\sigma_h^2}\left(\frac{\rho}{a_\beta^2}\right)^2.$$

For example, we take $\sigma_h \sim 0.5$ and consider the case $a_\beta^2 \sim 10\rho$. We find $\delta_0/\rho \sim -19$ (thus this example only makes sense for $\rho < 2\%$ or so), with the growth rate

reduced by a factor of five. (This choice of σ_h is essentially phenomenological and motivates the more precise treatment of Sec. C.)

b. Quadratic gain regime. Next we consider the limit in which μ is comparable to ρ. We look for a solution with $\delta_s << |\zeta|$, expanding in δ_s/ζ. we have

$$\zeta + \delta_0 \approx \frac{\mu^2}{\zeta}\left\{1 + \frac{1}{3}\left(\frac{\delta_s}{\zeta}\right)^2\right\} + \frac{8\,\rho^3}{\zeta^2}\left\{1 + \left(\frac{\delta_s}{\zeta}\right)^2\right\}.$$

We expand the root about the $\delta_s=0$ solution, $\zeta=\zeta_0+\zeta_1$, and obtain

$$\zeta_1 \approx \left(\frac{\delta_s}{\zeta_0}\right)^2 \frac{\left(\frac{1}{3}\mu^2\zeta_0 + 8\,\rho^3\right)}{\left(2\,\delta_0\zeta_0 + 3\,\zeta_0^2 - \mu^2\right)}.$$

As an example, we consider the correction to the root ζ_+, at the optimal detuning given by Eq. (3.132). In this case we have

$$\zeta_0 \approx \frac{8\,\rho^3}{\mu^2}(-1 + i),$$

$$\delta_0 = -\frac{1}{16}\frac{\mu^4}{\rho^3},$$

so that

$$\zeta_1 = -\frac{1}{2^4 3}(2+i)\frac{\mu^2\delta_s^2}{\rho^3}.$$

This gives a growth rate

$$\Im(\zeta_+) = \frac{8\rho^3}{\mu^2}\left\{1 - \frac{1}{2^7 3}\frac{\mu^4}{\rho^6}\delta_s^2\right\}$$
$$\approx a_\beta^2\left\{1 - \frac{1}{6}\left(\frac{\delta_s}{a_\beta^2}\right)^2\right\} \qquad (3.136)$$

Although the condition for the expansion amounts to $\delta_s << a_\beta^2$, this result should provide a useful estimate for more appreciable δ_s. For example, Eq. (3.136) predicts a factor of two reduction in growth rate for $\delta_s \sim 3^{1/2} a_\beta^2$.

In terms of axial momentum spread, Eq. (3.136) requires $q_s/q_z \sim O(a_\beta^2)$ or less. For a transverse energy spread $h_s \sim \sigma_h a_\beta^2/q_z$, Eq. (3.136) predicts a reduction in the growth rate by a factor $\vartheta \sim 1-\sigma_h^2/6$, which is of order unity.

We conclude from this that the quadratic gain regime is less sensitive to transverse energy spread than the cubic regime. It is slightly more sensitive to axial momentum spread, however, since the constraint on q_s/q_z is lower by a factor of order $O(a_\beta^2/\rho)$.

C. MAXWELL-VLASOV DISPERSION RELATION

In this section, we provide an alternate derivation of the dispersion relation using the method of characteristics applied to the Maxwell-Vlasov equations. This approach is especially useful in assessing the effects of detuning spread due to realistic beam profiles. After working out the dispersion relation, we will apply it to both the step profile and an arbitrary finite profile.

1. Phase space integrals

First we digress briefly to note certain helpful integrals. The normalization of the equilibrium distribution function f_0 is

$$\int d^3\, p\, dx\, dy\; f_0 = \frac{I}{ec}$$

and the average of some function F over the beam cross section is given by

$$\langle F \rangle = \frac{ec}{I}\int d^3\, p\, dx\, dy\; f_0 F \tag{3.137}$$

It will be convenient to convert this to an integral over parameters characterizing the unperturbed trajectories. We parameterize these

trajectories in terms of quantities θ_{x0}, θ_{y0} , q_x, q_y, q_z, and z_0 defined as follows. The betatron angles satisfy

$$\theta_y = \theta_{y0} + \omega_\beta \tau \ ,$$
$$\theta_x = \theta_{x0} + \omega_\beta \tau \ , \qquad (3.138)$$

where θ_{x0} and θ_{y0} are the values at τ=0. The transverse positions are

$$x = -\frac{c}{\omega_\beta}\frac{q_x}{q_z} cos\ (\theta_x) \ ,$$
$$y = -\frac{c}{\omega_\beta}\frac{q_y}{q_z} cos\ (\theta_y) \ . \qquad (3.139)$$

and the momenta are just $p_x=q_x sin(\theta_x)$, and $p_y=q_y sin(\theta_y)$. The axial velocity is given by

$$\frac{v_z}{c} = \frac{\bar{v}_z}{c} + \frac{1}{4q_z^2}\{q_x^2\ cos\ (2\theta_x) + q_y^2\ cos\ (2\theta_y)\} \ ,$$
$$\frac{\bar{v}_z}{c} = 1 - \frac{2 + q_x^2 + q_y^2}{4q_z^2} \ ,$$

and the axial position is given by

$$z = z_i + \bar{v}_z \tau + \frac{\xi_x}{k_z} sin(2\theta_x) + \frac{\xi_y}{k_z} sin(2\theta_y) \ ,$$
$$z_i = z_0 - \frac{\xi_x}{k_z} sin(2\theta_{x0}) - \frac{\xi_y}{k_z} sin(2\theta_{y0}) \ .$$

We recall the dimensionless quantities $\xi_{x,y}$

$$\xi_{x,y} = \frac{1}{8}\frac{k_z}{k_\beta}\frac{q_{x,y}^2}{q_z^2},$$

defined in Eq. (3.13).We may rewrite Eq. (3.133) by making a change of variables in the integrand, using

$$\begin{aligned} dy\, dp_y &= \frac{mc}{k_\beta q_z} q_y dq_y d\theta_{y0}, \\ dx\, dp_x &= \frac{mc}{k_\beta q_z} q_x dq_x d\theta_{x0}. \end{aligned} \tag{3.140}$$

This gives,

$$\langle F \rangle = \frac{m^2 e^2 c}{2k_p^2}(I_0/I)\int dq_z dq_x^2 dq_y^2 d\theta_{y0} d\theta_{x0} \frac{1}{q_z} F f_0$$

We consider the zeroth order distribution function, f_0, to be a function of $H_\perp$ and p_z, and it will be convenient to refer to the dimensionless transverse energy $h=H_\perp/mc^2$,

$$\begin{aligned} h &= \frac{1}{mc}\frac{(p_x^2 + p_y^2)}{2p_z} + \frac{1}{4}k_p^2(x^2 + y^2) \\ &= \frac{1}{2q_z}(q_x^2 + q_y^2) \end{aligned} \tag{3.141}$$

We may then convert <*F*> to an integral over q_y^2, q_z and h,

$$\langle F \rangle = \frac{m^2 e^2 c}{k_p^2} (I_0 / I) \int dq_z dh f_0 \int_0^{2hq_z} dq_y^2 \int_0^{2\pi} d\theta_{y0} \int_0^{2\pi} d\theta_{x0} F \quad . \tag{3.142}$$

When F is a function only of h and q_z, this gives,

$$\boxed{\langle F \rangle = 8\pi^2 \frac{m^2 e^2 c}{k_p^2} (I_0 / I) \int dq_z dh\, q_z h f_0 F} \tag{3.143}$$

It will also be necessary to compute integrals with derivatives of f_0, and we note for reference,

$$\left(\frac{\partial f_0}{\partial p_z}\right)\Big|_{p_x, p_y} = \frac{1}{mc}\left(\frac{\partial f_0}{\partial q_z}\right)\Big|_h - \frac{1}{mc}\left(\frac{\partial f_0}{\partial h}\right)\Big|_{q_z}\left\{\frac{p_x^2 + p_y^2}{2 p_z^2}\right\},$$
$$\left(\frac{\partial f_0}{\partial p_y}\right)\Big|_{p_x, p_z} = \frac{1}{mc}\left(\frac{\partial f_0}{\partial h}\right)\Big|_{q_z}\left(\frac{p_y}{p_z}\right). \tag{3.144}$$

2. *Method of Characteristics*

We proceed to apply the method of characteristics to derive the linearized dispersion relation for an electromagnetic wave copropagating with the beam through the ion-channel. Writing the perturbed distribution function as $f=f_0+f_1$, we the Vlasov equations is to linear order

$$\frac{df_1}{dt} = - F_{z1}\frac{\partial f_0}{\partial p_z} - F_{y1}\frac{\partial f_0}{\partial p_y}, \tag{3.145}$$

where d/dt is evaluated along the zeroth order trajectory. Taking a vector potential $A_y=(mc^2/e)bexp(i\zeta)$, gives

$$\begin{aligned} F_{z1} &= e\frac{v_y}{c}B_x = - imc\,be^{i\zeta}k_z v_y, \\ F_{y1} &= - e\left(E_y + \frac{v_z}{c}B_x\right) = - imc\,be^{i\zeta}(\omega - k_z v_z). \end{aligned} \tag{3.146}$$

f_1 is then given by

$$f_1(\vec{r},\vec{p},t) = \int_{-\infty}^{t} dt' \left\{ k_z v_y \frac{\partial f_0}{\partial p_z} + (\omega - k_z v_z)\frac{\partial f_0}{\partial p_y} \right\} (imc\,be^{i\zeta'}) \tag{3.147}$$

or, in terms of the Fourier transform,

$$f_1(\vec{r},\vec{p}) = \int_{-\infty}^{0} d\tau \left\{ k_z v_y \frac{\partial f_0}{\partial p_z} + (\omega - k_z v_z)\frac{\partial f_0}{\partial p_y} \right\} (imc\,be^{i(\zeta'-\zeta)}) \tag{3.148}$$

Here, the integrand is evaluated on the parameterized trajectory defined in Eqs. (3.138)-(3.140).

This result for f_1 is coupled to Maxwell's equations,

$$\left(c^2\nabla_\perp^2 + \omega^2 - c^2 k_z^2\right)b = \frac{4\pi e^2}{m}\int d^3 p\, f_1(\vec{r}, \vec{p})\frac{p_y}{p_z} \tag{3.149}$$

Note that the integral on the right-side is over the momenta at τ=0.

We assume b varies negligibly across the beam and define the mode area, Σ

$$\Sigma^{-1} = \frac{|b(r=0)|^2}{\int dx dy\, |b|^2} \tag{3.150}$$

Then the dispersion relation takes the form

$$\omega^2 - c^2 k_z^2 - c^2 k_\perp^2 = \frac{4\pi e^2 c}{m\Sigma}\int d^3 p\, dx\, dy \frac{q_y}{q_z} \sin(\theta_{y0}) \rightarrow \times \int_{-\infty}^{0} d\tau \left\{ k_z v_y \frac{\partial f_0}{\partial p_z} + (\omega - k_z v_z)\frac{\partial f_0}{\partial p_y} \right\} (imce^{i(\zeta' - \zeta)}), \tag{3.151}$$

where we make use of the parameterized trajectory given above. Defining the dielectric constant ε

$$\omega^2\varepsilon - c^2 k_z^2 - c^2 k_\perp^2 = 0, \tag{3.152}$$

and writing ε=1+ε_z+ε_y, we have

$$\varepsilon_z = -\frac{4\pi e^2 c}{m\Sigma\omega^2}\int d^3p\,dx\,dy\,\frac{q_y}{q_z}\sin(\theta_{y0})\int_{-\infty}^{0} d\tau\,k_z v_y\frac{\partial f_0}{\partial p_z}(imce^{i(\zeta'-\zeta)}),$$

$$\varepsilon_y = -\frac{4\pi e^2 c}{m\Sigma\omega^2}\int d^3p\,dx\,dy\,\frac{q_y}{q_z}\sin(\theta_{y0})\int_{-\infty}^{0} d\tau\,(\omega - k_z v_z)\frac{\partial f_0}{\partial p_y}(imce^{i(\zeta'-\zeta)}) \tag{3.153}$$

Next we make use of Eq. (3.144) to obtain

$$\varepsilon_z = -i\frac{4\pi e^2 c}{m\Sigma\omega^2}\int d^3p\,dx\,dy\,\frac{q_y}{q_z}\sin(\theta_{y0}) \rightarrow \times\int_{-\infty}^{0} d\tau\,k_z v_y\left\{\frac{\partial f_0}{\partial q_z} - \frac{\partial f_0}{\partial h}\left(\frac{p_x^2 + p_y^2}{2\,p_z^2}\right)\right\}e^{i(\zeta'-\zeta)},$$

$$\varepsilon_y = -i\frac{4\pi e^2 c}{m\Sigma\omega^2}\int d^3p\,dx\,dy\,\frac{q_y}{q_z}\sin(\theta_{y0}) \rightarrow \times\int_{-\infty}^{0} d\tau\,(\omega - k_z v_z)\left(\frac{\partial f_0}{\partial h}\right)\frac{p_y}{p_z}e^{i(\zeta'-\zeta)}. \tag{3.154}$$

Using Eq. (3.140), this may be written in terms of eikonal variables as

$$\varepsilon_{y,z} = -i\frac{8\pi e^2 m^2 c^3}{\omega^2 k_p^2\Sigma}\int dq_x\,dq_y\,dq_z\,d\theta_{x0}\,d\theta_{y0}\frac{q_x q_y^3}{q_z^3}\sin(\theta_{y0})\vartheta_{y,z}, \tag{3.155}$$

where,

$$\vartheta_y = \frac{\partial f_0}{\partial h}\int_{-\infty}^{0} d\tau\,(\omega - k_z v_z)\sin(\theta_y)e^{i(\zeta'-\zeta)}, \tag{3.156}$$

and

$$\vartheta_z = k_z c \int_{-\infty}^{0} d\tau \left\{ \frac{\partial f_0}{\partial q_z} - \frac{\partial f_0}{\partial h} \left(\frac{q_x^2 \sin^2(\theta_x) + q_y^2 \sin^2(\theta_y)}{2 q_z^2} \right) \right\} \sin(\theta_y) e^{i(\zeta' - \zeta)} \quad (3.157)$$

Several different integrals over τ appear in these expressions. For clarity we write them out separately

$$\begin{aligned}
\vartheta_1 &= \int_{-\infty}^{0} d\tau \sin(\theta_y) e^{i(\zeta' - \zeta)}, \\
\vartheta_2 &= \int_{-\infty}^{0} d\tau \cos(2\theta_x) \sin(\theta_y) e^{i(\zeta' - \zeta)}, \\
\vartheta_3 &= \int_{-\infty}^{0} d\tau \cos(2\theta_y) \sin(\theta_y) e^{i(\zeta' - \zeta)}, \\
\vartheta_4 &= \int_{-\infty}^{0} d\tau \sin^2(\theta_x) \sin(\theta_y) e^{i(\zeta' - \zeta)}, \\
\vartheta_5 &= \int_{-\infty}^{0} d\tau \sin^2(\theta_y) \sin(\theta_y) e^{i(\zeta' - \zeta)}.
\end{aligned} \quad (3.158)$$

In terms of these integrals,

$$\vartheta_y = \frac{\partial f_0}{\partial h} (\omega - k_z \bar{v}_z) \vartheta_1 + \frac{\partial f_0}{\partial h} k_z c \left(\frac{q_x^2}{4 q_z^2} \vartheta_2 + \frac{q_y^2}{4 q_z^2} \vartheta_3 \right) \quad (3.159)$$

$$\vartheta_z = k_z c \frac{\partial f_0}{\partial q_z} \vartheta_1 - k_z c \frac{\partial f_0}{\partial h} \left(\frac{q_x^2}{2 q_z^2} \vartheta_4 + \frac{q_y^2}{2 q_z^2} \vartheta_5 \right). \quad (3.160)$$

The term in the exponent in Eq. (3.158) is explicitly

$$\zeta' - \zeta = k_z \bar{v}_z \tau - \omega\tau \rightarrow$$
$$+ \xi_x \sin(2\theta_x) + \xi_y \sin(2\theta_y) - \xi_x \sin(2\theta_{x0}) - \xi_y \sin(2\theta_{y0}) \quad (3.161)$$

so that

$$e^{i(\zeta'-\zeta)} = exp\{-i(\xi_x \sin(2\theta_{x0}) + \xi_y \sin(2\theta_{y0}))\} \rightarrow$$
$$\times \sum_{m,n=-\infty}^{+\infty} J_n(\xi_x) J_m(\xi_y) exp\{2i(n\theta_{x0} + m\theta_{y0})\} \rightarrow$$
$$\times exp\{i(2(n+m)\omega_\beta \tau - \Omega)\tau\} \quad , \quad (3.162)$$

where

$$\Omega = \omega - k_z \bar{v}_z \quad . \quad (3.163)$$

Thus in general, the integrals of Eq. (3.158) are a bit complicated, involving a sum over odd harmonics, with coefficients given by infinite sums of products of Bessel functions. However, in the limit $\xi_x, \xi_y << 1$, these integrals reduce to a quite manageable form. (This is essentially the same approximation made in averaging the terms in Eq. (3.11)).

We have in this limit

$$\vartheta_1 \approx \frac{1}{2}\left\{\frac{e^{i\theta_{y0}}}{\Delta_{+1}} - \frac{e^{-i\theta_{y0}}}{\Delta_{-1}}\right\}, \quad (3.164)$$

where we assume $Im(\Omega)<0$ and we define the detuning from the k-th harmonic

$$\begin{aligned}\Delta_n &= \omega - k_z\bar{v}_z - n\omega_\beta \\ &= \omega - k_z c + k_z c\,\frac{1+q_z h}{2q_z^2} - n\omega_p\frac{1}{\sqrt{2q_z}}\end{aligned}, \tag{3.165}$$

The other integrals are

$$\begin{aligned}\vartheta_2 &\approx 0\ , \\ \vartheta_3 &\approx -\frac{1}{2}\vartheta_1\ , \\ \vartheta_4 &\approx \frac{1}{2}\vartheta_1\ , \\ \vartheta_5 &\approx \frac{3}{4}\vartheta_1\ ,\end{aligned} \tag{3.166}$$

and we discard terms that will vanish after integration over θ_{x0}. Noting that

$$\int_0^{2\pi} d\theta_{x0}\int_0^{2\pi} d\theta_{y0}\,\sin(\theta_{y0})\,\vartheta_1 = i\pi^2\left(\frac{1}{\Delta_+}+\frac{1}{\Delta_-}\right), \tag{3.167}$$

we may write

$$\varepsilon_{y,z} = \frac{8\pi^3 e^2 m^2 c^3}{\omega^2 k_p^2 \Sigma}\int dq_x\,dq_y\,dq_z\,\frac{q_x q_y^3}{q_z^3}\left(\frac{1}{\Delta_+}+\frac{1}{\Delta_-}\right)\tilde{\vartheta}_{y,z}\ , \tag{3.168}$$

where

$$\tilde{\vartheta}_y = \frac{\partial f_0}{\partial h}(\omega - k_z\bar{v}_z)(1) + k_z c\,\frac{\partial f_0}{\partial h}\frac{q_y^2}{4q_z^2}(-\frac{1}{2}),$$
$$\tilde{\vartheta}_z = k_z c\,\frac{\partial f_0}{\partial q_z}(1) - k_z c\,\frac{\partial f_0}{\partial h}\left\{\frac{q_x^2}{2q_z^2}(\frac{1}{2}) + \frac{q_y^2}{2q_z^2}(\frac{3}{4})\right\}. \qquad (3.169)$$

Recalling Eq. (3.14),

$$\frac{\bar{v}_z}{c} = 1 - \frac{2 + q_x^2 + q_y^2}{4q_z^2} = 1 - \frac{1 + q_z h}{2q_z^2}, \qquad (3.170)$$

we see that $\Delta_\pm$ depends on h, but not q_x or q_y individually. In this case, we may change variables to q_y and h, and integrate over q_y, to obtain.

$$\varepsilon_{y,z} = \frac{4\pi^3 e^2 m^2 c^3}{\omega^2 k_p^2 \Sigma}\int dh\,dq_z \frac{1}{q_z^2}\left(\frac{1}{\Delta_+} + \frac{1}{\Delta_-}\right)\int_0^{2q_z h} dq_y^2\, q_y^2\,\tilde{\vartheta}_{y,z}$$
$$= \frac{4\pi^3 e^2 m^2 c^3}{\omega^2 k_p^2 \Sigma}\int dh\,dq_z \frac{1}{q_z^2}\left(\frac{1}{\Delta_+} + \frac{1}{\Delta_-}\right)\hat{\vartheta}_{y,z} \qquad (3.171)$$

where

$$\hat{\vartheta}_{y,z} = \int_0^{2q_z h} dq_y^2\, q_y^2\,\tilde{\vartheta}_{y,z}, \qquad (3.172)$$

or

$$\hat{\vartheta}_y = 2\,q_z^2\,h^2\,\frac{\partial f_0}{\partial h}(\omega - k_z\bar{v}_z) - \frac{1}{3}k_z c\,\frac{\partial f_0}{\partial h}q_z\,h^3\,,$$
$$\hat{\vartheta}_z = 2\,q_z^2\,h^2\,\frac{\partial f_0}{\partial q_z}k_z c - \frac{4}{3}k_z c\,\frac{\partial f_0}{\partial h}q_z\,h^3\,. \tag{3.173}$$

Substituting this in Eq. (3.171), we have

$$\varepsilon = 1 + \frac{4\,\pi^3\,e^2\,m^2\,c^3}{\omega^2\,k_p^2\,\Sigma}\int d\,h\,dq_z(\vartheta' + \vartheta'')\,, \tag{3.174}$$

where

$$\vartheta' = \left(\frac{1}{\Delta_+} + \frac{1}{\Delta_-}\right)\left\{2\,h^2\,\frac{\partial f_0}{\partial h}(\omega - k_z\bar{v}_z)\right\},$$
$$\vartheta'' = \left(\frac{1}{\Delta_+} + \frac{1}{\Delta_-}\right)\left\{-\frac{5}{3}k_z c\,\frac{\partial f_0}{\partial h}\,\frac{h^3}{q_z} + 2\,k_z c h^2\,\frac{\partial f_0}{\partial q_z}\right\}. \tag{3.175}$$

We rewrite ϑ' as

$$\vartheta' = 2\,h^2\,\frac{\partial f_0}{\partial h}\left\{2 + \omega_\beta\left(\frac{1}{\Delta_+} - \frac{1}{\Delta_-}\right)\right\}, \tag{3.176}$$

and integrate by parts using

$$\frac{\partial \Delta_{\pm}}{\partial q_z} = \pm \frac{\omega_\beta}{2 q_z} - k_z c \frac{2 + q_z h}{2 q_z^3},$$
$$\frac{\partial \Delta_{\pm}}{\partial h} = \frac{k_z c}{2 q_z}, \tag{3.177}$$

so that

$$\vartheta' \equiv -4 h f_0 \left(2 + \omega_\beta \left(\frac{1}{\Delta_+} - \frac{1}{\Delta_-}\right)\right) + \frac{h^2 \omega_\beta k_z c}{q_z} f_0 \left(\frac{1}{\Delta_+^2} - \frac{1}{\Delta_-^2}\right), \tag{3.178}$$

and

$$\vartheta'' \equiv 5 k_z c f_0 \frac{h^2}{q_z}\left(\frac{1}{\Delta_+} + \frac{1}{\Delta_-}\right) - \frac{5}{6}(k_z c)^2 f_0 \frac{h^3}{q_z^2}\left(\frac{1}{\Delta_+^2} + \frac{1}{\Delta_-^2}\right) \rightarrow$$
$$\rightarrow + k_z c \omega_\beta f_0 \frac{h^2}{q_z}\left(\frac{1}{\Delta_+^2} - \frac{1}{\Delta_-^2}\right) - (k_z c)^2 \frac{h^2}{q_z^3} f_0 (2 + q_z h)\left(\frac{1}{\Delta_+^2} + \frac{1}{\Delta_-^2}\right). \tag{3.179}$$

From Eq. (3.174) this gives

$$\boxed{\varepsilon = 1 - \frac{\pi c^2}{\omega^2 \Sigma}\left(\frac{I}{I_0}\right)\langle X \rangle}, \tag{3.180}$$

where X is proportional to the dielectric susceptibility, and is given by

$$X = -\frac{5}{2}k_z c\,\frac{h}{q_z^2}\left(\frac{1}{\Delta_+}+\frac{1}{\Delta_-}\right)+\frac{5}{12}(k_z c)^2\,\frac{h^2}{q_z^3}\left(\frac{1}{\Delta_+^2}+\frac{1}{\Delta_-^2}\right)+\rightarrow$$
$$\rightarrow-\frac{h\,\omega_\beta k_z c}{2q_z^2}\left(\frac{1}{\Delta_+^2}-\frac{1}{\Delta_-^2}\right)+\frac{1}{2}(k_z c)^2\,\frac{h}{q_z^4}(2+q_z h)\left(\frac{1}{\Delta_+^2}+\frac{1}{\Delta_-^2}\right)\rightarrow$$
$$+\frac{2}{q_z}\left(2+\omega_\beta\left(\frac{1}{\Delta_+}-\frac{1}{\Delta_-}\right)\right)-\frac{h\,\omega_\beta k_z c}{2q_z^2}\left(\frac{1}{\Delta_+^2}-\frac{1}{\Delta_-^2}\right) \qquad (3.181)$$

Simplifying this somewhat gives

$$\boxed{\begin{aligned} X = &-\frac{5}{2}k_z c\,\frac{h}{q_z^2}\left(\frac{1}{\Delta_+}+\frac{1}{\Delta_-}\right)+\frac{2}{q_z}\left(2+\omega_\beta\left(\frac{1}{\Delta_+}-\frac{1}{\Delta_-}\right)\right)\rightarrow \\ &-\frac{h\,\omega_\beta k_z c}{2q_z^2}\left(\frac{1}{\Delta_+^2}-\frac{1}{\Delta_-^2}\right)+(k_z c)^2\,\frac{h}{q_z^4}\left(1+\frac{11}{12}q_z h\right)\left(\frac{1}{\Delta_+^2}+\frac{1}{\Delta_-^2}\right)\end{aligned}} \qquad (3.182)$$

In the next two sections we apply Eqs. (3.180) and (3.182) to compute the roots ω, of the dispersion relation determined by ε, for various beam distributions, f_0, corresponding to step radial, Gaussian, and parabolic density profiles.

It is worth noting the $h\rightarrow 0$, or cold-beam limit of Eq. (3.180),

$$\lim_{h\to 0}\varepsilon = 1-\frac{\tilde{\omega}_{beff}^2}{\omega^2}\,\frac{(\omega-k_z\bar{v}_z)^2}{(\omega-k_z\bar{v}_z)^2-\omega_\beta^2}, \qquad (3.183)$$

where we recall the effective beam plasma frequency, from Eq. (3.93),

$$\tilde{\omega}_{beff}^2 = \frac{4\pi c^2}{\Sigma}\left(\frac{I}{q_z I_o}\right). \tag{3.184}$$

This reduces to the expected results in the $\omega_\beta \to 0$ and $v_z \to 0$ limits. as we shall see below, the resonant part of this cold beam dielectric corresponds to the Π term in Eq. (3.103), and the μ^2 term in Eq. (3.104). It is straightforward to show that this ε gives rise to no instability, as we would expect from the discussion of the ponderomotive force of Eq. (3.70).

3. Step Radial Profile

To make contact with the results of the eikonal treatment, we consider first the case of a beam with uniform transverse energy,

$$f_0(h, q_z) = \frac{1}{8\pi^2}\frac{k_p^2}{m^2 e^2 c}(I/I_0)\frac{1}{h_0 q_{z0}}\delta(h - h_0)\,\delta(q_z - q_{z0}), \tag{3.185}$$

corresponding to a step radial variation in beam density, with beam radius, a, given by $h_0 = k_p^2 a^2/4$. The overlap integral is $\eta = \pi a^2/\Sigma$. We specialize to the case of small detuning from the fundamental, so that $\omega = \omega_0 + i\Gamma$, where $Re(\Gamma)$ corresponds to the growth rate to be calculated, and ω_0 is the resonant frequency, satisfying

$$\omega_0 - k_z v_z = \omega_\beta - \Delta\omega, \tag{3.186}$$

with $\Delta\omega << \omega_\beta$. In addition, we take ω_0 to satisfy the dispersion relation of Eq. (3.92),

$$\omega_0^2 = c^2\left(k_z^2 + k_\perp^2\right) + \tilde{\omega}_{beff}^2 . \tag{3.187}$$

Assuming $Re(\Gamma) << \omega_\beta$, we may neglect the Δ_{-1} terms in evaluating X, from Eq. (3.182). In this case the dispersion relation takes the form, identical to Eq. (3.104),

$$\Gamma(\Gamma + i\Delta\omega)^2 + \mu^2(\Gamma + i\Delta\omega)\omega_\beta^2 = i\left(2\rho\omega_\beta\right)^3 , \tag{3.188}$$

where the Pierce parameter ρ is given by

$$\rho^3 = \left(\frac{\eta I}{32 q_{z0} I_0}\right)\left(\frac{k_z c}{\omega_0}\right)\left\{\left(\frac{k_z c}{\omega_0}\right)\frac{\omega_0}{2 q_{z0}^2 \omega_\beta}\left(2 + \frac{11}{6}a_\beta^2\right) - 1\right\}, \tag{3.189}$$

with $a_\beta^2 = q_{z0} h_0$, as defined in Eq. (3.68). This is just Eq. (3.105) at lowest order in a_β^2, which we obtained by perturbing the electron equations of motion directly.

The dimensionless constant μ is

$$\begin{aligned}\mu^2 &= \frac{\pi c^2}{\Sigma}\left(\frac{I}{q_{z0} I_0}\right)\frac{1}{\omega_0 \omega_\beta}\left(1 - \frac{5}{4}\frac{k_z c}{q_z^2 \omega_\beta}a_\beta^2\right) \\ &= \frac{1}{4}\left(\frac{\eta I}{q_{z0} I_0}\right)\frac{2 q_z^2 \omega_\beta}{\omega_0}\frac{1}{a_\beta^2}\left(1 - \frac{5}{4}\frac{k_z c}{q_z^2 \omega_\beta}a_\beta^2\right),\end{aligned} \tag{3.190}$$

which is just Eq. (3.107) at lowest order in a_β^2. For example, for a fast-wave and zero detuning,

$$\mu^2 = 8\frac{\rho^3}{a_\beta^2}\left(1 - \frac{5}{2}a_\beta^2\right), \tag{3.191}$$

This result also shows that μ^2 vanishes for $a_\beta^2 \sim 0.4$.

From the work of this section, we conclude that the Maxwell-Vlasov treatment confirms the results of the eikonal model of the previous section. We turn to consider the effect of detuning spread.

4. Arbitrary, finite radial profile

One shortcoming of the step-profile model is that all particles have the same drift velocity in z. In general, we expect a spread in drift velocities, or equivalently, detuning, to produce Landau damping and to reduce gain, as discussed in Sec. B.3e. In this section, we consider the effect of such detuning spread and quantify its effect on gain.

We will consider an arbitrary finite distribution f_0, where by "finite" we mean that the first and second moments, $\langle h \rangle$ and $\langle h^2 \rangle$ are finite. This assumption (which excludes, for example, the Bennet profile) is necessary as we shall have occasion to refer to the fractional rms deviation in h

$$\sigma_h = \frac{1}{\langle h \rangle}\sqrt{\langle h^2 \rangle - \langle h \rangle^2} \quad . \tag{3.192}$$

a. Modified dispersion relation. We proceed to compute <*X*>, in order to derive the dispersion relation. We specialize as before to the case of small detuning from the fundamental, so that Δ_+ is small compared to ω_β at zeroth order. Now, for $\sigma_h \neq 0$, there is an instrinsic spread in detuning. (An exception to this is the case of a slow-wave.) Defining

$$a_\beta^2 = q_z \langle h \rangle \quad , \tag{3.193}$$

and defining a dimensionless rms detuning spread,

$$\begin{aligned} \delta_s &= \frac{1}{\omega_\beta}\left(\langle \Delta_+^2 \rangle - \langle \Delta_+ \rangle^2\right)^{1/2} \\ &= \frac{k_z c}{2 q_z^2 \omega_\beta} a_\beta^2 \sigma_h \end{aligned} \quad , \tag{3.194}$$

we see that the spread is of order $\sigma_h a_\beta^2$. We will assume $\sigma_h a_\beta^2 << 1$ so that we may neglect the Δ_- terms in Eq. (3.182). In this case,

$$X \approx \frac{4}{q_z} + \left(-\frac{5}{2} k_z c \frac{h}{q_z^2} + \frac{2}{q_z}\omega_\beta\right)\frac{1}{\Delta_+} + (k_z c)\frac{h}{q_z^2}\left(\frac{k_z c}{q_z^2}\left(1 + \frac{11}{12} q_z h\right) - \omega_\beta\right)\frac{1}{\Delta_+^2} \quad . \tag{3.195}$$

To compute <*X*> we evidently need to compute the integrals,

$$\vartheta_1 = \left\langle \frac{1}{\Delta_+} \right\rangle ,$$
$$\vartheta_2 = \left\langle \frac{h}{\Delta_+} \right\rangle ,$$
$$\vartheta_3 = \left\langle \frac{h}{\Delta_+^2} \right\rangle ,$$
$$\vartheta_4 = \left\langle \frac{h^2}{\Delta_+^2} \right\rangle . \tag{3.196}$$

In terms of these integrals, we have

$$\langle X \rangle \approx \frac{4}{q_z} - \frac{5}{2}\frac{k_z c}{q_z^2}\vartheta_2 + \frac{2\omega_\beta}{q_z}\vartheta_1 + \frac{k_z c}{q_z^2}\left\{\left(\frac{k_z c}{q_z^2} - \omega_\beta\right)\vartheta_3 + \frac{11}{12}\frac{k_z c}{q_z}\vartheta_4\right\} . \tag{3.197}$$

In general, Eq. (3.197) will result in a transcendental dispersion relation, analagous to, but more complicated than that of Eq. (3.134). As with Eq. (3.134), we may simplify this by assuming a small detuning spread, and expanding the dispersion relation to obtain the lowest order correction to the growth rate. Recalling Eq. (3.165),

$$\Delta_+ = \omega - k_z c + k_z c \frac{1 + q_z h}{2 q_z^2} - \omega_\beta . \tag{3.198}$$

it is convenient to write

$$\Delta_+ = -\Delta\omega + i\Gamma + \frac{k_z c}{2 q_z}\left(h - \langle h \rangle\right), \tag{3.199}$$

where $-\Delta\omega$ is the average of Δ_+ at zeroth order,

$$\Delta\omega = k_z c - \omega + \frac{k_z c}{2 q_z^2} + \omega_\beta + \frac{k_z c}{2 q_z}\langle h \rangle \tag{3.200}$$

We then write Eq. (3.198) as $\Delta_+ = \Delta_0 + \Delta_1$, where

$$\Delta_0 = -\Delta\omega + i\Gamma ,$$
$$\Delta_1 = \frac{k_z c}{2 q_z}\left(h - \langle h \rangle\right). \tag{3.201}$$

Defining $\varepsilon = \Delta_1/\Delta_0$, we assume that $|\varepsilon| << 1$, and expand the integrals of Eq. (3.195).

$$\vartheta_1 \approx \frac{1}{\Delta_0}\langle 1 - \varepsilon + \varepsilon^2 - \varepsilon^3 + \ldots \rangle ,$$
$$\vartheta_2 \approx \frac{1}{\Delta_0}\langle h\,(1 - \varepsilon + \varepsilon^2 - \varepsilon^3 + \ldots)\rangle ,$$
$$\vartheta_3 \approx \frac{1}{\Delta_0^2}\langle h\,(1 - 2\varepsilon + 3\varepsilon^2 + \ldots)\rangle ,$$
$$\vartheta_4 \approx \frac{1}{\Delta_0^2}\langle h^2\,(1 - 2\varepsilon + 3\varepsilon^2 + \ldots)\rangle . \tag{3.202}$$

To simplify matters, we will neglect the corrections higher order in $a\beta^2$ represented by ϑ_2 and ϑ_4. Keeping only terms through $O(1/\Delta_0^3)$, we have

$$\vartheta_1 \approx \frac{1}{\Delta_0} + \frac{1}{\Delta_0^3}\sigma_h^2\langle h\rangle^2\left(\frac{k_z c}{2q_z}\right)^2,$$

$$\vartheta_3 \approx \frac{1}{\Delta_0^2}\langle h\rangle - 2\frac{1}{\Delta_0^3}\sigma_h^2\langle h\rangle^2\left(\frac{k_z c}{2q_z}\right). \tag{3.203}$$

From Eq. (3.197) we write $\langle X\rangle = X_1 + X_2$ where

$$X_1 \approx \frac{4}{q_z} + \frac{2\omega_\beta}{q_z}\frac{1}{\Delta_0} + \frac{k_z c}{q_z^2}\left(\frac{k_z c}{q_z^2} - \omega_\beta\right)\frac{1}{\Delta_0^2}\langle h\rangle,$$

$$X_2 \approx -\frac{1}{\Delta_0^3}\sigma_h^2\langle h\rangle^2\frac{(k_z c)^2}{q_z^3}\left(\frac{k_z c}{q_z^2} - \frac{3}{2}\omega_\beta\right). \tag{3.204}$$

The term X_1 corresponds to the cold-beam susceptibility, while X_2 incorporates finite temperature effects.

Next we write out the modified dispersion relation. We take ω_0 to satisfy the dispersion relation of Eq. (3.92), and define $\zeta = (i\Gamma - \Delta\omega)/\omega_\beta$ as in Eq. (3.121). The modified dispersion relation is then

$$\zeta + \delta_0 \approx \frac{\mu^2}{\zeta} + \frac{8\rho^3}{\zeta^2} - \frac{\upsilon^4}{\zeta^3}, \tag{3.206}$$

where $\delta_0 = \Delta\omega/\omega_\beta$ is the average detuning. Note that the condition for the validity of the expansion, $|\varepsilon| << 1$, can be written $\sigma_h a_\beta^2 << |\zeta|$. The dimensionless parameters μ and ρ are defined as before in terms of ω_{beff} as in Eqs. (3.105) and (3.107). The dimensionless parameter υ is given by

$$\upsilon^4 = \frac{1}{8}\frac{\omega_{beff}^2}{\omega_0\,\omega_\beta^4}\sigma_h^2 a_\beta^4 \frac{(k_z c)^2}{q_z^5}\left(\frac{k_z c}{q_z^2} - \frac{3}{2}\omega_\beta\right), \tag{3.207}$$

and for a fast-wave,

$$\upsilon^4 \approx 8\,\rho^3\sigma_h^2 a_\beta^2 . \tag{3.208}$$

Now Eq. (3.206) is rather different from the result of Sec B.3.e, where we modelled detuning spread with a flat distribution. In that case, we found that the $O(1/\zeta^3)$ correction to the dispersion relation vanished, and we went on to compute the effect of the $O(1/\zeta^4)$ term. Such a distribution of detuning is a fair model of the effect of axial momentum spread. However, since the distribution of transverse energy is weighted by a factor of h (see Eq. [3.143]) we have found that in fact there is a non-vanishing $O(1/\zeta^3)$ term. We will now proceed to calculate the correction to the growth rate due to this term. We shall show that this effect is small, and in this way verify the simpler phenomenological model.

To compute the correction to the υ=0 root we expand $\zeta=\zeta_0+\zeta_1$ and find,

$$\zeta_1 = -\,\upsilon^4\left(\zeta_0^3 + \mu^2\,\zeta_0 + 16\,\rho^3\right)^{-1} . \tag{3.209}$$

b. Cubic regime. In the limit $\mu<<\rho$, Eq. (3.209) becomes

$$\zeta_1 \approx -\frac{\vartheta^4}{24\,\rho^3}\left(1-\frac{\mu^2}{\zeta_0^2}\right), \tag{3.210}$$

which in the fast-wave limit is

$$\zeta_1 \approx -\frac{1}{3}\sigma_h^2 a_\beta^2\left(1-\frac{\zeta_0}{a_\beta^2}\right). \tag{3.211}$$

Thus the shifted root is just

$$\zeta_0+\zeta_1 \approx -\frac{1}{3}\sigma_h^2 a_\beta^2+\zeta_0\left(1+\frac{1}{3}\sigma_h^2\right). \tag{3.212}$$

This implies that the growth rate is increased by a small factor

$$\vartheta \approx 1+\frac{1}{3}\sigma_h^2, \tag{3.213}$$

which is typically of order unity.

c. Quadratic regime. For $\mu>\rho$, we consider ζ_0 corresponding to the optimal detuning given by Eq. (3.132), so that

$$\zeta_0 = \frac{8\,\rho^3}{\mu^2}(-1+i),$$
$$\delta_0 = -\frac{1}{16}\frac{\mu^4}{\rho^3}. \tag{3.214}$$

In this case

$$\zeta_1 \approx -\frac{1}{16}\frac{\upsilon^4}{\rho^3}(1-i) \quad , \tag{3.215}$$

corresponding to a slight increase in the growth rate by a factor

$$\begin{aligned} \vartheta &\approx 1 + \frac{1}{128}\frac{\upsilon^4\,\mu^2}{\rho^6} \\ &\approx 1 + \frac{1}{2}\sigma_h^2 \end{aligned} \quad , \tag{3.216}$$

where in the last equality we take the fast-wave limit.

We proceed to compute the factors of Eq. (3.213) and (3.216) for two typical beam profiles.

d. Example: parabolic profile. We consider first a uniform distribution in transverse energy,

$$f_0(h, q_z) = \frac{1}{4\pi^2}\frac{k_p^2}{m^2 e^2 c}(I/I_0)\frac{1}{h_0^2 q_{z0}} H(h_0 - h)\,\delta(q_z - q_{z0}) \quad , \tag{3.217}$$

where H is the step function. This corresponds to a parabolic beam density profile,

$$n(r) = n_0\left(1 - \frac{r^2}{a^2}\right)H(a - r), \tag{3.218}$$

where the beam density on axis, n_0 and the current are related by $I=\pi a^2 e c n_0/2$. The beam radius, a is related to h_0 by $h_0=k_p^2 a^2/4$. For the parabolic profile Eq. (3.143) takes the form

$$\langle F\rangle = \frac{2}{h_0^2}\int_0^h dh\, hF(h)$$

Thus $\langle h\rangle=(2/3)h_0$ and $\langle h^2\rangle=(1/2)h_0^2$, and $\sigma_h^2=1/8$. Equation (213) then predicts an increase in growth rate of about 4% in the cubic regime, while Eq. (3.216) predicts a 7% increase in the quadratic regime.

e. Example: Gaussian profile. For a second example, we consider a Maxwell-Boltzmann distribution in transverse energy,

$$f_0(h, q_z) = \frac{1}{8\pi^2}\frac{k_p^2}{m^2e^2c}(I/I_0)\frac{1}{h_0^2 q_{z0}}\delta(q_z - q_{z0})\exp\left(-\frac{h}{h_0}\right),$$

This corresponds to a gaussian density profile,

$$n(r) = n_0 \exp\left(-\frac{r^2}{a^2}\right), \tag{3.219}$$

where the beam density on axis, n_0 and the current are related by $I=\pi a^2 e c n_0$. The beam radius, a is related to h_0 by $h_0=k_p^2 a^2/4$. Equation (143) takes the form

$$\langle F \rangle = \frac{1}{h_0^2}\int_0^\infty d\,h\,h\,exp\left(-\frac{h}{h_0}\right)F$$

Thus $\langle h\rangle=2h_0$ and $\langle h^2\rangle=6h_0^2$, and $\sigma_h^2=1/2$. Equation (213) then predicts a correction to the growth rate of about 16% in the cubic regime, while Eq. (3.216) predicts a 25% correction in the quadratic regime.

We conclude from this analysis that detuning spread due to a realistic beam profile does not seriously modify our estimates. Indeed, it appears that the most significant correction appears at order $O(1/\zeta^4)$ as indicated by the treatment in Sec. 3.B.e. No additional constraint has appeared in the course of this more rigorous calculation.

Finally, it is worth pointing out that this analysis establishes that the instability does not depend on an inverted distribution in h (e.g., $\delta(h-h_0)$).

D. RADIATION GUIDING

In this section, we calculate the overlap integral, η, in various regimes. The simplest estimate $\eta\sim1$ (perfect overlap) is adequate when the gain length is short compared to the Rayleigh length, $L_g<<L_R=\pi a^2/\lambda$, where $\lambda=2\pi c/\omega$. On the other hand,

$$L_R \approx \frac{a_\beta^2}{\pi}\lambda_\beta < \lambda_\beta ,$$

while $L_g > \lambda_\beta$. Thus diffraction is always important and, in this case, effects which provide guiding of the radiation must be included in our treatment.

In fact, the strength of guiding is rather critical, due indirectly to a combination of two constraints previously discussed. We know that to avoid detuning spread, we must have $a_\beta^2 < O(\rho)$. On the other hand, the condition that beam space-charge be negligible ($n_p >> n_b/\gamma^2$) can be written $\nu' << a_\beta^2$, where $\nu' = I/q_z I_0$. Now we observe from Eq. (3.106) that $\rho = (\eta\nu'/32)^{1/3}$ (in the fast-wave limit), and putting these two constraints on a_β^2 together, we have $\nu' << a_\beta^2 < (\eta\nu'/32)^{1/3}$, or $\eta >> \nu^2/32$. Thus guiding must not be so weak, and ρ so small, that the focussing strength consistent with small detuning spread is comparable to the beam self-fields. This constraint is not typically severe.

In this section, we consider: guiding by the ion-channel (viewed as a dielectric waveguide), guiding by a conducting waveguide, and optical guiding,[16] an effect which arises from the resonant contribution to the refractive index. In principle one should incorporate all these effects into a single model. However, we will consider each separately since, in practice, only one dominates.

We also should add a caveat that employing ion-channel dielectric guiding will depend on damping or reduction of the "electron-hose" instability, discussed in the previous chapter.

1. Ion-channel dielectric guiding

Neglecting collisions of plasma electrons, the channel serves as a cylindrically symmetric, dielectric waveguide, with step discontinuity in the dielectric constant,

$$\varepsilon(r,\omega) = \begin{cases} 1 & ; r < b \\ 1 - \dfrac{\omega_p^2}{\omega^2} & ; b \le r \end{cases} \tag{3.220}$$

where r is the radial coordinate, $r^2=x^2+y^2$.

Such a waveguide will always have at least one guided mode, the HE_{11} mode. We proceed to apply the results of Marcuse[17] to compute the overlap between this mode and the beam, in the limit $\omega>>\omega_p$. The transverse vector potential is,

$$A_y \approx \frac{mc^2}{e} A \sin(\zeta) \begin{cases} J_0(\kappa r) & ; r < b \\ \dfrac{J_0(\kappa b)}{K_0(\mu b)} K_0(\mu r) & ; b \le r \end{cases} \tag{3.221}$$

where J_n and K_n denote the n-th order Bessel functions.[18] Equation (221) shows that within the channel the vector potential decreases away from the axis on the scale κ^{-1}, and evanesces beyond the channel wall on the scale μ^{-1}. The quantities κ and μ are determined from Maxwell's equations,

$$\omega^2 = c^2 k_z^2 + c^2 \kappa^2 ,$$
$$\kappa^2 + \mu^2 = k_p^2 , \tag{3.222}$$

and the continuity condition at $r=b$

$$\kappa \frac{J_1(\kappa b)}{J_0(\kappa b)} = \mu \frac{K_1(\mu b)}{K_0(\mu b)} . \tag{3.223}$$

It is convenient to define a dimensionless "waveguide parameter"

$$V^2 = (\mu b)^2 + (\kappa b)^2 , \tag{3.224}$$

where, from Eq. (3.222),V is just the channel parameter of Eq. (2.15),

$$\boxed{V = k_p b} \tag{3.225}$$

In principle, V determines μb and κb through Eqs. (3.222) and (3.223), and, thus determines the efficacy of the guiding. It is not really surprising to see V appear again, since we are again considering shielding, albeit electromagnetic rather than just magnetic shielding.

The total power is related to the dimensionless amplitude, A, according to

$$P_{tot} = P_o \frac{\omega}{c} k_z b^2 A^2 \Lambda, \tag{3.226}$$

where $P_0=m^2c^5/e^2$~8.71 GW, and Λ is a dimensionless mode area ,

$$\boxed{\Lambda = \frac{1}{8}\left\{\frac{VJ_1(\kappa b)}{\mu b}\right\}^2} \tag{3.227}$$

The power flowing through the beam volume is, for $\kappa a<<1$

$$P_b = \frac{1}{8} P_o \frac{\omega}{c} k_z a^2 A^2 \tag{3.228}$$

Thus the overlap integral is

$$\eta = \frac{P_b}{P_{tot}} = \frac{a_\beta^2}{2 q_z V^2 \Lambda} \tag{3.229}$$

The Pierce parameter with dielectric guiding is then

$$\boxed{\rho = \frac{a_\beta^{2/3}}{2^{8/3} q_z^{2/3} \Lambda^{1/3}}}, \tag{3.230}$$

and the gain length (for $\mu=\delta=0$) is

$$L_g \approx \frac{2^{5/3}}{\pi 3^{1/2}} \lambda_\beta \left(\frac{\gamma^2 \Lambda}{a_\beta^2} \right)^{1/3} \tag{3.231}$$

(Although the actual gain length will of course depend on μ and δ, this is useful as a figure of merit.) Interestingly, the only explicit current dependence in L_g is through the dimensionless mode area, Λ.

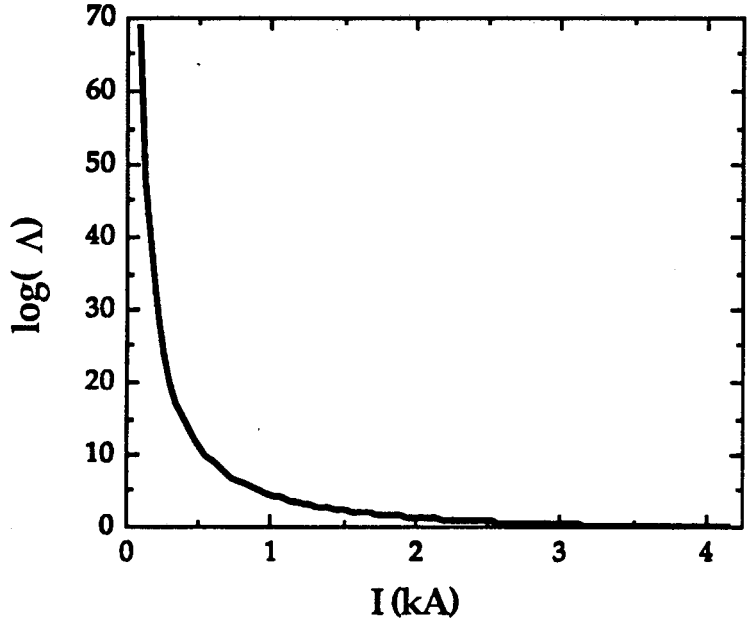

FIG. 3.10. The dimensionless mode area, Λ, of the HE_{11} mode of the ion-channel, decreases sharply as a function of beam current I for $I \leq 2$ kA. Plot of $log_{10}(\Lambda)$ versus $I(kA)$ shows that Λ passes through about 70 orders of magnitude for I varying from 100 A to 4 kA.

Now, characteristically plasmas shield currents on the scale of a plasma skin-depth, k_p^{-1}. On the other hand, in order for the radiation mode to

be confined to the channel, plasma currents must shield out the field over a length of order b. Thus for good guiding, we should require $b>k_p^{-1}$ or $V>1$. We make this more quantitative by solving for κ, μ and Λ explicitly in the limits of weak ($V\leq 1$), moderate ($1\leq V\leq 5$) and strong ($V>>1$) guiding.

a.Weak guiding. For $V\leq 1$ (i.e., $I\leq 4$ kA), the solution of Eq. (3.223) is

$$\mu b \approx 2\, exp\left(-\frac{1}{V}\frac{J_0(V)}{J_1(V)} - \gamma_E\right), \tag{3.232}$$

and $\kappa b \sim V$. The constant $\gamma_E \sim 0.5772$ is Euler's constant. In this regime, $\mu b<<1$ and the fields extend far beyond the channel. For example, $\mu b \sim 0.2$ for $V=1$.

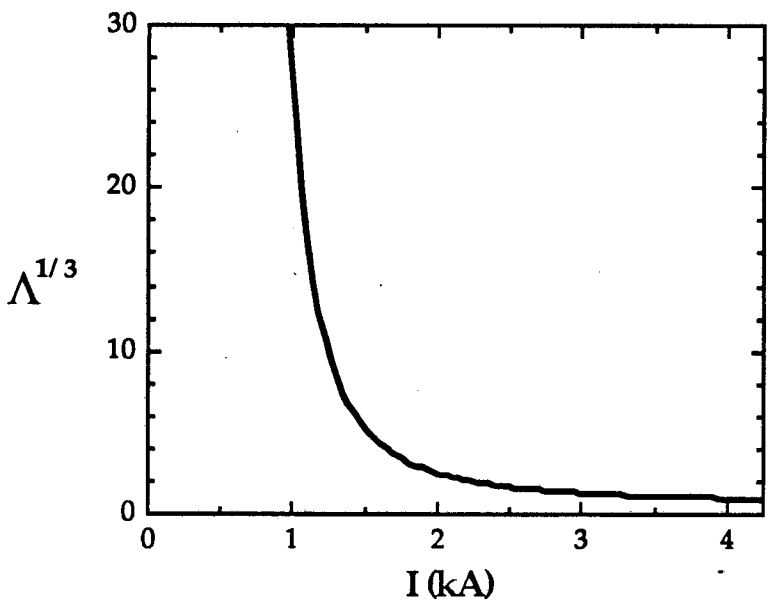

FIG. 3.11. Plot of $\Lambda^{1/3}$, the current dependent factor in the gain length of Eq. (3.231) varies by a factor of about 30 for I varying from 1 kA to 4 kA.

The mode area is

$$\Lambda \approx \frac{1}{32}\left\{V\, J_1(V)\, exp\left(\frac{1}{V}\frac{J_0(V)}{J_1(V)} + \gamma_E\right)\right\}^2 , \tag{3.233}$$

and is quite sensitive to current, as indicated in Figs. 3.10 and 3.11. For example, $\Lambda^{1/3}$ ranges from $\Lambda^{1/3}$~7x10^{10} for I=0.2 kA to $\Lambda^{1/3}$ ~2.4 for I~2 kA. For V=1, $\Lambda^{1/3}$~0.83.

The dispersion relation is

$$\omega^2 = c^2 k_z^2 + \omega_p^2 \cos^2(\alpha) , \tag{3.234}$$

where

$$\sin(\alpha) = \frac{J_1(V)}{\sqrt{8\Lambda}} . \tag{3.235}$$

The angle α is an increasing function of V, with α~12° at V=1. Thus for $V \leq 1$, most of the radiation propagates outside the channel, in quasineutral plasma.

b. Moderate guiding. For intermediate values of V ($1 \leq V \leq 5$) we have solved Eq. (3.223) numerically. In Fig. 3.5, $\Lambda^{1/3}$ is plotted for the corresponding range of current (4 kA<I<100 kA), and this plot complements Fig. 3.10. In Fig.

3.12, μb and κb are plotted versus V. Over this range μb is nearly linear and is well-fit by $\mu b \sim -0.92 + 1.11\ V$.

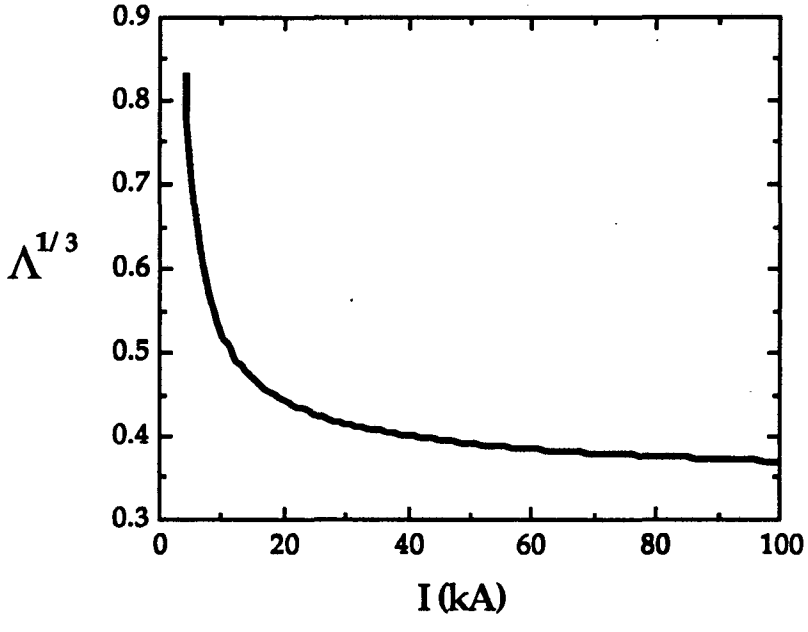

FIG. 3.12. The dimensionless mode area, Λ, of the HE_{11} mode of the ion-channel, as a function of beam current I for 4 kA$\leq I \leq$100 kA.

Now, the HE_{11} mode is unique in that it has zero cut-off and it should be noted that at high currents, other guided modes will appear. Each of these modes has a non-zero cut-off waveguide parameter, $V_c>0$, satisfying $J_n(V_c)=0$, where n is the radial mode number. For the ion-channel this means that for each mode there is a minimum beam current, $I_c \sim I_0(V_c/4)^2$, required for propagation. At a given V, the number of additional modes above cut-off is just the number of solutions of $J_n(V_c)=0$, with $V_c<V$. The next mode above the HE_{11} mode corresponds to $V_c=j_{0,1}=2.405$ (I_c=24.6 kA). Thus for I<24.6 kA

all modes are below cut-off, except the HE_{11} mode. The constant $j_{n,s}$ is the s-th zero of J_n. For reference, the first five mode cut-offs are listed in Table 3.2.[19]

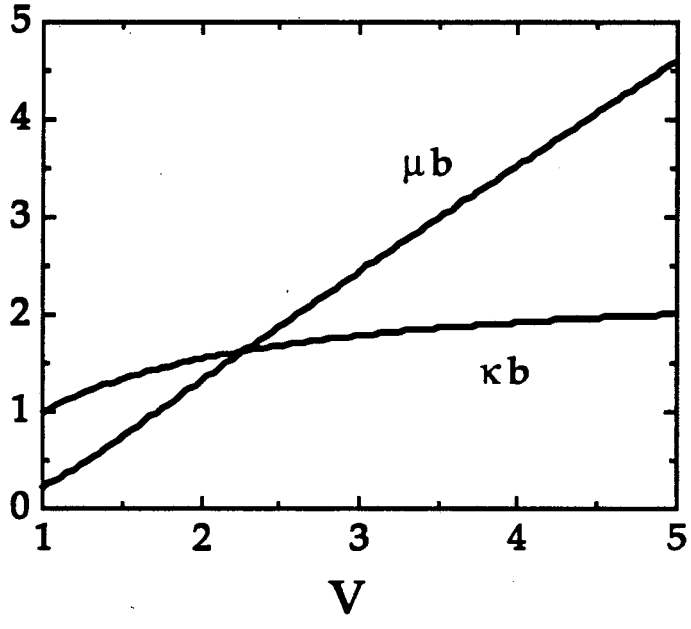

FIG. 3.13. The parameters κa and μa from Eq. (3.223) and (3.224), as a function of the waveguide parameter, V.

We also note that at high current the simple relation between V and I is altered. When the skin-depth is small, plasma electrons drift appreciably in z, and the resulting "vxB" force tends to expel them farther from the channel. Asymptotically, for $I>>I_0$, $b\sim a(2n_b/n_p)^{1/2}$, and V is bigger by a factor of order $2^{1/2}$. Thus the cut-off currents listed in Table 3.2 should be considered approximate values, accurate only to within a few tens of percents.

c. Strong guiding. For $V>>1$, $\mu b \sim V>>1$ and the field evanesces rapidly outside the channel. The solution of Eq. (3.223) for κb is

$$\kappa b \approx j_{0,1} \exp\left(-\frac{1}{V}\right), \tag{3.236}$$

and the mode area is

$$\Lambda \approx \frac{1}{8} J_1(\kappa b)^2 . \tag{3.237}$$

Thus Λ asymptotes to a constant ~3.34×10^{-2} independent of current. In this limit, the gain length from Eq. (3.231) is $L_g \sim 0.2\lambda_\beta(\gamma/a_\beta)^{2/3}$ and has no explicit current dependence. The dispersion relation is just $\omega \sim ck_z$, i.e., the fields are well confined to the channel and don't "see" the plasma.

Table 3.2: Approximate currents at cut-off for the ion-channel waveguide.

V_c	I_c (kA)
$j_{0,1}$=2.405	25
$j_{1,1}$=3.832	62
$j_{2,1}$=5.136	112
$j_{0,2}$=5.520	130
$j_{3,1}$=6.380	173

It is evident from these considerations that at high currents, typical, for example, of induction accelerators, dielectric guiding may be effective in

enhancing the overlap of the beam and radiation fields. In principle, this mechanism could be employed at very short wavelengths where machined waveguides would be inadequate, providing guiding of a sort not available for evacuated free-electron radiation devices. In fact, this mechanism can be tested and employed independent of the ion-channel laser instability. For example, it could be employed in an ordinary FEL to inhibit diffraction.

2. *Effect of Conducting Waveguide*

We shall find that, for operation of the ion-channel laser as a microwave amplifier, dielectric guiding is not quite as effective as guiding by a conducting waveguide. This may be seen from Eq. (3.232). For currents as high as a few kA and beam radii of 1 cm or so, the field evanesces radially on the scale of a fraction of a meter, a larger scale than that of the beam pipe. Thus in the microwave regime, it is necessary to consider modifications due to the presence of a conducting waveguide. Such modifications have been set down by Orzechowski *et al.*,[20] for the FEL, and we take them over directly for the ICL.

a. Rectangular waveguide. Consider first rectangular waveguide with dimensions $w_x > w_y$. We consider operating in the TE_{10} mode, rather than the usual TE_{01} mode used in FEL work. This is possible since the beam electrons make only small excursions off-axis, unlike in the FEL. This choice of mode has the added advantage that, depending on the waveguide parameters, higher order modes may be below cut-off. The dispersion relation is

$$\omega^2 = c^2 k_z^2 + c^2 k_\perp^2 , \tag{3.238}$$

where $k_\perp = \pi/w_x$. We neglect the effect of the plasma in modifying the dispersion relation, in the limit $k_\perp >> k_p$. The overlap factor is

$$\eta = \frac{2\pi a^2}{w_x w_y} , \tag{3.239}$$

and we assume $a << w_x$, so that the field does not vary appreciably across the beam.

b. Circular waveguide. Next, we consider a circular waveguide of radius R, operated in the TE_{01} mode. The dispersion relation is that of Eq. (3.238) with $k_\perp = j'_{01}/R$, where $j'_{01} \sim 3.832$ is the first zero of J_0'. We will neglect the effect of the plasma in modifying the dispersion relation. The overlap factor is

$$\eta = \frac{1}{j_{10}^2 J_2(j_{10})^2} \frac{a^2}{R^2} \approx 0.42 \frac{a^2}{R^2} , \tag{3.240}$$

using $J_2(j_{10}) \sim 0.4027$. We assume $a << R$, so that the field does not vary appreciably across the beam. Note that three additional modes are above cut-off, the TE_{11} ($k_\perp = j'_{11}/R$, $j'_{11} \sim 1.841$), the TM_{01} ($k_\perp = j_{01}/R$, $j_{01} \sim 2.405$), and the TE_{21} ($k_\perp = j'_{21}/R$, $j'_{21} \sim 3.054$). The incorporation of multiple mode effects in the

particle dynamics can be accomplished in a manner analagous to that for the FEL.[21,22]

3. Optical Guiding

It is evident from the dielectric constant given by Eq. (3.180) and (3.182) that the fast-wave interaction results in a modified index of refraction, which is complex and varies radially. This suggests the possibility of a waveguide effect due to the resonant interaction itself, regardless of other conducting or dielectric boundaries. Such an effect was noted by Scharlemann *et al.*,[16], and Moore,[23] for the FEL. This "optical guiding" or "active guiding" and related topics have been studied in detail by Xie[24,25] and others.[26] In this section, we shall give a simple approximate treatment of this effect in the ICL, which is valid in the limit of weak guiding.

We return to and rewrite Eq. (3.152), in the form

$$\omega^2 - c^2 k_z^2 - c^2 k_\perp^2 \approx \frac{\pi c^2}{\Sigma}(I/I_0)\langle X \rangle , \tag{3.241}$$

using Eqs. (3.180) and (3.182). We remove the average over the radiation mode cross-section,

$$\left(\nabla_\perp^2 + \frac{\omega^2}{c^2} - k_z^2\right) b \approx \frac{1}{a^2}(I/I_0) X H(a - r) b , \tag{3.242}$$

restoring the mode profile, b. We consider a step radial profile for illustration, so that H is the step function. We may describe this result in terms of a radially varying, complex dielectric constant

$$\varepsilon(r) \approx \begin{cases} 1 - \frac{c^2}{\omega^2 a^2}(I/I_0)X & ; r < a \\ 1 & ; a \le r \end{cases} \tag{3.243}$$

Consulting Eq. (3.182), we observe that this may be written,

$$\varepsilon(r) \approx \begin{cases} 1 - \frac{2\omega_\beta}{\eta\omega_0}(\zeta + \delta) & ; r < a \\ 1 & ; a \le r \end{cases}, \tag{3.244}$$

where ζ and δ are defined by Eq. (3.121). This corresponds to an index of refraction, $n=n_r+in_i$, where, for $r<a$,

$$\begin{aligned} n_r &\approx 1 - \frac{\omega_\beta}{\eta\omega_0}\Re(\zeta + \delta), \\ n_i &\approx -\frac{\omega_\beta}{\eta\omega_0}\Im(\zeta). \end{aligned} \tag{3.245}$$

Typically one distinguishes between gain guiding, where n_i dominates, and refractive guiding, where n_r dominates. In general, both contribute.

We look for a solution for the radial mode of the form,

$$b(r) = \begin{cases} J_0(\kappa r) & ; r < a \\ \dfrac{J_0(\kappa a)}{K_0(\mu a)} K_0(\mu r) & ; a \le r \end{cases} \tag{3.246}$$

The quantities κ and μ are determined from Maxwell's equations,

$$\frac{\omega^2}{c^2} = k_z^2 - \mu^2 ,$$
$$(\mu a)^2 + (\kappa a)^2 = V^2 , \tag{3.247}$$

and the continuity condition at $r=b$

$$\kappa \frac{J_1(\kappa a)}{J_0(\kappa a)} = \mu \frac{K_1(\mu a)}{K_0(\mu a)} . \tag{3.248}$$

In Eq. (3.247) we have introduced the (complex) waveguide parameter

$$\boxed{V^2 = -\frac{\delta a^2 \beta}{\eta}(\zeta + \delta)} \tag{3.249}$$

and it will be convenient to express V in terms of amplitude V_0 and phase θ, $V=V_0 e^{i\theta}$. From Eq. (3.246) we see that the mode evanesces radially on a length scale $1/Re(\mu)$. In particular, we require $Re(\mu)>0$.

We will consider only the weakly guided regime, so that $Re(\mu)a<<1$. We will make the additional assumption $|\mu a|<<1$. In this case, Eq. (3.248) may be solved approximately using the small argument expansions for the modified Bessel functions,[27]

$$K_0(z) \approx -\ln\left(\frac{z e^{\gamma_E}}{2}\right),$$
$$K_1(z) \approx \frac{1}{z},$$

to find,

$$\mu a = 2\ exp\left\{-\frac{J_0(V)}{V J_1(V)} - \gamma_E\right\}. \tag{3.250}$$

We may simplify Eq. (3.251) somewhat in the limit $V_0<1$,

$$\mu a \approx 2\ exp\left(-\frac{1}{V^2} - \gamma_E\right)$$
$$\approx 2\ exp\left(-\frac{e^{-2i\theta}}{V_0^2} - \gamma_E\right). \tag{3.251}$$

Writing μ in terms of amplitude and phase we have $\mu=\mu_0 exp(i\phi)$, where

$$\mu_0 a \approx 2\ exp\left\{-\frac{\cos(2\theta)}{V_0^2} - \gamma_E\right\},$$
$$exp(i\phi) = exp\left\{i\frac{\sin(2\theta)}{V_0^2}\right\}. \tag{252}$$

Thus $\phi=sin(2\theta)/V_0^2$ modulo 2π, and $-\pi/2<\phi<\pi/2$ is required for guiding so that $Re(\mu)>0$.

Now, Eq. (3.252) is implicit in that the overlap factor, η, depends on μ, which in turn depends on V, which depends on η. To close this set of equations we need to compute η in terms of μ. Having taken $b(0)=1$, the mode area is[28]

$$\begin{aligned}\Sigma &= 2\pi\int_0^\infty r\,dr\,|b(r)|^2 \\ &\approx 2\pi\left|\frac{J_0(\kappa a)}{K_0(\mu a)}\right|^2\int_0^\infty r\,dr\,|K_0(\mu r)|^2 \\ &\approx \frac{2\pi}{\mu_0^2}\frac{1}{|K_0(\mu a)|^2}\frac{\phi}{sin(2\phi)}\end{aligned} \tag{3.253}$$

Equation (255) gives for the overlap integral $\eta=\pi a^2/\Sigma$,

$$\eta \approx \frac{1}{2}(\mu_0 a)^2\,|K_0(\mu a)|^2\,\frac{sin(2\phi)}{\phi} \tag{3.254}$$

As we would expect, in the limit $\phi\to\pi/2$ (so that $Re(\mu)\to 0$), the mode extends to infinity and we find $\eta\to 0$. Equation (254) may be rewritten explicitly in terms of V_0 and θ, using Eq. (3.252),

$$\eta \approx \frac{2}{V_0^4} exp\left\{-2\frac{cos\ (2\theta)}{V_0^2} - 2\gamma_E\right\} \frac{sin\left(2\frac{sin\ (2\theta)}{V_0^2}\right)}{\left(\frac{sin\ (2\theta)}{V_0^2}\right)} \tag{3.255}$$

Combining Eq. (3.255) with Eq. (3.249) provides an iterative algorithm for determining η and V. Now, in principle θ must be solved for as well, however, we may distinguish two regimes where θ is determined immediately and only V_0 (or η) need be solved for (self-consistenly for the assumed regime). We discuss these regimes in turn.

a. Small μ, δ limit (cubic regime). In the cubic gain regime, ζ_+ is given by Eq. (3.112), $\zeta_+=2\rho exp(2i\pi/3)$, so that

$$V_0^2\, e^{2i\theta} = exp(-i\pi/3)\frac{16\, a_\beta^2\, \rho}{\eta} \tag{3.256}$$

Thus $\theta=-\pi/6$, and $\phi=-3^{1/2}/2V_0^2$. The requirement $\phi>-\pi/2$ then restricts V_0 to $V_0\geq 0.743$. Eq. (3.255) becomes

$$\eta \approx \frac{4}{3^{1/2}}\frac{1}{V_0^2} exp\left\{-\frac{1}{V_0^2} - 2\gamma_E\right\} sin\left(\frac{3^{1/2}}{V_0^2}\right).$$

To solve this, we define ρ_0 such that $\rho^3=\eta\rho_0^3$ (ρ_0 is the Pierce parameter for perfect overlap), and a dimensionless parameter $\sigma=64\rho_0^{3/2}a_\beta^3$. Then from Eq. (3.256), $\eta=\sigma/V_0^3$, and we have

$$\sigma \approx \frac{4}{3^{1/2}}V_0 exp\left\{-\frac{1}{V_0^2}-2\gamma_E\right\}sin\left(\frac{3^{1/2}}{V_0^2}\right). \tag{3.257}$$

Since σ is formally independent of η Eq. (3.259) is easily inverted numerically to give V_0 as a function of σ. This is plotted in Fig. 3.14(a). The corresponding overlap integral η is plotted versus σ in Fig. 3.14(b).

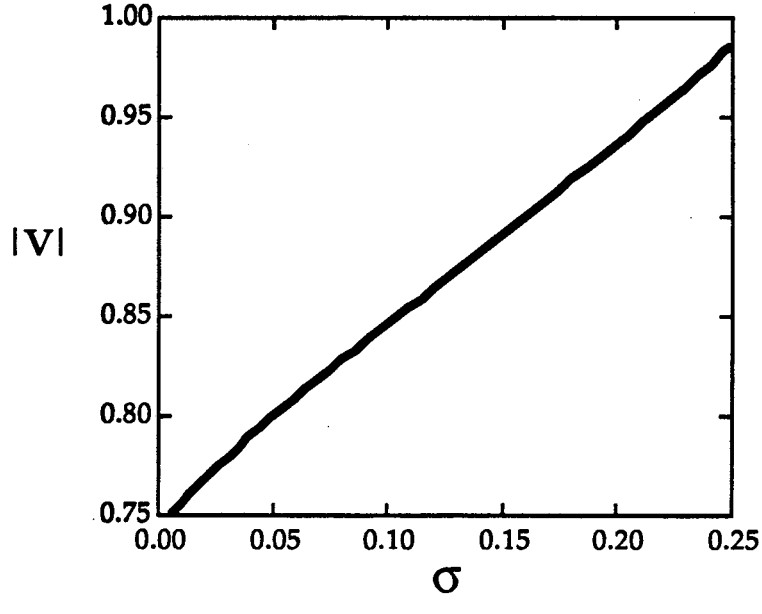

FIG. 3.14 (a)The modulus of the waveguide parameter $|V|=V_0$ as a function of the dimensionless parameter $\sigma=64\rho_0^{3/2}a_\beta^3$, in the small μ,δ limit ("cubic regime"). This result is well-fit by $V_0\sim0.74+0.94\sigma$.

For $\sigma<0.05$, we may extract a simple analytic scaling law by approximating the curve of Fig. 3.14(b), with $\eta\sim2.3\sigma$. Taking $a_\beta^2=\alpha\rho$ for some $\alpha\sim O(1)$ we find $\eta\sim2.2\ 10^4\ \rho_0^6\alpha^3$, and $\rho\sim28\rho_0^3\alpha\sim\alpha(I/q_zI_0)$. Thus $\rho\sim\alpha(\nu/\gamma)$ where $\nu=(I/I_0)$ is Budker's parameter. On the other hand, the condition that beam space-charge be negligible ($n_p>>n_b/\gamma^2$) can be written $\nu<<a_\beta^2$. Thus we must have $\alpha^2>>O(1)$. This is incompatible with $\alpha\sim O(1)$.

Essentially this argument shows that for effective optical guiding in the cubic regime, $\sigma>0.05$ is required (i.e., larger η). Otherwise ρ is so small that the constraint on a_β^2, $a_\beta^2<O(\rho)$, (imposed by the limit on detuning spread) ultimately implies that focussing is too weak,$a_\beta^2\sim\nu$.

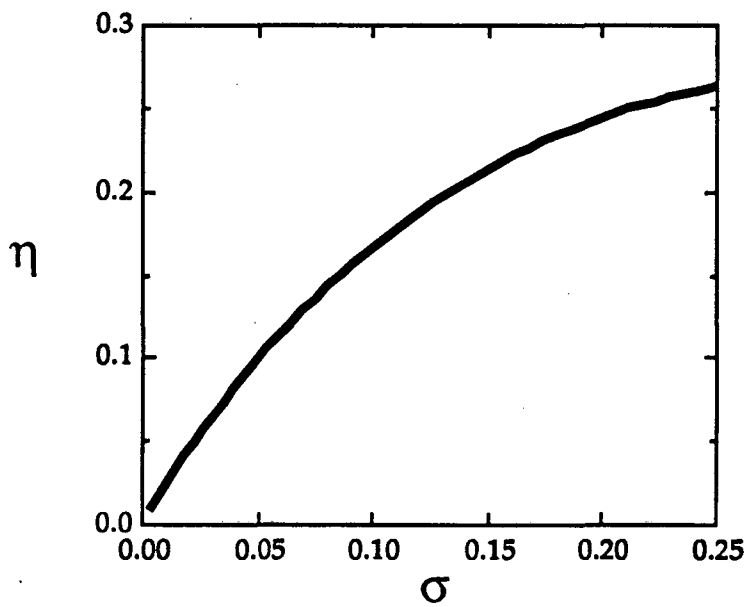

FIG. 3.14 (b)The overlap integral for the optically guided mode in the cubic gain regime, as a function of the dimensionless parameter $\sigma=64\rho_0^{3/2}a_\beta^3$, corresponding to the solution of Eq. (3.256) as depicted in Fig. 3.14(a). For $\sigma<0.05$, this result is well-fit by $\eta\sim2.3\sigma$.

b. Large δ limit. We turn then to consider operation at large detuning. In this case, from Eq. (3.130), we have $\delta+\zeta_+\sim\delta$, so that guiding is primarily refractive. The waveguide parameter is,

$$V_0^2 = -\frac{8a_\beta^2\delta}{\eta},$$

and will assume $\delta<0$ so that V is real and $\theta=\phi=0$.

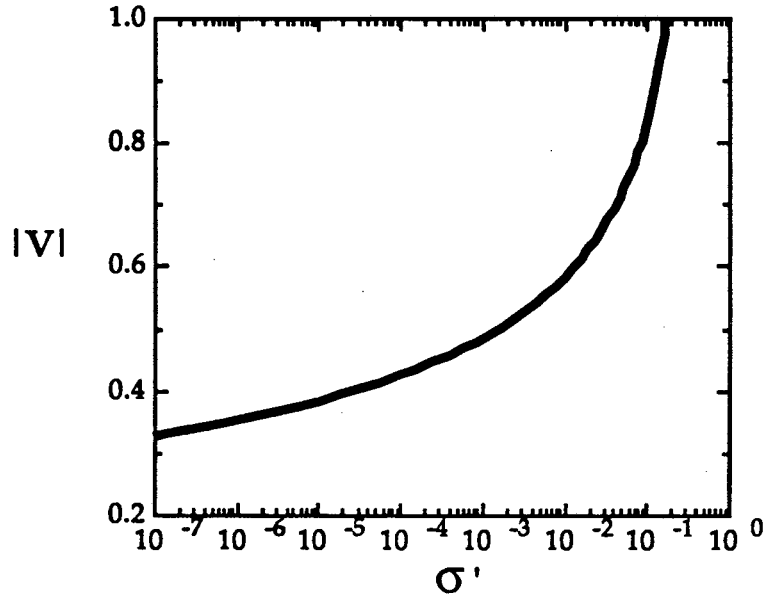

FIG. 3.15. (a)The modulus of the waveguide parameter $|V|=V_0$ as a function of the dimensionless parameter $\sigma'=8a_\beta^2|\delta|$, in the limit of large detuning, as given by Eq. (3.258).

The overlap integral is

$$\eta \approx \frac{4}{V_0^4} exp\left\{\frac{-2}{V_0^2} - 2\gamma_E\right\},$$

and we note that this expression is just the usual weak guiding result (as in

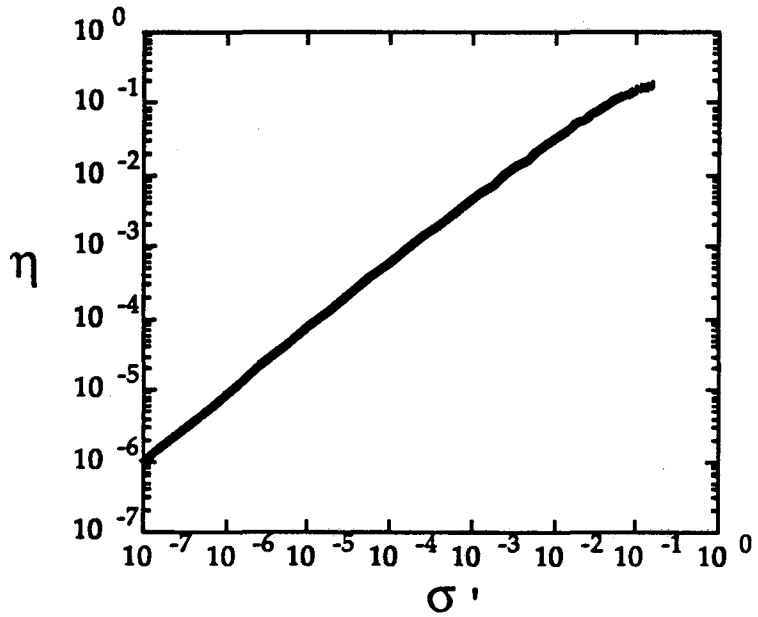

FIG. 3.15 (b) The overlap integral for the optically guided mode in the limit of large detuning, as a function of the dimensionless parameter $\sigma'=8a_\beta^2|\delta|$, corresponding to the solution of Eq. (3.258) as depicted in Fig. 3.15(b). For $\sigma'<10^{-3}$, this result is well-fit by $\eta \sim 2.032\ (\sigma')^{0.903}$.

Eq. (3.229), with appropriate modifications). We define a parameter $\sigma'=8a_\beta^2|\delta|$, which is formally independent of η. Using $V_0^2=\sigma'/\eta$, we obtain V_0 implicitly as a function of σ' (analagous to Eq. (3.257),

$$\sigma' \approx \frac{4}{V_0^2} exp\left\{-\frac{2}{V_0^2} - 2\gamma_E\right\}. \tag{3.258}$$

The dependence of V_0 and η on σ' is depicted in Figs. 3.15a,b.

With a bit of algebra it is not hard to see that this refractive guiding regime scales more robustly than the zero detuning case. For illustration, we select the optimal detuning given by Eq. (3.132). In this case,

$$\zeta_+ = \frac{8\rho^3}{\mu^2}(-1+i) \approx a_\beta^2(-1+i),$$

$$\delta = -\frac{1}{16}\frac{\mu^4}{\rho^3} \approx -4\frac{\rho^3}{a_\beta^4},$$

so that $\sigma'=32\eta^{2/3}\rho_0^2/\alpha$, where we take $a_\beta^2=\alpha\rho$ for some $\alpha\sim O(1)$. For $\sigma'<10^{-3}$, we fit $\eta(\sigma')$ by $\eta\sim 2.032\ (\sigma')^{0.903}$. It is then straightforward to solve for ρ and we find $\rho\sim 24.9\rho_0^{2.513}/\alpha^{0.756}$, or

$$\rho \approx 1.36\ \alpha^{-0.756}\ \nu^{0.838}.$$

The condition $a_\beta^2>>\nu$ may then be written, $\alpha>0.28\nu^{0.672}$ and this is not usually inconsistent with the requirement $\alpha<O(1)$. For example, consider a 50 MeV beam with I=100A. At this current, ion-channel dielectric guiding is ineffective, while the wavelength will likely be in the infrared making the use of a waveguide impractical. For this example, we compute $\nu\sim 6\times10^{-5}$, and taking $\alpha\sim 0.5$, we find $\rho\sim 6\times10^{-4}$. For the same current, at 2 MeV energy, we

find ρ~1%, corresponding to an output power at saturation on the order of 1 MW.

We also note that for a controlled experiment it may be important to remove the quasineutral plasma surrounding the ion-channel (by lowering the intensity of the ionizing laser and producing fewer free electrons). In this case, active guiding will be important even for high currents. As an example, taking I=4 kA and 50 MeV, we find ρ~1%, corresponding to an output power on the order of 2 GW.

We may conclude from this work that refractive guiding in the large detuning limit will be quite useful depending on the regime of interest.

E. EXAMPLES

In this section, we apply the scalings derived in Secs. B-D, to fashion several numerical examples of ion-channel laser performance from microwave to X-Ray wavelengths. We consider four numerical examples for which parameters are given in Table 3.4. The results have been checked with a many-particle simulation based on Eqs. (3.22)-(3.26) and (3.98). The first example was also checked with a simulation following the full equations of motion derived from Eq. (3.4) (i.e., Eqs. (3.6)-(3.8) and (3.98)). We postpone discussion of numerical results to the next chapter. The numerical values quoted assume ion-channel dielectric guiding, and the gain lengths and efficiencies are for $\mu=\delta=0$. Nevertheless, other regimes are of interest as well

(Table 3.3) and we will explore these in the numerical work of the next section.

Table 3.3. Minimum gain length scalings

Cubic gain regime ($a_\beta^2 > \rho$)*:*

$$L_g \approx \begin{cases} \dfrac{\lambda_\beta}{2\pi 3^{1/2}\rho} & ;\delta_0 = 0 \ , \ \delta_s < \rho \\ \dfrac{\lambda_\beta}{16\pi}\left(\dfrac{\delta_s^2}{\rho^3}\right) & ;\delta_0 \approx -\dfrac{1}{16}\dfrac{\delta_s^4}{\rho^3} \ , \ \delta_s > \rho \end{cases}$$

Quadratic gain regime ($a_\beta^2 < \rho$)*:*

$$L_g \approx \frac{\lambda_\beta}{2\pi a_\beta^2}\left\{1 - \frac{1}{6}\left(\frac{\delta_s}{a_\beta^2}\right)^2\right\}^{-1} \qquad ;\delta_0 = -4\,\frac{\rho^3}{a_\beta^4}$$

It is also worth noting that, in the first example (microwave regime), it would be most natural to confine the radiation in a conducting waveguide. Taking a 3 cmx5 cm waveguide, operated in the TE_{10} mode, the overlap factor is η~0.2, and the Pierce parameter is ρ~8%, for a gain length of L_g~45 cm. The output power would be on the order of 600 MW. The beam parameters for this example are quite practical, corresponding roughly to what has already been achieved with induction linear accelerators.[29]

Table 3.4: Examples of Ion Channel Laser Scalings.

	Microwave	Millimeter	Infrared	X-Ray
$\lambda(cm)$	2	$5\ 10^{-2}$	$1\ 10^{-3}$	$1\ 10^{-6}$
$E(MeV)$	2	4	10	100
$I(kA)$	4	4	4	4
$\varepsilon_n(cm\text{-}rad)$	$3\ 10^{-1}$	$1\ 10^{-2}$	$5\ 10^{-4}$	$3\ 10^{-5}$
$n_p(cm^{-3})$	$6\ 10^{10}$	$8\ 10^{12}$	$1\ 10^{15}$	$2\ 10^{19}$
$L_g(cm)$	70	16	4	0.2
$\lambda_\beta(cm)$	$4\ 10^{1}$	5	$6\ 10^{-1}$	$2\ 10^{-2}$
$\tau_i(ns)$	$2\ 10^{1}$	1	0.1	$1\ 10^{-3}$
a_β	0.6	0.5	0.4	2
$a(cm)$	1	$7\ 10^{-2}$	$3\ 10^{-3}$	$4\ 10^{-5}$
$\rho(\%)$	5	3	1	1
$P_{sat}(GW)$	0.4	0.5	0.6	3
N_h	3	6	11	14

In selecting these examples, the most severe constraint was found to be the condition $a_\beta^2 < O(\rho)$, which is marginally satisified in the first three examples. To exhibit the consequences of this constraint, the fourth example was designed with a large a_β. It should be emphasized, however, that such an X-Ray laser could not be realized without a sharp distribution in axial velocity, corresponding to a step radial profile, a spinning or otherwise specially prepared beam. In the first three examples, the plasma densities required are not out of the ordinary. For the fourth example, the plasma density is high; however, it need only be maintained over a few centimeters.

For completeness, we review the considerations of Chapter 2, for these examples. Scattering with the neutral atoms and ions of the gas will results in emittance growth. The increase in normalized emittance in one betatron wavelength is $\Delta\varepsilon_n=4\pi r_e Z^2 \ln(\theta_{max}/\theta_{min})/f$, where f is the ionization fraction, r_e is the classical electron radius and $\theta_{max}/\theta_{min} \sim 5.26\ 10^4/(AZ)^{1/3}$. Z is the atomic number, and A is the atomic weight. For the examples, below, we take Z~50, A~100 and $f \sim 10\%$, corresponding to $\Delta\varepsilon_n \sim 10^{-6}$ cm-rad. This is typically small.

Most beam-plasma instabilities will be rather benign for typical parameters; however, growth of the ion-hose instability[30] is not always negligible and the number of ion hose e-folds at saturation, N_h, becomes severe at shorter wavelengths. However, it can be reduced by further shortening of the REB pulse length, τ.

To summarize, we have seen that the ion-channel laser is viable high-power, high-efficiency source of coherent radiation across the spectrum. Needless to say, before proposing a practical experiment based on any of these examples, one should ask whether any experiment has already been performed which might in some way confirm theory. This appears to be the case, as we shall discuss next.

F. ION-CHANNEL LASER IN THE OVERDENSE REGIME

Ion neutralization of the beam on the ω_i^{-1} time scale imposes a significant constraint on beam length and this motivates the study of the analogous instability of a magnetically self-focussed beam ($n_b<n_p$). This regime is also of special interest in that experimental evidence has already been found, of coherent radiation from intense electron beams injected into overdense, unmagnetized plasmas.[31,32] Explanations offered for the high microwave power levels observed have included streaming instabilities, strong-turbulence, and virtual cathode oscillations. Kato *et al.*,[31] remark on the possibility of an FEL analogy based on jitter motion in "large-amplitude electrostatic waves generated by instability"; however, to date, no satisfactory theory has been set down to explain the measured power levels. We propose the ICL instability as a possible mechanism.

Examining the single particle motion, we observe that the Hamiltonian of Eq. (3.3), takes the form

$$H = \sqrt{m^2c^4 + \left(p_z + \frac{e}{c}A_z\right)^2 c^2 + p_x^2c^2 + \left(p_y + \frac{e}{c}A_y\right)^2 c^2}$$
$$\approx p_z c + \frac{m^2 c^3}{2\,p_z} + \frac{p_x^2 c}{2\,p_z} + \frac{p_y^2 c}{2\,p_z} + e\,A_z + e\,\frac{p_y}{p_z}A_y \quad , \qquad (3.261)$$

where p_z is the canonical axial momentum

$$p_z = m\gamma v_z - \frac{e}{c}A_z \ .$$

In Eq. (3.261), we have set $\varphi \sim 0$ from quasi-neutrality. The axial vector potential, A_z, is due to the axial beam current, together with any plasma return current.[33] For a step radial profile (a crude approximation, in particular, for the plasma return current)

$$A_z \approx \frac{1}{c} I_{net} \frac{r^2}{a^2} \ . \tag{3.262}$$

Note that here the assumption of a step radial profile takes on additional significance in that, with it, the restoring force is linear. For realistic beams, nonlinearities in focussing will introduce detuning spread and reduce gain.

With this approximate form for the Hamiltonian, the problem is formally identical to that describe by Eq. (3.3), i.e., the potential of Eq. (3.1) is replaced by eA_z. There are some important differences, of course, even in this idealized model. For example, now "γ" is constant at zeroth order (whereas previously it suffered a small jitter). We still have p_z constant at zeroth order, from translational invariance.

Table 3.5. Parameters for the experiment of di Capua, *et al.*

——	I=50 kA	I_{net}~25 kA
	τ=60 ns	R~33cm
	a~ 7.5 cm	n_p~4 x10^{10} cm^{-3}
	λ_β~44 cm	L~50 cm

Although this problem is deserving of a detailed analysis in its own right, we may make some simple estimates merely by identifying, $k_\beta \sim (2I_{net}/\gamma I_0)^{1/2}/a$ and $a_\beta \sim (\gamma I_{net}/I_0)^{1/2}$, and carrying over the scalings laws developed for the underdense case. We consider then the experiment of di Capua, *et al.* [32] Parameters are listed in Table 3.5 (where R is the circular beam pipe radius and L is the propagation length), and analytic estimates are given in Table 3.6. In this experiment, microwave emission was measured from a relativistic electron beam propagating through an unmagnetized plasma. The power as a function of time was measured in frequency bins ranging from 2-47 GHz.[34]

Table 3.6. Estimates for the experiment of di Capua, *et al.*

$a_\beta \sim 2.3$	$\rho \sim 45\%$
$V \sim 3.4$	$L_g \sim 9$cm
$f_p \sim 3$ GHz	$2\gamma^2 f_\beta/(1+a_\beta^2) \sim 3$GHz
$2\gamma^2 f_\beta \sim 19$ GHz	$P_{out} \sim 32$ GW

A number of features of this experiment presented anomalies. Two of these were the large microwave power radiated (they estimate 4% conversion of beam power to microwave power), and the spectrum, which extended far above ω_p, and resisted explanation. A number of the observations in the paper are particularly notable:

> *" . . . Electron acceleration due to the self-magnetic field of the beam is capable of producing synchroton radiation. However, the power levels previously observed are substantially higher than those expected on the basis of a single-particle model, indicating that it is necessary to have bunching of the electron beam as well. The growth of the radiation could conceivably provide the mechanism for such bunching, but it is not at all clear to what extent that occurs in our experiment."*

and later

> *". . . The Compton boost model proposed in [8] [K. Kato, et al., Phys. Fluids 26, 3636 (1983)] predicts a frequency upshift in the emission from f_p to $\gamma^2 f_p$. In our experiment, this would correspond to emission at about 35 GHz; we do observe emission at this frequency and beyond. Unlike the results of [8], however, we observe a decaying spectrum, not one in which the emitted microwave power is uniformy distributed over a wide range of frequencies . . ."*

Thus the experimentalists observed large microwave emissions at frequencies far above ω_p, and theory did not provide them with any qualitative or quantitative explanation for their observation. Of course, there are a number of factors which complicate any clear understanding. Among these are time variation in plasma density (also anomalously high) and virtual cathode oscillations. Recognizing that this experiment does not represent an ideal test of ICL theory, we may nevertheless make simple comparisons.

Now, the experimental results are characterized by overall efficiency of about 4% (mostly at ω_p) and a broad-band spectrum extending far above ω_p.

The naive estimate of efficiency gives 45%, which of course one has no reason to expect given the highly nonlinear focussing and spreads in momenta, associated with the large value of a_β~2.3. Thus comparison of efficiency is not particularly fruitful. On the other hand, the spectrum as given in Fig. 3 of Ref. 31 is quite interesting. For late times (t>120 ns), when the current has dropped to I~10 kA (corresponding to a reduced a_β~1), it reveals a plateau in the 18-20 GHz and 20-22 GHz windows, bracketing, the expected resonance near $2\gamma^2 f_\beta$~19 GHz. In this time range all other frequency windows give no reading observable on their plot. This is indicative of a sharp resonance. This could be explained tentatively from the result for the resonant frequency: $\omega - k_z v_z \sim \omega_\beta$. An electron with small transverse energy (small a_β) is resonant with $\omega \sim 2\gamma^2 \omega_\beta$, while electrons with large transverse energies are resonant with $\omega \sim 2\gamma^2 \omega_\beta / a_\beta^2$. At later times, many more electrons have small a_β.

One other feature should be noted. Based on the estimates of Sec. D, we would expect dielectric and active guiding to be quite strong. Now the detectors used in the experiment were mounted on the side of the beam pipe, 33 cm from the center of a 7.5 cm radius beam. Even in the overdense regime, one expects an optical fiber effect (analagous to ion-channel dielectric guiding) due to the radial variation in plasma electron density. A simple estimate gives a fiber parameter of V~3.4. Consulting Fig. 3.13, we see that the radial mode would then evanesce on a length scale of $a/3$~2.5 cm. Thus the power at the wall would be much reduced from that flowing through the beam volume. We may conclude that the power levels measured were not

accurately calibrated and probably represent underestimates of the total radiated power. This is particularly true of higher frequencies, and may explain in part the observed exponential fall-off in the spectrum.

One cannot cite these experimental results as evidence confirming the theory of the ICL as set forth here. However, they don't contradict theory, and they provide strong motivation for further, more controlled, experimental work.

As for other experimental evidence, it seems likely that some form of the ion-channel laser instability will appear naturally, in astrophysical circumstances and its applicability to solar bursts merits further study.[31,35]

G. SUMMARY

In conclusion, we have presented the concept of the ion-channel laser, together with a theoretical formulation. Several novel features were noted. First, the electromagnetic instability itself, and the resonant damping of the transverse motion for a weakly driven oscillator. We examined the dielectric guiding effect of the ion-channel, noting that it may ultimately prove to be problematic due to the electron-hose instability. We also found that, as in the FEL, there is an optical guiding mechanism which is quite effective depending on the regime of operation.

Given the practical difficulties typically associated with manipulating plasmas, it is important to recognize the advantages to be gained. Perhaps the

primary advantage of the ICL over the FEL, is the short betatron wavelength achievable in a plasma. To reach a given wavelength with the ICL, a lower beam energy may be used than in an FEL, resulting in higher efficiency and a more compact accelerator. Indeed, with optical guiding, operation in the visible spectrum with under 100 MeV appears possible. Economically, plasmas are "cheap", since one trades the cost of magnets and power supplies, for the cost of a laser.

A disadvantage of the ICL is that the "pump-field" is unstable. Fortunately, ion-motion represents a cumulative, electrostatic instability, with zero group velocity, while the ICL instability is electromagnetic, propagating with a beam slice, with only small slippage. Thus, a reduction in the pulse length, τ, lowers the growth of ion instabilities, while not reducing the peak laser power, or efficiency.

Another disadvantage is that in using a plasma, results will be subject to axial and radial variation in the plasma density. Axial variation in n_p, especially on the scale of a betatron period, will tend to disrupt the resonance. Radial variation in n_p will make focussing nonlinear, damping growth. Thus in any proof-of-principle experiment, control of and diagnostics for the plasma will be rather crucial.

Of course, before proposing a practical experiment based on any of these examples, one should perform detailed numerical simluations to confirm the theory. This is the subject of the next chapter.

References

[1]Ref. 1, Ch. 1.

[2]Ref. 2, Ch. 1.

[3]B. Levush, T.M. Antonsen, W.M. Manheimer, and P. Sprangle, Phys. Fluids **28**, 2273 (1985).

[4]T.P. Hughes and B.B. Godfrey, Phys. Fluids **29**, 1698 (1985).

[5]T. M. Antonsen and B. Levush, IEEE J. Quant. Electron. **QE-23**, 1621 (1987).

[6]Y. Carmel, *et al.*, Phys. Rev. Lett. **62**, 2389 (1989).

[7]C. A. Frost, J. R. Woodworth, J. N. Olsen And T. A. Green, Appl. Phys. Lett. **41**, 813 (1982).

[8]Ref. 14, Ch. 2.

[9]N.M. Kroll, P.L.Morton, and M.N. Rosenbluth, IEEE J. Quant. Elec. **QE-17**, 1436 (1981).

[10]Milton Abramowitz and Irene A. Stegun, *Handbook of Mathematical Functions*, (Dover, New York, 1972), p. 590. For reference, we note

$$K(k^2) = \int_0^{\pi/2} d\theta \left\{1 - k^2 \sin^2(\theta)\right\}^{-1/2},$$

$$E(k^2) = \int_0^{\pi/2} d\theta \left\{1 - k^2 \sin^2(\theta)\right\}^{1/2}.$$

[11]N. M. Kroll and W. A. McMullin, Phys. Rev. A **17**, 300 (1978). See in particular, Eqs. (3.19) and (3.20), and related discussion.

[12]K. R. Chu and J. L. Hirshfield, Phys. Fluids **21**, 461 (1978).

[13]R. Bonifacio, C. Pellegrini, and L. M. Narducci, Opt. Commun. **50**, 373 (1984).

[14]This terminology is used by analogy with that for the FEL (Ref. 13). Such a parameter, proportional to $I^{1/3}$ was originally used by J. R. Pierce in his description of travelling wave tubes. See J. R. Pierce, *Travelling Wave Tubes*, (D. Van Nostrand, New York, 1950) p.174.

[15] W. B. Colson and A. M. Sessler, Ann. Rev. Nucl. Part. Sci. **35**, 25 (1985).

[16]E. T. Scharlemann, A. M. Sessler, and J. M. Wurtele, Phys. Rev. Lett. **54**, 1925 (1985).

[17]D.Marcuse, *Theory of Dielectric Optical Waveguides*, (Academic Press, New York, 1974).

[18] Ref. 7, Ch. 2, pp. 951- 981.

[19]Ref. 10, p. 409.

[20]T.J.Orzechowski, *et al.*, IEEE J. of Quantum Electronics, **QE-21**, 831 (1985).

[21]Jonathan S. Wurtele, "Multiple Waveguide Mode Effects in Free-Electron Lasers", (Ph. D. Thesis, unpublished, 1985)

[22]Efrem J. Sternbach, "Multiple Frequency Effects in Waveguide Free-Electron Lasers", Lawrence Berkeley Laboratory Report No. 27294 (Ph. D. Thesis, unpublished, 1989)

[23]G. T. Moore, Opt. Comm. **52**, 46 (1984), and **54**, 121 (1985).

[24]M. Xie and D. A. G. Deacon, Nucl. Instrum. Methods **A250**, 426 91986).

[24]M. Xie and D. A. G. Deacon, Nucl. Instrum. Methods **A250**, 426 91986).

[25]M. Xie, D. A. G. Deacon, and J. M. J. Madey, "Eigenmode Analysis of Optical Guiding in Free electron Lasers," (submitted to Phy. Rev. A), Lawrence Berkeley Laboratory Report No. 26987.

[26]L. H. Yu and S. Krinsky, *Short Wavelength Coherent Radiation: Generation and Applications*, edited by D. T. Attwood and J. Bokor, Rita G. Lerner, series editor, AIP Conf. Proc. **147**, (AIP, New York, 1986), pp. 299-309.

[27]Ref. 7, Ch. 2, p. 961.

[28]Ref. 7, Ch. 2, p. 673.

[29]W. Turner, "High-Brightness, High-Current Operation at ETA II", Energy and Technology Review, August 1989, Lawrence Livermore National Laboratory.

[30]Ref. 30, Ch. 2.

[31]K.G. Kato, G. Benford, D. Tzach, Phys. Rev. Lett. **50**, 1587 (1983).

[32]M. S. Di Capua, J. F. Camacho, E. S. Fulkerson, and D. Meeker, IEEE Trans. Plasma Sci. **16**, 217 (1988).

[33]Roughly, the plasma return current becomes significant when $k_p a>1$, and decays appreciably if the pulse length is longer than a magnetic diffusion time$\sim(k_p a)^2/\nu$, with ν the plasma electron collision rate.

[34]The frequency bins were (in GHz) 2-6, 6-12, 12-18 , 18-20 , 20-22, 22-24, 24-26, 26-32, 32-40 and 40-47.

[35]V.V. Zheleznyakov, *Radio Emission of the Sun and Planets*, translated by H. S. H. Massey, edited by J. S. Hey (Pergamon Press, Oxford, 1970)

Chapter 4: Numerical Simulations

" . . . this free-electron laser is to be three or four miles long, its main apparatus buried in concrete tunnels beneath the desert . . . just cooling the giant laser will require an estimated 450 million gallons of water a year . . ."
-William J. Broad, "Anti-Missile Laser Project Is Delayed Nearly 2 Years", New York Times, 4/17/88

In this chapter we study numerically some example ion-channel laser "designs". These numerical simulations provide us with an opportunity to check the theoretical scalings, and to confirm the eikonal model. The numerical approach also provides us with a straightforward method of following the dynamics through saturation, and studying the effect of detuning spread on gain length and efficiency.

In Sec. A, we describe the numerical codes we will use. With these codes, we proceed to examine the examples set down in Table 3.4.

In Sec. B, we consider variants on the microwave design. We compare ECL, FULLCL and theory, finding good agreement. We examine the consequences of optical guiding, ion-channel dielectric guiding and the

introduction of a waveguide. We also examine the effect of detuning spread due to spreads in axial momentum and due to a spread in transverse energy. Finally we consider the effect of errors in plasma density.

Having established confidence in the theoretical scalings in Sec. B, we go on in subsequent sections to consider examples at shorter wavelength, in somewhat less detail.

In Sec. C we consider variants on the sub-millimeter example. We first consider a high gain experiment using a beam typical of induction linacs. We then consider a low gain example making use of a low current, low emittance beam typical of a storage ring.

In Sec. D, we consider a high gain 10 μm amplifier, and, in Sec. E, we consider an X-ray laser, which, is severely constrained by the requirement on detuning spread, and probably cannot be realized practically at present. This example, does however, provide considerable motivation for further work.

In Sec. F, we offer some conclusions for future numerical and experimental work.

A. THE CODES: ECL AND FULLCL

We will use two codes, ECL and FULLCL, each running on a VAX 8650. The code ECL solves the betatron-averaged equations, Eqs. (3.22)-(3.26), combined with Maxwell's equations, Eq. (3.95). The code FULLCL solves the full equations of motion, Eqs. (3.6)-(3.8) and (3.95). Each codes relies on a

fourth-order Runge-Kutta advance in t. Each makes use of a complex field variable ($B=Ae^{i\varphi}$), advancing the real and imaginary parts.

Note that, consistent with Eq. (3.95) there is no radial solver, and no slippage. The codes merely follow one beam slice and its comoving eikonal, a system of ordinary differential equations, rather than the full partial differential equations. Thus we cannot fully model sidebands, oscillators, lethargy, diffraction, or optical guiding. We also cannot incorporate beam break-up, or cumulative plasma effects. Needless to say, all these effects should eventually be modelled. On the other hand, simple simulations such as discussed here provide considerable graphic insight into the beam dynamics, finite temperature effects, and the approach to saturation. These codes are also enormously faster.

Each code checks energy conservation through the integral of Eq. (3.97)

$$E = \eta\omega_b^2\langle H\rangle + \frac{1}{2}\omega^2 mc^2\langle A^2\rangle ,$$

and quotes a fractional numerical error given by

$$\varepsilon_{num} = \frac{E_f - E_i}{\eta\omega_b^2\langle \Delta H\rangle} , \tag{4.1}$$

where $<\Delta H>$ is the average change in energy of beam electrons. E_f and E_i are the final and initial values of E. Thus for example a numerical error of $\varepsilon_{num}\sim 1\times 10^{-2}$ (a typical value) for a result of 100 MW of output power,

corresponds to an absolute error of 1 MW. The integrals, Φ_x, Φ_y, and Φ_z of Table 3.1 could also be used to double-check the accuracy of the numerical algorithms, however this has not been implemented yet.

The initialization and time constraints of each code are rather different so we discuss them separately.

1. Eikonal ICL Equation Solver (ECL)

In this code, the particle variables are $\chi=k_z z-\omega t+\theta_y$, q_x , q_y, and q_z, as defined in Eqs. (3.9) and (3.94). Note that the variables θ_y and θ_x are ignorable. ECL integrates the betatron-averaged equations, Eqs. (3.22)-(3.26), combined with Maxwell's equations, Eq. (3.95), using a standard fourth-order Runge-Kutta algorithm.

a. Inputs. The inputs for ECL are:

ε_n	*rms normalized emittance,*
I	*beam current,*
H	*beam energy,*
λ	*resonant wavelength (free-space),*
P_0	*input signal power,*
$\Delta\omega$	*detuning.*

In addition, the user specifies momentum spread (σ_h or $\Delta p_z/p_z$) and numerical variables, N_χ, N_α, N_h, ε, N_t as described below. The user also specifies the guiding option of which there are three:

(1)ion-channel dielectric guiding (code computes overlap),

(2)conducting waveguide (user specifies dimensions, code computes overlap, k_z, $k_\perp$, etc.)

(3)user-specified overlap (code assumes fast-wave, $\omega=ck_z$).

Other significant quantities are determined implicitly from the following relations:

$$\omega - k_z v_z = \omega_\beta - \Delta\omega \,, \qquad \textit{[resonance relation, Eq. (3.16)]}$$

$$\omega^2 = c^2 k_z^2 + c^2 k_\perp^2 \,, \qquad \textit{[dispersion relation, Eq. (3.238)]}$$

$$\varepsilon_n = \frac{1}{4} q_z k_\beta a^2 = \frac{1}{2}\frac{a_\beta^2}{q_z k_\beta} \,, \qquad \textit{[emittance, Eqs. (3.81), (3.69)]}$$

$$n_b = \frac{I/I_0}{\pi\, r_e a^2} \,, \qquad \textit{[beam density]}$$

$$k_p = k_\beta \sqrt{2 q_z} \,, \qquad \textit{[plasma wavenumber Eq. (3.1)]}$$

$$n_p = \frac{k_p^2}{4\pi\, r_e} \,, \qquad \textit{[plasma density]}$$

where r_e is the classical electron radius, $r_e=e^2/mc^2\sim2.8\times10^{-13}$cm. ECL solves these equations iteratively, rejecting a parameter choice which would result in an overdense plasma ($n_p>n_b$).

b. Initialization. Particles are initialized in χ, with a uniform distribution $-\pi<\chi<\pi$, over N_χ values. The initialization in q_x and q_y corresponds to $q_x=q_0 sin(\alpha)$, $q_y=q_0 cos(\alpha)$, where α is distributed uniformly over

the interval $0<\alpha<(1-\varepsilon)\pi/2$, with N_α values. Results are not sensitive to the value of ε, and typically, $\varepsilon\sim10^{-2}$. The quantity $q_0=2^{1/2}a_\beta$, for a step profile. To model a more realistic profile, we use a distribution of N_h values of q_0 satisfying $<q_0^2>\sim2a_\beta^2$, and a user prescribed value of the rms deviation

$$\sigma_h = \frac{1}{\langle q_0 \rangle}\sqrt{\langle q_0^2 \rangle - \langle q_0 \rangle^2}\ , \tag{4.2}$$

where the subscript "h" refers to the transverse energy, of Eq. (3.141) which is proportional to q_0. The quantity a_β is determined from the normalized emittance of the beam, and the user specified resonant frequency.

Detuning spread is modelled with a uniform distribution over q_z, $q_{z0}-q_s<q_z<q_{z0}+q_s$, or, alternatively, with the distribution over q_0 mentioned above. It will be convenient to refer to the dimensionless detuning spread,

$$\delta_s = 1.5\,\frac{q_s}{q_0}\ , \tag{4.3}$$

and to the total fractional momentum spread,

$$\frac{\Delta p_z}{p_z} = 2\,\frac{q_s}{q_0}\ . \tag{4.4}$$

In Eq. (4.3) the factor 1.5 appears instead of 1.0 (as in an FEL) due to the relativistic mass dependence of the betatron frequency.

Note that δ_s should be distinguished from the average detuning of the ensemble, δ_0

$$\delta_0 = \frac{1}{\omega_\beta}\left\langle k_z v_z - \omega + \omega_\beta \right\rangle, \tag{4.5}$$

where the angle brackets denote an average over the ensemble.

c. Numerical requirements. For a cold beam (no detuning spread) all particles are initialized with the same q_z and q_0. The number of macroparticles needed may be detemined from the requirement that the initial values of $\langle sin\chi \rangle$, $\langle cos\chi \rangle$, $\langle sin(2\chi) \rangle$ and $\langle cos(2\chi) \rangle$ are small (theoretically, they are zero). This requirement, which insures that the beam is not prebunched, can be satisfied by any distribution which is symmetric under the transformations $\chi \rightarrow -\chi$ and $\chi \rightarrow \chi + \pi/2$. For N values specified on the interval $[0,\pi/2]$, $N_\chi = 4N$ macroparticles are required. As for the variable α, results are not sensitive to the distribution, provided the value of $\langle q_y^2 \rangle$ is correctly fixed at $\langle q_y^2 \rangle = a\beta^2$. Thus in general the number of macroparticles required to model a cold beam is of order $N_p = N_\alpha N_\chi \sim 10^2\text{-}10^3$. Modelling momentum spread requires $N_p = N_h N_\alpha N_\chi \sim 10^3\text{-}10^4$, i.e., an additional factor of ten or so in the number of macroparticles.

The number of steps in t, N_t, required to evolve the system through to saturation is typically quite small, on the order of 100-500. This is because all quantities vary as the larger of the growth rate or the detuning (and because we are using a fourth-order differencing). Thus the number of betatron

periods does not enter the time-step scaling, making this code particularly efficient for low gain simulations.

2. *Full ICL Equation Solver (FULLCL)*

In this code, the particle variables are x, p_x, y, p_y, ζ, and p_z, where $\zeta=k_z z-\omega t$. The code integrates the full equations of motion, Eqs. (3.6)-(3.8) and (3.95), using a standard fourth-order Runge-Kutta advance in t.

a. Inputs. The inputs for FULLCL are:

ε_n	*rms normalized emittance,*
I	*beam current,*
H	*beam energy,*
n_p	*plasma density,*
ω	*input signal frequency*
P_0	*input signal power,*

In addition, the user specifies the number of particles, N_p, and the number of time-steps N_t. There are three guiding options as for FULLCL. If a waveguide is used and ω is below cut-off, or, if the self-consistent beam density is less than n_p, the parameter choice is rejected. Unlike ECL, there are no implicit algebraic relations to solve. FULLCL computes a_β, intializes the beam and integrates in t.

b. Initialization. The initialization is most easily described in terms of eikonal variables. (Note however, that eikonal variables are not actually used

to solve for the particle motion.) Particles are initialized in θ_x, θ_y uniformly over $(-\pi, \pi)$. The initialization in q_x and q_y corresponds to $q_x=q_0 sin(\alpha)$, $q_y=q_0 cos(\alpha)$, where α is distributed uniformly over $0\leq\alpha\leq\pi/2$, and $q_0=2^{1/2}a_\beta$. There are $N_p^{1/3}$ values for each distribution (i.e., in α, θ_x, θ_y). Particles begin at $t=0$ with the same ζ and p_z.

c. Numerical requirements. From the reasoning given in Sec. 1, we see that the number of particles required will be of order $N_p \sim 10^3$-10^4. In practice, we find fair agreement with ECL and theory for as few as $\sim 10^3$.

The number of steps in t (N_t) required to evolve the system through to saturation scales directly with the number of betatron periods. (With the fourth order differencing, one may use as few as 30 steps per betatron period.) This constraint, combined with the large number of particles required, generally limits the application of this code to problems where gain is high, and saturation is reached in about ten betatron periods. This typically corresponds to the microwave regime. Due to the large number of particles and time-steps required, this code does not model detuning spread.

We proceed to study the examples of Table 3.4, using the codes ECL and FULLCL.

B. MICROWAVE EXAMPLES

In this section, we consider ICL designs in the microwave regime, with parameters as given in Table 4.1, but subject to different guiding mechanisms,

and for various values of detuning spread. These beam parameters are typical of what can be achieved with an induction accelerator. The wavelength was chosen somewhat arbitrarily within the range 11-23 GHZ. This range has attracted considerable interest in the microwave power source community, for application in a future TeV-energy linear collider.

Our discussion of this example will be fairly detailed. We will first consider an ICL relying solely on ion-channel dielectric guiding. We will go on to consider the effect of optical guiding and we will find that it is in fact very important. We will also consider the effect of introducing a 3cmx5cm waveguide and we will find that it provides an overlap integral (η) comparable to that from optical guiding. In presenting the results based on these three guiding mechanisms, we will have established that a practical experiment is possible and that the signature of the different guiding mechanisms would be clear, experimentally.

In addition, we will use these examples to check the conclusions of Chapter 3, relating to particle motion, gain, effects of detuning and detuning spread and the like. Our analysis and survey of parameter-space will not be exhaustive, but, hopefully illustrative. In the course of this more or less tutorial example, we will have shown that, even in the presence of realistic momentum spreads, significant amplification (i.e., a positive experimental result) can be expected.

Table 4.1. Parameters for Microwave Examples

$\lambda(cm)$	1.75
$E(MeV)$	2
$I(kA)$	4
$\epsilon_n(cm\text{-}rad)$	0.25
$n_p(cm^{-3})$	$6.2\ 10^{10}$
$\lambda_\beta(cm)$	36
$a(cm)$	1
a_β	0.57
P_0	50 kW

1. Ion-channel dielectric guiding example

For this first example, we will assume that the beam pipe is sufficiently large that ion-channel dielectric guiding dominates. Now the channel radius is $b \sim a(n_b/n_p)^{1/2} \sim 2$cm, and the fiber parameter is $V \sim 1$, from Eq. (3.225), while, from Fig. 3.13, $\mu \sim 0.25/b$. Thus the ion-channel, HE_{11} mode evanesces radially on a length scale $\mu^{-1} \sim 8$ cm. We assume a beam-pipe radius of perhaps~30 cm or more and proceed to compute the cubic gain regime scalings for this example.

At 4 kA, the dimensionless HE_{11} mode area is from Eq. (3.233) (or Fig. 3.11), $\Lambda \sim 0.7$. We compute an overlap integral $\eta \sim 6.3 \times 10^{-2}$, from Eq. (3.229). From Eq. (3.106) this gives a Pierce parameter $\rho \sim 5.5\%$, and a gain length from Eq. (3.118) of $L_g \sim 67$ cm. The beam power is about 6 GW, so we expect the

saturated output power to be about 5.5%x6 GW~330 MW. We will assume an input power P_0~ 50 kW (a typical figure for a magnetron), and this implies roughly a length of L_{sat}~$0.5\ L_g\ ln(9P_{sat}/P_0)$~4 m, for saturation, where the factor of 9 arises from Eq. (3.114).

Table 4.2. Comparison of ECL, FULLCL and Cubic Gain Results

	Psat	*efficiency*	L_{sat}
Cubic Gain	330 MW	5.5%	4 m
ECL	392 MW	6.6%	4.8 m
FULLCL	384 MW	6.4%	4.6 m

a. Summary of ECL Results. We turn next to compare these predictions to the results of simulation. We followed the eikonal equations through twenty betatron periods, using N_t=198 steps in t and N_p=1600 particles. The initial values of the the sine and cosine averages were $\langle sin(\chi)\rangle$~-3x10^{-11} and $\langle cos(\chi)\rangle$~3x10^{-8}. These are sufficiently small that we may consider the beam unbunched. Results from ECL are depicted in Figs. 4.1-4.3. Saturation is reached at L_{sat}~4.75 m, with an output power of 392 MW, for an efficiency of 6.5%. The numerical error in energy conservation is ε_{num}~3x10^{-2} % (12 MW).

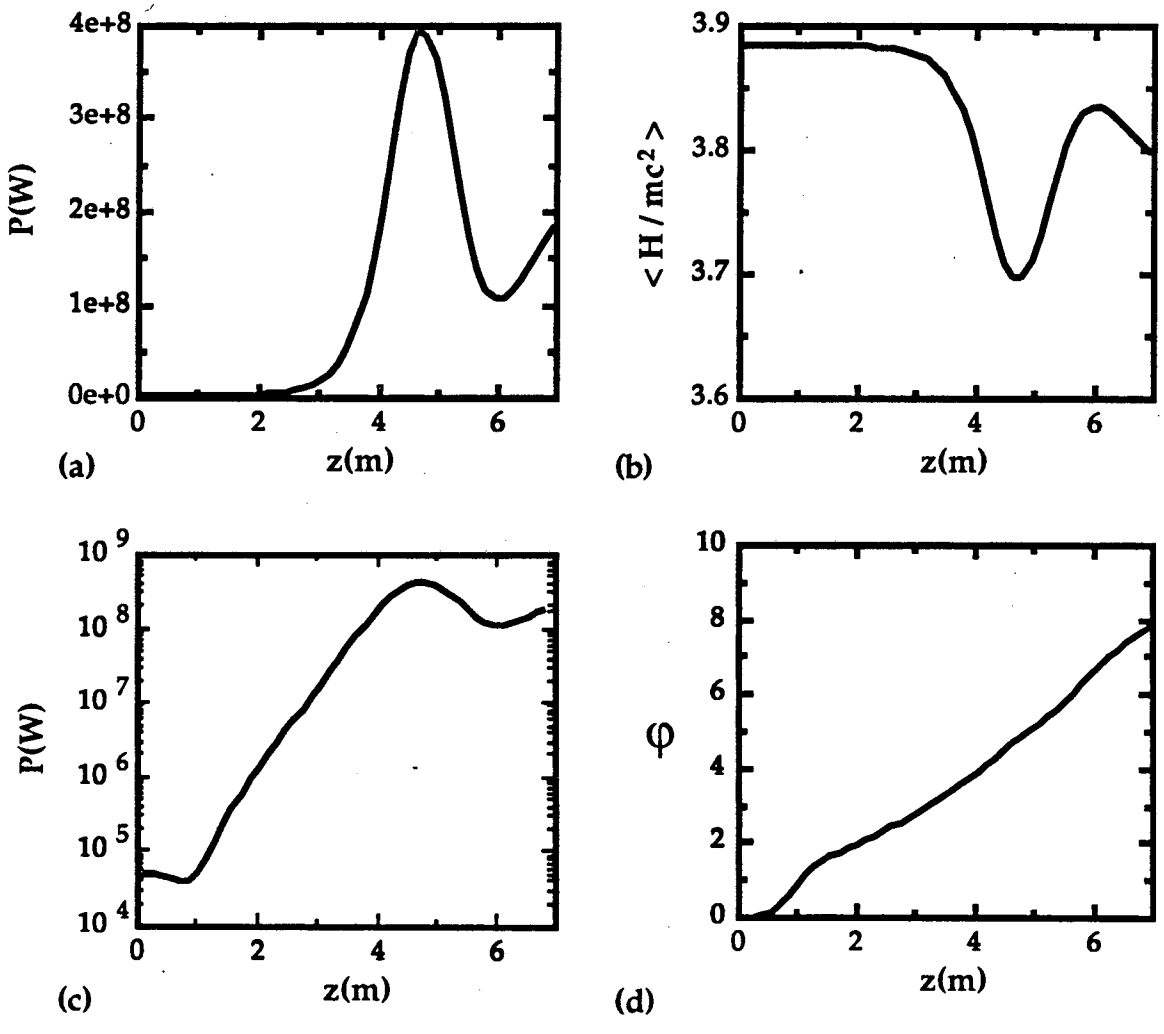

FIG. 4.1. Results from the eikonal equation solver, ECL, for (a) power in GW versus z (b) beam energy versus z, (c)power in watts on a log scale (compared with the analytic result of Fig. 3.4a) and (d)eikonal phase, φ in radians versus z (to be compared with Fig. 3.4b). Parameters are as in Table 4.1, and we assume only ion-channel dielectric guiding.

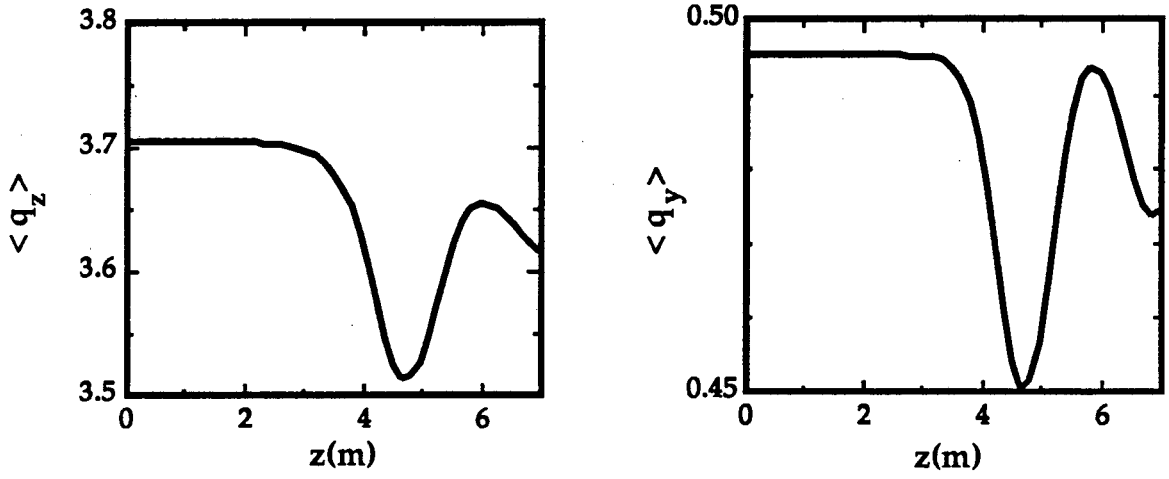

FIG. 4.2. ECL result for (a)dimensionless average axial momentum and (b)dimensionless transverse momentum amplitude, for the parameters of Table 4.1. Comparing this plot with Fig. 4.1(b), we see that $<p_z>$ follows H, as would be expected from the integral Φ_z, of Eq. (3.73).

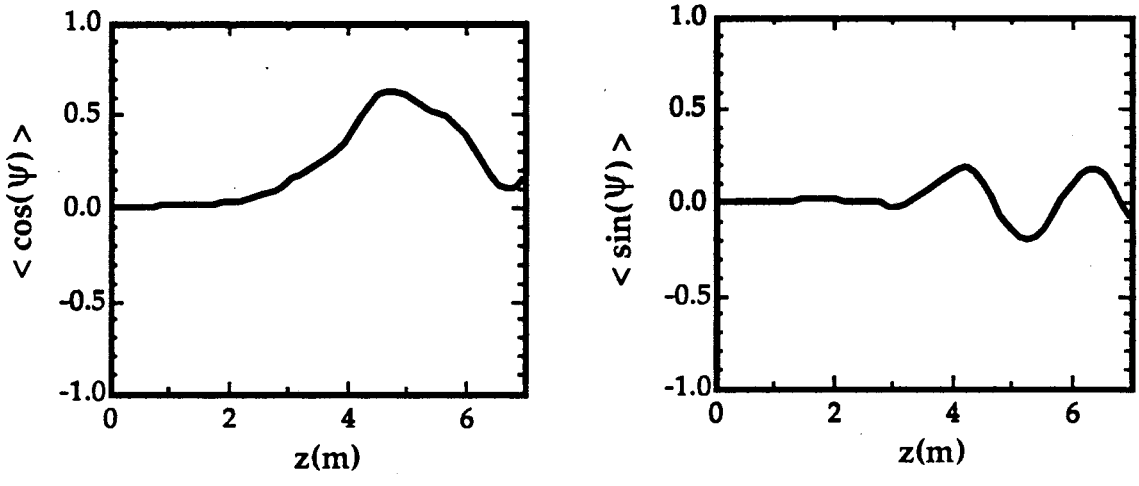

FIG. 4.3. ECL result for (a)the average of $cos(\psi)$ and (b)the average of $sin(\psi)$ over the ensemble, versus z. We observe that peak power in Fig. 4.1a, and the zero of $<sin(\psi)>$ coincide, as would be expected from Eq. (3.96).

b. Comparison with FULLCL Results. Next we compare these results to those obtained from FULLCL, by solving the full equations of motion. We used N_t=500 steps in t, and N_p=1000 particles. The initial values of the the sine and cosine averages were $<sin(\theta_{x,y})>\sim 10^{-10}$ and $<cos(\theta_{x,y})>\sim -10^{-7}$. We find saturation at z~4.6 m (versus 4.8 m for ECL), with an output power of 384 MW (versus 392 MW for ECL, for a difference of about 2%). The numerical error in energy conservation is $\varepsilon_{num}\sim 1\times 10^{-2}$ % (i.e. 4 MW). Generally agreement between theory, ECL and FULLCL is good as we can see by inspecting Fig. 4.4 (also, Table 4.2). A comparison of the results for phase advance is plotted in Fig. 4.5, also giving good agreement.

We also observe in Fig. 4.4, a discrepancy between the slope of the cubic gain regime analytic curve and the numerical results. This is due to the nonnegligible value of $\mu/\rho\sim 1.2$. Consulting Fig. 3.8a, we see that the growth rate will be only 87% of the μ=0 value, corresponding to the lower slope observed in Fig. 4.4.

The FULLCL code also shows that the beam centroid develops a coherent oscillation, as depicted in Fig.4.6. Inspecting this plot we see that the amplitude is $<p_y>\sim 0.25$ in rough agreement with the theoretical estimate of Eq. (3.120) $<p_y>\sim a_\beta/2^{3/2}\sim 0.21$. In addition, we find a decrease in the rms normalized y-emittance from 0.25 cm-rad to 0.20 cm-rad, or $\Delta\varepsilon_{ny}/\varepsilon_{ny}\sim 20\%$. this is in rough agreement with the theoretical estimate of Eq. (3.82), $\Delta\varepsilon_{ny}/\varepsilon_{ny}\sim(\Delta H/H)/a_\beta^2\sim 14\%$. Emittance versus z is depicted in Fig. 4.7.

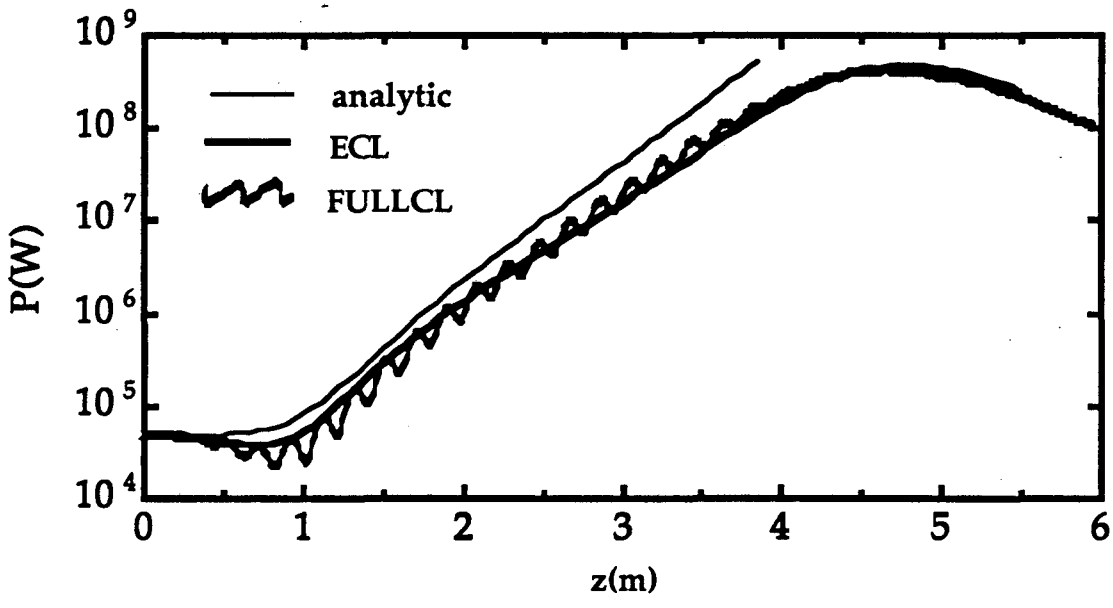

FIG. 4.4. Comparison of theory (straight line) with the results of the ECL (smooth curve) and FULLCL (tortuous curve) results for power in gigawatts vs z.

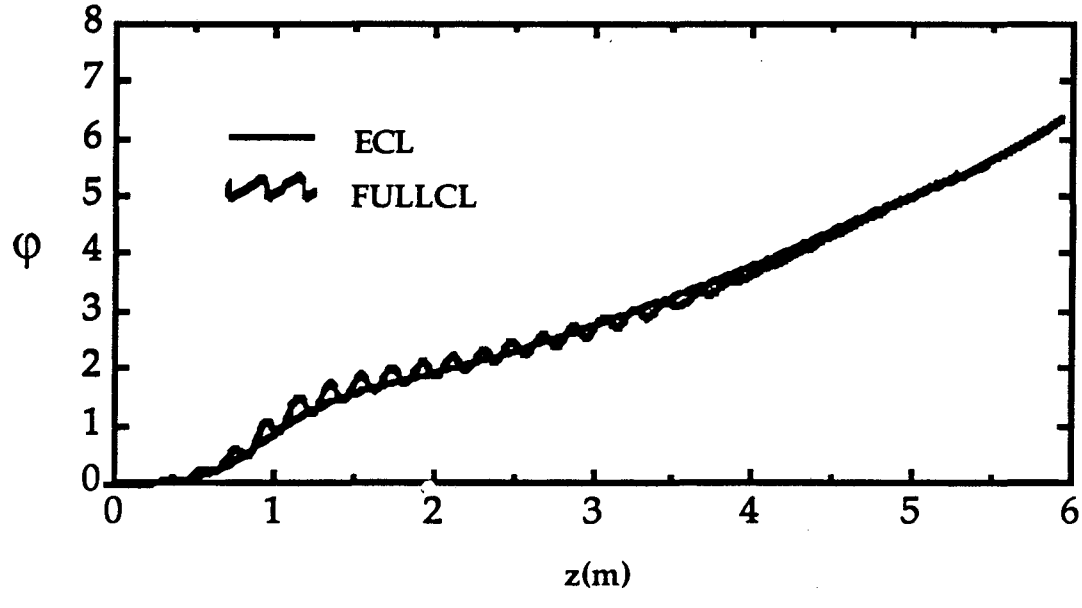

FIG. 4.5. Comparison of the phase advance computed by the ECL code (smooth curve) with that of FULLCL (tortuous curve).

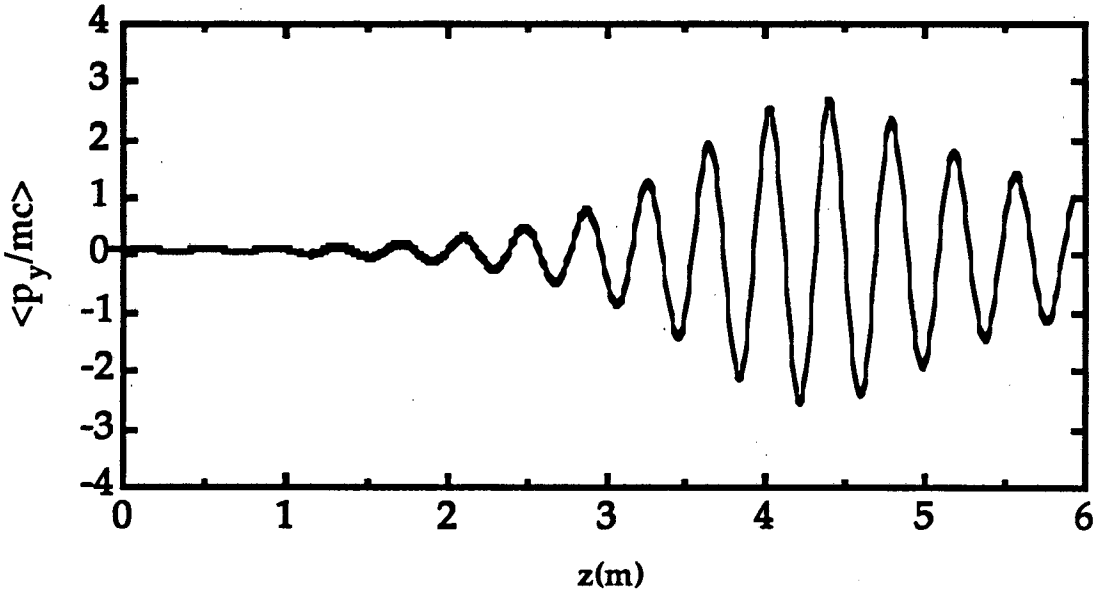

FIG. 4.6. The y-momentum, averaged over the ensemble is plotted versus z. As the beam approaches saturation a noticeable coherent oscillation of the beam centroid develops.

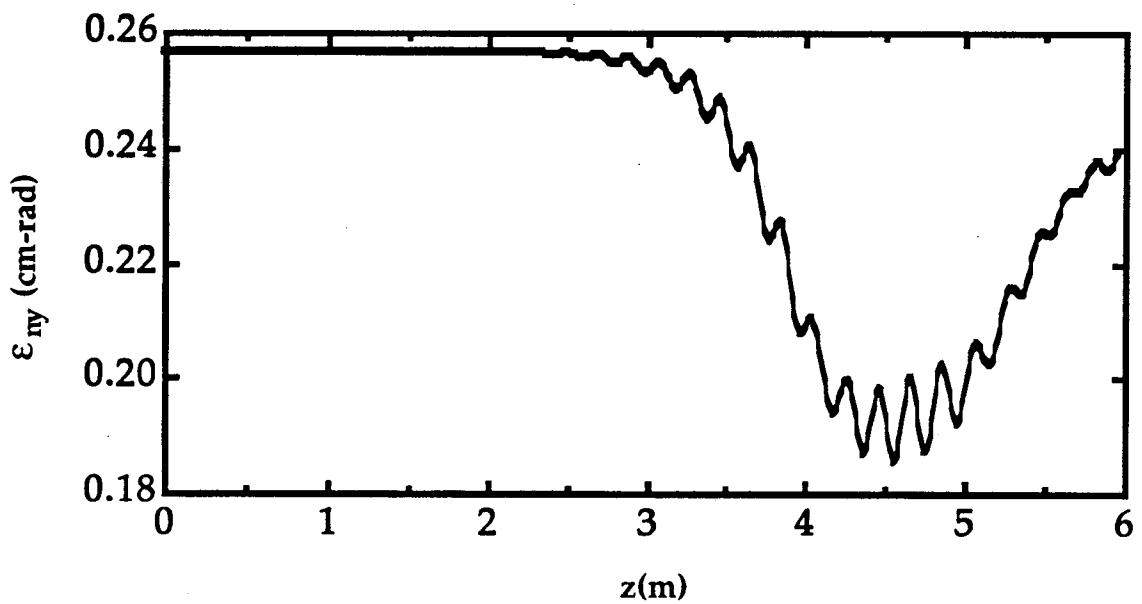

FIG. 4.7. The normalized rms y-emittance decreases near saturation, consistent with conservation of Φ_y [Eq. (3.77)].

c. Particle Motion. With working codes in hand, it is straightforward to follow the particle motion in detail. Making use of ECL, we plot a reperesentative sample of the beam (particles #600-#700), in the ψ-q_z plane, at various positions in t, in Figs. 4.8(a)-(d). Rather than simply depicting a "snapshot", each of these plots includes a range of values in t, so one can view the particles position and the tangent, and thereby discern the character of the motion.

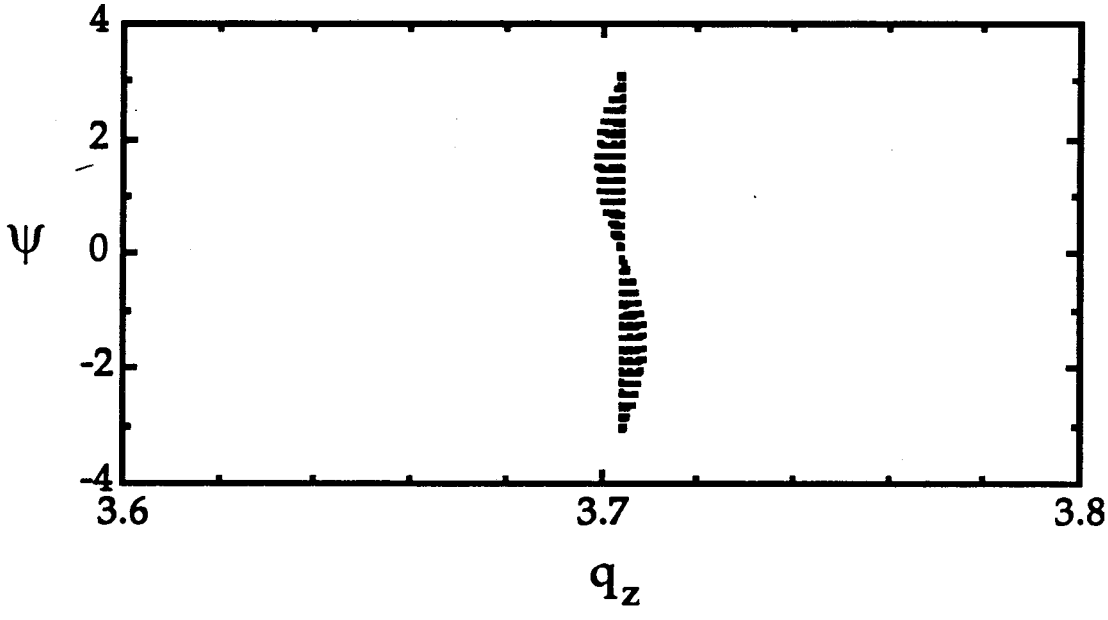

Fig. 4.8(a). Orbit segments for one-hundred representative particles for 0<z<0.4 m. We see that particles were intialized on the interval $(-\pi,+\pi)$, all with q_z~3.7. We also observe that particles with $sin(\psi)>0$ initially drift backward in q_z (lose energy) and vice versa for $sin(\psi)<0$, all as one would expect from Eq. (3.24), i.e., $dq_z/dt \propto -sin(\psi)$.

Inspecting these figures we observe three qualitatively different kinds of orbit. One class of orbits resembles very much what one observes in the

FEL, while the others appear to be more weakly perturbed. This can be understood from Eq. (3.32), and the variation of the bunching parameter Σ with q_y. In the sample of particles we have taken, there are three different values of q_y, and hence three qualitatively different orbits.

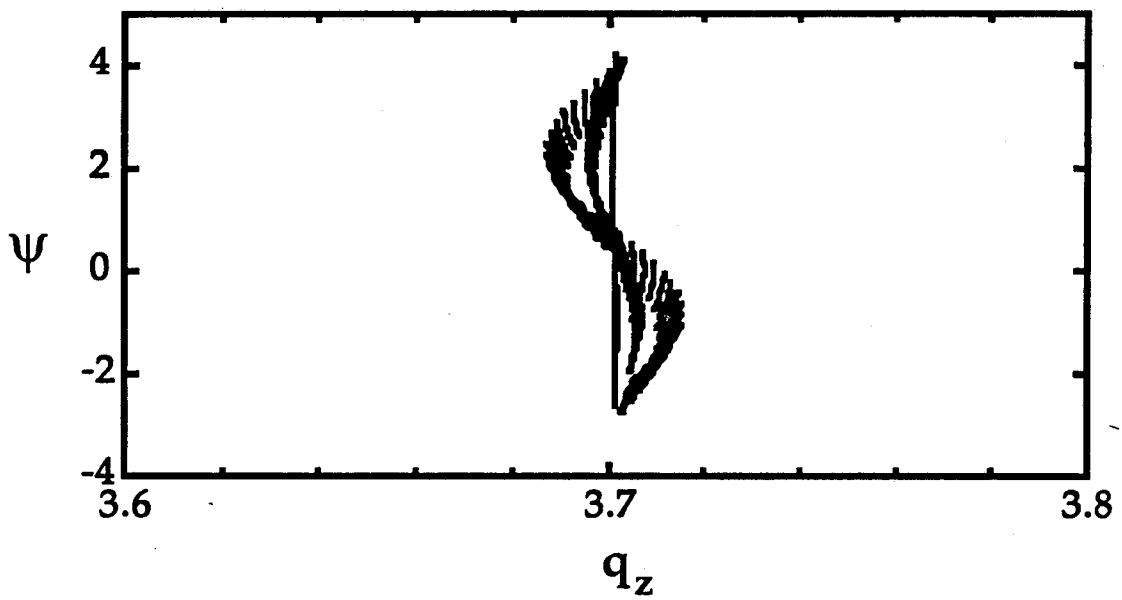

Fig.4.8 (b). Orbit segments for the particles of Fig. 4.8(a), for 0.7<z<1.1 m. We observe that some particles are remaining nearly stationary in q_z. These are just the particles initialized with small q_y.

These plots illustrate the competition between axial bunching and forced debunching, i.e., the effect of the "Π'" term (debunching) in Eq. (3.65) in competition with the "Ξ" (bunching) term. The transverse motion of small q_y particles is strongly perturbed by the growing fields, and these particles oscillate with ever large amplitude, extracting energy from the fields through the ponderomotive force of Eq. (3.65). The transverse motion of high q_y

particles is on the other hand only weakly perturbed and they bunch axially (or in ψ as we see in Fig. 4.8(d). Low q_y particles are also detuned, as seen in Eq. (3.27), and in Fig. 4.8 in their vertical motion in the ψ-q_z plane.

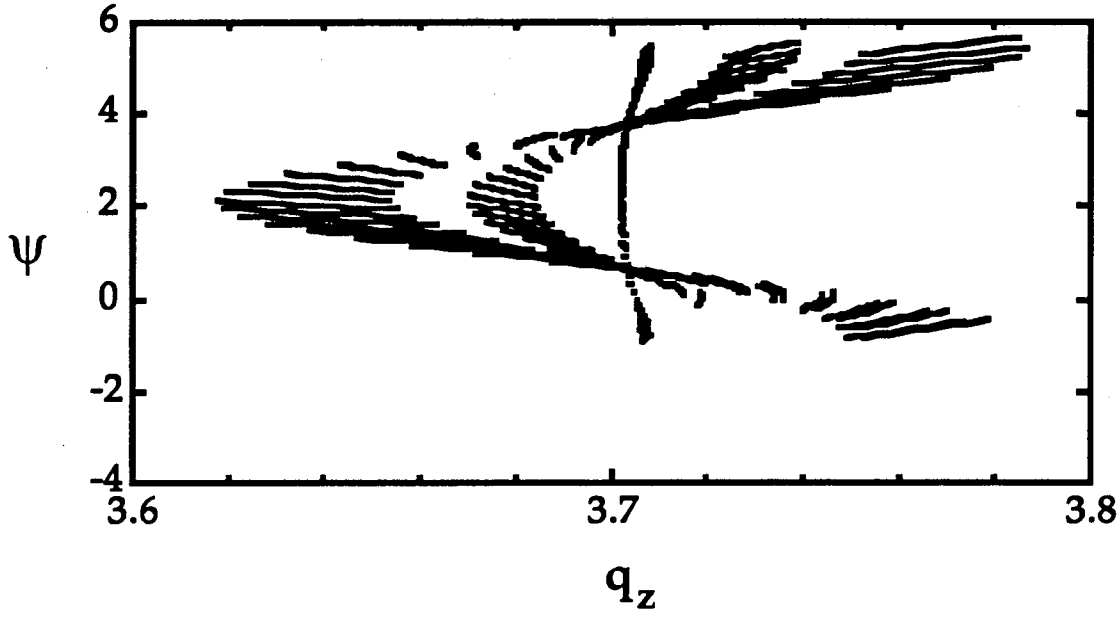

Fig. 4.8(c). Orbit segments for the particles of Fig. 4.8(a), for 2.2 m<z<2.6 m. The three populations corresponding to three different values of q_y are now very clearly distinguished. Larger q_y particles have drifted farther back in q_z, giving up more energy to the fields.

To make this inspection of the phase-space a bit more quantitative, we select two specific groups of five particles, and observe their motion in detail. Fig. 4.9 depicts motion in the ψ-q_z plane and Fig. 4.10 depicts q_z as a function of z, for these particles. Each group of particles has initial phases distributed throughout $(-\pi,+\pi)$. However the first group, depicted in Figs. 4.9(a) and 4.10(a). has a large $q_y \sim a_\beta$, while the second group, in Figs. 4.9(b) and 4.10(b) has

a small $q_y \sim 0.05 a_\beta$. In Figs. 4.9(c) and 4.10(c), both groups are plotted together.

Inspecting Fig. 4.9 we see that high-q_y particles tend to give up energy to the fields, while low q_y particles tend to absorb energy from the fields (as they are driven to higher q_y by the transverse Lorentz force). Fig. 4.10(c) shows that the peak loss (gain) of high (low) q_y particles occurs at roughly the same point in z, corresponding to the saturation point and maximum radiated power.

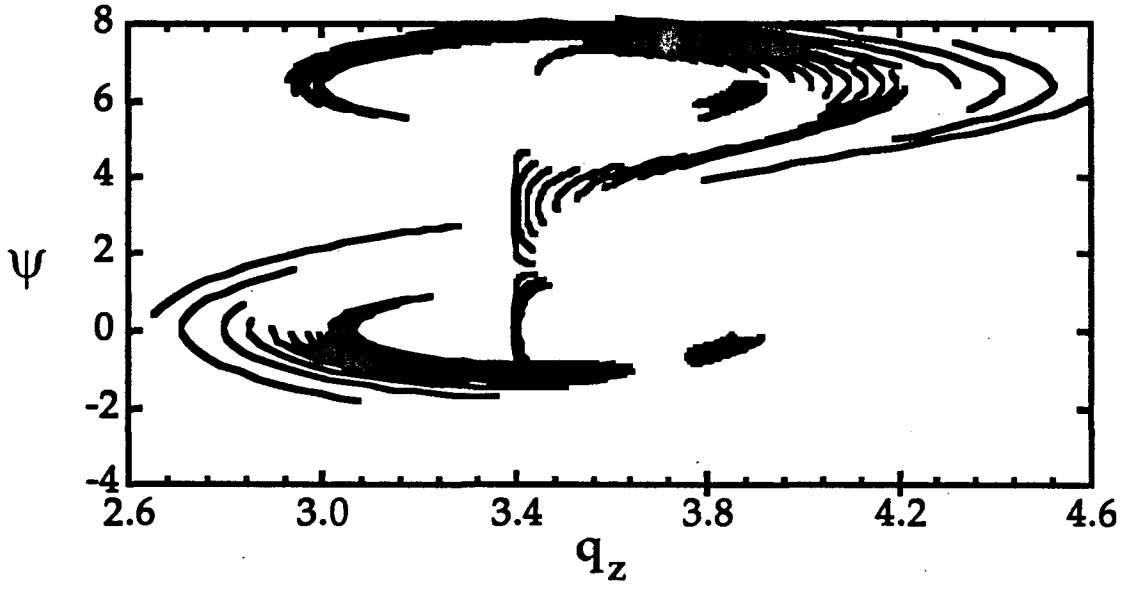

Fig. 4.8(d). Orbit segments for the particles of Fig. 4.9(a), for 4.4 m<z<5.1 m, including the saturation point at z~4.8m. Large q_y particles have completed one synchrotron oscillation, and are exceuting bound orbits governed approximately by the bounce Hamiltonian of Eq. (3.36). Small q_y particles (the dark clumps near q_z~3.8) have gained energy from the fields.

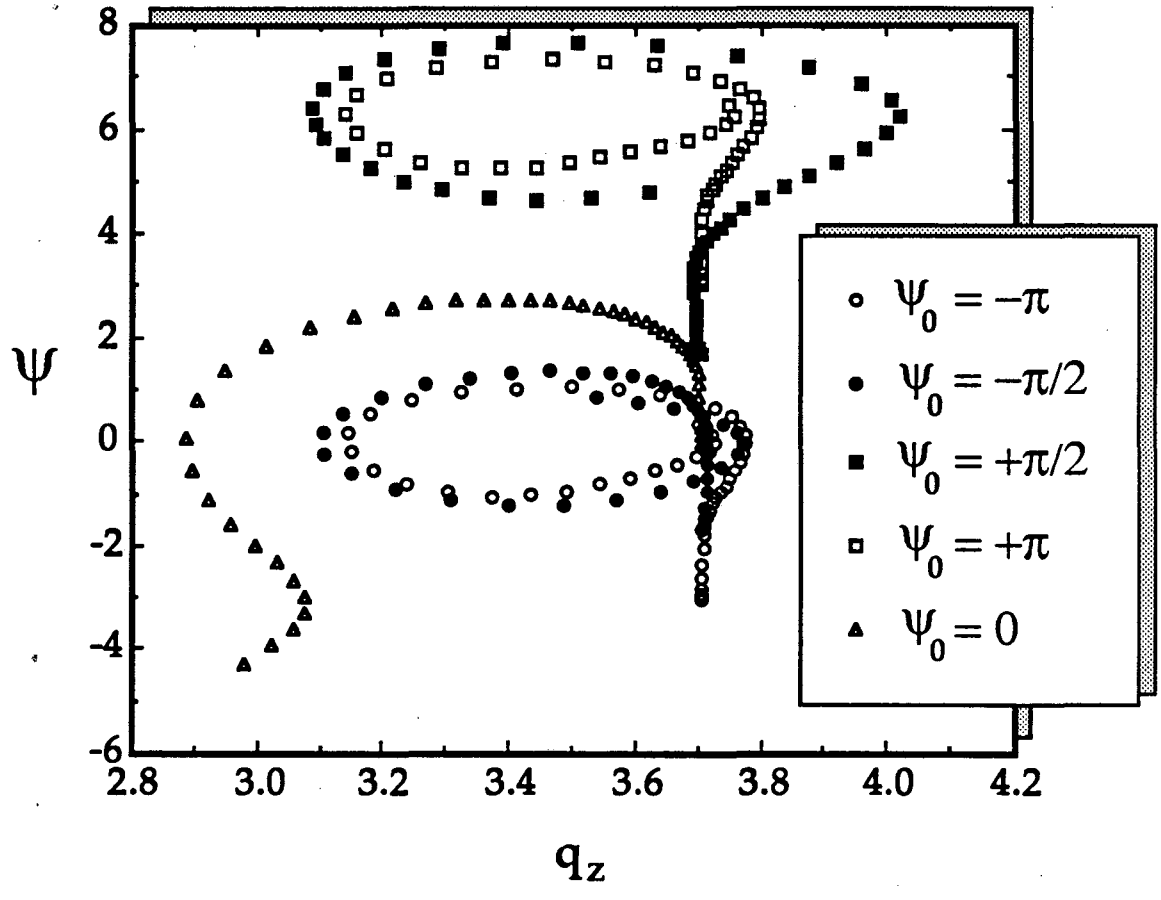

Fig. 4.9(a). Depicted is the motion computed with ECL for 0<z<7.3m for a representative collection of five particles with $q_y \sim a_\beta$. This motion is to be compared with that of a simliar collection, with $q_y \sim 0.05 a_\beta$, depicted in Fig. 4.9(b). Evidently, large q_y particles bunch in ψ and give up energy (moving to the left in the figure). From Fig. 4.9(b) we see that small q_y particles gain a little, and from Fig. 9(c), we see that the difference is positive, leaving some energy to be taken away by the fields .

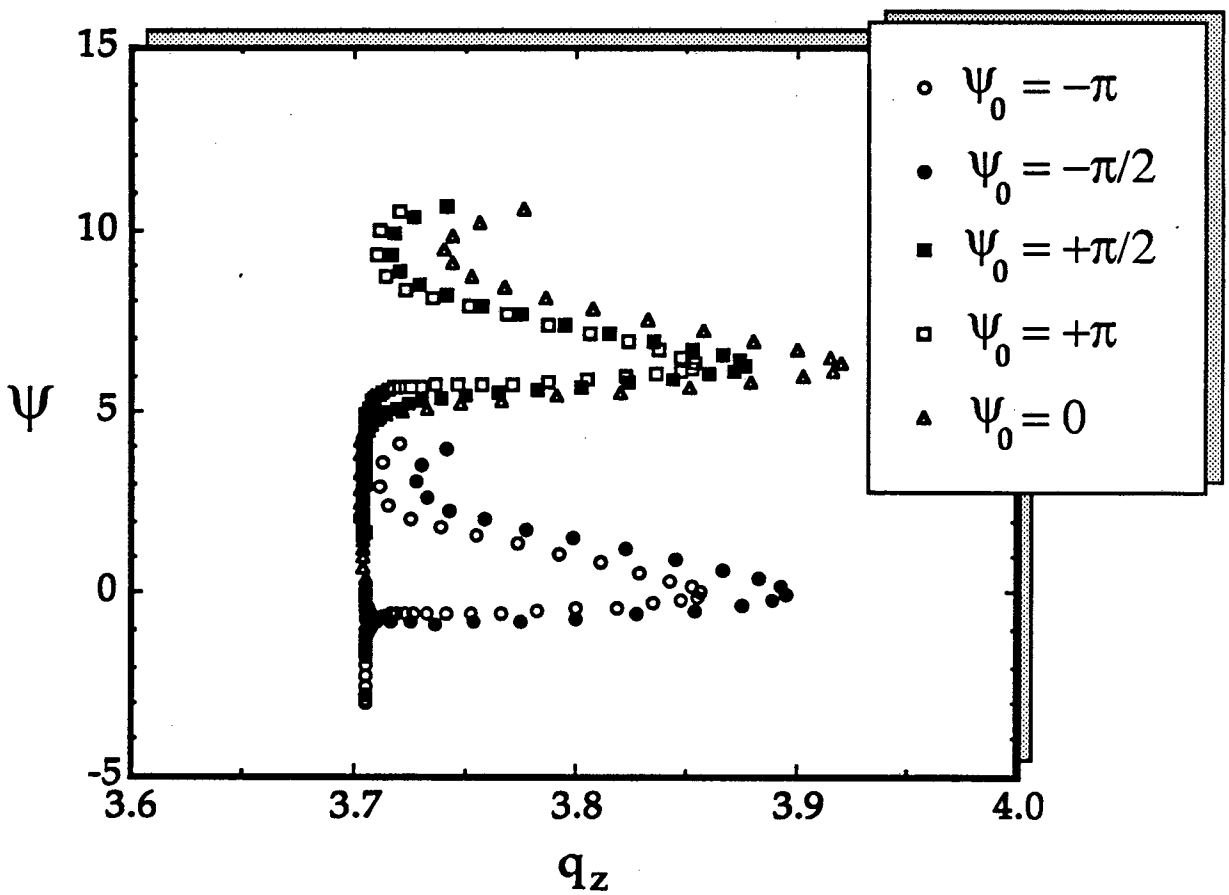

Fig. 4.9(b). The motion in ψ and q_z of five representative macroparticles with small $q_y \sim 0.05 a_\beta$. Because q_y is small, the transverse motion of these electrons is strongly perturbed by the signal field. As a result they oscillate with growing amplitude, aborbing energy from the field. None of them give up energy, as discussed in connection with Eq. (3.77).

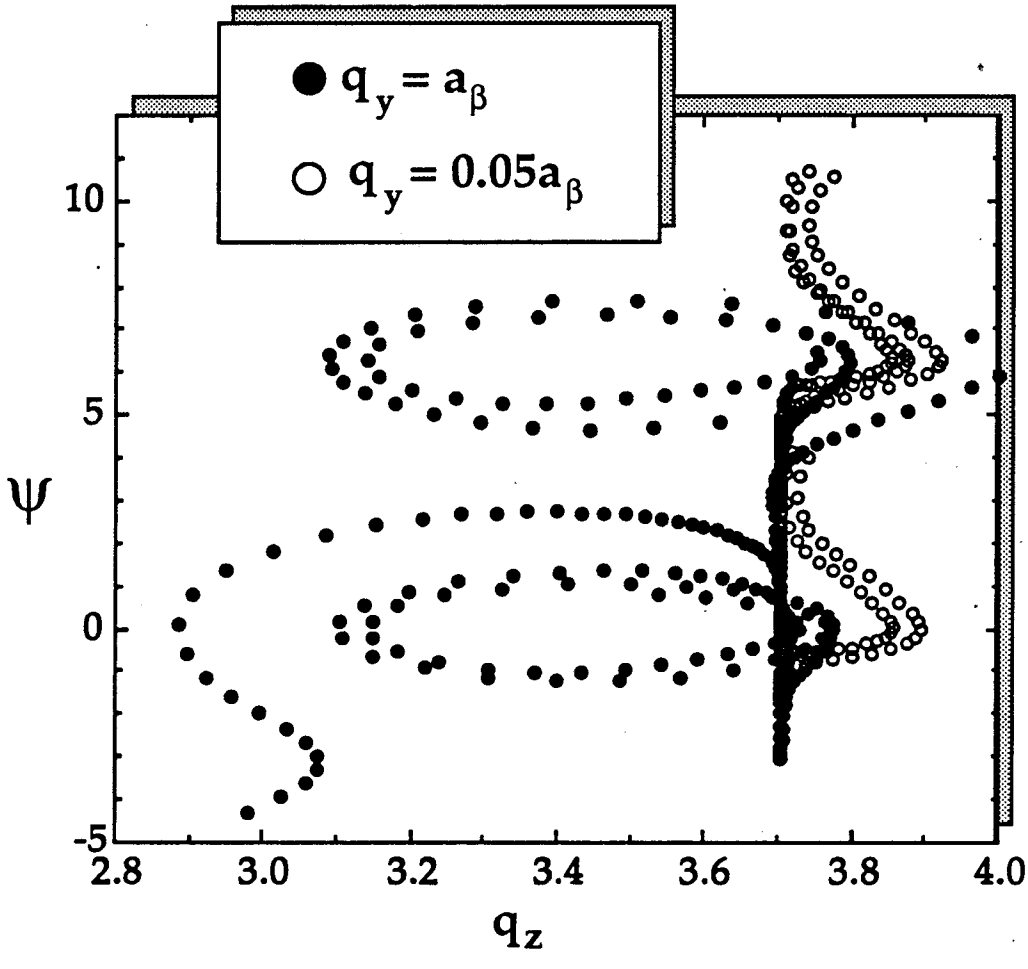

Fig. 4.9(c). Orbits in the ψ-q_y plane of particles with small q_y (white dots) and particles with large q_y (dark dots). Small q_y particles *gain* a small amount of energy. Large q_y particles *lose* a large amount of energy. The difference is taken away by the fields.

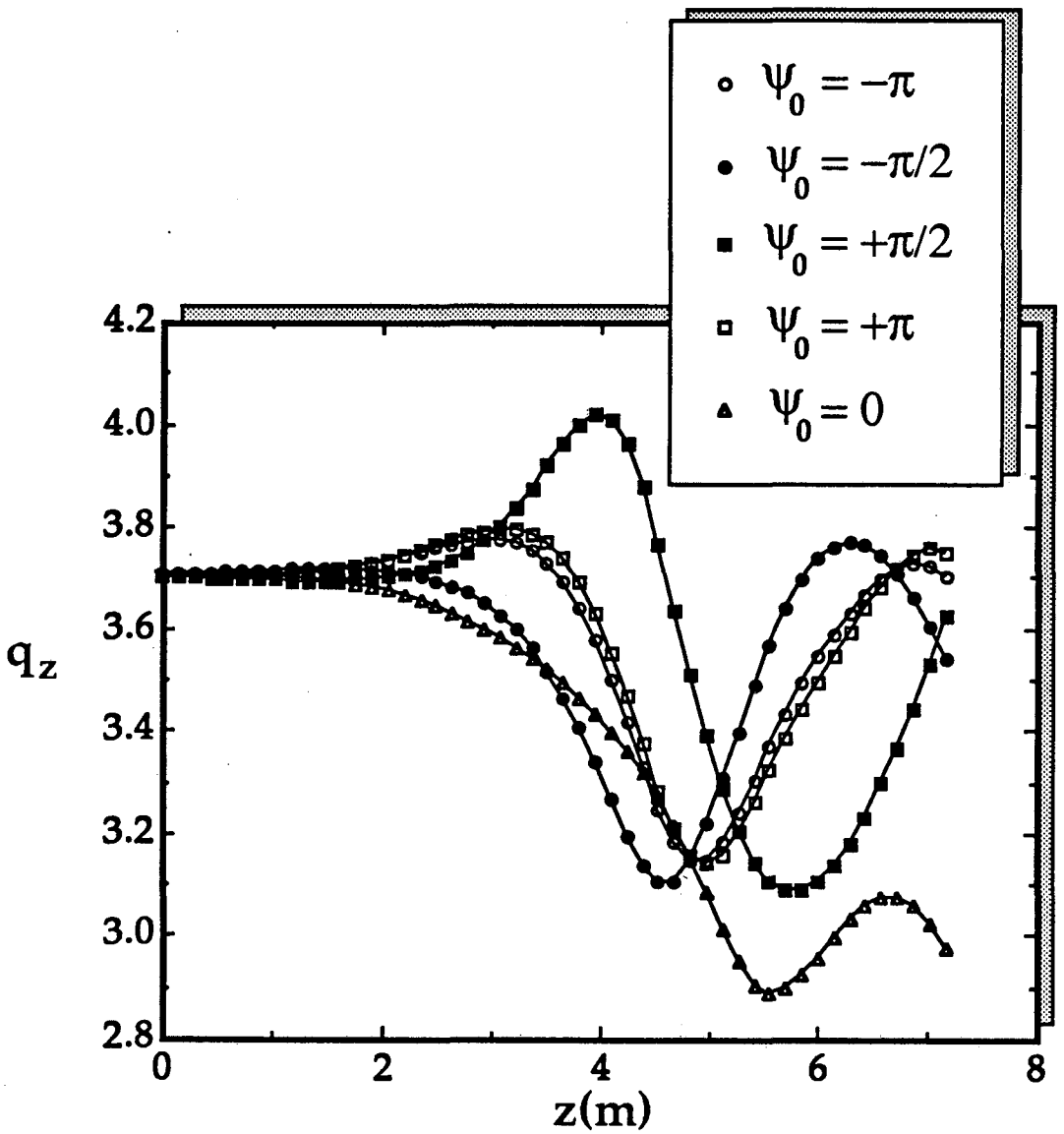

Fig. 4.10(a). Near saturation large q_y particles lose a significant amount of energy. On the other hand, (b) small q_y particles actually gain energy near saturation. This is clearer in (c) where both ensembles are depicted together.

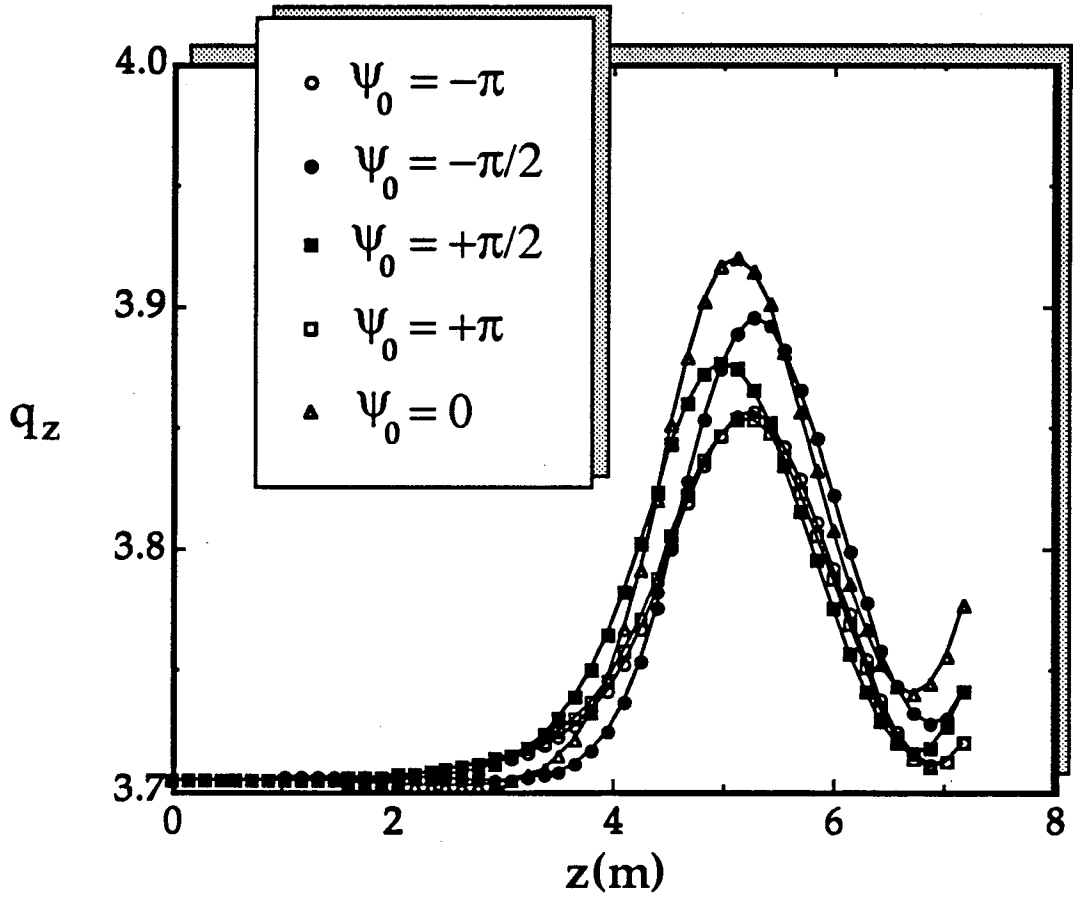

Fig. 4.10(b). Depicted is q_z versus z for the five representative low q_y particles of Fig. 4.9. Evidently, these particles gain energy near saturation (z~5 m).

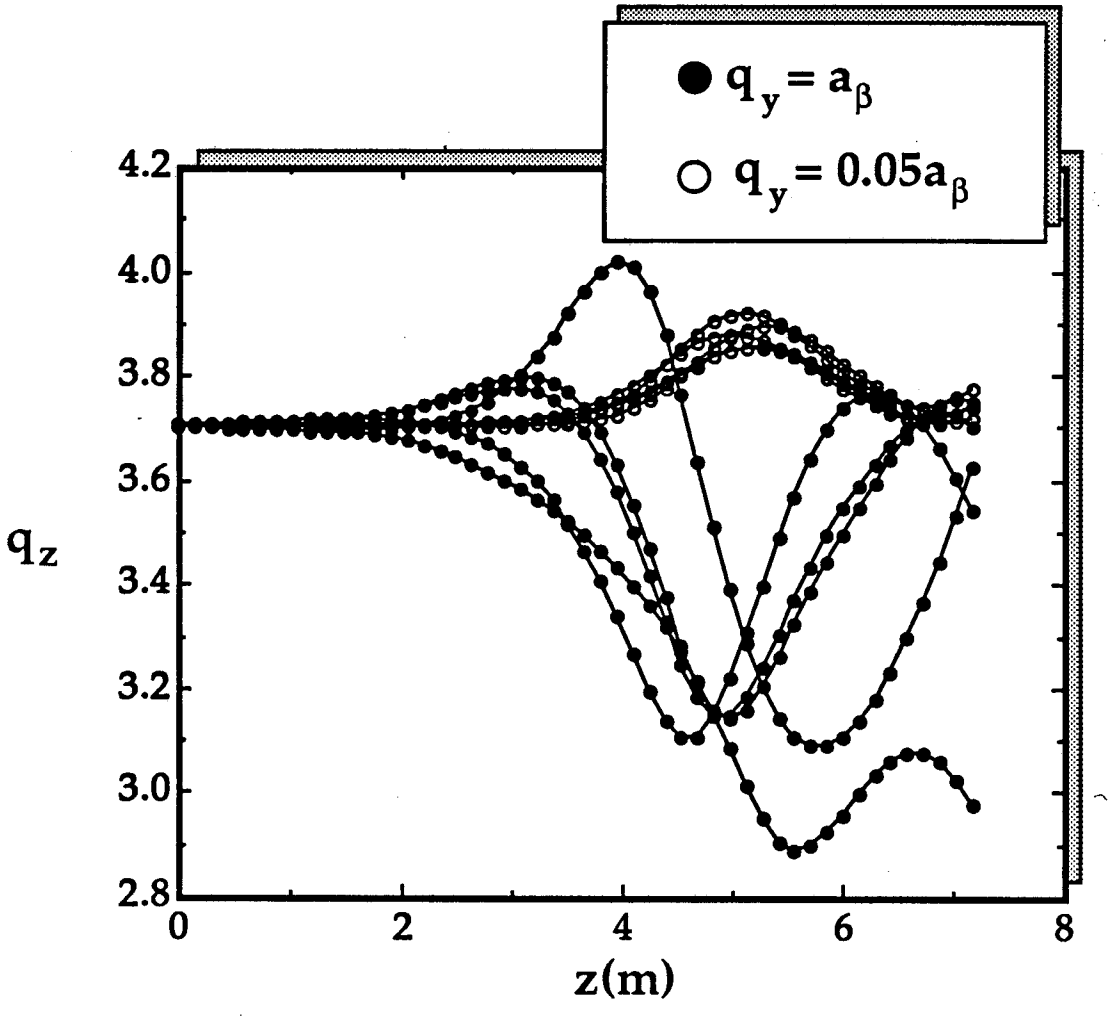

Fig. 4.10(c). Depicted is q_z versus z for the representative particles of Fig. 4.9. While low q_y particles gain energy, high q_y particles lose energy. The average results is a loss for the beam.

Inspection of Figs. 4.9 and 4.10 qualitatively confirms the conclusions of our discussion of bunching, in particular the ponderomotive force of Eq. (3.70) and the invariant Φ_y of Eq. (3.73).

d. Effect of detuning spread. Next, we turn to consider the effect of detuning spread on the saturation length and output power. There are in principle at least three important effects: (1) detuning spread due to spread in axial momentum (2) detuning spread due to spread in transverse energy ("realistic radial profile") and effective detuning spread due to beam space charge. The beam density is n_b~1.7x10^{11}, and the Lorentz factor is γ~3.9, so that the spread in k_β due to beam self-fields ($\Delta k_\beta/k_\beta \sim \nu/2\gamma a_\beta^2$) will be of order 7%. The spread in detuning due to a non-ideal radial profile will be of order $\delta_s \sim \sigma_h a_\beta^2$~20% (depending on the beam profile). The code ECL allows us to model detuning spread in two ways: spread in q_z, or spread in h. We consider each in turn.

First, we consider spreads in axial momenta. Results for power versus z for various spreads in momenta are depicted in Fig. 4.11. A summary of peak power and saturation length is depicted in the plot of Fig. 4.12. We observe that power is rather insensitive to even significant spreads. This is not surprising, given the discussion of Eq. (134) (modified dispersion relation, including momentum spread) since the Pierce parameter is relatively large. In this connection note that the actual detuning spread δ_s as defined by Eq. (3.134) is given by Eq. (4.2) as $\delta_s = 1.5 q_s/q_z$, where particles are distributed

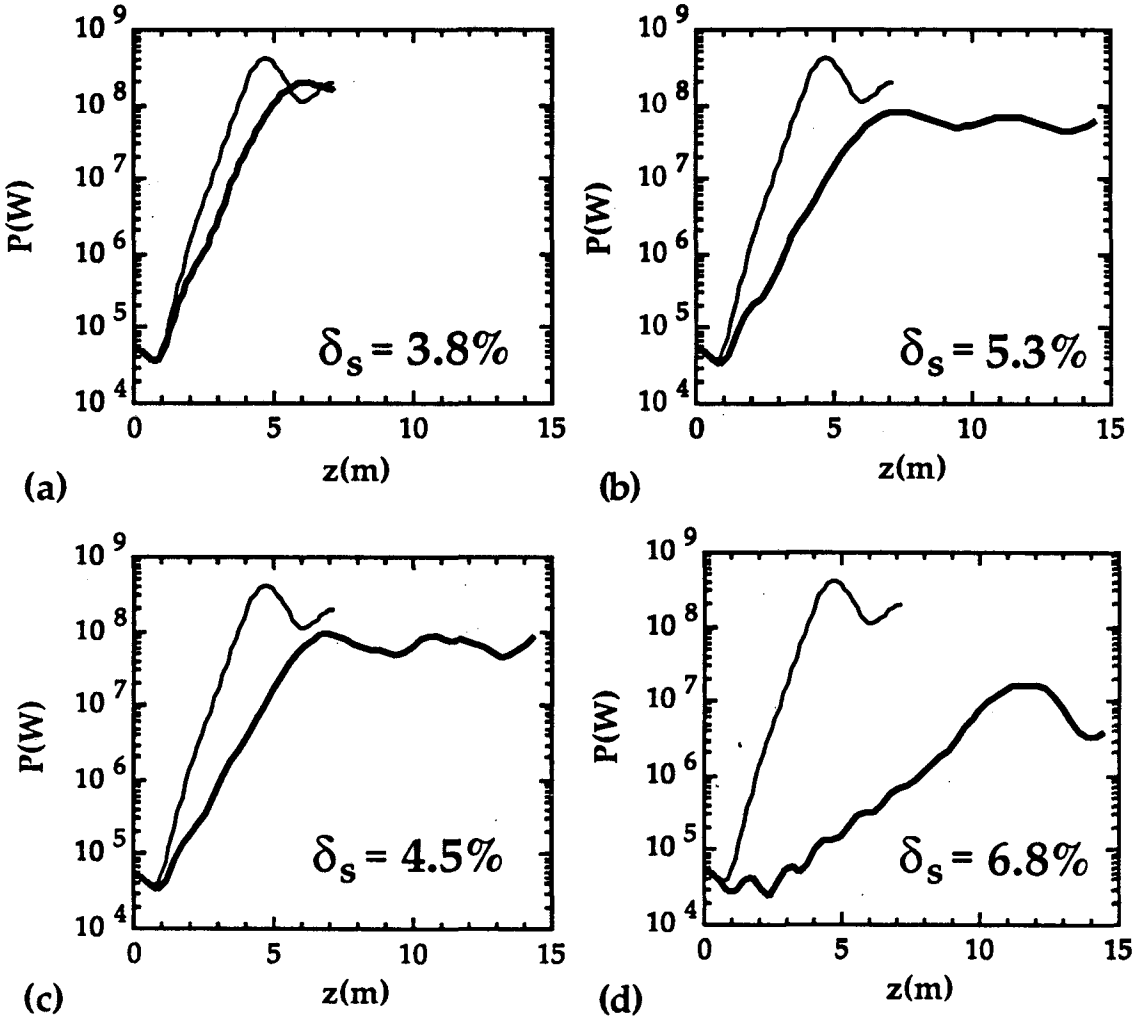

FIG. 4.11. (a)-(d) Curves for power versus z for the parameters of Table 4.1, with an assortment of different spreads in axial momenta (dark curves) plotted with the result for zero detuning spread (light curve, the result of Fig. 4.1 (a)), for reference. The corresponding momentum spreads ($2q_s/q_z$) are (a) 5% (b) 6% (c) 7% and (d) 9%.

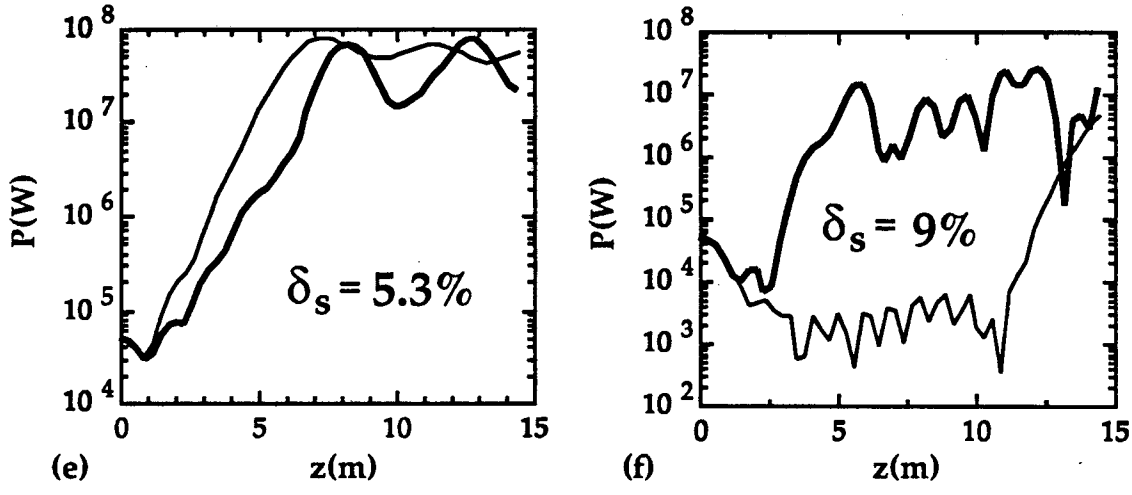

FIG. 4.11. (e)-(f). Stabilization due to detuning spread manifests itself numerically as a sensitivity to the number of points used to model the momentum distribution. So for example, (a)the result of 4.11(c) is relatively insensitive to a decrease in the particle number by a factor of four (the dark curve corresponds to 700 particles, the light curve, 2800). On the other hand for δ_s~9%, the result varies dramatically with particle number. By increasing the number of particles it is possible to show that the power curve of 4.11 (f) flattens out. The curve of 4.11(e) merely converges, and in fact, has more or less converged with the result of 4.11(c).

uniformly in momenta on the interval $[q_z-q_s,q_z+q_s]$. (The results for saturation power and length are summarized in Table 4.3 and in Fig. 4.12.

To illustrate the approach to stabilization, in Fig. 4.11 (e) and (f) we compare results corresponding physically to reduced growth (e) and no growth (f). Numerically, the physically stable system is numerically sensitive to the number of particles. In principle, this sort of result can be avoided altogether by routinely using 20-40 values of momenta. However, this is not always numerically efficient.

The results of Figs. 4.11(a)-(d) are summarized in Fig. 4.12, giving peak power and saturation length as a function of δ_s, based on these four runs.

Table 4.3. Effect of axial momentum spread for ion-channel guiding

δ_s	P_{sat}	L_{sat}	*efficiency*	$\Delta p_z/p_z$
0	392 MW	4.8 m	6.5%	0
3.8%	189 MW	6.1 m	3.2%	5%
4.5%	91 MW	7.0 m	1.5%	6%
5.3%	78 MW	7.3 m	1.3%	7%
6.8%	16 MW	11.7 m	0.3%	9%
9%	—	(stabilized)	—	12%

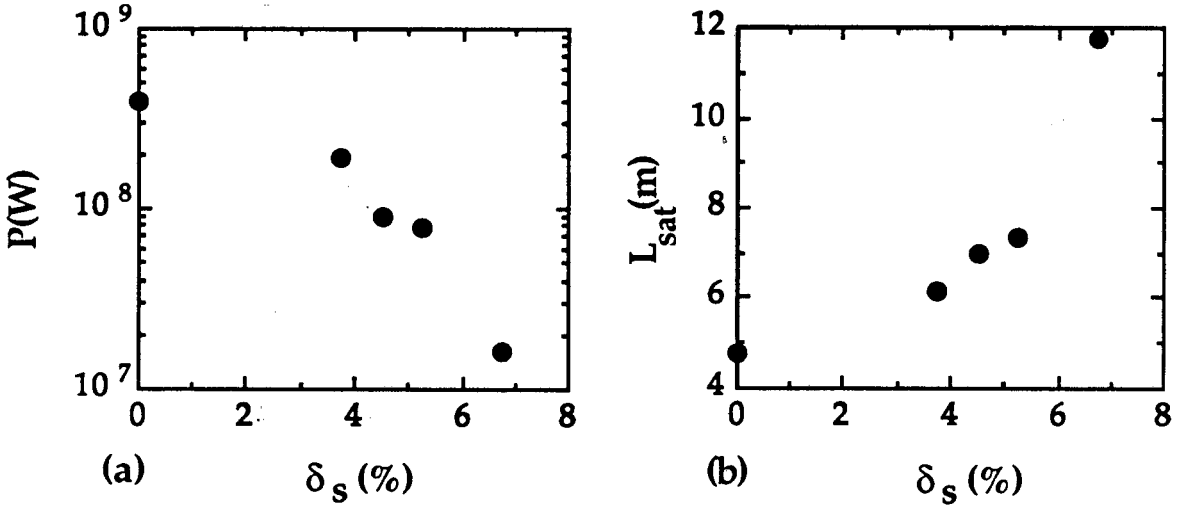

FIG. 4.12. (a) Power at saturation versus detuning spread, based on the data of Fig. 4.11, and (b) length for saturation. For these plots, the first appreciable peak in power was selected (even though, frequently, the second peak is slightly larger).

From these runs we see that a detuning spread $\delta_s<\rho$ has only a small effect on the output power (a factor of two), in accord with the results of Ch. 3, Sec. B.4. For $\delta_s>\rho$, we observe an approximately exponential decrease in power with detuning spread, as we would expect when δ_s enters the gain length scaling, as in Eq. (3.135).

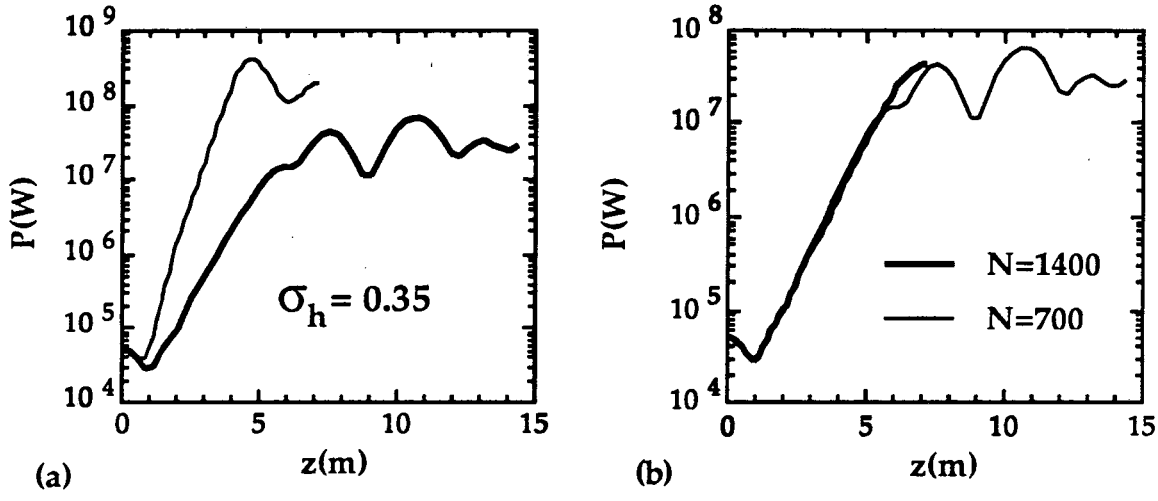

FIG.13. (a)Power versus z for the parameters of Table 4.1, with a spread in transverse energy corresponding to a parabolic radial profile. The "equivalent" detuning spread is δ_s~11%. (b) The result of (a) compared to the same result for twice as many particles.

In addition to detuning spread due to axial momentum spread, there is a detuning spread due to the spread in transverse energy associated with a realistic beam profile (as discussed in Ch. 3, Sec. C). To quantify the effect of such an "intrinsic" detuning spread, we consider a distribution in the dimensionless transverse energy h with an rms fractional deviation in

transverse energy σ_h~0.35, equivalent to a parabolic beam profile. The equivalent detuning spread is of order $\delta_s \sim \sigma_h a_\beta^2 \sim 12\%$. Results are depicted in Fig. 4.13. Saturation occurs at z~7.6 m with P_{sat}~41 MW. The peak power is 61 MW at z~10.7 m, corresponding to a factor of 10 reduction in power, and an efficiency of about 0.6%.

This result is mildly surprising, since for an 11% detuning spread due to axial momentum spread the beam is stabilized. On the other hand, particles with the largest detuning, i.e., the smallest transverse energy, interact negligibly with the wave. They tend to gain energy, but as we see in Figs. 4.9(c) and 10(c), this gain is relatively small. Thus the rms detuning $\sigma_h a_\beta^2$ is not quite "equivalent" to a numerically equal detuning due to momentum spread. Detuning due to energy spread is reduced by a weighting increasing with h.

We performed simliar runs for σ_h~0.71 (equivalent to a Gaussian beam) and found that the instability was stabilized. This is not surprising since the equivalent detuning spread is an enormous 22% ($>4\rho$). However, this has sobering implications for a practical experiment. Results will depend in detail on the character of the transverse energy distribution. On the other hand, the situation improves for smaller a_β^2/ρ as we shall see in the next example.

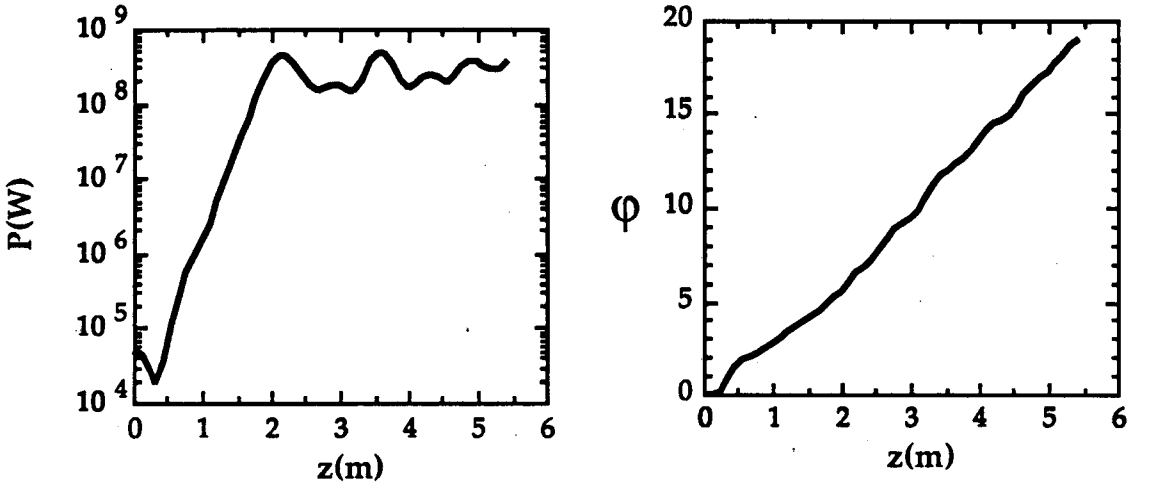

FIG. 14. The result from the code ECL, for (a)power in watts and (b)phase in radians versus z for the example of Table 4.1. This differs from Fig. 4.1 (a) because we have included the effect of optical guiding. Saturation occurs at L_{sat}~2.2 m, with P~440 MW.

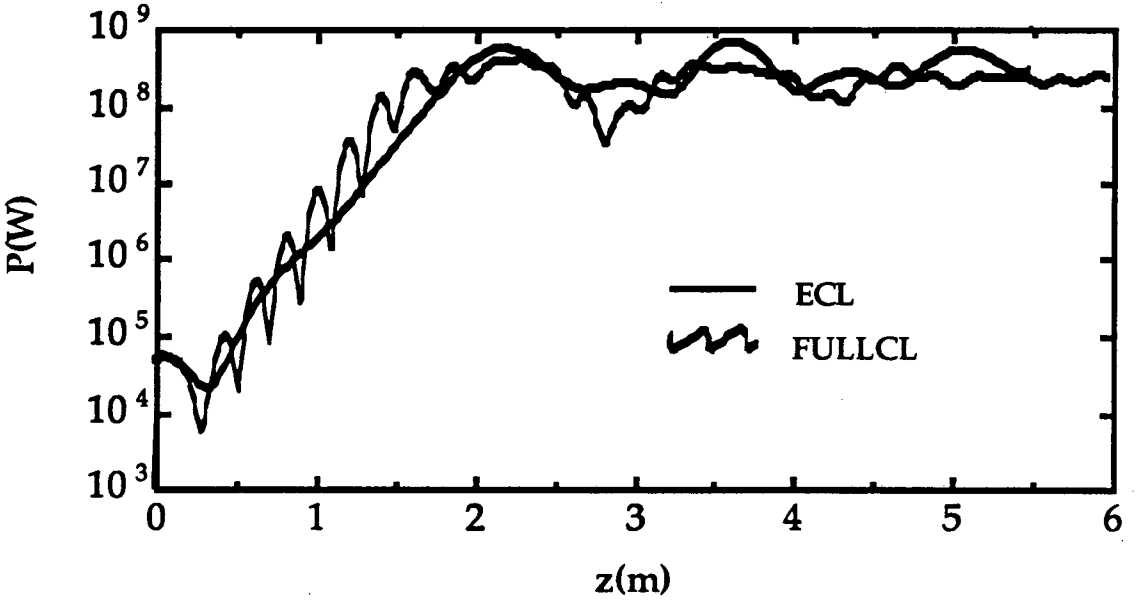

FIG. 4.15. The results from the code FULLCL (wiggling curve) and ECL, for power versus z, for the example of Table 4.1, including optical guiding. FULLCL predicts saturation at L_{sat}~2.3 m, with P~370 MW.

2. *Effect of Optical Guiding*

All of the previous discussion of Sec. 1 assumed guiding by the HE_{11} mode of the ion-channel. On the other hand, a simple estimate of the effect of optical guiding for the parameters of the previous example shows that it will be quite important. From Eq. (3.258) we find $\sigma=64\rho_0^{3/2}a_\beta^3\sim1.5$, which is too large to apply the weak-guiding results of of Sec. 3.D, and indicates that $\eta\sim1$ is probably a good approximation. This gives a corrected Pierce parameter $\rho\sim12.4\%$ and a gain length $L_g\sim27$ cm. The output power at saturation would be $P_{sat}\sim744$ MW. The length for saturation would then be $L_{sat}\sim1.6$ m, or about 5 betatron wavelengths. We conclude from this that the parameters of Table 4.1 would provide a fair test of optical guiding. Since in this case the gain length is less than a betatron wavelength, this example also provides an interesting test of the eikonal formalism beyond its presumed range of validity.

a. Comparison of ECL and FULLCL results. Taking $\eta\sim1$, we performed ECL and FULLCL simulations as described above. Results for power versus z are depicted in Fig. 4.14. The code ECL predicts saturation at $z\sim2.1$m, with $P_{sat}\sim440$ MW, corresponding to an efficiency of about 7.3%. FULLCL predicts saturation at $z\sim2.3$ m with $P_{sat}\sim370$ MW, for an efficiency of about 6.2% (Fig. 4.15).

Thus the power levels are somewhat less than the cubic gain regime predictions. This is partially due to corrections to the eikonal approximation

in the limit $L_g<\lambda_\beta$, and also due to the larger value of μ/ρ, which lowers the growth rate as discussed in connection with Eq. (3.126). For this example, we have $\mu/\rho\sim1.8$, which from Fig. 3.8(a) predicts a peak growth rate 75% of the $\mu=0$ value (and somewhat less for zero detuning).

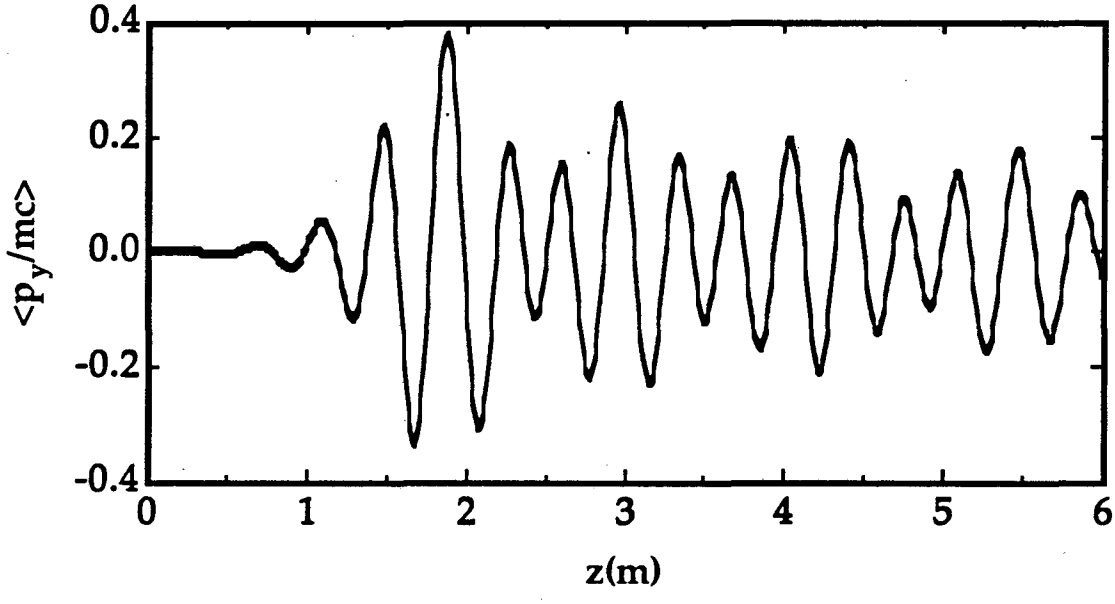

FIG. 4.16. The y-momentum, averaged over the beam slice is plotted versus z, for the parameters of Table 4.1, including optical guiding. Following saturation the beam centroid continues to oscillate coherently.

b. Effect of detuning spread. With optical guiding we have seen that the Pierce parameter is larger by about a factor of two. With a larger ρ, the condition $\delta_s<\rho$ is eased and we can expect performance to be much less sensitive to detuning spreads. This is seen in the results of Fig. 4.17, which are summarized in Table 4.4 and Fig. 4.18. For example, with a 7.5% spread, the peak power is reduced by only a factor of 3.

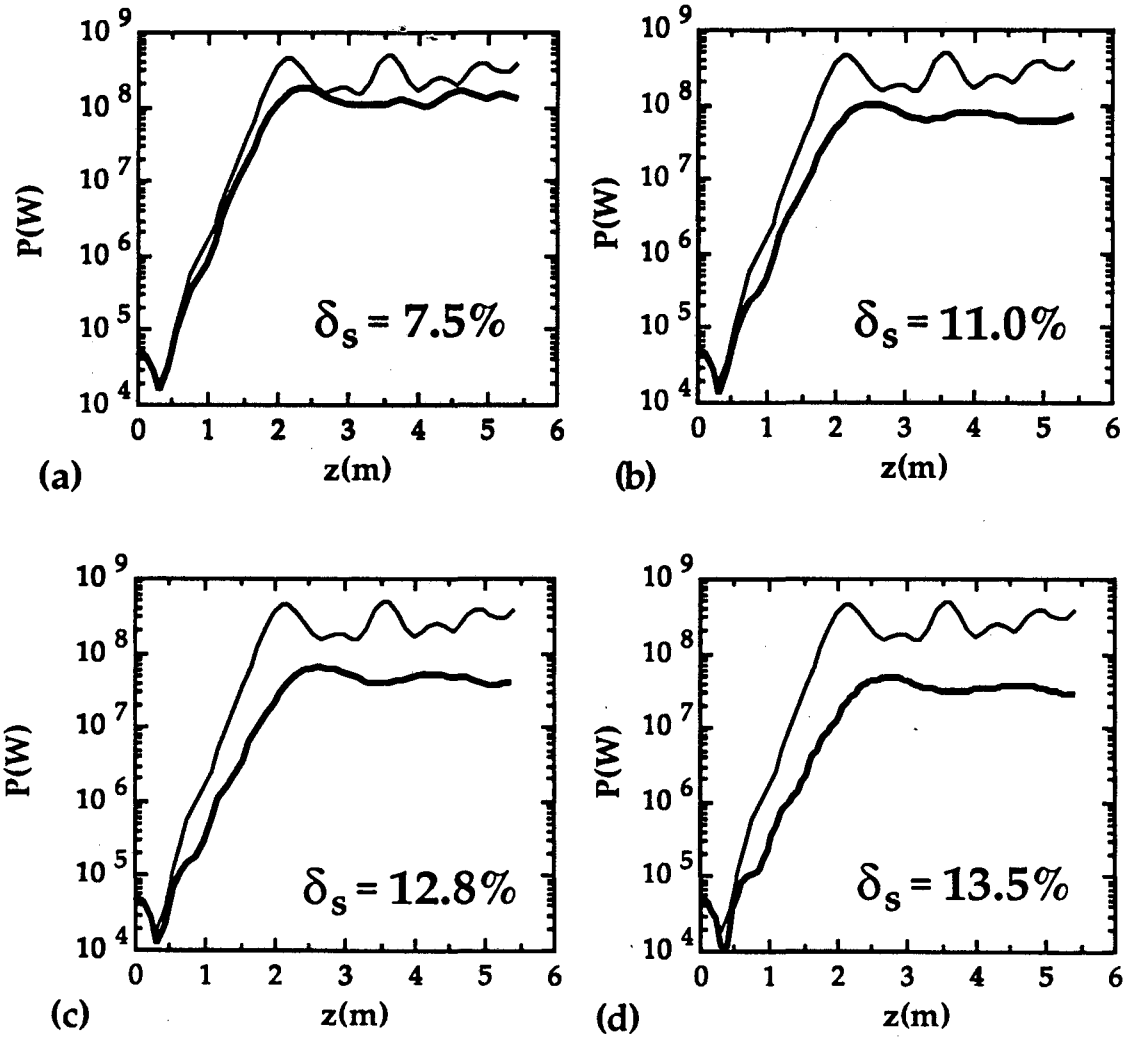

FIG. 4.17. (a)-(d) ECL results for power versus z with various detuning spreads (dark curves), compared to the cold beam result of Fig. 4.14 (a) (light curves). Optical guiding has increased ρ, and as a result the power is less sensitive to detuning spread.

Table 4.4. Effect of axial momentum spread for optical guiding example.

δ_s	P_{sat}	L_{sat}	*efficiency*	$\Delta p_z/p_z$
0	440 MW	2.2 m	7.3%	0
7.5%	170 MW	2.4 m	2.8%	10%
11.3%	98 MW	2.5 m	1.6%	15%
12.8%	61 MW	2.6 m	1.0%	17%
13.5%	46 MW	2.8 m	0.8%	18%
15%	—	(stabilized)	—	20%

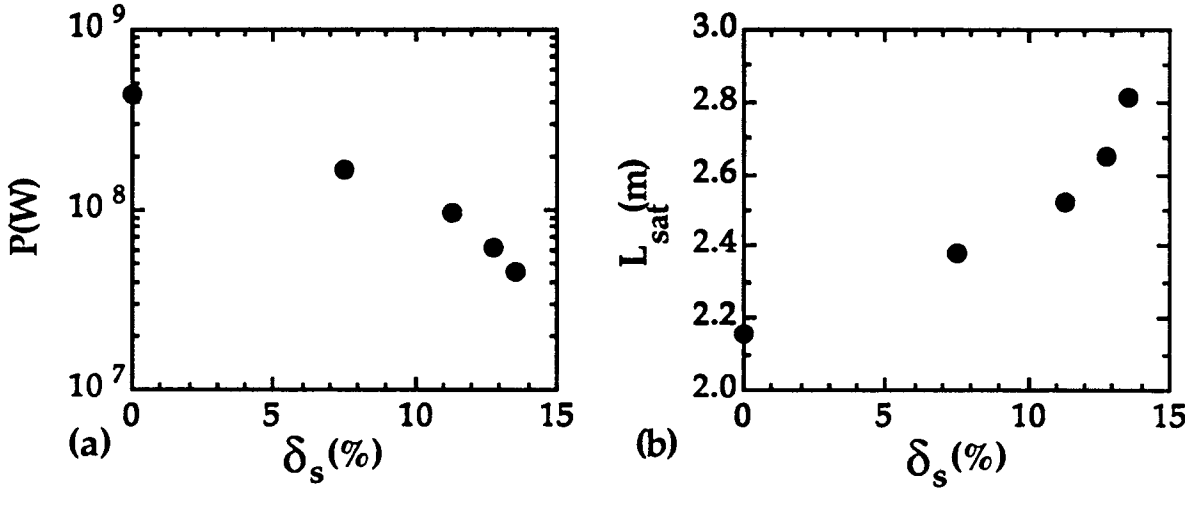

FIG. 4.18. (a) Power at saturation versus detuning spread, based on the data of Fig. 4.17, and (b) length for saturation. For these plots, the first appreciable peak in power was selected (even though, frequently, the second peak is the largest).

In Fig. 4.19, we have collated the results for peak power and saturation length as a function of δ_s/ρ, for this example (optical guiding) and the

previous example (ion-channel guiding). We observe that the results are well-correlated, even though they apply to Pierce parameters differing by a factor of two, and different μ/ρ values. This gives us a fair measure of confidence in the condition for gain,

$$\frac{\Delta p_z}{p_z} < \rho \quad ; \quad (\delta_0 = 0) \,, \tag{4.6}$$

Where in parenthesis we note for clarity that we have only considered zero average detuning.

By the same reasoning, since ρ is large we expect the performance to be much less sensitive to realistic spreads in transverse energy. This is observed

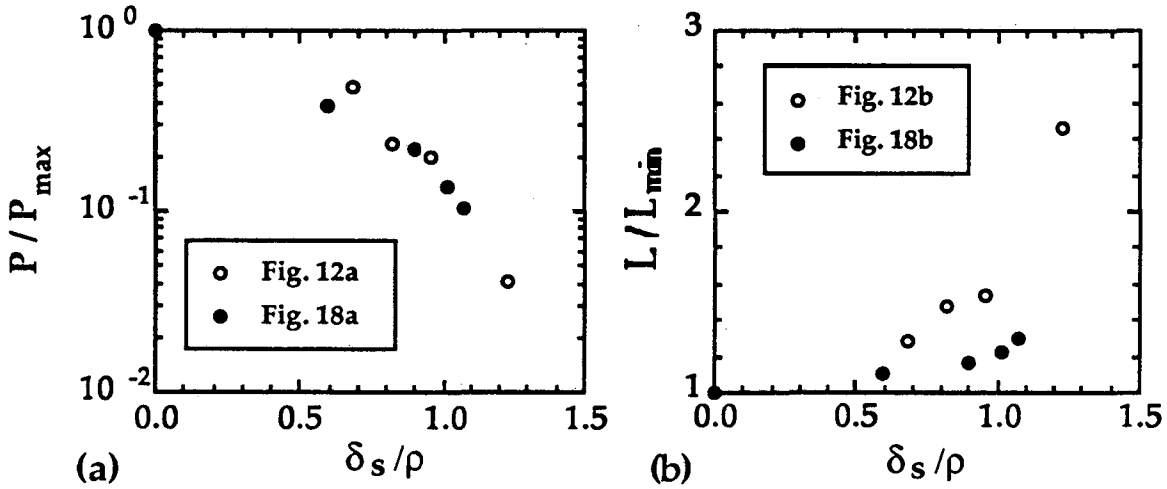

FIG. 4.19. A collation of the results of Figs. 4.12 and 4.18. (a) Power at saturation normalized by the cold beam value, versus detuning spread normalized by the Pierce parameter (b) length for saturation normalized by the cold beam value.

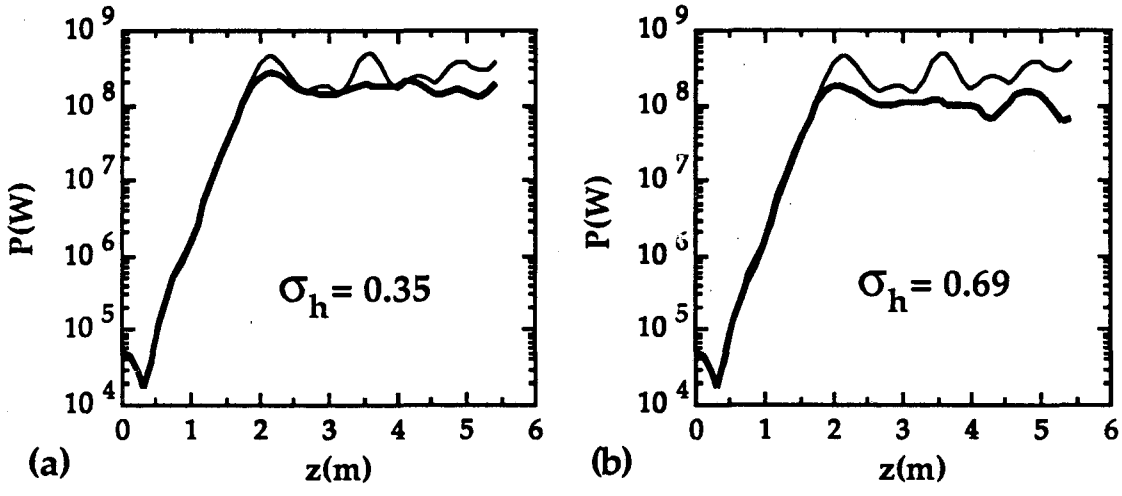

FIG. 4.20. ECL results for power versus z with fractional rms spreads in transverse energy (dark curves) of (a) 35% and (b)70%(dark curves), compared to the cold beam result of Fig. 4.14 (light curve). (a)For the parabolic beam of the peak power is 270 MW, at 2.2 m, (56% of the step-profile result). (b)For the case of σ_h comparable to a Gaussian beam, the peak power is 173 MW at 2.1 m (36% of the step-profile result) .

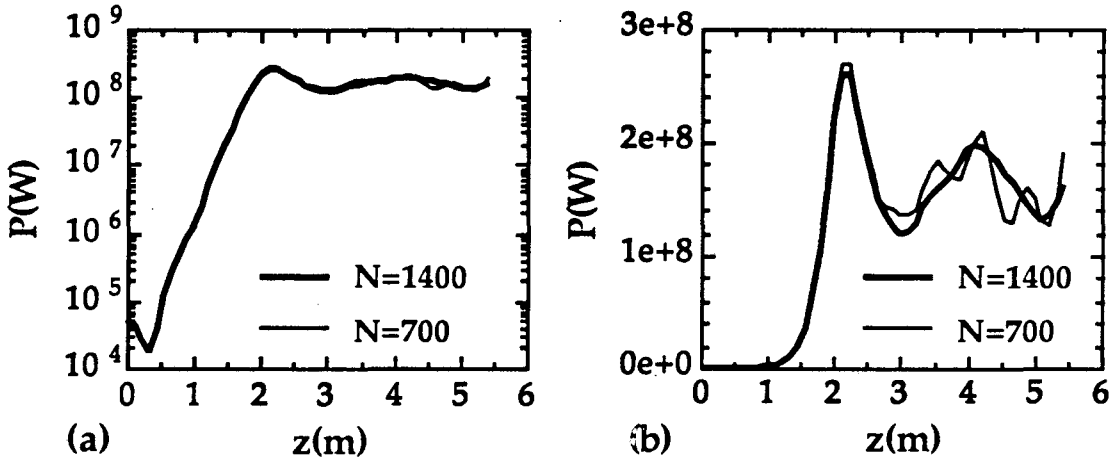

FIG. 4.21. Example of the insensitivity of the numerical result to a change in the number of particles used to model energy spread for N=700 and 1400, corresponding to 5 and 10 different h-values respectively and σ_h=35%. In (a) we see that the linear growth rates agree well, and in (b) we see that the peak power levels agree well. Note that the larger number of particles has resulted in more realistic phase-mixing and a noticeably smoother power variation in (b).

in the results of Fig. 4.20. As a check on the results we varied the particle number, obtaining roughly the same results, as shown in Fig. 4.21. We conclude that with optical guiding, a positive experimental result would not depend on the beam profile, or the momentum spread, within reasonable limits.

3. Waveguide example

Next we consider the effect of introducing a waveguide for the parameters of Table 4.1. We select (somewhat arbitrarily) a 3cmx5cm guide, and increase the plasma density to 1.3×10^{11} cm^{-3}, (corresponding to λ_β~23.6cm) in order to maintain resonance at 1.7 cm.

The phase velocity is β_φ~1.016, and q_z~3.6, corresponding to a reduction in the Pierce parameter by a factor F~0.341, from Eq. (3.110). Thus ρ~3.3%. From Eq. (3.118) we expect a gain length of $L_g \sim 0.09\lambda_\beta/\rho \sim$ 64 cm and an output power P_{sat}~200 MW, with saturation at L_{sat}~3 m.

a. FULLCL results. The numerical result for power versus z is depicted in Fig. 4.22. FULLCL predicts P_{sat}~280 MW, with saturation in 2.3 m. for an efficiency of 4.7%.

b. Error in plasma density In practice one expects shot-to-shot variations in the plasma density, and it is natural to ask what effect this might have on the output power. Taking the last example, we decreased the plasma density by about 50% to 9×10^{10} cm^{-3}, keeping all other inputs fixed. In this case λ_β~28.6 cm and the resonant frequency is now 12.7 GHz.

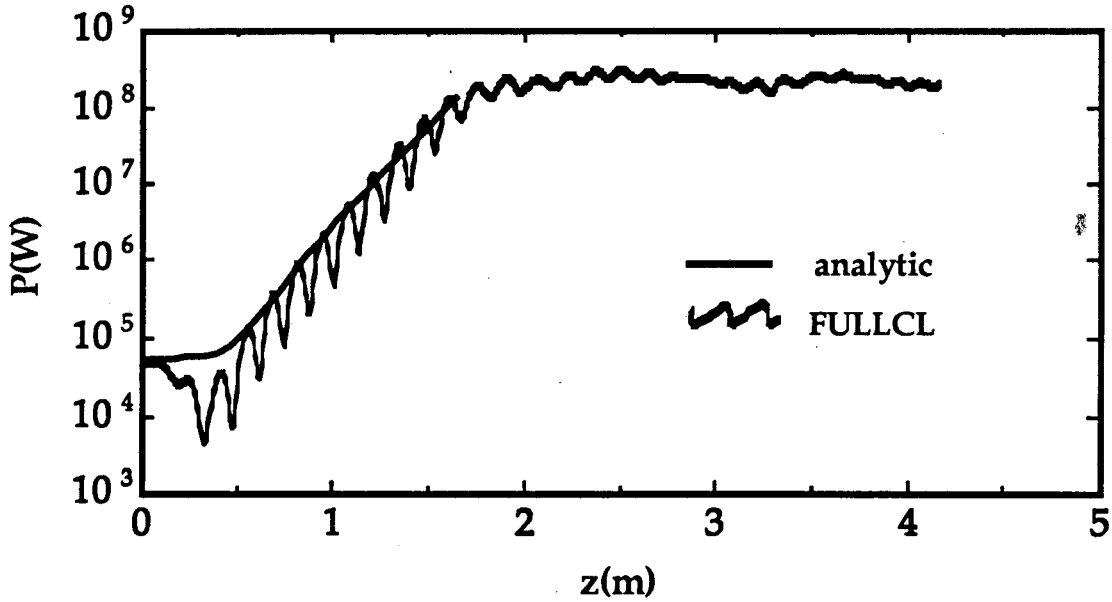

FIG. 4.22. The results from the code FULLCL for power in gigawatts, versus z for the example of Table 4.1, with modications due to a 3cmx5cm waveguide. The analytic result is overlayed for comparison.

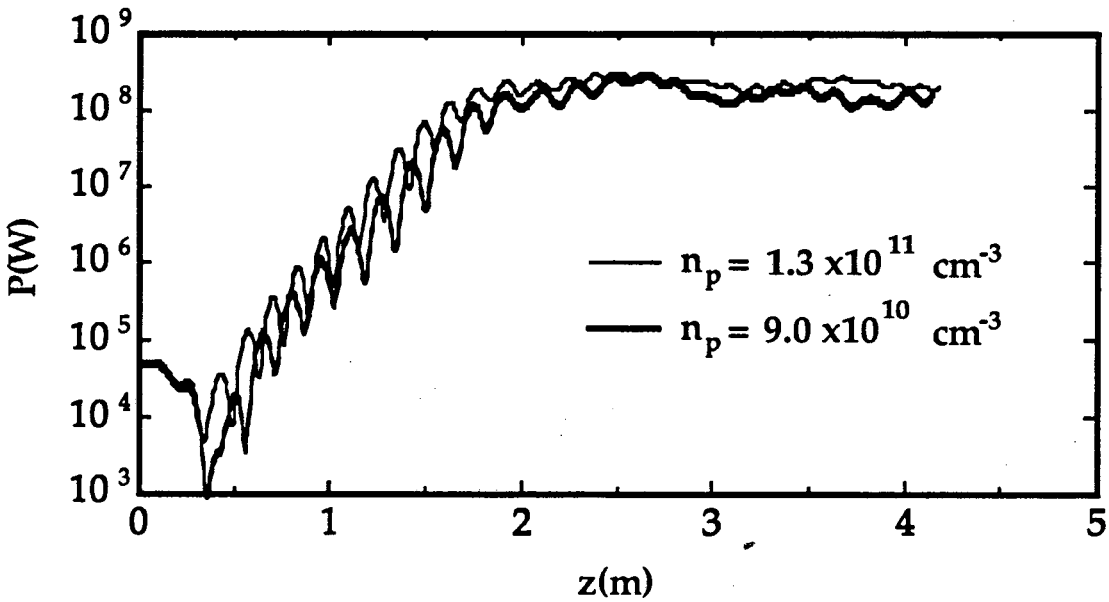

FIG. 4.23. Comparison of the result of Fig. 4.22 for power versus z (light curve), with the result for a 50% error in plasma density (dark curve).

FULLCL predicts saturation at L_{sat}~2.6 m with a saturated power of 260 MW (Fig. 4.23), about 7% less than the result for a 50% more dense plasma. The rf phase at z~410 m has changed by about 388 degrees due to the plasma error. Thus the error in power is small, while the error in phase is quite large. This is not really surprising, since waveguide corrections tend to diminish the detuning. Indeed, even though the resonant frequency is off by about 50% (6 GHz), the detuning is only $\delta \sim \Delta\omega/\omega_\beta \sim -12\rho \sim -40\%$ (i.e., $\Delta\omega \sim -2.6$GHz). Consulting Fig. 3.7, we see that the growth rate will still be appreciable at this detuning. (Note that since FULLCL follows the full motion, it should be accurate even for a detuning of order unity).

We conclude from this that for applications requiring good phase control, the plasma density will have to be repeatable from shot-to-shot, to good precision. However, a positive experimental result will not depend on extraordinary control of the plasma density.

4. Discussion

For completeness we should note the practical constraints on these examples, due to plasma effects. The chief constraint is due to ion-motion and imposes a limit on the pulse length. The time for ion-neutralization of the beam (assuming an atomic weight of ~100) is about 15 ns. Typically, induction linacs provide pulse lengths in the range 10 ns - 100's of ns, so this is a bit short, but acceptable. The ion-hose growth length computed from a rigid beam model is L_h~8 cm, and with about four e-folds after five meters. In fact,

this represents a conservative estimate since it neglects nonlinearities in the ion-motion. In addition, the use of ion-channel dielectric guiding has been rendered problematic due to the "electron-hose" instability, as discussed in Chapter 2. However, electron-hose growth has been quantified only relatively recently, and it may be that other mechanisms may arise, or be devised to reduce it.

We conclude from the work of this section, that this example would provide a highly efficient, and compact source of high peak power radiation in the 10-30 GHz range, comparing favorably with the FEL.[1] We summarize our observations:

> *(1)The codes ECL and FULLCL agree with each other and theory, despite the fact that they solve different equations, on different time-scales. Theory is more or less confirmed with respect to simple estimates of efficiency, gain length, saturated power, length for saturation, and the details of particle dynamics.*
>
> *(2)The result for power versus z assuming only ion-channel guiding is fairly sensitive to realistic spreads in axial and transverse momenta . . .*
>
> *(3) . . . However, optical guiding is predicted to be more effective than ion-channel guiding for this example. With optical guiding, ρ is large and the design is relatively insensitive to spreads in transverse energy, or axial momenta.*
>
> *(4) Operation in a 3cmx5cm waveguide gives a performance comparable to that predicted by optical guiding theory and . . .*
>
> *(6) . . ., as a footnote, we observe, that the result for power versus z is not very sensitive to a 50% error in plasma density.*

Of course, more exhaustive surveys of the δ_s, δ_0, β_φ, n_p, μ/ρ parameter space remain to be performed. However, based on our examples here, and theoretical work of the last chapter, one has a good idea of what to expect from such a survey. Our purpose here has been merely to illustrate and test the scaling laws of Chapter 3. With a fair understanding of the design constraints in hand, we devote the remainder of this chapter to a brief discussion of ICL examples at shorter wavelengths.

C. SUB-MILLIMETER EXAMPLES

In this section we consider two examples in the sub-millimeter regime. The first is a high gain experiment that could be performed with an induction linac beam. The second is a low gain experiment that could be performed with a beam more typical of a storage ring.

1. High gain example.

First we consider the example parameters of Table 4.5. We assume for the moment that ion-channel dielectric guiding dominates. The overlap integral from Eq. (3.229) is $\eta \sim 1.8 \times 10^{-2}$. The Pierce parameter is then $\rho \sim 2.6\%$. the beam power is $P_b \sim 14$ GW, so we expect a power at saturation $P_{sat} \sim 2.4\% \times 14\text{GW} \sim 360\text{MW}$. The betatron wavelength is $\lambda_\beta \sim 4.7$ cm, so that the

gain length is $L_g \sim 0.1\lambda_\beta/\rho \sim 18$ cm. We assume an input power $P_0 \sim 1$kW so we expect saturation in a length $L_{sat} \sim 0.5 L_g ln(9P_{sat}/P_0) \sim$ 1 m.

The results of ECL are depicted in Fig. 4.24 with the analytic result overlayed. We find a peak power of 500 MW in about 2.1 m for an efficiency of about 3.6%. The gain is about 27dB/m. Incorporating a spread in transverse energy $\sigma_h \sim 0.35$ we find the system is stabilized at zero detuning. as we would expect since the effective detuning spread, $\delta_s \sim \sigma_h a_\beta^2 \sim 9\% \sim 3\rho$. (We have not studied variation with δ_0 for this example).

Incorporating optical guiding, we find $\sigma \sim 0.17$, so that $\eta \sim 0.39$. The Pierce parameter is then $\rho \sim 7\%$. The gain length is $L_g \sim 6.6$ cm and the length for saturation would be of order $L_{sat} \sim 0.5$ m with an output power of $P_{sat} \sim 1$ GW. The detuning spread due to space charge effects would be $\delta_s \sim 7\% \sim \rho$, and this is an acceptable amount, as is that due to spread in h.

We conclude that this example would provide a highly efficient, and compact source of high peak power radiation in the 300 GHz range, comparing favorably with the FEL.[2] This would be suitable, for example, for plasma heating[3] and military applications.[4]

Table 4.5. Parameters for High-Gain Sub-Millimeter Example

$\lambda(cm)$	5×10^{-2}
$E(MeV)$	4
$I(kA)$	4
$\varepsilon_n(cm\text{-}rad)$	1×10^{-2}
$n_p(cm^{-3})$	7×10^{12}
$\lambda_\beta(cm)$	5
$a(cm)$	6×10^{-2}
a_β	0.5
$P_0(W)$	10^3

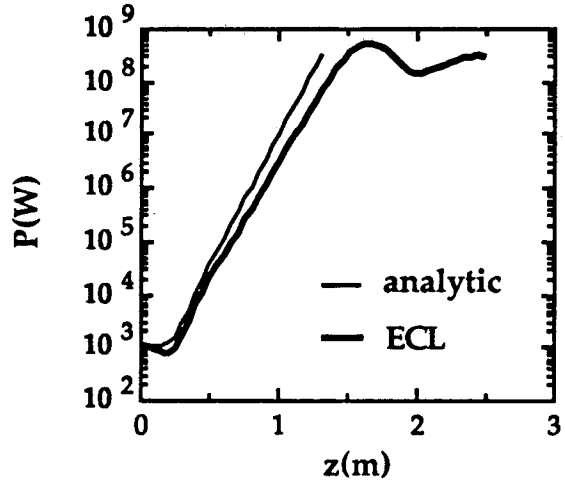

FIG. 4.24. Result for power vs z for the high gain example of Table 4.6, from ECL (dark curve) with a step-radial profile (no spread in transverse energy) compared to the analytic result (light curve).

2. *Low gain example.*

As a different millimeter-wave example we consider a low gain experiment which could be performed with the high-quality low-current beam typical of a storage ring.[5] Parameters are given in Table 4.6.[6] For this example we will also assume operation in a 1cmx1cm waveguide. The overlap integral is $\eta \sim 8.4 \times 10^{-4}$, so that the Pierce parameter is $\rho \sim 1.6 \times 10^{-3}$, and the gain length is $L_g \sim 2.3$m. For this simulation we assumed an input power of $P_0 \sim 1$ kW, and we find $P \sim 100$ kW after 15 meters, still in the exponential gain regime, as shown in Fig. 25(a). Taking into account the spread in transverse energy this is reduced to about 25 kW, as shown in Fig. 4.25 (b).

Table 4.6. Parameters for Low-Gain Millimeter Example

$\lambda(cm)$	1×10^{-1}
$E(MeV)$	5
$I(kA)$	0.05
$\varepsilon_n(cm\text{-}rad)$	3×10^{-3}
$n_p(cm^{-3})$	1×10^{12}
$\lambda_\beta(cm)$	15
$a(cm)$	5×10^{-2}
a_β	0.14
$P_0(W)$	10^3

We conclude that this example would provide a useful proof-of principle for parameters typical of a storage ring. Extended to shorter wavelengths, operation with such a beam would have applications in the

study of solid-state phenomena,[7] in a wavelength range which, except for the FEL, is devoid of other tunable sources.

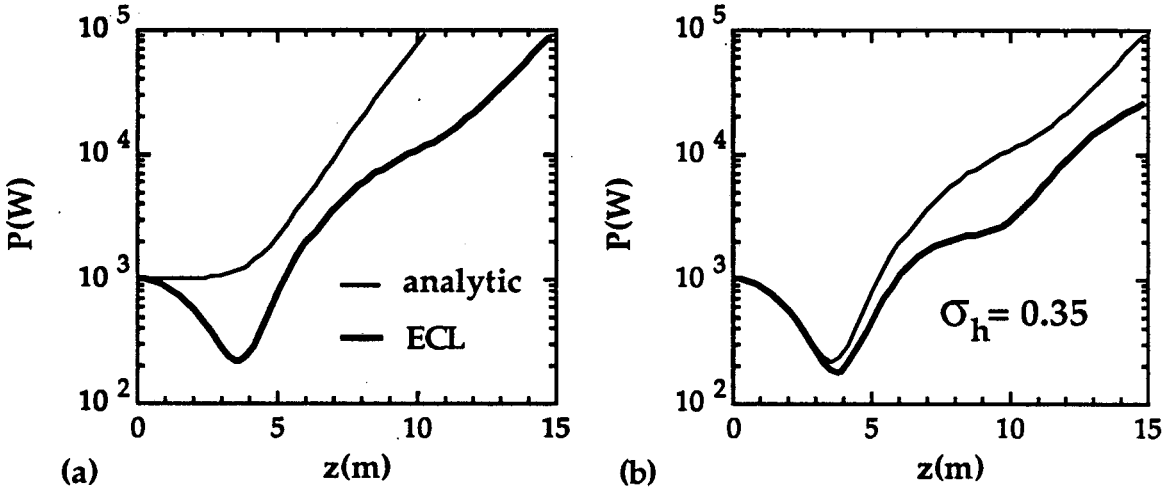

FIG. 4.25. (a)ECL result for power versus z (dark curve), for the low-gain millimeter wave example of Table 4.6, compared to the analytic result (light curve). (b)ECL result for an rms spread in transverse energy σ_h~0.35 (comparable to a parabolic profile) compared to the cold beam result of (a) (light curve).

D. INFRARED EXAMPLE

For the next example, we consider amplification of 10μm radiation from a CO_2 laser, the goal of recent FEL experiments.[8] Instead of the 50 MeV beam typically required in FELs (due to the longer wiggler wavelength), we consider a 10 MeV beam, with other parameters as in Table 4.7. This lower energy has numerous advantages, among these are: shorter device length (more compact), lower beam break-up growth (lower emittance), and higher Pierce parameter (higher efficiency).

Using the HE_{11} mode overlap we have $\eta \sim 7 \times 10^{-3}$, $\rho \sim 1.4 \times 10^{-2}$ and $L_g \sim 4$ cm. We expect a saturated power of $P_{sat} \sim 0.6$ GW, and assuming an input power of 1 kW, saturation should occur in a length $L_{sat} \sim 0.3$ m. ECL predicts saturation in 22 cm with an output power of $P_{sat} \sim 0.94$ GW, as depicted in Fig. 4.26(a). This corresponds to a gain of 154 dB/m and an overall efficiency of 2.5%.

Table 4.7. Parameters for Infrared Example

$\lambda(cm)$	1×10^{-3}
$E(MeV)$	10
$I(kA)$	4
$\varepsilon_n(cm\text{-}rad)$	5×10^{-4}
$n_p(cm^{-3})$	1×10^{15}
$\lambda_\beta(cm)$	0.6
$a(cm)$	3×10^{-3}
a_β	0.4
$P_0(W)$	10^3

We also examined the effect of detuning, $\delta_0 \neq 0$ (not detuning spread, δ_s) as shown in Fig. 4.26(b). For large negative detuning, growth is still in the (quadratic) exponential gain regime after 80 cm, where $P \sim 3.4$ MW. For large positive detuning, the system is stabilized (within numerical accuracy), in qualitiative agreement with theory.

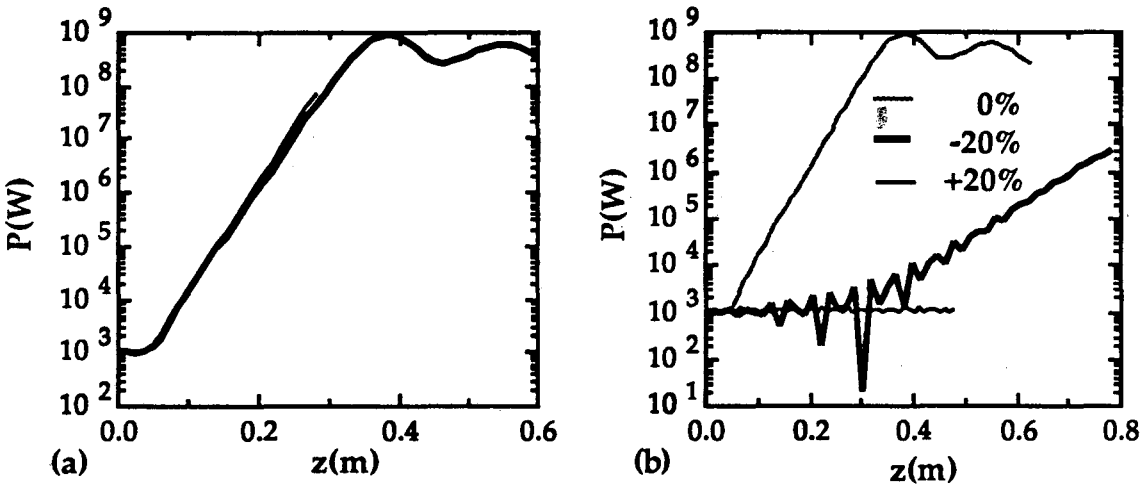

FIG. 4.26. (a) ECL result for power versus z (dark curve), for the infrared example of Table 4.8, predicting gain of roughly 154dB/m, with saturation in 38 cm. Plotted with it is the analytic result (light curve) which agrees well, due to the low value of μ ($\mu \sim 1x10^{-2} \sim \rho$). (b) ECL result for power versus z for detunings $\delta_0 \sim -20\%$(dark curve), $\delta_0 \sim 20\%$(light curve), compared to the result of (a) for zero detuning (dashed curve). As predicted by theory, the result for the large positive detuning (light curve) is stable.

Inspecting Fig. 26(b) further we observe that the result for $\delta_0 \sim -20\%$ is rather irregular suggestive of possible numerical instability. To check this we doubled the number of steps in z (to 798) and found an indistinguishable result. Energy was conserved to within 6% of gain (i.e. the beam had lost 3.6 MW, while the signal had gained only 3.4 MW). This result was also insensitive to particle number.

We also examined the effect of a spread $\sigma_h \sim 0.35$ in transverse energy, as indciated in Fig. 4.27. We conclude that the system is stabilized for this value

of σ_h at zero detuning. This is not surprising since the equivalent detuning spread is δ_s~5.6%~4ρ.

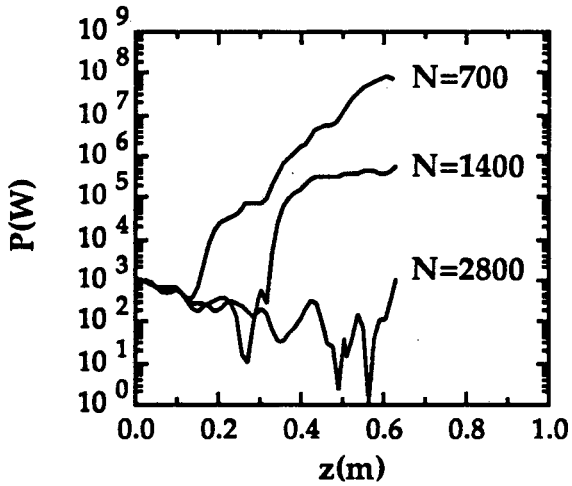

Fig. 4.27. The example of Fig. 4.26 is stabilized by the detuning spread associated with a realistic beam profile. It is instructive to see how this appears in the numerical data. Here depicted is power versus z of runs with different numbers of particles. The numerical variables are N_χ=28, N_α=5 and N_h values of transverse energy where N_h=5, 10, and 20. This dependence on N_h is characteristic of the proximity to the stability boundary in δ_s. When the system is *physically* unstable, it is *numerically* insensitive to the value of $N_h \geq 5$.

In this connection we note that when σ_h or δ_s is sufficienctly large to stabilize the system, ECL will still give growth, but the growth depends on the number of values used to model the distribution (N_h), and can be reduced arbitrarily by increasing N_h. On the other hand, when the system is physically unstable, the result is insensitive to the number of values in the distribution (see, e.g., Fig. 4.21).

Including optical guiding, we find σ~7.5x10^{-2}, so that η~0.17, giving a Pierce parameter, ρ~4%. The gain length is then L_g~1.4 cm and the length for saturation would be of order L_{sat}~0.1 m with an output power of P_{sat}~1.5 GW. The detuning spread due to space charge effects would be δ_s~4%~ρ, and this is an acceptable amount, as is that due to spread in h.

We conclude that this example would provide a highly efficient, and compact source of high peak power radiation in the 10 μm range.

E. X-RAY EXAMPLE

For our last example we consider generation of 100 Angstrom radiation from a 100 MeV beam with other parameters as given in Table 4.8. Two of these parameters are rather problematic: emittance and a_β. The emittance is lower by a factor of ten or more than is currently achievable at this current. The value for a_β is larger than theory has considered and for a realistic beam profile would correspond to considerable detuning spread. Nevertheless the example is useful insofar as it provides some motivation for further work on the large a_β limit.

Using the HE_{11} mode overlap we have η~0.1, ρ~1.6x10^{-2} and L_g~1.6x10^{-2} cm. We expect a saturated power of P_{sat}~6 GW, and assuming an input power of 1 W, saturation should occur in a length z~0.2 cm. ECL predicts saturation in 0.5 cm with an output power of P_{sat}~15 GW, corresponding to a gain of 2x10^4 dB/m and an overall efficiency of 4% .

Unfortunately, but not surprisingly, this example will suffer in practice from a huge detuning spread $\delta_s \sim \sigma_h a_\beta^2 \sim 9 >> 1 >> \rho$, which stabilizes the system. To surpass this obstacle, would require a rather special manipulation or preparation of the beam, which we leave as a topic for further work.[9]

Table 4.8. Parameters for X-Ray Example

$\lambda(cm)$	1×10^{-6}
$E(MeV)$	100
$I(kA)$	4
$\varepsilon_n(cm\text{-}rad)$	3×10^{-5}
$n_p(cm^{-3})$	6×10^{20}
$\lambda_\beta(cm)$	2×10^{-3}
$a(cm)$	2×10^{-5}
a_β	5
$P_0(W)$	1

F. SUMMARY

We conclude this chapter noting that the numerical work has confirmed theory in essentially all respects. Simple estimates of efficiency, gain length, saturation power, emittance variation and the like give the correct answers to within a few tens of percents, which is what one expects from simple scaling laws. From this work the theory of the ICL is advanced to the state where goals for practical experiments can be planned, and

perfomance can be estimated incorporating the ever-present effects of energy spread.

Further studies of detuning and detuning spread are of course important. In fact, a practical conclusion from this work is that control of detuning spread will be the key to a successful experiment. In practice, this means a small spread in axial momentum $\Delta p_z/p_z<O(\rho)$, and a low emittance, such that $\sigma_h a_\beta^2 \leq O(\rho)$.

At the same time there is much more elaborate numerical modelling to be done. Important problems include: (1) implementing a radial field solver to demonstrate, numerically, optical guiding, (2) modelling multiple mode effects in the microwave regime, (3) incorporating slippage and side-bands, (4) detailed studies of tapering, (5) numerical investigation of oscillator configurations, (6) incorporation of ion-motion and the resulting detuning sweep along the beam, and investigation of the ion-coupled dispersion relation, and its consequences for beam break-up in the ion-focussed regime.

References

[1] T. J. Orzechowski, *et al.*, Nucl. Instrum. Methods **A250**, 144 (1986).

[2]K. Thomassen, *Free-Electron Lasers and Applications*, edited by Donald Prosnitz, SPIE Proc. 1227, (SPIE, 1990) pp. 94-104.

[3]R. A. Jong and E. T. Scharlemann, Nucl. Instrum. Methods **A259**, 254 (1987).

[4]W. O. Eckhardt, J. G. Small, and F. Chilton, *Microwave and Particle Beam Sources and Propagation*, edited by Norman Rostoker, SPIE Conf. Proc. 873, 112 (1988).

[5]S. Chattopadhyay, Ref. 2, pp. 160-175.

[6]These are more or less the design parameters for the pre-injector for the Advanced Light Source at Lawrence Berkeley Laboratory.

[7]T. C. Marshall, *Free-Electron Lasers*, (Macmillan, New York, 1985), pp. 10-13.

[8]This was essentially the goal of the Paladin FEL experiment at Lawrence Livermore National Laboratory.

[9]Specifically, one would have to remove the emittance related velocity spread in a thermal beam. Since such a "beam tuner" would not violate any fundamental theorem (Liouville's theorem, energy conservation, etc.), there appears to be no theoretical constraint preventing us from designing such a device, e.g., via mixed electrostatic and magnetic focussing, as recently suggested by Sessler.

Chapter 5: Conclusions

" Never trust the artist. Trust the tale."
-D. H. Lawrence

In this chapter we summarize the discussion of plasma constraints of Ch. 2, the theoretical scalings of Ch. 3, and the numerical results of Ch. 4. We go on to consider prospects for future experimental tests of theory, and for practical applications.

A. SUMMARY

In this work we have answered essentially three questions:

1. Under what conditions is an ensemble of relativistic simple harmonic oscillators subject to an electromagnetic instability?

2. Do these conditions apply to realistic relativistic electron beams propagating the ion-focussed regime?

3. Is the gain length short enough, and the frequency high enough to make this instability a viable source of efficient, coherent radiation?

The answer to question (1) lies in the formulae of Ch. 3, and in the examples simulated in the last chapter. The answer to questions (2) and (3) is yes.

More specifically, in answer to (1) and (2), we have seen that for small betatron parameter (and small spread in axial momentum) detuning spread is small, and amplification occurs. The answer to (3) depends on the beam of course. Specifically, we have seen that design of an ICL parameter set proceeds from assumed values for current (I), energy ($mc^2\gamma$), normalized emittance (ε_n), and the resonant frequency of interest ($\omega \sim 2\gamma^2\omega_\beta$). Current and energy determine the Pierce parameter for perfect overlap (ρ_0). The plasma frequency is determined from ω, and then determines a_β. With these parameters in

hand, the overlap integral (η) can be computed (whether it be due to ion-channel dielectric guiding, optical guiding or waveguide overlap).

From these parameters, we may derive the key figures of merit: (a)the efficiency (ρ), (b)the gain length (L_g), and (c)the detuning spread due to transverse energy spread ($\sigma_h a_\beta^2$). The design can be judged roughly in terms of these figures of merit. The gain length determines whether saturation can be reached in a reasonable length. The Pierce parameter determines the efficiency. The betatron parameter represents a correction to the gain length and the efficiency, and this correction must be taken into account when $a_\beta^2 > \rho$.

For any given design, practical constraints due to plasma effects must also be taken into account. In Ch. 2 we found that these are primarily due to ion-motion. The effects of ion-motion may be put in three categories for conceptual purposes. As the ions collapse inward to neutralize the beam, the betatron frequency drifts upward. Thus each slice finds itself at a slightly different detuning, and samples a different part of the gain curve. In addition, the ion density becomes nonuniform, and focussing becomes anharmonic. Finally, focussing is with respect to the ion-column center of mass, which will oscillate in response to the beam centroid oscillations (ion-hose). We have accepted these effects as a constraint on pulse length. In practice, it will be interesting to see just how stringent these constraints are, and this requires more elaborate numerical work or, better yet, experimental work.

B. PROSPECTS

The usefulness of all this theoretical work is in laying the groundwork for designing, planning and proposing practical experiments, whether they be with high current induction linac beams, or low current (but high quality) beams typical of synchrotron sources. Much further theoretical work can be done of course. In particular, incorporation of space-charge in the analytic model will be important for low energy beams. On the numerical side, *2-D* solution of the Schrodinger/eikonal equation for the vector potential could usefully buttress our simple model of optical guiding. Non-axisymmetric, fully-electromagnetic, *3-D* (or at least *2-D*) particle-in-cell simulations of channel formation and propagation can be used to assess ion-motion effects. However, given the numbers of the last chapter (short gain lengths, high efficiencies, short wavelengths) there is every reason to proceed with a practical experiment.

Indeed there are many applications for which the ICL merits investigation. These include the ground-based laser concept,[1] the two-beam accelerator (linac microwave power source),[2] UV/X-ray laser applications,[3] and others. In addition, it is likely that this electromagnetic instability will appear in a natural way in astrophysical circumstances. At the same time, in experiments relying on ion-focussing, the coupling of the beam centroid to the ion-motion will result in beam break-up and emittance growth in a long

pulse---an electromagnetically-coupled ion-hose. Thus an understanding of the ion-coupled dispersion relation will be important in characterizing emittance growth in the ion-focussed regime.

Reviewing the volumes of work published in just the last ten years on the FEL alone, one realizes that it would be impossible to cover the equivalent ground in one thesis. However, with this work we have at least shown that the ICL merits serious attention. It is amusing to note that this electromagnetic instability, and the electron-hose, are just two instabilities, revealed by a bit of careful attention to the short-pulse beam-plasma regime. Each has rather serious consequences for our understanding of the IFR. One can't help but wonder what other discoveries await us there.

References

[1]T. W. Meyer, R. L. Gullickson, B. J. Pierce, and D. R. Ponikvar, Nucl. Instrum. Methods **A285**, 369 (1989).

[2]A. M. Sessler, E. Sternbach, and J. S. Wurtele, Nucl. Instrum. Methods **B40/41**, 1064 (1989).

[3]D. J. Nagel, *High Intensity Laser Processes*, edited by A. John Alcock, SPIE Conf. Proc. **664**, 142 (1986).

LAWRENCE BERKELEY LABORATORY
UNIVERSITY OF CALIFORNIA
INFORMATION RESOURCES DEPARTMENT
BERKELEY, CALIFORNIA 94720